FACULTY
OF MATHEMATICS
AND PHYSICS
Charles University

DOCTORAL THESIS

Zhansaya Sadakbayeva

Microstructure, swelling and deformation behavior of methacrylate hydrogels with interpenetrating network structure

Institute of Macromolecular Chemistry
Czech Academy of Sciences

Supervisor of the doctoral thesis: Miroslava Dušková-Smrčková, PhD

Study programme: Physics

Specialization: 4F4 – Biophysics, chemical and macromolecular physics

Prague 2017

Acknowledgements

Dedicated

To My Dear Mother

Rassima Sadakbayeva

R.I.P.

"Per aspera ad astra"

Lucius Annaeus Seneca

I declare that I carried out this doctoral thesis independently, and only with the cited sources, literature and other professional sources.

I understand that my work relates to the rights and obligations under the Act No. 121/2000 Coll., the Copyright Act, as amended, in particular the fact that the Charles University in Prague has the right to conclude a license agreement on the use of this work as a school work pursuant to Section 60 paragraph 1 of the Copyright Act.

In…....... date............

Zhansaya Sadakbayeva

Title: Microstructure, swelling and deformation behavior of methacrylate hydrogels with interpenetrating network structure

Author: Zhansaya Sadakbayeva

Department: Department of Macromolecular Physics, Faculty of Mathematics and Physics, Charles University in Prague

Supervisor: Ing. Miroslava Dušková-Smrčková, Dr., Institute of Macromolecular Chemistry, Czech Academy of Sciences

Consultant: Prof. Ing. Karel Dušek, DrSc., Institute of Macromolecular Chemistry, Czech Academy of Sciences

Abstract: This work is devoted to interpenetrating polymer network (IPN) hydrogels prepared by sequential processes of redox-initiated radical polymerization of the first network prepared from 2-hydroxyethyl methacrylate (HEMA), and UV-initiated radical polymerization of the second network prepared from 2-hydroxyethyl methacrylate (HEMA) or glycerol methacrylate (GMA). Microstructure, swelling and deformation responses of the IPN hydrogels and their constituent network hydrogels were tested by various techniques. The microstructure of the first poly(HEMA) network was found sensitive to polymerization conditions. A novel route for one-step synthesis of double-porous poly(HEMA) cryogel was proposed. The formation of the second poly(GMA) network in the environment of non-porous and macroporous poly(HEMA) parent networks was quantitatively studied using the ATR FTIR, UV-spectrophotometer, sol-extraction, and rheology techniques. The scattering of irradiation generated by the microstructure of parent network considerably enhanced the polymerization rate. This acceleration effect was quantified by careful optical analysis. The gelation point of the second poly(GMA) network in the environment of the parent network was detected rheologically and formation of covalently crosslinked network structure within the IPN was confirmed. The development of inhomogeneities during the network formation studied by SWAXS was ascribed to intra- and intermolecular associations resulting in dense hydrophobic domains. DLS analysis of reaction mixtures showed the organization of HEMA or GMA molecules into nanosized hydrophobic domains when diluted with water already prior to polymerization. The poly(HEMA) parent network in IPNs exhibited surprisingly high swelling capacity when incorporated into the IPN with more hydrophilic poly(GMA). The combination of macroporous poly(HEMA) as the first network, which by itself exerts very low modulus, with poly(GMA) or poly(HEMA) as the second network offered interpenetrating polymer networks (IPNs) of superior mechanical properties compared to the properties of their constituents. The rubber elasticity theory was adapted to swollen non-porous homogeneous IPN hydrogels.

Keywords: hydrogel, interpenetrating polymer networks, *in-situ* formation, microstructure, swelling, mechanical properties

Contents

Chapter 1. Theoretical part

1. Interpenetrating polymer networks

1.1. Classification of IPNs

"Interpenetrating polymer networks" comprise two or more networks that are at least partially interlaced on a molecular scale but not covalently bonded to each other and cannot be separated unless chemical bonds are broken[1] (IUPAC definition of IPN). From a synthetic standpoint, IPNs can be classified as "simultaneous" or "sequential" depending on the way of their preparation (Figure 1). Simultaneous IPNs are prepared by mixing the precursors of both networks followed by simultaneous independent polymerization reactions. Sequential IPNs are prepared by swelling of a pre-formed single network by a reaction mixture of the second network followed by its polymerization.

● precursors of Network I
● precursors of Network II

Simultaneous IPN

Network I   ● precursors of Network II   Sequential IPN
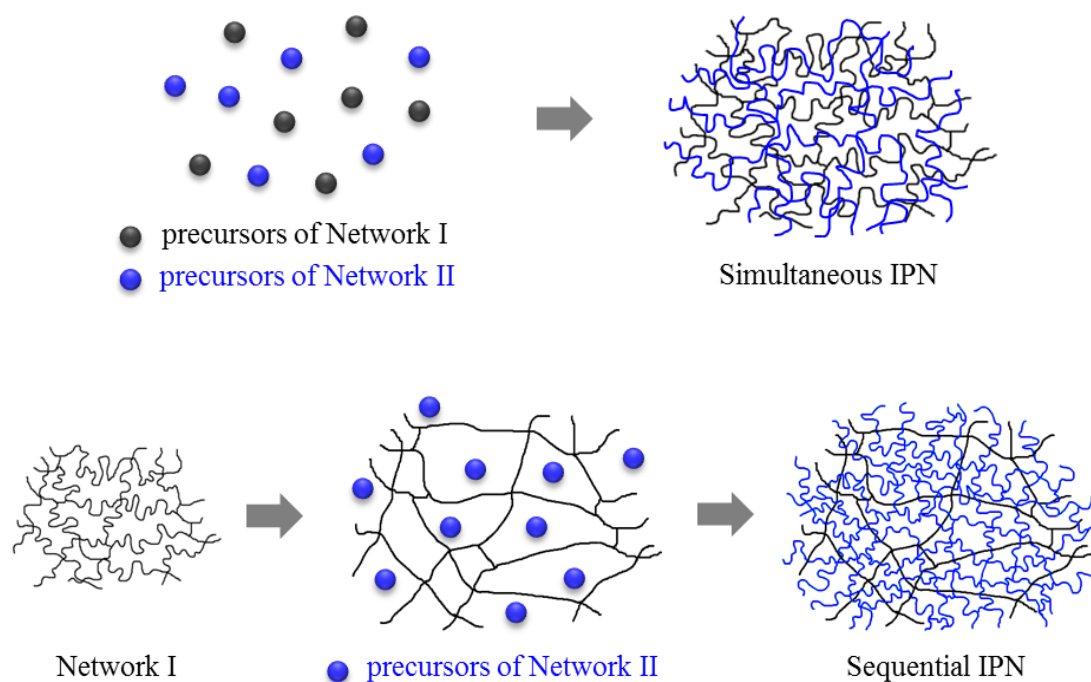
Figure 1. Scheme of IPNs formation.

If the second polymer is crosslinked, a "full-IPN" is formed. Otherwise, a linear second polymer incorporated into the first network results in "semi-IPN" (Figure 2).
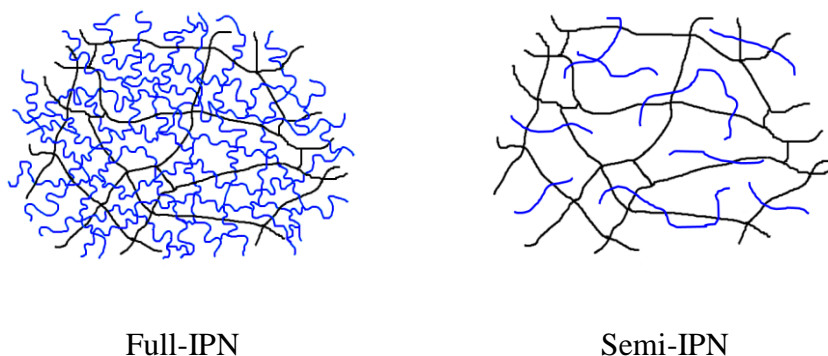
Full-IPN	Semi-IPN

Figure 2. Scheme of full-IPN and semi-IPN.

When the IPN consists of identical networks, it is called "homo-IPN". When the networks are chemically different, the IPN is called "hetero-IPN". In terms of grafting of the second network to the first network, one can distinguish "pseudo-IPN", when the grafting takes place, or "true-IPN", when two networks are not chemically connected.

1.2. Remarks on terminology

The first known person who invented in 1914 the IPNs based on phenol formaldehyde, natural rubber and sulfur was Jonas Aylsworth.[2] He attempted to obtain tough material to make phonograph records, but he never called this material an IPN. Since that period, the idea of interpenetrating polymer networks was forgotten and reinvented several times. In 1946, Tobolsky[3] used a term "two networks" for dual molecular network of vulcanized natural and synthetic rubbers, in which one network was in its relaxed (unstretched) state, while the other was in stretched state. The term "interpenetrating polymer networks" was coined by Millar[4] in 1960. He described homo-IPNs (also called "Millar IPNs") prepared by sequential polymerization of styrene and divinylbenzene. Early academic laboratories interested in IPNs include the groups of Frisch, Klempner, Sperling, and Lipatov. Their early works were published, for example, here.[5,6,7] Recently, the term "double network" (DN) hydrogels has been coined by the group of Gong.[8] Double network hydrogels are just a special case of interpenetrating networks consisting of two chemically different networks and revealing a high toughness and a special energy dissipation mechanism when undergoing the deformation.

2. Interpenetrating polymer network hydrogels

The concept of IPNs was extended towards hydrogels and can be a route to materials with new and tunable properties due to manifold varieties of networks combination. Moreover, the embedding of networks sensitive to external stimuli such as temperature, pH, ionic strength of the aqueous medium, light (UV, visible or near infrared), oscillating magnetic or electric fields, into the IPNs structure can modify the responsiveness of the latter. Hydrogels with IPNs architecture are interpenetrating networks swollen in aqueous media, and, therefore can be considered as three-component systems (network 1, network 2 and solvent).

In this part of the thesis, various types of IPN hydrogels such as chemically homogeneous IPNs, chemically heterogeneous IPNs, special double networks, and multiple networks will be discussed.

2.1. Chemically homogeneous IPN hydrogels

In this thesis, the term "chemically homogeneous IPN hydrogels" (also called homo-IPNs) is attributed to the case, when the first and the second networks were made of the same monomer. The *whole term* "chemically homogeneous IPN hydrogels" does not carry information on networks structure or morphology of IPN hydrogels. Whereas the separate utilization of terms "homogeneous" or "heterogeneous" further may be attributed to networks structure as well as to morphology of gels depending on the context.

There are not so many reports on synthesis of chemically homogeneous IPN hydrogels. Those that exist are devoted to IPN hydrogels based on poly(2-hydroxyethyl methacrylate) (PHEMA), poly(acrylic acid) (PAA), polyacrylamide (PAAm) full-IPNs and PAAm semi-IPNs. Usually, the homo-IPN hydrogels are prepared sequentially, i.e., the first network after it is formed swells in the reaction mixture of monomers and the second network is formed by its polymerization. Depending on the interactions between segments of the first and the second networks and several other parameters, the formed double networks can be homogeneous or phase separated. The topological independence of homogeneous sequential interpenetrating networks can be questioned, e.g., because of grafting.[9]

One of the rare examples of PHEMA-PHEMA homo-IPNs was described in reports[10,11,12,13] in terms of their ophthalmological application. In designing a new type of artificial cornea consisting of transparent homogeneous PHEMA optical core

and porous PHEMA skirt, the transparent cornea core was bonded to the porous skirt by monomer penetration and subsequent polymerization.[10] Both parts of artificial cornea were modified by IPN concept to reduce the ability of transparent core to uptake calcium ions[11,12] and to improve the mechanical properties of porous skirt.[13] The PAA-PAA and PAAm-PAAm homo-IPNs were examined to assess only the effect of physical entanglements of the polymer chains on their structure and properties, while avoiding the chemical interactions between moieties of chemically different networks. The effective network chain length and equilibrium water content are governed by the density of physical entanglements increasing with the concentration of monomer. The IPNs and corresponding single networks have similar compressive moduli, but different strains, – lower in case of IPNs due to the lower effective chain length and therefore increased brittleness.[14] Synthesis of chemically homogeneous semi-IPN hydrogels based on crosslinked and linear PAAm resulted in materials with altering swelling properties.[15] Shrinkage response in acetone/water mixture was faster when linear PAAm was introduced into the matrix of crosslinked PAAm forming a semi-IPN hydrogel compared to shrinkage of single PAAm network. Semi-IPNs containing the first crosslinked PAAm network and the second and the third linear PAAm revealed a fracture stress of up to 5.7 MPa and 10 MPa, respectively, which were significantly higher than a fracture stress of a single PAAm network (0.15 MPa).[16] Enhanced mechanical properties of semi-IPNs were explained by the inhomogeneous (wide mesh size distribution) structure of the first crosslinked PAAm network estimated by static light scattering technique. Larger degree of inhomogeneity, as a result – better mechanical properties, can be achieved by changing the *N,N'*-methylene-bis-(acrylamide) (BAAm) crosslinker to poly(ethylene glycol) dimethacrylate (PEG-DM).

2.2. Chemically heterogeneous IPN hydrogels

A great majority of IPN hydrogels are made by combining chemically different networks, so called "chemically heterogeneous IPN hydrogels". The constituent networks can be natural or synthetic polymers, hydrophilic or hydrophobic, stimuli-responsive, or of different morphology. Moreover, each component can be either a covalently crosslinked network or a linear polymer. The general idea is that the networks are combined in a way of producing an advanced multicomponent system with a new profile. The most commonly used networks are

hydrophilic natural or synthetic polymers with hydrophilic functional groups such as –COOH, –OH, –CONH$_2$, –SO$_3$H, –NR$_2$ and –R$_4$N$^+$, and –OR.[17]

The morphology of the IPN hydrogels (non-porous or porous) plays a crucial role when considering their potential application. In biological applications, the presence or absence of porosity affecting the cells proliferation and viability can be a decisive factor of integration of the artificial material into the body. The majority of the vast literature on the IPN hydrogels involves non-porous gels. If the pre-formed first network is non-porous or porous, and the synthesis of the second network is not accompanied by the phase separation, then the formation of non-porous IPN hydrogel is likely. As an example, the formation of hydrophilic poly(2-hydroxyethyl acrylate) (PHEA) network inside the macroporous hydrophobic poly(methyl methacrylate) (PMMA) or poly(ethyl acrylate) (PEA) networks in the absence of any diluents resulted in non-porous IPN hydrogels.[18] The hydrophobic macroporous first network matrix imparts the mechanical strength to the IPN, while the hydrophilic second network is responsible for the swelling characteristics. In this example, at room temperature, the hydrophobic first PMMA and PEA networks were glassy and rubbery, respectively. Therefore, the swelling of the IPN hydrogel driven by the hydrophilic PHEA network is better when PHEA is incorporated into the rubbery PEA network.

There are also reports devoted to porous IPN hydrogels[13,18,19,20,21]. Addition of a diluent into the reaction mixture of the second network may cause the phase separation leading to the formation of porous IPN hydrogel[18]. Another interesting example of porous IPN hydrogel based on methacrylated hyaluronan HA (PHA) and *N,N'*-dimethylacrylamide (DAAm) was studied by Weng and coworkers.[19] Both networks were photocrosslinked sequentially and the IPN hydrogel after the lyophilization revealed macroporous structure of pore size ranging from 10 to 20 μm. Indeed, such macroporous structure of the hydrogel causes a very high swelling (up to 90 %), while the fracture stress is also increased up to 5.2 MPa due to the IPN approach. "Squeeze-soak-squeeze" repetitive technique, when the reaction monomers are expelled from the pores of the first network but remained in the polymer matrix, is another approach for preparation of macroporous IPN hydrogels with enhanced mechanical properties.[13] Utilization of templates serving as porogens during the IPN gels formation allows to control the size and shape of pores and obtain the materials with narrow distribution of pore size.[20] On the other hand, the

spatial distribution of template particles is usually stochastic, and therefore the preparation of high volume of communicating pores is unlikely. A cryogelation implying the polymerization at temperatures below zero, which is accompanied by freezing of diluent and, thus, formation of pores, was used to prepare independently crosslinked PAAm/chitosan full-IPN hydrogel with interconnected pores and high sorption capacity.[21] The crosslinking under cryo-conditions of the first PAAm network with trapped chitosan molecules was followed with crosslinking of the chitosan with epichlorohydrin under alkaline conditions.[21]

There is a quite wide field of IPN hydrogels responsive to multiple environmental stimuli. Incorporation of natural polymers and their derivatives into stimuli-responsive IPN hydrogels may improve the biocompatibility of IPNs. For instance, to obtain the hydrogel responsive to both pH and temperature, it is enough to incorporate into the IPN structure ionizable and thermosensitive functional groups. Hydrogels responding to both pH and temperature are usually represented by copolymers with pH responsive moieties such as *N,N'*-diethylaminopropyl methacrylamide or acrylic acid and temperature responsive moieties such as *N*-isopropylacrylamide (NIPAAm).[22] The permeability of PNIPAAm/PMA IPNs for the purpose of membrane or drug release application can be controlled by both pH and temperature.[23] Sometimes unique properties that are unattainable by single constituent networks can be achieved when these constituent networks are incorporated into the IPN structure. For instance, poly(vinyl alcohol) (PVA) network interpenetrated with PAAm network becomes responsive to temperature in the range from 40 to 50 °C, whereas neither polymer exhibits temperature responsiveness in this range.[24]

2.3. Double networks as a special case of IPNs

Certain class of tough IPN hydrogels are called "double network" (DN) hydrogels. This term promoted by Gong[8] et al. implies a subset of interpenetrating polymer networks, where the first network is always a tightly cross-linked polyelectrolyte and the second network is always a loosely crosslinked or uncrosslinked neutral polymer. Mechanically weak ionized poly(2-acrylamido-2-methyl-1-propanesulfonic acid) (PAMPS) reinforced with mechanically weak neutral polyacrylamide (PAAm) exhibits nonlinear enhancement of mechanical strength. Such combination of networks resulted in IPN hydrogel containing 60-90 % of water

and possessing high both hardness and toughness. The effect is achieved due to the ductile second network holding the brittle first network and preventing it from damage.[25] The proposed structure of the PAMPS-PAAm DN hydrogel is shown in Figure 3.[26,27] It is suggested that the PAMPS hydrogel has inhomogeneous network structure and consists of large "voids". According to Wu[28,29,30] et al., large "voids" can be formed when: (a) the rate of growing of polymer "clusters" is significantly higher than their relaxation rate (diffusion) and (b) the voids between polymer "clusters" (microgels) are larger than the mesh size between crosslinked chains inside the microgels. The PAAm second network occupies these "voids" and acts as a "molecular crack stopper" preventing the growing of crack to a macroscopic level.[26] The second PAAm network not only interpenetrated to the PAMPS network, but also forms a soft continuous network due to the physical entanglements.[27] The mechanical strength of DN hydrogels is affected by structural parameters such as molar ratio of the first network to the second and crosslinking density of both networks. Formation of DN hydrogels with extraordinary mechanical performances requires that both the swelling capacity and the cross-link density of the first network must be high.[8]
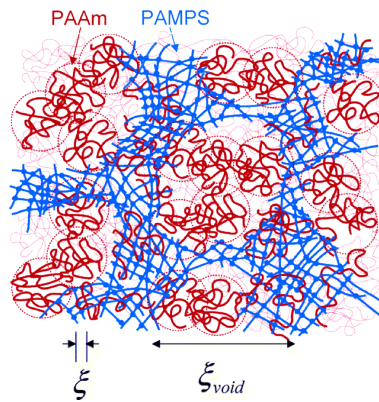
Figure 3. Inhomogeneous structure of tightly crosslinked ionized PAMPS/loosely crosslinked neutral PAAm double network hydrogel.[27]

Inspired by the work of Gong and co-workers, Frank and co-workers proposed another way to design IPNs with enhanced modulus and fracture strength for an artificial cornea application.[31,32,33,34] The general idea is changing the synthesis order of ionized and neutral networks and, thus, obtaining double network hydrogels that are "inverse" of the double networks prepared by Gong et al. A tightly crosslinked poly(ethylene glycol) (PEG) network is interpenetrated with a loosely

crosslinked ionizable second poly(acrylic acid) (PAA) network. Each of these single networks is mechanically weak and fragile. However, their combination causes the increase in compressive modulus and fracture strength of IPNs over 3 times compared to that of single PEG network with the same polymer volume fraction.[34]
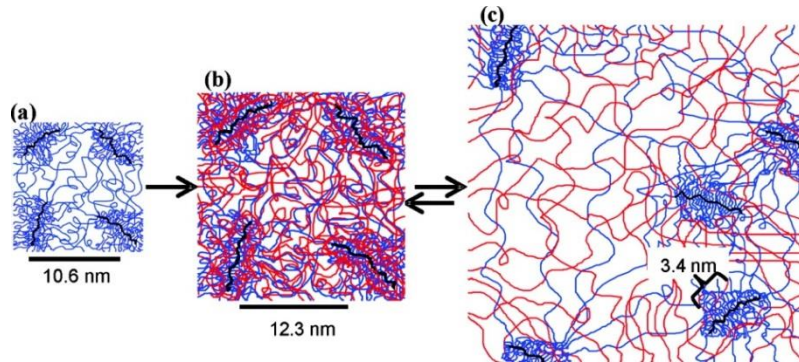
Figure 4. Inhomogeneous structure of "inverted" double network hydrogel – tightly crosslinked neutral PEG/loosely crosslinked ionized PAA: (a) single PEG network, (b) PEG/PAA IPN at low pH 3.0, (c) PEG/PAA IPN at high pH 7.4.[34]

PEG network itself has flexible rod-like crosslink junctions of high functionality, which resemble "molecular bottle-brush" morphology (Figure 4a).[35] It is known that PEG and PAA networks tend to complexation;[36,37,38] the extent of complexation is in consistent with the swelling and depends on pH. At low pH 3, the volume of the entire IPN hydrogel slightly increases, but the weakly ordered structure of the PEG network remains (Figure 4b).[34] The total volume fraction of polymers gets high due to the hydrophobic interpolymer hydrogen-bonding complexation between PEG and PAA. At high pH 7.4, two networks in the frame of the DN hydrogel completely dissociate from one another and the hydrogel exhibits extensive swelling. However, the constraints in the IPN do not allow PAA network to dissociate from the PEG on a large scale. Therefore, there is a separation on a nanoscale level – between the PEG-rich high functionality crosslink joints and the PAA network within the IPN (Figure 4c).[34] Moreover, such a high value of pH causing the swelling of PAA network disrupts the weak ordering of domains in PEG network. The improvement of the modulus of PEG/PAA IPN hydrogel is caused by the non-Gaussian conformation and the finite extensibility of the PEG network chains within the first tightly crosslinked network.

Thus, in both cases: (a) one network is neutral while the other network is ionized, and (b) one network is tightly crosslinked while the other network is loosely

8

crosslinked. The crucial difference is in the order of networks incorporation into the IPN structure. DN hydrogels based on tightly crosslinked ionized first network and loosely crosslinked neutral second network prepared by Gong's group reveal high-tear-strength properties. The improvement of mechanical properties was achieved by the neutral second network suppressing the propagation of cracks during the deformation of the DN hydrogel. Whereas the IPN hydrogels prepared by Frank's group were synthesized in an opposite way. High swelling degree of the loosely crosslinked ionized second network causes high extension of the neutral first network. But since its extensibility is finite, the first network prevents the IPN hydrogel from rupture. Such combination of networks results in IPN hydrogels with enhanced modulus and fracture strength rather than an enhanced tear strength.[34]

DN hydrogels with extraordinary mechanical properties confined only to polyelectrolytes are limited in their widespread application. In this connection, Okay and co-workers have studied nonionic DN hydrogels based on polyacrylamide (PAAm) and poly(*N*,*N'*-dimethylacrylamide) (PDMA) networks.[16] The first network was always crosslinked (PAAm or PDMA), while the second network was linear. Obtained hydrogels exhibited improved mechanical strength. Despite remarkable increase of fracture stress and compressive modulus (MPa range) of eventual multinetwork hydrogel, the content of water remains high – about 90 %. Shams Es-haghi[39] et al. also prepared nonionic PAAm/PAAm DN hydrogel, the both networks of which are crosslinked loosely. High extensibility and high stress in this hydrogel is caused by the increase of an average crosslink density of the resulting structure due to the fact, that networks not only interpenetrate each other, but also are chemically crosslinked (black chains in Figure 5.).
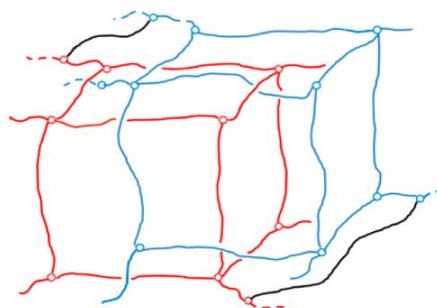
Figure 5. Double network hydrogel comprised of loosely crosslinked PAAm neutral networks.[39] Red and blue chains represent two networks; black chains represent the

grafted links between two networks.

The networks in DNs as well as in all IPN hydrogels can be crosslinked not only by chemical covalent bonds but also by physical bonds. Generally, chemically crosslinked single polymer networks are mechanically stronger compared to physically crosslinked single networks. However, due to irreversible bond breaking, chemically crosslinked networks do not reveal self-healing, self-recovery and fatigue resistance properties. To take advantage of both chemical and physical crosslinks, the differently crosslinked polymer networks can be combined into the DN structure. For instance, the physically crosslinked Agar network interlocked with the chemically crosslinked polyacrylamide (PAAm) network results in unique hybrid-linked Agar/PAAm DN gel, which has the fracture energy similar to fully chemically crosslinked PAMPS/PAAm gels (10^2-10^3 J/m^2) and can be recovered to some extent after damage or fatigue.[40] Combination of two physically crosslinked networks (Agar/hydrophobically associated linear PAAm) also results in strong DN gel, the mechanical properties of which are comparable with those of fully chemically linked DN gels and hybrid-linked DN gels; moreover, fully physically crosslinked DN gels reveal rapid self-recovery and self-healing properties without any external stimuli at room temperature.[41]

2.4. Multiple network gels

The concept of interpenetrating networks has a great potential in terms of the possibility to generate new materials by introducing more and more independent networks into the structure of hydrogels. This technique is supposed to improve the mechanical properties of single network hydrogels, but sometimes for IPN hydrogels of a certain rank, the efficiency of the method become lost and a worsening of mechanical properties can be observed.[39] The combination of three and more independent yet interpenetrating networks with well-defined network structure and identified functional roles of each network in mechanical behaviors of multiple network gels is challenging. Preparation and properties of multiple homo-IPN hydrogels (PHEMA-based,[12] PAAm-based[16,39] and PDMA-based[16]) and multiple hetero-IPN hydrogels (PAMPS/PAAm/PAMPS and PAMPS/PAAm/PAMPS (linear),[42] SAPS/PAAm/PAAm and SAPS/PAAm(linear)/PAAm,[43] HA/PDMA/PDMA[44]) were reported.

2.4.1. Multiple homo-IPNs

Synthesis of a multiple chemically homogeneous PHEMA-PHEMA IPN hydrogel was considered as a route for reducing the size of nanodomains existing in a single network hydrogel, in which undesirable calcium ions would accumulate.[12] Swollen triple network polyacrylamide (PAAm) hydrogel and poly(*N,N*-dimethylacrylamide) (PDMA) hydrogel, in which only the first constituent is a crosslinked network while the second and third ones are linear polymers, exhibit high swelling degree (about 90% for both types of triple networks), high fracture stress (up to 10 MPa for PAAm, up to 19 MPa for PDMA), and the Young's modulus (1-2 MPa for PDMA).[16]

A set of multiple PAAm homo-IPN hydrogels (double, triple and quadruple networks) was prepared by Shams Es-haghi[39] et al. Each generation of networks was synthesized sequentially by UV-initiated radical polymerization and was loosely crosslinked (0.01 mol% of MBAA crosslinker to AAm monomer). Stress-strain behavior of multiple networks PAAm hydrogels showed that the stress at break of IPN of the next rank increased drastically, while the decrease in strain at break values was not significant. Each subsequent polymerization step led to increase of the overall crosslink density due to the some grafting of each network to the previous one and heterogeneous distribution of crosslinks in the IPN resulting in areas of brittle clusters of crosslinks[45]. The tensile deformation of such hydrogel may cause the strain localization producing the localized fracture of the cluster structure. Since the average crosslink density of area surrounding the cluster structures is lower compared to average density of clusters, the fracture of the cluster does not propagate and macroscopic gel remains ductile, which explains the increase of stress of the triple network and quadruple network hydrogels.

2.4.2. Multiple hetero-IPNs

Kaneko[42] and co-workers, reported on three component PAMPS/PAAm/PAMPS hydrogels, the third component of which was either crosslinked PAMPS network (triple network) or linear PAMPS polymer (linear polymer penetrated the double network). These gels were tested as potential materials for human artificial cartilage exhibiting low frictional coefficients. Fracture stress and elasticity of both hydrogels were high enough (in MPa range) to withstand extremely high pressures exerted on articular cartilage in synovial joints (10^3-10^5

Pa). The low frictional coefficients of triple network hydrogel and the hydrogel, in which the linear polymer penetrated the double network, also corresponded to the real conditions. However, the latter hydrogel revealed an ultra-low-frictional coefficient ($\mu \sim 10^{-5}$) due to the highly mobile chains of the third linear PAMPS component contributing to the reduction of friction.

Hydrogels constituted of a tightly crosslinked hyaluronic acid (HA) of various degrees of methacrylation as a first network and loosely crosslinked PDMA as a second and a third networks exhibit superior mechanical properties.[44] While the single network HA hydrogel itself can withstand only 40% of compression strain and up to 0.02-0.05 MPa of stress, the HA/PDMA withstands a fracture stress of above 10 MPa and fracture strain of 96 %, and HA/PDMA/PDMA, in which the ratio of the ductile network is enhanced, withstands the compressive stress above 20 MPa.

The introduction of the loosely crosslinked PAAm network as a third network into the structure of 3-sulfopropyl acrylate potassium salt (SAPS)/PAAm (linear or crosslinked) semi-IPN and full-IPN hydrogels prevents the typical for those IPNs necking upon tensile deformation and leads to strain hardening.[43]

3. Application of IPN hydrogels in biomedicine

3.1. Scaffolds for tissue engineering

The IPN concept results in hydrogels of enhanced or controlled mechanical properties and swelling that is a good output for designing various scaffolds and materials in tissue engineering. High performance IPN hydrogels of suitable viscoelasticity, high mechanical strength, low friction, durability, biocompatibility, and resistance to wear and to biodegradation within the living body are good candidates for artificial cartilage application. Cells sense and respond to mechanical stimuli and topography of the microenvironment.[46,47,48,49] The mechanical properties of the artificial hydrogel substrate are supposed to be similar to the real cartilage in order to evoke the growth of cells. The mechanical characteristics of real cartilage are the following: Young's modulus[50] – 0.45-0.8 MPa, tensile strength at break[51] – 15-35 MPa, elongation at break[52] – 80 %, compressive strength[53] – 14-59 MPa, equilibrium compressive aggregate modulus[54] – 0.1-2 MPa, equilibrium shear modulus[55] – 0.05-0.25 MPa, coefficient of friction (μ)[56,42] – 10^{-1}.

A general procedure of artificial articular tissue engineering is presented in Figure 6.[57] Three main components are needed to be properly selected for successful tissue replacement: cells, biomaterial scaffold and environment including mechanical stimuli and bioactive factors (growth factors, oxygen tension, gene, drugs and bioreactors).
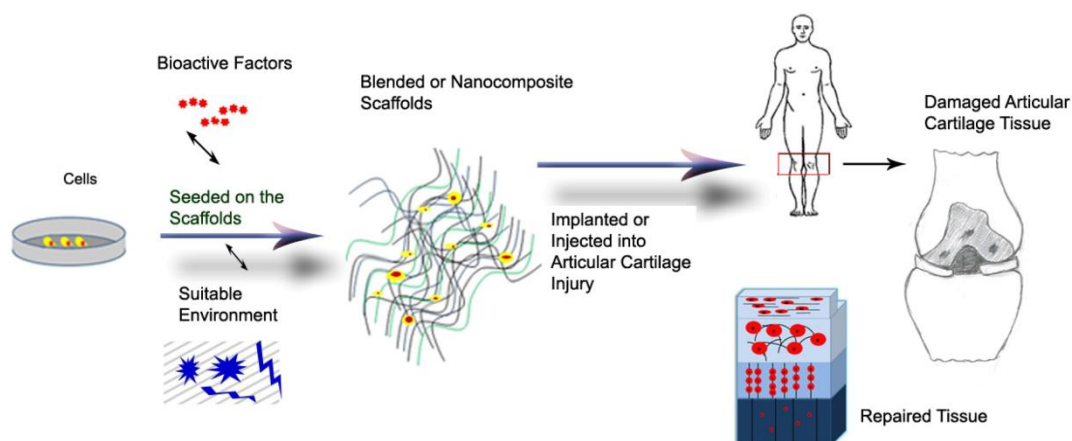
Figure 6. Articular cartilage tissue engineering procedure.[57]

Many different IPN hydrogels were tested as potential artificial cartilages in terms of their mechanical properties as well as cells viability within the microstructured artificial tissue. Some of the examples of IPN hydrogels are

summarized in Table 1 and attributed to fully synthetic, fully bio, or hybrid synthetic/bio networks.

Table 1. Examples of IPN hydrogels as potential artificial cartilages.

IPN hydrogel: Network 1/Network 2		Parameters	Values	References
Synthetic	PAMPS/PAAm[42]	Elasticity Fracture stress Fracture strain Coefficient of friction	0.84 MPa 4.6 MPa 65 % 10^{-2} - 10^{-1}	[42]
	PAMPS/PAAm/ PAMPS(linear)[42]	Elasticity Fracture stress Fracture strain Coefficient of friction	2.1 MPa 9.2 MPa 70 % 10^{-5}	[42]
	PAMPS/ PDMAAm[58]	Compressive failure stress Compressive failure strain Elastic modulus	3.1 MPa 73 % 0.2 MPa	[58]
Bio	Bacterial cellulose/gelatin[59]	Fracture stress Compressive strain	3.7 MPa 30 %	[59]
	Gellan gum methacrylate (GGMA)/gelatin methacrylamide (GelMA)[60]	Compressive failure stress Compressive failure strain	6.9 MPa 80 %	[60]
Synthetic/ Bio	Oligo(2,2-dimethyltrimethylene carbonate)-poly(ethylene glycol)-oligo(2,2-dimethyltrimethylene carbonate)-diacrylate/ methacrylated hyaluronic acid DPD-DA/HA-GMA[61]	Fracture stress	8.38±0.67 MPa	[61]
Bio/ Synthetic	HA/PDAAm[19]	Fracture stress	5.2 MPa	[19]

It was shown, that the fully synthetic DN hydrogel composed of poly(2-acrylamido-2-methylpropanesulfonic acid) (PAMPS) and poly(*N,N'*-dimethylacrylamide) (PDMAAm) acting as a plug can induce the spontaneous

regeneration of hyaline-cartilage with large osteochondral defect.[62] Complete regeneration was achieved in 4 weeks. The bonding of natural tendon and cartilage to bone is extremely tough (interfacial toughness is around 800 J/m^2).[63,64] Therefore, the strong adhesion between IPN hydrogels and solid surfaces is important. Kurokawa[65] et al. estimated the bonding of PAMPS/PAAm DN hydrogels to *porous* solid substrates (glass, polyethylene and sponge) by peeling test. The highest achieved bonding strength was ~1000 J/m^2. Zhao and co-workers[66] showed, that tough PAAm/alginate IPN hydrogels provide a strong interfacial bonding (strength from 1200 to 1500 J/m^2) to various *non-porous* silanized solid substrates due to the chemically anchoring the long-chain networks.

3.2. Suitability of methacrylate-based gels for ophthalmic application

Biomedical application of crosslinked hydrophilic single network of PHEMA as soft contact lenses was developed in 1960s by Wichterle and Lim.[67] Since that time, PHEMA is commonly used for corneal implants[68], intraocular lenses[69], vitreous substitutes.[70] For many of ophthalmic applications, the polymer materials should have high water-content, appropriate refractive index and good mechanical properties to withstand the intraocular environment. Therefore, to date, PHEMA is used in combination with other polymers to create materials with improved properties. The input data, which have to be taken into the account when designing a new material for ophthalmic application are, for instance, the normal intraocular pressures averaging between 12-22 mmHg. The human cornea is optically clear (refractive index 1.376)[71] and nearly 80 % water with tensile strength of several MPa (3.81 MPa)[72]. Depending on the age and intraocular pressure, the Young's modulus of human cornea varies in the range from 159-961 kPa.[73]

In the hydrogel applications, the IPN concept was used especially in ophthalmology where the interpenetration serves as a joint between tissue and implant.[74,75,76,77] Although the application of hydrogels in ophthalmology demands optically clear gel, translucent or opaque materials also have a great potential in ocular implants and devices that do not demand optical clarity. For successful biointegration, the artificial cornea should be designed as a "core-and-skirt" system with optically clear core (central part) and porous peripheral skirt to improve the tissue attachment and diffusion of nutrients for cellular function.[78,10,32,77] It was found, that the strongest attachment between the core and periphery can be achieved

by interpenetrating polymer network concept as compared to clamping, screwing or gluing of artificial cornea sections.[10] This concept was used by Chirila[10] et al. to create a new type of artificial cornea made from PHEMA and consisting of transparent homogeneous optical PHEMA core, porous PHEMA skirt, and the PHEMA/PHEMA IPN interface bounding together the core and skirt (Figure 7a). Another example of artificial cornea consisting of transparent PEG/PAA double-network core with high strength and high water content interpenetrating the created by photolithography microperforated PHEA hydrogel skirt was created by Myung[32] et al. (Figure 7b). Both components were modified with collagen type I to provide the epithelialization. Recently, to control the porosity of the skirt and improve its biointegrability via creation of an environment conductive to the ingrowth of stromal cell, sintered polystyrene microspheres have been used as templates for the PEG/PAA IPN skirt[77] (Figure 7c). After the polymerization, templates were leached from IPN scaffold using methyl ethyl ketone (MEK). The advantage of this technique implies the utilization of a specially constructed annular PDMS mold for fabricating artificial cornea in a single seamless piece without creation a potentially weak interface joints between the core and skirt. The mold is constructed in such a way, that only the periphery is templated while the central core remains non templated. As a result, the designed artificial core consists of transparent non-porous PEG/PAA IPN core and porous PEG/PAA IPN skirt.

a   b   c
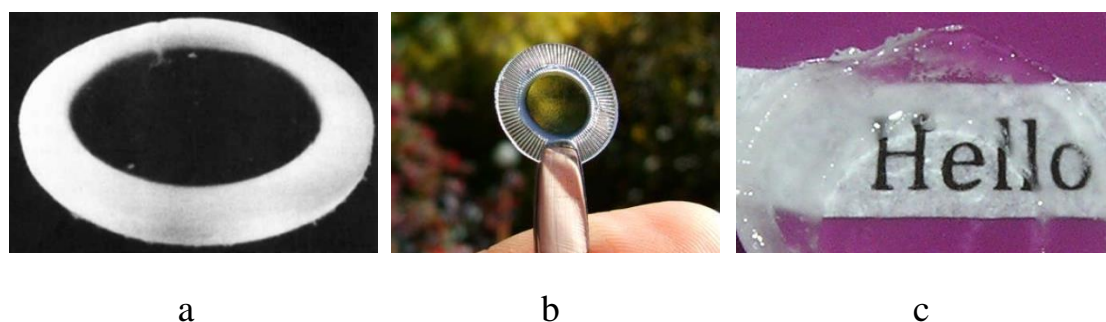
Figure 7. A few examples of artificial cornea: (a)[10] non-porous PHEMA optical *core* –PHEMA/PHEMA IPN *interface* – spongy macroporous PHEMA *skirt*, (b)[32] non-porous PEG/PAA DN optical *core* – PEG/PAA/PHEA *interface* – microperforated by photolithography PHEA *skirt*, and (c)[77] non-porous PEG/PAA optical *core* – templated porous PEG/PAA *skirt*.

The IPN hydrogel design provides the adjustability of gel mechanical properties by choosing the constituent polymers, changing the crosslinker concentrations in both networks and polymerization mechanisms. Single PHEMA network itself has relatively low water content (up to 40 %) and low permeability to glucose,[79] which is a drawback in terms of proper implant epithelialization. This issue can be overcome by interpenetration of PHEMA network with other polymer networks. For instance, methacrylic anhydride modified gelatin interpenetrated into the PHEMA network improved its swelling properties from 30.4 % to 74.4 % of water in equilibrium and, hence, created suitable conditions for corneal epithelial cell attachment and proliferation.[68] Biocompatible PHEMA/PAA IPN hydrogels containing ZnS nanoparticles are shown to have 60.2 % of water and refractive index in swollen state of 1.49.[80] In the IPN gels, PHEMA network is commonly responsible for sample strengthening. Collagen-immobilized PEG/PHEMA IPN hydrogels[81] are shown to be potential biomaterials for artificial cornea. Among the studied compositions of IPNs, gels of appropriate transmittance (about 90%) have demonstrated tensile strength of 6.3 – 7.5 MPa depending on the amount of incorporated PHEMA network.

3.3. Other applications

Antifouling properties: the most commonly used mechanically poor poly(ethylene glycol) (PEG)-based hydrogels[82] and zwitterionic poly(carboxybetaine methacrylate) (PCBMA) hydrogels with moderate mechanical properties[83] reveal excellent surface resistance to protein adsorption and cell adhesion. So, they could be embedded in the DN structure to obtain antifouling tough materials. Among the tough DN hydrogels, those exhibiting also antifouling properties are: (1) PAMPS/PCDME (poly(2-acrylamido-2-methylpropanesulfonic acid)/ poly((N-carboxymethyl)-*N,N*-dimethyl-2-(methacryloyloxy) ethanaminium, inner salt)),[84] (2) Agar/PAAm,[85] (3) PNVA/PAAm (poly(N-vinylacetamide)/poly(acrylamide)),[86] and (4) PAMPS/PAAm.[87] The latter[87] was tested against barnacles for a long time in the real marine environment. The antifouling activity of the PAMPS/PAAm DN hydrogel lasted 330 days.

Drug delivery systems are another group of systems, for which IPN hydrogels can be efficient. DN hydrogels with high mechanical strength can serve as stable carriers to control the release of drugs or biomolecules[88,89] and retain the entrapped

biomolecules with native or functional conformations.[90,91] IPN drug delivery hydrogels responsive to light,[92] pH,[93,94] temperature[95,96] or both pH/temperature[94,97,23] are reported.

Other applications of PHEMA-based IPNs includes the combination of PHEMA network with poly(2-methacryloyloxyethyl phosphorylcholine) for better protein adsorption resistance and ion permeability;[98] with acrylic acid for separation of cationic dyes and heavy metal ions;[99] with PHEMA[12] for reducing the calcification; with PEG,[100] PVP,[101,102] PVA[103] and gelatin[104] to improve water-sorption characteristics; with itaconic acid and PVP[105] to obtain antimicrobial materials; with chitosan to reduce the protein adsorption[106] or to remove metal ions from aqueous solutions.[107]

4. Kinetics of IPNs formation

Control of the kinetics of IPNs formation is important, since it significantly affects the morphology and properties of the final IPN products. The formation of networks in the IPNs is somewhat different than the formation of individual single networks regardless of the way of networks synthesis (sequential or simultaneous). In sequential IPNs, where the networks are synthesized one by one, the formation of the second network is affected by the presence of the pre-formed first network, which acts as a diluent for the second network. In simultaneous IPNs, where the networks are supposed to be formed simultaneously, due to the different polymerization rates the network formed earlier creates the medium for the formation of the second network and serves as a matrix.[108]

The parameters influencing the reaction kinetics during the individual single network formation also influence the kinetics of IPNs formation. Networks in both cases are mostly synthesized by free-radical polymerization consisting of initiation, propagation and termination steps. The relative rates of each step determine the overall rate of polymerization. Moreover, for crosslinked networks, these relative rates determine the final structure of the material and its properties.[109] The polymerization is usually initiated by irradiation, temperature, or redox systems. The type of initiator, crosslinker and solvent may also affect the rate of polymerization as well as gelation time. Before considering the features of polymerization kinetics in IPNs, it is important to summarize the general factors affecting the kinetics of single networks formation. Therefore, the kinetics of PHEMA-based single networks formation will be considered below.

4.1. Formation of an individual single network

4.1.1. *Bulk polymerization of 2-hydroxyethyl methacrylate*

Bulk polymerization process of 2-hydroxyethyl methacrylate (HEMA) and similar monomers can be roughly divided into three regions:[110] (1) the polymerization region without diffusional control, (2) the autoacceleration region (Trommsdorff effect) with diffusion-controlled termination but not controlled propagation, and (3) the autodeceleration region with reaction-controlled termination and propagation.

Crosslinking photopolymerization of 2-hydroxyethyl methacrylate and di(ethylene glycol) dimethacrylate (HEMA/DEGDMA) system reveals similar

regions (Figure 8): initial rise of the polymerization rate followed with diffusion limited termination (autoacceleration) and diffusion limited propagation (autodeceleration).[111] At the very beginning of the reaction, when propagation and termination are not diffusion controlled, the rate of polymerization is almost constant. The conversion of monomer to polymer during the polymerization is usually accompanied by an increase in viscosity, which in turn leads to a decrease in translational and segmental diffusion of the polymer. Once the termination by recombination or disproportionation becomes limited by diffusion, the concentration of living radicals increases greatly and the propagation due to the mobile unreacted double bonds continues. Such situation results in autoacceleration process with great increase of the polymerization rate. With further domination of the reaction-controlled termination mechanism over the propagation mechanism, the reaction starts to autodecelerate.
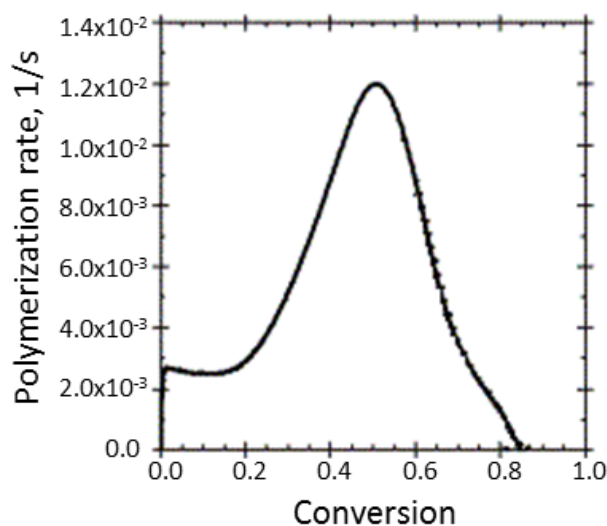
Figure 8. Polymerization rate of HEMA/DEGDMA (99/1 wt%) system vs. conversion. Photopolymerization in the presence of Irgacure 651 initiator at $I = 4.8$ mW/cm^2 and $T = 25$ °C.[111]

Incomplete conversion of functional groups in crosslinked systems is often caused by vitrification effects occurring during the bulk polymerization. The mobility of reactive species can be enhanced by polymerization at temperatures above the temperature of vitrification. For instance, Huang[112] et al. reported that during the thermally initiated crosslinking bulk polymerization of 2-hydroxyethyl methacrylate and ethylene glycol dimethacrylate (HEMA/EGDMA) system the conversion of C=C double bonds is complete at curing temperature above 90 °C. The

intensity of UV light is another parameter that can provide for high conversions. Bowman and co-workers[111] reported that the increase of UV light intensity from 0.5 mW/cm^2 to 13 mW/cm^2 increases the conversion in HEMA/DEGDMA (99/1 wt.-%) system from 86 % to 92 %. Moreover, an increase of UV light intensity and hence, initiation rate, causes an increase in polymerization rate. High initiation rate increases the concentration of short radicals and makes the termination easier.

The crosslinker concentration also influences the rate of polymerization and the conversion. The polymerization is faster at higher concentration of crosslinker, however when the system becomes sufficiently crosslinked, the diffusion limitation of the propagation results in a decrease of the rate. The conversion of vinyl groups as well as the polymerization rate increases as the weight ratio of EGDMA crosslinker increases in EGDMA/HEMA system.[112] If one compares the effect of functionality of crosslinking monomers, then the trivinyl copolymerization (trimethylolpropane trimethacylate, TMPTMA) reacts more rapidly than the divinyl copolymerization (diethylene glycol dimethacrylate, DEGDMA) because the increased crosslinking results in considerable autoacceleration.[113]

4.1.2. Polymerization of 2-hydroxyethyl methacrylate in solution

Formation of polymer network in the presence of a solvent shifts the glass transition temperature of network to lower values and prevents the vitrification of the system upon crosslinking polymerization. The resulting material after the polymerization in solution is elastic, while the one prepared without solvent is glassy.

Free radical polymerization of multifunctional monomers forms heterogeneous network structures due to the intramolecular cyclization (primary or secondary).[114,115,116] Crosslinking and formation of cycles are competitive processes. The rates of these two processes are controlled by the concentration of radicals in the bulk solution and the effective concentration of radicals on the same propagating chain as the pendant double bond.[116] The size of crosslinking agent molecule affects the rate of cyclization: smaller the crosslinking molecules, higher the rate of formation of primary cycles.[117] Cyclization causes the formation of more loosely crosslinked network. It has been observed that the polymerization in the presence of solvent increases the rate of primary cyclization and ends up with less crosslinked network of larger mesh size (distance between crosslinks).[117,118] Dilution of

monomers decreases the consumption of monomeric double bonds and the rate of pendant crosslinking, and hence, decreases the propagation rate. Increase of solvent concentration increases the probability of cyclization rather than intermolecular crosslinking. When the solvent content is low, the concentration of double bonds surrounding the radical is relatively high, which leads to a faster rate of propagation and less opportunity for the radical to cycle by reacting with its own pendant double bond (Figure 9a). When the solvent content is high, the concentration of double bonds is low as well as the rate of propagation; the probability of cyclization is increased (Figure 9b).

Low solvent concentration (a)   *High solvent concentration (b)*

More likely to crosslink   *More likely to cycle*
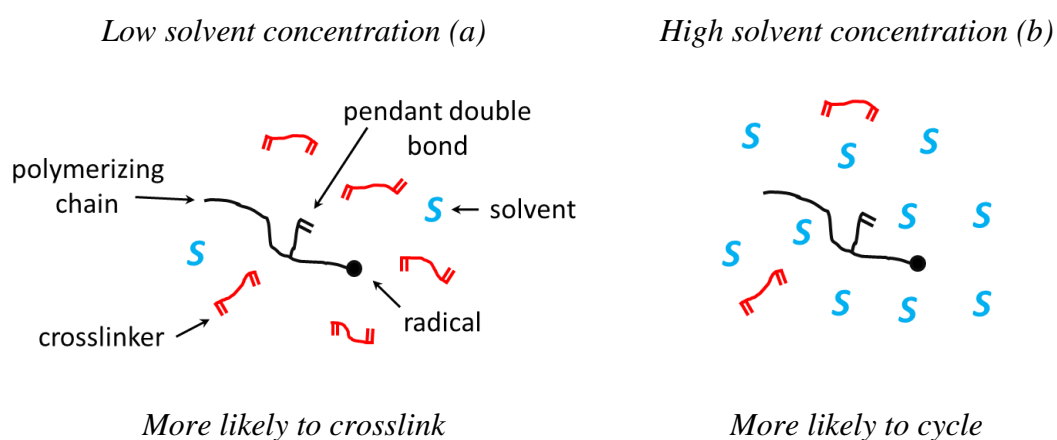
Figure 9. Solvent concentration effect on cyclization.[117]

The quality of solvent is also crucial and affects the parameters such as: diffusion of polymer chains, intermolecular termination rate, primary chain length, viscosity, gel point, reactivity ratios, and extent of primary and secondary cyclization.[119,120,121,122] If the interaction between polymer and solvent is good, the radical on the growing polymer chain prefers to move away from the pendant double bond, and the probability to form a cycle is reduced (Figure 10a). Whereas the poor interaction between the polymer and solvent causes the coiling of growing polymer chain, and the probability to form a primary cycle is high due to the increased proximity of the pendant double bond (Figure 10b).

Better solvent (a)   *Poor solvent (b)*

Less likely to cycle   *More likely to cycle*
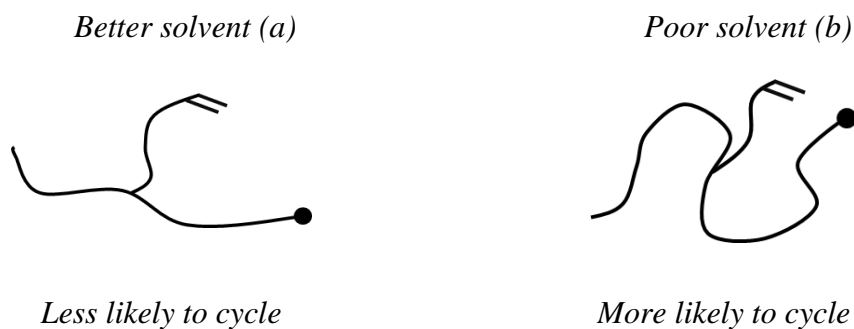
Figure 10. Conformation of propagating chain in good and poor solvent.[118]

The effect of water content at network preparation (0 – 60 wt.-%) and the UV intensity (0.25 – 40 mW/cm^2) during the photopolymerization on the polymerization rate and gelation of HEMA/DEGDMA hydrogel was studied by Li[123] et al. The increase of the UV intensity enhanced the polymerization rate. However, too high intensity of UV had an opposite effect on the rate of polymerization. Dilution at preparation reduced the concentration of reactants, hence slowing down the reaction rate. The crosslinking polymerization of multifunctional HEMA/DEGDMA monomers leads to the formation of pendant double bonds on the growing radicals, which can react with propagating radicals through either intra- or intermolecular reactions. Intramolecular reactions result in cyclization leading to microgels formation, while intermolecular reactions contribute to the formation of network. Usually at certain period of time the microgels and network coexist in one crosslinking system. The relative rates between these two processes are controlled by the composition of the monomers mixture, solvent content and light intensity. The gelation of HEMA/DEGDMA was significantly delayed with the more dilution of the reaction mixture and irradiation of the reaction mixture with UV of too high intensity. The reason is that the dilution of the reaction mixture increases the distance between radicals, hence making the intramolecular reactions more preferable. Whereas too high UV intensity causes rapid initiation of the reaction, formation of more radicals and pendant double bonds in the system leading to the domination of the cyclization over the formation of the infinite network.

4.2. Formation of IPNs

4.2.1. Special features of polymerization of the second monomer in the presence of the first network

The kinetics of IPNs formation is affected by the presence of the pre-formed first network. First of all, the presence of the preliminary formed networks causes the total change in the viscosity of the reaction medium. An increase of viscosity accelerates the reaction due to the limitation of termination because it is diffusion controlled. Second, the various groups of growing polymer chains of both networks may physically interact.[108] When networks are synthesized simultaneously, one of the forming networks may act as a solvent for another network. So, the latter being incorporated into the IPN structure may result in higher conversion of functional groups compared to conversion achieved during its polymerization alone ("solvent effect").[124] Immiscibility of polymers often causes the phase separation in IPNs, which can be controlled by the kinetics of IPNs formation. Complete miscibility of polymers is not always needed, as physical entanglements can effectively prevent the phase separation. The extent of phase separation can be arranged as domains of micrometer-size (incompatible), of nanometer-size (intermediate) and of no resolvable domain structure (completely compatible).[124] It was found, that more homogeneous simultaneous IPNs can be formed, when: (1) the rates of polymerization and crosslinking are fast, and (2) processes of both networks formation are as simultaneous as possible.[125] At high reaction rates, there is no enough time for diffusion of monomers and subsequent phase separation. After the complete crosslinking, the phase separation cannot occur due to topological constraints. Phase separation in IPNs begins typically at very low conversions, where the rheological changes govern the kinetics of polymerization, propagates with increase of conversion and does not influence the kinetics.[126,127]

4.2.2. Gelation of IPNs

As the polymerization and crosslinking reactions proceed, the molecular weight of the macromolecules increases leading to formation of linear and/or branched chains and eventually to formation of first infinite network, which become bonded together irreversibly in the form of a network. The macroscopic viscosity and the molecular weight of the forming network grow to infinity. Such transition from soluble system into a partially insoluble one passes through the point called ***gel***

point.[128,129,130] At gel point (critical conversion), the first infinite structure containing the elastically active network chains (EANCs) is formed. Only crosslinking reaction implying the consumption of pendant vinyl groups by other macroradical is responsible for gelation, while the cyclization do not change the degree of polymerization of the macroradicals.[115]

Gel point determination: there are several methods for gel point determination. The solubility test implies the visual examination of solution, containing the solvent and certain portion of reaction mixture, under mechanical agitation in given time.[131,132] The gel point is the first time, at which insoluble fraction is registered. The crossover of storage modulus (G') and loss modulus (G'') is the empirical criterion of the gel point.[133] According to the Winter-Chambon criterion, the gel point is reached when the loss factor (tan δ) becomes frequency independent.[134]

There are not many reports on monitoring the *in-situ* gelation of IPNs. Among existing, mostly the formation of semi-IPN hydrogels[135,136,137] and simultaneous IPN hydrogels[138,139] was studied, whereas the reports on gelation of the second network in the matrix of the pre-formed first network are missing. The formation of PHEMA/chitosan semi-IPN was studied in terms of effect of the molecular weight of chitosan and the length of the crosslinker on the gel point.[135] The gelation time in this report was determined by measuring the time at which the dynamic storage modulus (G') starts to be higher than the dynamic loss modulus (G''). Faster gelation of HEMA was observed in the medium of higher molecular weight chitosan dissolved in 1 % acetic acid. The latter had a high viscosity caused the autoacceleration of the crosslinking polymerization due to the diffusion-controlled termination. The length of a crosslinker was the other parameter affecting the gel point. The gelation of PHEMA/chitosan semi-IPN crosslinked with ethylene glycol dimethacrylate (EGDMA) was faster than that of semi-IPN crosslinked with poly(ethylene glycol) diacrylate (PEGDA). In viscous medium of chitosan solution, the gelation time is determined by the mobility of monomer molecules. The shorter EGDMA crosslinker is more mobile compared to the PEGDMA crosslinker, and therefore resulted in faster gelation. Jandt[136] and co-workers followed the gelation of PNIPAM in the presence of linear PVA as diluent by rheometer. The gel point was achieved very quickly and both moduli reached the plateau region within 12.5 minutes. Neither the concentration nor the molecular weight of the PVA polymer

affected the gelation time. Whereas the increase of the PVA concentration caused the delay in gelation of the PAA network when forming PAA/PVA semi-IPN hydrogel.[137] Interpenetrating network hydrogels composed of oxidized dextran and thiolated chitosan were formed simultaneously without any small molecule crosslinker.[138] The interpenetrating network structure was created by disulfide bonds and Schiff base formations, respectively. It was found that the IPN hydrogel is crosslinking first via Schiff base formation and then by disulfide bonding. The gelation of IPN was much faster than the self-gelation of thiolated chitosan (60s vs. 1300s). Fibrinogen/alginate simultaneous IPN crosslinked with thrombin/Ca^{2+} demonstrated rapid gelation.[139] The gelation slowed down with the decrease of crosslinker concentration.

4.2.3. Methods for monitoring the kinetics of IPNs formation

Here, the common methods used for monitoring the kinetics of polymerization and network formation are briefly listed. The <u>Fourier transform infrared spectroscopy</u> (FTIR) allows monitoring the conversion of functional groups with time. The polymerization rate can be determined from evolution of heat during the polymerization reaction monitored by the <u>differential scanning calorimeter</u> (DSC). Gravimetric method of determining a <u>sol-gel fraction</u> gives information on conversion of functional groups. Choosing an appropriate method for sol extraction is very important in terms of correct quantitative determination of sol fraction. <u>Dilatometry</u> can be used as an indirect way of following the kinetics of network formation via volume changes of sample during the polymerization. This technique needs the preliminary calibration using one of the mentioned above methods or other in order to relate the volume of sample at a certain time to a proper conversion. The gelation of polymer network can be followed by <u>chemorheological measurement</u> of dynamic storage (G') and loss (G'') moduli, and loss factor (tan δ) or by <u>dielectric spectroscopy</u> assessing the dielectric constant (ε'), dielectric loss (ε''), and electrical constant (M') and loss moduli (M'').

5. Microstructure of IPN hydrogels

5.1. Phase separation in IPN formation

Phase separation phenomenon is common in IPNs and depends on the degree of polymer miscibility.[124,140] When highly incompatible polymers are used for IPNs synthesis, phase separation may not be prevented due to thermodynamic reasons leading to phase separation before the crosslinking can hinder it, while phase separation can be completely avoided when polymers are miscible. However, complete miscibility is not always a crucial factor to achieve complete phase mixing, since the permanent crosslinks can prevent the phase separation. The extent of phase separation in IPNs depends on factors such as concentration of each polymer component, crosslinking density, ratio between components.[141] Moreover, the phase separation occurs not only in hetero-IPNs, but also in homo-IPNs.[4,142,143,144,145] To understand the mechanisms of phase separation in IPNs, it is important to analyze the general principles of phase separation of the reaction mixture during the network formation described by Dušek.[146] A general condition for phase separation was formulated as the equality between the maximum swelling of the network in equilibrium with the diluent or diluent-monomer mixture $(1 - \varphi_2)$ and the instantaneous dilution of the network $(1 - \varphi_2^0)$, i.e., $\varphi_2 = \varphi_2^0$, where φ_2 is a volume fraction of polymer in the gel swollen to equilibrium and φ_2^0 is a volume fraction of all polymerizable substances at preparation. Phase separation occurs due to deterioration of solvent power (χ-syneresis) or increase in crosslink density (ν-syneresis). The χ-syneresis (micro- and/or macrosyneresis, often combined with ν-syneresis) in the crosslinking system[147,148] causes formation of gels phase-separated into microsized domains and leads to generation of discontinuous or continuous pores of the size of the order of 10^0-10^2 μm, the topology of pores being governed by the system composition including volume network/diluent ratio; the shape and pore distribution can be affected by surface active agents.[149] When considering IPNs, we have similar "network-diluent" system, when the network 2 is formed in the matrix of the pre-formed network 1, which acts as a diluent for the network 2 and at certain concentration also can cause phase separation of networks.

The microstructure of IPNs depends on the mechanism of phase separation, which can be either nucleation and growth or spinodal decomposition. Phase separation in simultaneous IPNs occurs due to the spinodal mechanism, while in

sequential IPNs – due to the nucleation and growth mechanism.[108] The mechanism of nucleation and growth was proposed by Sperling[150,151,152] et al. and schematically represented in Figure 11. Three main states of networks during the domain formation can be considered: state 1 – single polymer network 1, state 2 – polymer network 2 swollen in the reaction mixture of the monomer 2 including crosslinker, and state 3 – almost simultaneous formation and separation of network 2 into spherical domain surrounded by shell of network 1. The crosslink density in network 1 as well as the concentration ratios between two networks affect the size and the shape of domains of network 2.[153] Although the model is simplified, it allows to predict the size of domains. It was shown, that the experimental and theoretical domain sizes for full- and semi- poly(n-butyl acrylate)/polystyrene IPNs were in a good agreement.

a   *b*   *c*
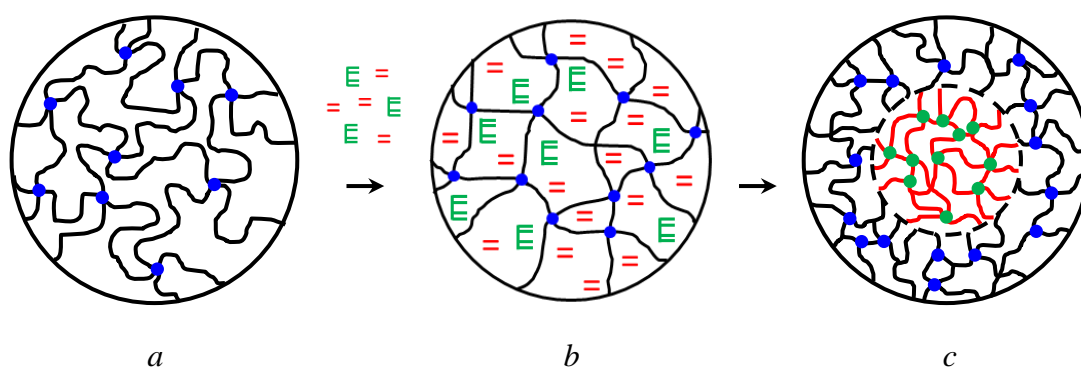
Figure 11. Phase separation in IPNs:[152] (a) network 1 and monomer 2, (b) network 1 swollen in monomer 2, (c) domain of network 2 (core) surrounded by network 1 (shell).

Another model based on the application of Flory-Huggins equation and describing the nucleation and growth rate in epoxy resin-rubber system allowed to predict the fraction, composition, average radius of domains as well as distribution of domain dimensions.[154,155] It was shown, that the structure of rubber-modified thermosets depended on the relation between the location of the reaction extent (p_c) at which phase separation occurred and gel conversion (p_{gel}). If $p_c \approx p_{gel}$, the low diffusion coefficient will prevent significant phase separation. If $p_c << p_{gel}$, the low density rubbery phase in a medium of low viscosity will lead to macroscopic phase separation.

The theory of spinodal decomposition was developed by Cahn and Hillard in 1958.[156] Concerning the phase separation in IPNs caused by spinodal decomposition, one can say that this mechanism involves the spontaneous formation and continuous

growth of one phase in the unstable "mother" phase. The decomposition occurs with fluctuations of small amplitude leading to the continuous growth of the second phase. Phase separation may start already at the very beginning of the reaction, when the conversion is very low. The high viscosity of the reaction mixture and the diffusion limitations may cause the incompleteness of the phase separation process with the formation of interfacial region separating the phase regions in the IPNs.[157] Therefore, the final structure of the phase separated two network IPNs consists of three different regions. The kinetics of IPNs formation affects the degree of phase separation and the fraction of the interfacial region, which depends on: the rate of reaching the critical molecular weight when networks become incompatible, the molecular weight of both components at the phase separation, the degree of conversion at which phase separation begins, reaction rates of the formation of both components, and the ratio of components in the initial reaction mixture.[157]

5.2. Non-porous and porous IPN hydrogels

The investigation of microstructures of polymer network hydrogels is crucial as it can be a way to improve their mechanical properties. Combination of two networks into one IPN structure gives even more options to control the morphology of hydrogels, for example, by changing the preparation conditions.[21,94,158] There are several factors influencing the microstructure of final IPN hydrogels. The first factor is the type of IPNs synthesis: simultaneous or sequential. To obtain a non-porous simultaneous IPN hydrogel, the networks must be miscible and should be formed with similar rates not to cause the phase separation; otherwise the resulting IPN hydrogel may have pores of micro- (< 2 nm), meso- ($2 - 50$ nm) or macrosize (> 50 nm)[1] or possess domains. The microstructure of sequential IPN hydrogels depends on the morphology of the first network and on the technique used for synthesis of the second network. The formation of the second network (Network 2) without diluent in the matrix of the pre-formed non-porous first network (Network 1) generally results in non-porous IPN hydrogel. However, the resulting material is typically heterogeneous due to special density fluctuations. If the first network is porous, then two scenarios are possible: (1) uniform distribution of the second network in the matrix of the first polymer network and in the pores, and (2) formation of pores during the second network formation. The latter can be achieved by several techniques such as gelation under cryo-conditions,[21,159] reaction induced phase

separation (macro- and microsyneresis), extraction of monomers of the second network from pores of the first network prior to crosslinking polymerization, etc.

Certain treatment of final IPN hydrogels may also change the morphology of the material. For instance, transformation of porous IPN hydrogels during the drying-reswelling processes is not always reversible. Drying at elevated temperature above T_g under the vacuum may cause the collapse of pores, so that further reswelling in a solvent will not result in hydrogel of the same morphology as before drying. In this sense, drying of porous IPN hydrogels by lyophilization is safer. However, lyophilization conditions involve rapid cooling and it may distort the initial morphology. For milder drying of hydrogels one can use the solvent exchange technique, when the initial solvent is gradually replaced with another more volatile solvent, which then can be easily removed from the gel without irreversible change of morphology.

5.3. Methods for hydrogel morphology characterization

Utilization of the most of hydrogels is concerned with their swelling ability. Therefore, it is very important to study the morphology of hydrogels in their native swollen state. To date, there are several available techniques for studying the morphology in wet state. And the selection of the proper one is important, since the observation conditions as well as sample preparation may create some issues in data interpretation by distorting the real morphology of materials.[160,161,162,163] The most common techniques to observe swollen gels are light microscopy (LM), laser scanning confocal microscopy (LSCM), atomic-force microscopy (AFM), environmental scanning electron microscopy (ESEM). Cryo-SEM is also used for studying the swollen gels but in preliminary frozen state. Freezing of swollen hydrogels is challenging since it should be as quick as possible to prevent the formation of ice crystals destructing the sample and causing the morphology distortions. Scanning electron microscopy (SEM) is used for dry samples only and requires the specimen to be electrically conductive. Therefore, the sample preparation involves preliminary drying and coating of non-conductive dry hydrogel with an ultrathin conducting material deposited on the sample by low-vacuum sputtering or high-vacuum evaporation. Such treatment prevents the charging of non-conductive hydrogel by electron beam and hence, occurrence of artifacts, and provides significantly better resolution. Dehydration of samples should be very

careful and a proper method of drying is recommended to be selected according to the sample properties. Dehydration of porous hydrogels at elevated temperature under the vacuum is risky due to the possible collapse of pores, whereas the lyophilization of highly swollen non-porous hydrogels or hydrogels of small pores size (micro-, meso-) is risky due to the wrong observation of porous structure with overestimated size of pores or observation of porous structure instead of non-porous one. Advantages and disadvantages of microscopy techniques for hydrogels morphology observation are shown in Table 2.

Table 2. General advantages and disadvantages of microscopy techniques used for hydrogels morphology observation.

Observation technique	State of sample	Advantages of technique	Disadvantages of technique
LM	wet	• examination of hydrated sample; • quick and simple sample preparation; • non-destructive for sample; • unaffected by magnetic fields; • observation of colored samples;	• low resolution ($\approx$ 200 nm); • limited magnification ($\approx 10^3$); • restriction in depth of field;
LSCM	wet	• examination of hydrated sample; • non-destructive for hydrogel; • high contrast due to fluorescent dyes; • Z-axis scanning; • reconstruction of 3D image;	• sample preparation requires staining; • staining may introduce artifacts; • moderate resolution (XY: 100 – 200 nm, Z: 300 – 400 nm);
ESEM	wet	• examination of hydrated sample; • quick and simple sample preparation; • non-destructive for sample;	• requires finding a proper pressure at which a droplet of water fixing the sample disappears, while the sample structure appears; • lower resolution ($\approx$ 2 nm) compared to SEM;
Cryo-SEM	wet (frozen)	• observation of swollen sample morphology in frozen state; • relatively quick sample preparation; • high resolution ($\approx$ 1 nm);	• improper sample freezing introduces artifacts;
SEM	dry	• high resolution ($\approx$ 1 nm); • high magnification ($\approx 10^5$);	• complex and time consuming sample preparation; • examination of dry sample; • drying introduces artifacts;
AFM	wet	• examination of hydrated sample; • quick and simple sample preparation; • high resolution ($\approx$ 0.1 nm); • high magnification ($\approx 10^6$);	• information on the topography of the surface only;

The pore size distribution and the total pore volume (porosity) of dry hydrogels can be estimated by mercury porosimetry.[164] Major limitations of the

method are connected with the inability of the intruding mercury to pass through the closed and blind pores (not interconnected with other pores) and the fact that it measures the size of the largest entrance towards a pore, but not the actual inner size of a pore.

The morphology of hydrogels on nanoscale level can be explored by scattering techniques (SWAXS, SANS), which are sensitive to the presence of inhomogeneities in gels including small clusters, nanodomains, or pores in the nanometer range[165]. These techniques are a powerful tool characterizing the morphology of water-swollen hydrogels in their native state and allowing the monitoring of the kinetics of structuring during the network formation. Investigation of the IPN hydrogels structures by SWAXS/SANS methods are reported[166,34,167] and found to be valuable for interpretation of the enhancement of mechanical properties and for proposing the mechanisms of hydrogels strengthening.

6. Swelling of hydrogels

One of the important characteristics of hydrogels is their ability to swell in a thermodynamically good solvent and retain structural integrity due to the chemically or physically crosslinked network structure (Figure 12). During the swelling, hydrogel undergoes a reversible volume change from shrunken to swollen states. In the dry state, gel is usually glassy, while in swollen state it behaves like an elastomer capable to withstand large deformations. The swelling pressure in almost dry gel, which is in contact with water, can reach several hundreds of MPa. The weight and volume changes of hydrogel upon isotropic swelling in water are influenced by the morphology of sample. The values of these parameters are likely equal for non-porous hydrogels, but may be different for porous samples with different distribution of water between the polymer matrix and pores. Besides drying/swelling processes, the coiling state of network chains (shrinkage/swelling) can be controlled by external stimuli such as pH, temperature, ionic strength, light, electric field, etc.

weight and volume
$\rightleftharpoons$
changes

dry network
(xerogel)

swollen network
(hydrogel)
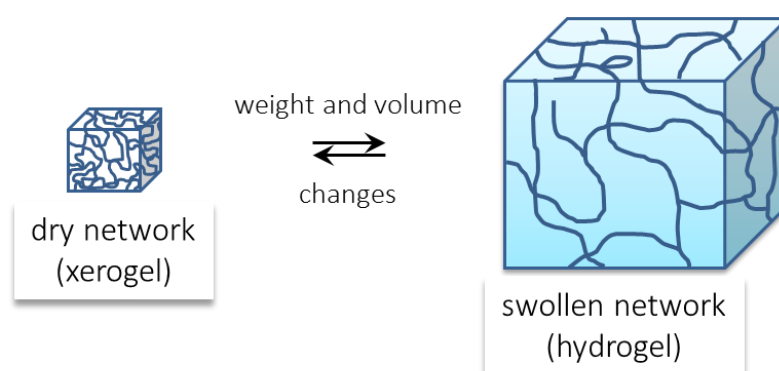
Figure 12. Scheme of polymer network swelling.

Swelling equilibrium implies the equality between osmotic forces and retraction forces of chains, which means, that the chemical potential of the solvent (μ_s) inside and outside the gel is equal. The main factors controlling the swelling degree of polymer networks are the polymer-solvent interaction, the crosslink density, the dilution during the network formation, the presence of charged groups, the finite chain extensibility (non-Gaussian networks), the applied external forces causing (an)isotropic deformation. The competition between the crosslinking and cyclization processes during the network formation affects the final structure of the network and, in turn, diffusion of solvent through the gel and it's swelling properties[117]. At high crosslink density, the overall structure of network is tightly

held together adding the rigidity and high strength to the system, but reducing its swelling ability. At high density of cycles, the overall structure of network is filled with loops, and the backbone polymer chains are loosely crosslinked and able to swell further. The canonical theoretical treatment of swelling phenomena based on Flory and Erman theoretical approach to crosslinked macromolecular systems (for single networks only) is given in this text below – cf. the paragraph 8 of the Theoretical part. For the theoretical treatment of the swelling IPNs – in the case of chemically and microscopically homogeneous systems – we propose our own physical model. It will be worked out in the Part "Results and Discussion" of this text.

Equilibration of network with solvent under no mechanical constraints (free swelling) results in homogeneous and isotropic expansion, when the molecules of water distribute in the gel homogeneously. However, the swelling of polymer network can be affected by external forces or geometrical confinements.[168,169,170] In that case, the deformation of network during the swelling is anisotropic. The constraints may occur upon swelling of crosslinked polymer films adhered to non-swelling substrates, core-shell particles with cores and shells of different swelling capacity, composites with fillers, in which crosslinked matrix has a good or bad adhesion to non-swelling solid particle. The interface region between two differently swelling parts of the system is characterized by gradient stresses and gradient degrees of swelling.[168] The co-existence of two differently swelling networks in IPN system also causes topological constraints imposed by physical entanglements between two networks.

The swelling properties of single network poly(2-hydroxyethyl methacrylate) (PHEMA) hydrogels depending on their morphology were thoroughly studied in many works; for example, here.[171,172] Non-porous PHEMA hydrogels prepared without dilution or at moderate water content (0 – 40 wt.-%) absorb up to 40 % of water, while the swelling degree of porous PHEMA hydrogels is larger and increases with the increase of sample porosity. More hydrophilic poly(glycerol methacrylate) (PGMA) single network can absorb larger amount of water compared to PHEMA network of similar composition due to the presence of two hydroxyl groups in its monomer unit.[173,174,175] For instance, bulk crosslinking polymerization of glycerol methacrylate (GMA) and 0.03 wt.-% of tetraethylene glycol dimethacrylate monomers resulted in hydrogel with equilibrium swelling degree of 63 % (in

water)[173]. Dilution of GMA monomer with water at preparation (from 35 % to 93 %) led to formation of hydrogels with swelling degrees changing from 75 % to 98 %, respectively.[173] The hydrogels obtained by copolymerization of both monomers into one network structure revealed the swelling degrees that are higher than that of pure PHEMA network, but lower than that of pure PGMA network.[176] The combination of PHEMA and PGMA networks into the IPN structure was never reported.

6.1. Swelling of IPN hydrogels

The moderate swelling capacity of hydrophilic PHEMA single network can be improved by incorporation of more hydrophilic second network or linear polymer to form the full- or semi-IPN hydrogel, respectively.[100,101,102,103] The hydrophilic linear polymer incorporated into the PHEMA network improves the swelling of the IPN better than the hydrophilic second network. Indeed, depending on composition of the IPN hydrogel, the combination of PHEMA network with linear poly(ethylene glycol) (PEG)[100] increased the IPNs swelling up to 83 %; with poly(N-vinylpyrrolidone) (PVP)[101] network – up to 72 %, with linear poly(N-vinylpyrrolidone) (PVP)[102] – up to 87 %, with linear poly(vinyl alcohol) (PVA)[103] – up to 83 %, and with poly(vinyl alcohol) (PVA)[103] network – up to 76 %. For single network hydrogels or copolymers, the improvement of swelling properties usually means lowering of mechanical properties. However, for IPN systems it is not necessarily so. Due to the entanglements between the networks chains, one can obtain IPN gels with excellent mechanical properties without compromising the swelling properties[25] or at least with insignificant decrease of swelling capacity.[177]

Since both networks take part in solvent uptake, the swelling capacity of the final IPN depends on the coiling states of networks chains, which can differ depending on the way of IPNs preparation. The chains of both networks in simultaneous IPN hydrogels are in state-of-ease (relaxed state) after the polymerization. The formation of sequential IPNs implies the formation of the second network in the presence of the first network. This means that after the polymerization, the first network is already stretched due to the swelling in the reaction mixture of the second monomer, while the chains of the second network are in relaxed state. The extent of the first network stretching depends on the nature of the second network monomer, i.e., on the capacity of the first network to absorb the second monomer.

7. Deformation behavior of swollen hydrogels

Swollen hydrogels behave like elastic or viscoelastic materials.[178] The elastic behavior of swollen hydrogels to external stresses involves a high extensibility and nearly instantaneous and complete recovery after removal of the applied load. If the complete recovery after removal of the load is slow, the behavior is called viscoelastic. The time-dependent recovery is caused by the movement of the segments of the polymer chains.

The viscoelastic behavior of hydrogels originates from two basic models characterizing the behavior of ideal elastic solid body (Hooke's law) and ideal viscous liquid (Newton's law). There are two basic classical models mathematically describing the viscoelastic behavior of hydrogels: Maxwell model describing the stress relaxation process when the system is subjected to a constant strain and Kelvin-Voigt model describing the creep behavior when the strain is changing with time at a constant stress.

Compared to creep and relaxation experiments, the oscillating mode is more versatile and covers a wide range of conditions.[179,180] Dynamic mechanical analysis in the form of oscillations provides quantitative information on the viscoelastic and rheological properties of materials measured under periodic stress or strain. In case of a non-destructive oscillation technique, a sinusoidal oscillating stress wave is applied to a material and the resulting strain wave is measured (Figure 13). For a purely elastic solid, the stress is in phase with the strain (phase angle is $\delta = 0°$). For a purely viscous liquid, the stress is 90° out of phase. For a viscoelastic material, the phase angle is in between ($0° < \delta < 90°$).
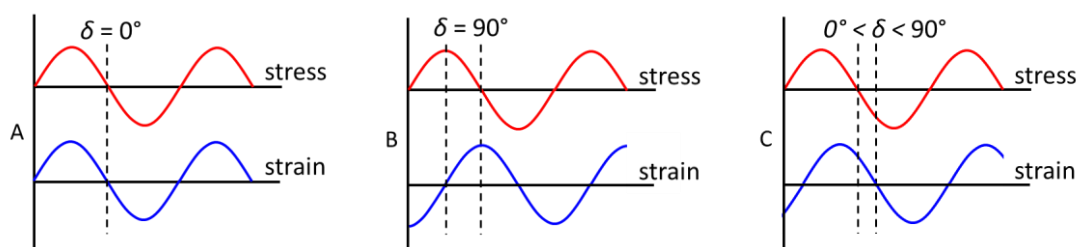
Figure 13. Dynamic oscillation test representing the stress-strain relationship of purely elastic (a), purely viscous (b) and viscoelastic (c) materials.

The overall resistance of a material to deformation is assessed by the complex modulus (G^*), which is resolved into two components – storage modulus (G') and loss modulus (G'') – representing the elastic and viscous components of material behavior:

$$G^* = G' + iG'' = \frac{\sigma^*}{\varepsilon^*}$$

(Equation 1.1)

The tangent of the phase angle (δ) – the loss factor (tan δ) – shows the ratio of energy lost to energy stored during the oscillatory deformation and is defined as:

$$\tan\delta = \frac{G''}{G'}$$

(Equation 1.2)

The response of the material to loading can be characterized by several parameters, among which are Young's modulus (E), describing the linear part of strain response only to uniaxial stress, and equilibrium shear modulus (G), describing the response to shear stress. For isotropic materials these moduli are related as:

$$E = 2G(1 + v)$$

(Equation 1.3)

where v is a Poisson's ratio ranging in $-1 < v < 0.5$.

One of the important characteristics of materials is their resistance to rupture.[180] There are two main responses of the material to the load: it can break immediately or undergo plastic deformation (Figure 14). In the first case, the brittle failure occurs at a very low strain. If before failure the sample undergoes the plastic deformation, then the behavior is called ductile failure with yield. The necking means the abrupt reduction of the cross section, in which the polymer molecules become reoriented and the material continues to extend (cold drawing). A new orientation of molecules results in a stiffer material (strain-hardening phenomenon).
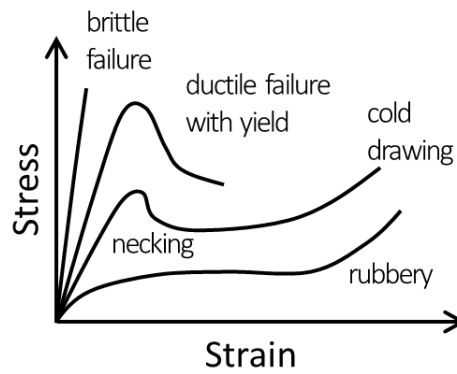
Figure 14. Stress-strain range for materials of various fracture and yield.[180]

7.1. Accuracy and precision of mechanical measurements

Among the applied deformation modes of the hydrogels, the most common are: uniaxial elongation and compression, and the deformation in shear. Each type of deformation test has its own shortcoming. First of all, the examination of hydrogels should be carried out in swollen state, i.e., the sample is immersed into the solvent (water) to prevent the evaporation of latter. Uniaxial elongation implies the application of a tensile force to the material held between two grips. The sample and the grips should be correctly aligned as any off-center loading will exert bending loads on the sample.[181] The contact between the sample and the grips should be strong enough to prevent the sample release during the elongation and, on the other hand, there should be no slippage between them to prevent the deformation by grip pressure contributing to an error. The main disadvantage of compression test is the bulging of hydrogel under compression and difficulty in uniform application of pressure.[182] To overcome this issue, the hydrogel could be confined around its outer edge, but such manipulations change the nature of the measurement.

Deformation of hydrogels in shear involves several important parameters influencing the results of measurement. For a good contact between the sample and plates, the hydrogel specimen should be parallel providing uniform contact with upper and lower plates through the entire area of both surfaces, and the surface roughness issues should be overcome. The procedure of finding a correct gap between rheometer plates implies finding such compressive stress, at which the dewatering and structure changing as well as the slippage are avoided.[172]

7.2. Deformation behavior of swollen IPN hydrogels

Single network hydrogels have often poor mechanical properties due to the high content of water and randomly crosslinked network structure, the chains of which reveal a low resistance to breakage and crack propagation due to an insufficient energy dissipation mechanism. In general, the failure of material can be considered as two sequential processes of the initial fracture formation (nucleation) and the following fracture propagation (growth).[25] Designing a material with superior mechanical properties means diminishing the number of factors causing initial fracture deformation. The concept of multicomponent interpenetrating polymer networks (IPNs) has been introduced to mixing immiscible polymers very often leading to improve of intrinsic mechanical properties of hydrogels. The mechanical properties of single network hydrogels are governed by the parameters such as the polymer structure, the number of elastically active network chains, the effective molecular weight between crosslinks, and the ratio between cyclization and crosslinking.[178] Basically, the same parameters are valid for IPNs There are examples when the combination of two weak networks results in IPN material with good mechanical properties.[8,31,183] For those specific cases, several main parameters affecting the structure and, hence, the mechanical properties of IPN hydrogels were distinguished: the nature of networks (polyelectrolytes or neutral networks), the molar ratio between the first and the second network monomers, the concentration of a crosslinker in both networks, and the molecular weight of polymer chains between crosslinks in the second network.[25,184] The correct proportion between the components contributes to hydrogels with enhanced mechanical properties.

The PHEMA-based IPN hydrogels are usually made for diverse purposes. In some cases,[98,99,104,105,135] additionally to the main purpose of the research work the enhancement of mechanical properties was achieved. For instance, the Young's modulus of swollen full-IPN hydrogel, in which the gelatin network was incorporated into the porous PHEMA network, was 80 kPa.[104] This was higher than the Young's moduli of constituent networks: 56 kPa for porous PHEMA prepared at 70 wt.-% of dilution and 46 kPa for glutaraldehyde-crosslinked gelatin.[104] Or, another example, when chitosan was incorporated into non-porous poly(2-hydroxyethyl methacrylate-*co*-sodium methacrylate) network prepared at 30 wt.-% of water resulting in semi-IPN hydrogel with the Young's modulus of 235 kPa compared to the PHEMA single network prepared at 30 wt.-% of water with the

Young's modulus of 114 kPa.[135] Opposite effect of worsening of the mechanical properties of PHEMA network when interpenetrated with the second network was also observed.[81,185] Despite of that, the materials were still suitable for biomedical application. For instance, the tensile strengths and Young's moduli of collagen-immobilized PEG/PHEMA[81] or methacrylated gelatin/PHEMA[68] IPN hydrogels were slightly lower than that of constituent networks, but they were still greater than that of the human cornea.[72,73] Eventually, there are only a few reports addressing the problem of improving the mechanical properties of PHEMA-based IPN hydrogels. And even less number of reports proposing the mechanisms of strengthening or toughening.

8. Theoretical background of swelling and elasticity of single network hydrogels

The free swelling of polymer network implies the mixing of separate phases of the polymer chains of network and the solvent inducing the deformation of elastically active network chains (EANC). The change of the Gibbs energy on equilibrium swelling considered to be an additive function of mixing and elasticity:[186]

$$\Delta G_{sw} = \Delta G_{mix} + \Delta G_{el}$$

(Equation 1.4)

The Flory-Huggins formulation modified by Koningsveld and Staverman[187] gives for mixing of an infinite uncrosslinked molecule:

$$\Delta G_{mix} = kT(N_1 \ln \phi_1 + g(\phi_2)N_1\phi_2)$$

(Equation 1.5)

where N_1 is number of solvent molecules, ϕ_1 and ϕ_2 are volume fractions of solvent and polymer, respectively, $g(\phi_2)$ is the concentration dependent interaction function. For concentration independent $g(\phi_2)N_1 = \chi$, the mixing contribution to the chemical potential of solvent is obtained as:

$$\frac{\Delta\mu_{1,mix}}{RT} = \frac{1}{RT}\left[\frac{\partial\Delta G_{mix}}{\partial N_1}\right]_{p,T} = \frac{\Delta\mu_{1,mix,n}}{RT} = \ln\phi_1 + \phi_2 + \chi\phi_2^2$$

(Equation 1.6)

For the elastic contribution ΔG_{el} which includes effect of chains crosslinking on the entropy change one gets:

$$\frac{\Delta G_{el}}{kT} \approx \frac{\Delta F_{el}}{kT} = \frac{AN_e}{2}\left(\lambda_x^2 + \lambda_y^2 + \lambda_z^2 - 3\right) - BN_e \ln\left(\frac{V}{V_0}\right)$$

(Equation 1.7)

where λ_x, λ_y, λ_z are deformation ratios relative to the reference state, N_e is the number of elastically active network chains, V/V_0 is the swollen volume relative to the reference volume λ_x, λ_y, $\lambda_z = V/V_0$, A and B are front factors in the Flory-Erman junction fluctuation theory; $A = (f_e - 2)/f_e$, $B = 0$ for phantom network, and $A = 1$, $B = 2/f_e$ for affine network.

For free swelling, $\lambda = \lambda_x = \lambda_y = \lambda_z$ and $V/V_0 = \lambda^3$.

So, that:

$$\frac{\Delta G_{el}}{kT} = \frac{AN_e}{2}(3\lambda^2 - 3) - BN_e \ln \lambda^3$$

(Equation 1.8)

by passing from N_e to the concentration ν_e and from the elastic contribution to the volume fractions $V/V_0 = \lambda^3 = \phi_2^0/\phi_2$ (ϕ_2^0 being the volume fraction of network at state of network formation) assuming the network chains are in the reference state at the network formation conditions, the solvent chemical potential is obtained in the form:

$$\frac{\Delta \mu_{1,el}}{kT} = \left[\frac{\partial(\Delta G_{el}/kT)}{\partial N_1} \right]_{p,T} = \frac{\partial(\Delta F_{el}/kT)}{\partial \lambda} \frac{\partial \lambda}{\partial N_1}$$
$$= AV_{1m}\nu_e(\phi_2^0)^{2/3}\phi_2^{1/3} - BV_{1m}\nu_e\phi_2^{1/3}$$

(Equation 1.9)

where V_{1m} is the molar volume of the solvent, if one lattice site is occupied by one solvent molecule.

At equilibrium swelling, the chemical potentials of solvent in each of the phases should be equal. Since the gel is in equilibrium with pure solvent, the chemical potential of which is by definition equal to zero, the following condition holds:

$$\ln \phi_1 + \phi_2 + \chi\phi_2^2 + V_{1m}\nu_e\left(A(\phi_2^0)^{2/3}\phi_2^{1/3} - B\phi_2^{1/3}\right)$$

(Equation 1.10)

Elasticity of single network

For deformation of any geometry, we start from equation (above):

$$\frac{\Delta G_{el}}{kT} \approx \frac{\Delta F_{el}}{kT} = \frac{AN_e}{2}\left(\lambda_x^2 + \lambda_y^2 + \lambda_z^2 - 3\right) - BN_e \ln\left(\frac{V}{V_0}\right)$$

(Equation 1.11)

and introduce the bounds between deformation components.

The deformation ratios related to the reference state ($\approx$ state at network formation) or related to "practical" deformation ratios related to the isotropic (swollen) and undeformed state:

43

$$\lambda_j = \frac{L_j}{L_{j0}} = \Lambda_j \frac{(L_j)_{iso}}{L_{j0}} = \Lambda_j \phi_2^{-1/3} (\phi_2^0)^{1/3}$$

(Equation 1.12)

Thus, for *simple shear* $\Lambda_x = \Lambda$, $\Lambda_y = 1$, $\Lambda_x \Lambda_y \Lambda_z = V/V_{iso}$, $\Lambda_z = (V/V_{iso})\Lambda^{-1} \approx \Lambda^{-1}$.

With this bound:

$$\frac{\Delta F_{el}}{kT} = \frac{A\phi_2^{-2/3}(\phi_2^0)^{2/3}N_e}{2}(\Lambda^2 + \Lambda^{-2} - 2) - BN_e \ln\left(\frac{V}{V_0}\right)$$

(Equation 1.13)

Transforming $\gamma = \Lambda - \Lambda^{-1}$ and differentiating with respect to γ, one gets the shear stress:

$$\left(\frac{\partial \Delta F_{el}}{\partial \gamma}\right)_{T,V} = \sigma_{sh,sw} = AN_e kT \phi_2^{-2/3}(\phi_2^0)^{2/3}\gamma$$

(Equation 1.14)

and, finally, the shear stress reads (per swollen cross-section and passing to concentrations):

$$\sigma_{sh,sw} = RTA\nu_e \phi_2^{1/3}(\phi_2^0)^{2/3}\gamma = G_{sw}\gamma$$

(Equation 1.15)

and the shear modulus:

$$G_{sw} = RTA\nu_e \phi_2^{1/3}(\phi_2^0)^{2/3}$$

(Equation 1.16)

For *uniaxial extension/compression*, the axial bonds bounds are:

$\Lambda_x = \Lambda$, $\Lambda_y = \Lambda_z$, $\Lambda_x \Lambda_y \Lambda_z = V/V_{iso}$, $\Lambda_y^2 = \Lambda_z^2 = (V/V_{iso})\Lambda^{-1} = (\phi_{2,iso}/\phi_2)\Lambda^{-1} \approx \Lambda^{-1}$

$$\frac{\Delta F_{el}}{kT} = \frac{AN_e \phi_2^{-2/3}(\phi_2^0)^{2/3}}{2}(\Lambda^2 + 2\Lambda^{-1} - 3) - BN_e \ln\left(\frac{V}{V_0}\right)$$

(Equation 1.17)

The uniaxial force, f_{ec} to achieve deformation Λ (subscript "ec" stands for extension/compression):

44

$$\left(\frac{\partial \Delta F_{el}}{\partial L_x}\right)_{T,V} = f_{ec} = AN_e kT \phi_2^{-2/3} (\phi_2^0)^{2/3} \left(\Lambda - \left(\phi_{2,iso}/\phi_2\right)\Lambda^{-2}\right)$$

$$\approx AN_e kT \phi_2^{-2/3} (\phi_2^0)^{2/3} (\Lambda - \Lambda^{-2})$$

(Equation 1.18)

Passing to concentrations and stress, f_{ec}, per unit cross-section area of undeformed, isotropic sample, one gets:

$$\sigma_{ec} = \frac{f_{ec}}{S_{iso}} = A\nu_e RT \phi_2^{1/3} (\phi_2^0)^{2/3} (\Lambda - \Lambda^{-2})$$

(Equation 1.19)

The Young's modulus, E, in uniaxial extension defined as:

$$\sigma_{ec} = E\varepsilon = E(\Lambda - 1)$$

(Equation 1.20)

is not constant but varies with deformation; only for very small $\varepsilon = \Lambda - 1$, it is equal to $3G$ as can easily be seen by expanding σ_{ec} into power series of $\Lambda - 1$.

Chapter 2. Aims and scope

The principal goal of this work is to understand the process of formation of interpenetrating polymer networks (IPN) from selected methacrylate hydrophilic monomers and the role of the formed IPN microstructure in its swelling and mechanical properties and set the conditions under which the concept of macromolecular network interpenetration will lead to mechanical reinforcement of the hydrogels. The studied IPN systems will be based on the two chemically identical or two chemically different hydrophilic methacrylate-based constituent networks.

To achieve the goal, the particular aims of the work address the following issues:

1. Study the effect of the first network hydrogel as the parent matrix on the properties of the sequentially prepared IPNs. Focus on the effect of the first network morphological structure on the microstructure, swelling and mechanical behavior of the resulting IPN hydrogels. The hydrogel matrices of interest will have porous vs. non-porous morphology.

2. Study the rate and mechanism including the gelation of the second network formation in the first network milieu.

3. Explore the effect of mechanical reinforcement in equilibrium swollen IPN hydrogels via the network interpenetration concept.

The hydrophilic analogs of 2-hydroxyethylmethacrylate (HEMA) have been one of the most important monomers in ophthalmologic biomedical areas and became the material standard for contact lenses, soft intraocular lenses, body implants and tissue engineering matrices to name the most important ones. The IPN concept is envisaged to broaden the range of relevant swelling and mechanical performance of HEMA and its analog, glycerol methacrylate (GMA)-based systems. Therefore the goal of the theses is also to contribute to presently limited information on the particular HEMA-HEMA and HEMA-GMA–based IPN hydrogels.

In scope of these aims, the results are presented and discussed as follows:

Section 1 offers the overview of all experimental series prepared and discussed in this work: the preparation of selected single network hydrogels by crosslinking polymerization of HEMA and GMA monomers leading to hydrogels of different microstructure and porosity utilizing the *in situ* phase separation or cryogelation and preparation of corresponding IPN hydrogels based on these matrices is described in detail.

Section 2 presents insight into the formation of the second network in the first network environment studied by monitoring the conversion of monomer double bonds due to polymerization by ATR FTIR spectroscopy and by monitoring the change of UV light absorption and scattering using UV-VIS spectroscopy. The gelation of single and interpenetrating crosslinking systems was studied by rheological measurements.

In Sections 3–5, the structure-properties relationships for PHEMA-PHEMA and PHEMA-PGMA IPNs and their constituent networks are addressed. In particular, Section 3 brings study of the microstructure of hydrogels by SWAXS and links it with the macroscopic hydrogel appearance.

Section 4 deals with the swelling behavior of single and IPN hydrogels in water as the most important solvent for these materials and in solvents thermodynamically better than water bringing structural information. The capacity of extension of network chains of the single network embedded within the IPN structure upon swelling was quantified.

In Section 5, the deformation responses of the prepared single and IPN networks swollen to equilibrium in water are determined by application of small-strain and large-strain deformations. Small-strain shear and tensile deformation provided information on equilibrium moduli, while large-strain deformation provided stress-strain dependencies up to ultimate sample failure – thus, we obtained the stress and strain at break. Effect of water content at preparation and crosslinker concentration in both networks is discussed in this context. Comparisons are made between all IPN hydrogels on the basis of moduli and degrees of swelling. A theoretical treatment of swelling and deformation responses of IPNs of homogeneous structure and chemically equal networks 1 and networks 2 is put forward and some experimentally obtained parameters are compared with the predicted ones.

Chapter 3. Experimental part

1. Chemicals

1.1. Monomers, initiators, and solvent

2-hydroxyethyl methacrylate (HEMA) (Rohm and Haas) contained 0.14 wt.-% of ethylene glycol dimethacrylate (EGDMA) and 105 ppm of 4-methoxyphenol (MEHQ); 2,3-dihydroxypropyl methacrylate (glycerol methacrylate, GMA) (BASF) contained 0.03 wt.-% of glycerol dimethacrylate (GDMA). The crosslinker, i.e., di(ethylene glycol) dimethacrylate (DEGDMA), the catalyst, i.e., *N,N,N',N'*-tetramethylethylenediamine (TEMED), initiators, i.e., ammonium persulfate (APS) and 2,2′-azobis(2-methylpropionitrile) (AIBN), and swelling solvent, i.e., dimethyl sulfoxide (DMSO), were purchased from Sigma-Aldrich, 2-hydroxy-2-methyl-1-phenyl-propane-1-one (DAROCUR 1173) initiator was purchased from Ciba. The chemicals were used as received.

1.2. Fluorescent labels

Fluorescein isothiocyanate isomer I (FITC), DY-677-NHS (amine coupling asymmetric cyanine ester), and *N*-(3-aminopropyl) methacrylamide hydrochloride as methacryloylation agent were purchased from Sigma-Aldrich and further chemically modified to introduce polymerizable groups utilized in gel structure visualization by laser scanning confocal microscopy.

2. Preparation of samples

2.1. Synthesis of the first network: PHEMA

2.1.1. Synthesis of soft hydrogels

The poly(2-hydroxyethyl methacrylate) (PHEMA) hydrogels, as the first network of IPNs, were prepared using redox-initiated free-radical polymerization using diethylene glycol dimethacrylate (DEGDMA) as a crosslinker and ammonium persulphate (APS) with *N,N,N',N'*-tetramethylethylenediamine (TEMED) as a redox-initiating system. Aqueous solutions containing various amounts of mixtures of HEMA with the crosslinker DEGDMA (0.2 – 6 mol-% per monomer) and 0.75 wt.-% of APS initiator per monomers were prepared and stirred for 5 minutes while purged with nitrogen. Then, the co-initiator TEMED was added and the reaction mixture was quickly injected between two glass plates 8 × 8 cm, separated by a

silicone rubber spacer serving as a frame. The reaction was carried out at room temperature overnight. Next day, the sample was taken out of the mold and washed with distilled water to remove all unreacted species. The soaking and replacement cycles were repeated several times until constant weight of the swollen hydrogel was reached. The amount of sol was determined gravimetrically and did not exceed 5 wt.-% per initial monomers.

2.1.2. Synthesis of hydrogels via bulk polymerization

The reaction mixture containing HEMA monomer, DEGDMA crosslinker and 2,2′-azobis(2-methylpropionitrile) (AIBN) thermal initiator was stirred for 5 minutes while purged with nitrogen, injected between two glass plates with a silicone spacer, and placed into an oven at 70 °C for 12 hours. Then the sample was removed from the mold, washed by swelling-replacement cycle and swollen to its equilibrium volume in water.

2.1.3. Synthesis of cryogels

The reaction components (HEMA, DEGDMA, APS/TEMED and water) were first pre-cooled in a refrigerator and then quickly mixed and gently stirred for 2-3 minutes while purged with nitrogen. The monomer solution was then injected into the pre-cooled glass plate mold, and placed in a freezer at -14°C. The sample was taken out after 24 hours, conditioned at laboratory temperature, removed from the mold, washed by swelling-replacement cycle and swollen to its equilibrium volume in water. In the case of the double-porous cryogels synthesis, 0.5 M aqueous solution of NaCl was used instead of pure water, otherwise the procedure was absolutely the same.

2.2. Synthesis of the reference second network hydrogels: PGMA or PHEMA

Reference single network poly(glycerol methacrylate) (PGMA) or PHEMA hydrogels were synthesized by photopolymerization of the respective monomer containing 0.3 mol-% of DEGDMA crosslinker (per monomers) and 0.5 wt.-% of 2-hydroxy-2-methyl-1-phenyl-propane-1-one (DAROCUR 1173) photoinitiator. The reaction mixture was stirred for 5 min, bubbled with nitrogen, injected between two glass panels separated by a silicone rubber frame and exposed to a UV light source composed of four Repti-Glo 8.0 UVB EXO-TERRA 15 W fluorescent lamps with the incident intensity of 10 mW/cm^2 for 90 min. The distance of the sample from the

UV source was kept constant in all gel preparations. When the full conversion was reached (time was tested previously in a preliminary polymerization), the sample was thoroughly washed with distilled water again to remove possible unreacted material.

2.3. Synthesis of IPN hydrogels

The IPN hydrogels were prepared by a sequential two-step free-radical procedure; the first network was formed by a polymerization using redox initiation, while the second one by UV polymerization using photoinitiator. The PHEMA hydrogel first network swollen in water was immersed into the reaction mixture of the second monomer, i.e., GMA, 0.3 mol-% of the crosslinker (DEGDMA), and 0.5 wt.-% of initiator (2-hydroxy-2-methyl-1-phenyl-propane-1-one). Before starting the second polymerization by UV irradiation, the equilibrated reaction mixture was replaced by a fresh one, and this was repeated 3-4 times in order to replace completely water by monomers. The composition of swelling liquid surrounding the gel was checked by determining the refractive index of the liquid. During swelling in the monomer mixture, the samples were kept in a dark cabinet to prevent photoinitiation by ambient light. Constant volume of the swollen gels at room temperature was attained in 10 days. The specimens were then exposed for 90 min to ultraviolet light of the intensity of 10 mW/cm^2 to get them polymerized. After that time, the residual uncrosslinked monomers were removed by washing with distilled water.

2.4. Coding of samples

The single network gels were coded as, for example,

H80/1 or **G0/0.3**

Here, the first letter (H or G) means the HEMA or GMA monomer used for polymerization, respectively, the numbers following the letter define the concentration of water in wt.-% used as the diluent in the polymerization and the numbers following the slash mean crosslinker concentration in mol-% in the mixture of monomers. The IPN hydrogels were coded as, for example,

H80/1–G0/0.3

where the first part of the code describes the composition of the first network, and the second part following the hyphen describes the composition of the second network. Letter and numbers have the same meaning as above.

3. Characterization of gels

3.1. Kinetics of gel formation

3.1.1. ATR FTIR measurements

The infrared spectra were recorded on a Nexus Nicolet 870 FTIR spectrometer purged with dry air and equipped with a liquid nitrogen cooled MCT (mercury cadmium telluride) detector. The spectra of the solutions and hydrogel samples were acquired using the Golden Gate single reflection ATR cell (Specac) equipped with a diamond internal reflection element. When the first network swollen in the GMA monomer was transferred onto the diamond crystal, the spectrum was obtained without applying any force and without covering the sample. When a sample of the IPN being formed was placed onto the crystal, then, if the time of UV irradiation was equal to or longer than 7 min, a pressure was applied to the sample using the arm of the ATR accessory. The spectra were recorded with a resolution of 4 cm^{-1}; 32 scans were averaged to form a spectrum. After subtracting the spectrum of the atmosphere, baselines were corrected (linear baseline correction) and an advanced ATR correction was applied. The spectra were normalized using the integrated intensity of the C–H stretching vibration bands; the region between 3050 and 2650 cm^{-1} was used for integration.

To monitor the rate of the photopolymerization during the single network hydrogel formation, the reaction mixture containing the GMA monomer was divided into aliquots which were placed into open containers and exposed to UV light of intensity of 10 mW/cm^2. Before starting the irradiation with UV, a spectrum of one of the aliquots was recorded, corresponding to the time $t = 0$ min. Next, over a period of 100 minutes, always a new container with a mixture irradiated for given time was used to record a spectrum of the forming PGMA.

In the case of the IPN formation, prior to irradiation with UV light, the PHEMA network swollen in the GMA monomer mixture was cut into pieces and placed onto a Nescofilm to remove the excess monomer of GMA. Then, all samples were exposed to the same UV source and irradiated for given time interval and then transferred onto the ATR crystal with their top surface in contact with the crystal. The corresponding spectra were acquired over a period of 90 minutes. A piece of the monomer-swollen gel not irradiated with UV was measured at time 0 min and taken as a reference.

3.1.2. Sol extraction

A series of six samples of parent PHEMA hydrogels swollen in monomers mixture of network 2 were irradiated within 0 and 60 minutes. At a given time, the irradiation of each sample was stopped, and the sample was placed into a solvent – dimethyl sulfoxide (DMSO) for sol extraction. The extracting medium was replaced with a fresh portion of DMSO several times. After the complete sol extraction, the IPN gel was washed with water and then dried. The sol fraction was calculated as:

$$\omega_{sol} = \frac{m_{net2}^{sol} - m_{net2}}{m_{net2}^{sol}}$$

(Equation 3.1)

where m_{net2}^{sol} is the weight of dry network 2 and sol, while m_{net2} is the weight of dry network 2; m_{net2}^{sol} is the difference between the weight of the IPN after the irradiation ($m_{net1+net2}^{sol}$) and the weight of dry network 1 (m_{net1}), while m_{net2} is the difference between the weight of dry IPN after sol extraction ($m_{net1+net2}^{dry}$) and the weight of dry network 1 (m_{net1}).

3.1.3. UV-VIS spectrophotometry

The kinetics of the polymerization was also followed using UV-VIS optical extinction measurements. Liquid and solid samples were measured in a mold assembled using two flat quartz glasses and a silicone rubber spacer. The thickness of the silicone rubber spacer and of each quartz glass was 1 mm. The mold filled with the sample was irradiated outside the spectrophotometer using UV light of 10 mW/cm^2 intensity, and at defined periods of time transferred into the spectrophotometer for spectra acquisition. The total irradiation time was 90 minutes. The optical transmission spectra of the samples were acquired using a PerkinElmer Lambda 950 spectrophotometer in the wavelength range from 190 to 800 nm. The samples were attached directly to the solid state sample holder and measured with unpolarized light using a common beam depolarizator. Alternatively, the samples were attached to the input port (aperture diameter 2.5 cm) of the 60 mm integrating sphere for the diffuse optical transmission measurements.

3.1.4. SWAXS measurements

X-ray scattering experiments were performed using a pinhole camera (Molecular Metrology SAXS System) attached to a microfocus X-ray beam generator (Bede, Durham, UK) operating at 45 kV and 0.66 mA (30 W). The camera

was equipped with a multiwire, gas-filled area detector with an active area diameter of 20 cm and 512×512 pixels (Gabriel design). A PIN diode was part of the beamstop. This configuration served not only to protect the detector from the primary beam but, at the same time, to measure its intensity. Measurements were conducted in a momentum transfer range ($5 \times 10^{-2} < q < 11$) nm^{-1} ($\lambda = 0.154$ nm). Scattering measurements covering this region are usually denoted as SWAXS small and (near) wide angle X-ray scattering. The measured intensities were put on the absolute scale using a glassy carbon standard. In the case of monitoring the changes during gelation in single (not interpenetrating networks) hydrogels, the reaction components were mixed immediately prior to SWAXS measurements leaving out TEMED to slow down the reaction rate, the solution was placed in a standard capillary, placed in the sample holder, and the reaction was followed *in situ* at the room temperature. In the case of monitoring the IPNs formation, the thin strips of the pre-formed first network swollen in the monomers of the second network were irradiated outside the camera; and after a certain time of irradiation (0, 15, 30, 45, 60 and 90 min) each stripe was placed in a standard capillary, placed in the sample holder and measured.

3.1.5. Chemorheological determination of the gel point

Chemorheological measurements were carried out using a Bohlin Gemini HR Nano oscillatory rheometer (Malvern, UK) equipped with a Peltier measuring table for temperature control. The viscoelastic response of the sample due to gelation was monitored on the basis of changes in the storage (G') and loss (G'') shear moduli during the crosslinking reaction. The deformation responses of the *in situ* crosslinking gel was monitored in an oscillation–time sweep mode at a frequency of 0.05 Hz. First, the initial curing region up to the liquid−solid transition was monitored by the stress-control mode, and then, when the system passed through the gel, the mode of deformation control was switched to the strain-control mode. This ensured that the condition of the so-called linear viscoelastic region applied throughout the entire curing cycle, and at the same time, the applied and measured forces and strains were relevant. The dynamic storage G' and loss G'' moduli were plotted as functions of the gelation time. To prepare hydrogels, an aliquot of GMA reaction mixture (HEMA, DEGDMA and AIBN) or PHEMA hydrogel swollen in the GMA reaction mixture were placed between two parallel plates of 40 mm diameter.

The reaction was initiated by AIBN thermal initiator at 70 °C. A special solvent trap was used to avoid the evaporation of the monomer mixture during the reaction.

3.2. Differential scanning calorimetry

Differential scanning calorimetry (DSC) records were obtained using TA Instruments Q2000 calorimeter. Nitrogen was used as a purge gas at a flow rate of 50 mL/min. Heat flow was calibrated with a standard sample of indium. The samples of about 20 mg were placed inside aluminum pans and subjected to annealing treatments. The enthalpy of polymerization was recorded in a temperature range 20 – 150 °C at a heating rate of 3 °C/min.

3.3. Dynamic light scattering

Dynamic light scattering (DLS) experiments were performed using Zetasizer Nano-ZS instrument, model ZEN3600 (Malvern Instruments, UK). Two series of solutions were prepared: (1) "monomer–water" mixtures of various ratios and (2) "monomer–water–crosslinker" solutions, in which the content of water was constant (40 wt.-%), while the concentration of crosslinker varied in the range from 0 to 6 mol-% per monomer. The scattering intensities and hydrodynamic diameter of aggregates (D_h) were measured at a scattering angle of $\theta = 173°$. The DTS (Nano) software was used to evaluate the data. The intensity-weighted value of the apparent D_h was chosen to characterize the dispersity of the aggregates in solutions.

3.4. Morphology studies

3.4.1. Cryo-Scanning Electron Microscopy (Cryo-SEM)

The morphology of the flash-frozen hydrogels was studied by means of low-vacuum cryo-scanning electron microscopy (cryo-LVSEM). The scanning electron microscope (Quanta 200 FEG, FEI, Czech Republic) was equipped with a Peltier cooling stage and a secondary electron detector working under vacuum (large-field detector, LFD). A small piece of wet hydrogel was flash-frozen in liquid nitrogen, fixed with ice onto the pre-cooled stage (at -10 °C) and then the thin frozen top layer of the specimen was cut off with a razor blade. The freshly open frozen surface of the sample was observed under low-pressure cryo-conditions and using secondary electrons imaging at an accelerating voltage of 10 kV.

3.4.2. Light microscopy (LM)

Light microscopy studies of wet hydrogels were performed with Leica DM6000 M (Leica, Austria) microscope equipped with a digital camera and extra-large working distance objectives with extended depth of focus and possibility of bright field and dark field imaging in both transmitted and reflected light. The samples were submerged in water at all times. A thin slice of hydrogel cut with a sharp blade was placed between the support and cover glasses and observed in the light microscope at room temperature.

3.4.3. Laser scanning confocal microscopy

The structure of hydrogels in the wet state was visualized by laser scanning confocal microscopy (LSCM) Fluoview FV1200 (Olympus, Japan). After its formation, the single network hydrogel H80/1 was stained with fluorescein isothiocyanate (FITC). First, methacryloylated FITC was dissolved in phosphate-buffered saline (PBS) solution. Then, macroporous hydrogel was immersed into the 0.01 wt.-% PBS solution of methacryloylated FITC and let swell to achieve uniform staining. After 3-4 days, samples were thoroughly washed by pure PBS solution to remove the excess fluorescein from interstitial spaces within the pores.

The preparation of H80/1–G0/0.3 IPN hydrogel for structure visualization was different. Two types of dyes were used to distinguish two networks of the IPN. Methacryloylated fluorescein isothiocyanate with the excitation spectrum peak at 495 nm was covalently embedded in the first PHEMA network and the methacryloylated fluorescent dye, DY-677, exerting the main excitation peak at 673 nm was incorporated in the second PGMA network. Both dyes were covalently modified with methacrylate functionality (the procedure is described in Supporting Information). Each modified dye with attached polymerizable double bond was copolymerized into the backbone chain of the corresponding polymer network. An argon ion laser and diode laser providing emissions at wavelengths of 488 nm and 635 nm, respectively, were used to excite the labeled hydrogels. Fluorescence images were captured with an objective with the magnification 50 and using double digital zoom. The materials were visualized at a room temperature.

3.5. Swelling degree

3.5.1. Swelling in monomers and solvents

The *volume swelling ratio* (Q_V) of disc-shaped hydrogel samples was assessed by measuring the discs dimensions achieved in the equilibrium swollen state (V_{sw}) and after drying (V_d) in vacuum oven at 100 °C to constant weight; it was defined as:

$$Q_V = \frac{V_{sw}}{V_d}$$

(Equation 3.2)

The chain *dilation factor* (α) was related to reference network chain dimensions (volume at network formation) and calculated from the volume swelling ratio as:

$$\alpha = \sqrt[3]{V/V_{nf}}$$

(Equation 3.3)

where V and V_{nf} are actual (at a given state) volume and volume at network formation, respectively.

When relation (3.3) is applied to macroporous gels, it is assumed that network chains in pore walls at the end of gel preparation are in their reference states and are randomly oriented. During drying of such gels, some smaller pores may collapse by capillary contraction or the pore walls shrink non-affinely with external dimensions, so that the value of $\alpha < 1$ as a measure of network chain contraction is only approximate.

The *weight swelling ratio* (Q_m) of the disc-shaped hydrogel samples was assessed by measuring the weight of disc in the equilibrium swollen state (m_{sw}) and after drying (m_d) in vacuum oven at 100 °C to constant weight; it was defined as:

$$Q_m = \frac{m_{sw}}{m_d}$$

(Equation 3.4)

The *equilibrium solvent or water content* (**ESC or EWC**) was determined using a gravimetric method. Weights of swollen (m_{sw}) and dry (m_d) hydrogels were used in the following expression:

$$\text{ESC, EWC} = \frac{m_{sw} - m_d}{m_d}$$

(Equation 3.5)

The *swelling degree (SD)* was determined using a gravimetric method. Weights of swollen (m_{sw}) and dry (m_d) hydrogels were used in the following expression:

$$\text{SD} = \frac{m_{sw} - m_d}{m_{sw}}$$

(Equation 3.6)

3.5.2. Swelling of gel phase in water vapor. Determination of the porosity

Preliminarily freeze-dried gels were placed into the desiccator equipped with a sensor detecting the humidity and temperature inside (Figure 15). The high humidity (according to the sensor as high as 99.9 %) was provided by the wet tissue located at the bottom of the chamber and kept constant due to a good sealing, while the temperature inside was corresponding to a room temperature. The sample was inserted into the vial, which was kept open during the entire swelling experiment. Prior to weighing, the vial with sample was quickly taken from the chamber and closed.
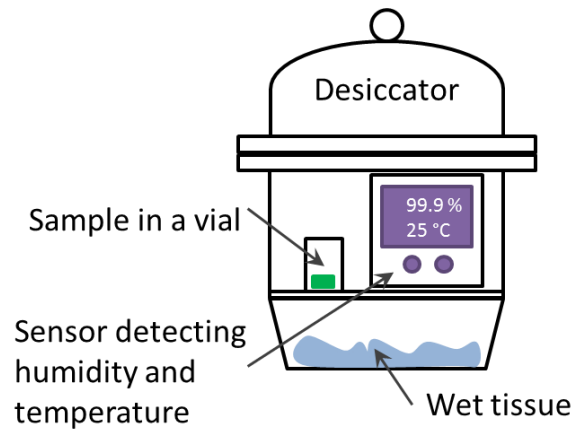
Figure 15. Swelling of gels in water vapor.

The *equilibrium water content* (**EWC**$_G$) *in the gel phase* was determined as:

$$\text{EWC}_G = \frac{m_{sw}^V - m_d^L}{m_d^L}$$

(Equation 3.7)

where (m_{sw}^{V}) and (m_{d}^{L}) are weights of hydrogels swollen in water vapor and freeze-dried.

The **porosity (P)** of gels was assessed from the weight of sample fully swollen in water (m_{sw}) and the weight of sample the gel phase of which is swollen in water vapor (m_{sw}^{V}):

$$P = \frac{m_{sw} - m_{sw}^{V}}{m_{sw}}$$

(Equation 3.8)

3.5.3. Determination of gel porosity by swelling in cyclohexane

Preliminarily freeze-dried gels were immersed into cyclohexane for 1 hour and quickly weighed afterwards. This was repeated at least three times for each gel. The **porosity (P)** of gels was assessed from the weight of sample the pores of which were filled with cyclohexane (m_{sw}^{CH}) and the weight of freeze-dried sample (m_{d}^{L}):

$$P = \frac{m_{sw}^{CH} - m_{d}^{L}}{m_{sw}^{CH}}$$

(Equation 3.9)

3.5.4. Gel porosity assessed by calculation of fraction of pores

The porosity of macroporous gels can roughly be assessed by calculation of **fraction of pores (φ_{pores})**:

$$\varphi_{pores} = \frac{(ESC_x - ESC_{40}) \cdot \rho_{gel}}{(1 + ESC_x) \cdot \rho_{solv}}$$

(Equation 3.10)

where (ESC_x) and (ESC_{40}) are equilibrium solvent contents in considered gel and in PHEMA gel prepared with 40 wt.-% of water, respectively, while (ρ_{gel}) and (ρ_{solv}) are densities of considered gel and solvent, respectively. The detailed derivation procedure is available in appendix (appendix 2).

3.6. Deformation behavior

3.6.1. Tensile tests

Tensile mechanical measurements were performed on Linkam TST 350 equipment with maximum load of 50 N at ambient temperature. All hydrogels were tested after complete equilibration after immersing in distilled water. The samples were patterned into dog-bone shaped pieces of 8 × 4 mm (central part). The thickness of gels was dependent on their swelling properties and varied within 1 and 3 mm. Hydrogels were fixed in the grips and the extension speed was 10 μm/s. For each hydrogel composition, at least five samples were measured. The stress was expressed as force per initial specimen cross-section area and strain was expressed as

$$strain = 100 \times \frac{L - L_i}{L}$$

(Equation 3.11)

where L_i is the initial (isotropic) sample length (distance between clamps) and L is the extended sample length at given stress. The relation between strain and deformation ratio λ is $strain = 100 \times (\lambda - 1)$, where $\lambda = L/L_i$. The true strength is defined as:

$$\sigma_{true} = (\lambda - 1)\sigma_{break}$$

(Equation 3.12)

where σ_{break} is the value of stress at break.

3.6.2. Rheological measurements

Bohlin Gemini HR Nano (Malvern Instruments, UK) equipped with a Peltier element temperature controller was utilized to assess dynamic viscoelastic properties of swollen hydrogels (Figure 16). Stainless steel parallel plate-plate geometry of 20 mm diameter was used for rheological measurements of hydrogels at a gap size (distance of measuring plates) between 1 and 4 mm. A bottom of a special solvent dish filled with water during measurement served as a lower plate preventing drying out of the swollen sample. Thus, each hydrogel was always immersed in water during the measurement.
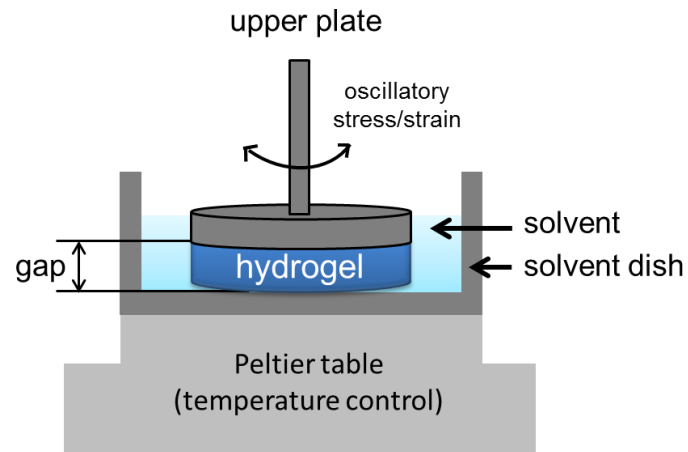
Figure 16. Measuring cell of rheometer consisting of a Peltier element temperature controller, measuring plate-plate geometries, and a solvent dish.

The correct gap between the plates is considered to be found, when sliding of the sample does not occur, full contact between plates and sample is achieved and deswelling does not occur. Viscoelastic behavior of the hydrogels was studied in the stress-control mode of the frequency sweep test at 25 °C covering a range of frequencies from 0.003 to 100 Hz. The stress value was chosen within linear viscoelastic range determined from the amplitude sweep test.

Chapter 4. Results and discussion

1. Overview of systems studied in thesis

1.1. Selection of monomers and sample coding

In this work, as model systems, the monomers of methacrylate class were used because of facile preparation of polymers and applicability. The structural formulas of monomers used in our work are given in Figure 17. Both 2-hydroxyethyl methacrylate (HEMA) and glycerol methacrylate (GMA) monomers are infinitely miscible with water. Due to the additional hydroxyl group, the GMA monomer is even more hydrophilic than the HEMA monomer. Monomers were used as purchased without removing the hydroquinone inhibitor (MEHQ), the concentration of which was around 100 ppm. The effect of inhibitor was suppressed by relatively high concentrations of added initiators (0.5 – 0.75 wt.-%), that were ammonium persulfate (APS), 2,2′-azobis(2-methylpropionitrile) (AIBN), and 2-hydroxy-2-methyl-1-phenyl-propane-1-one (DAROCUR 1173).
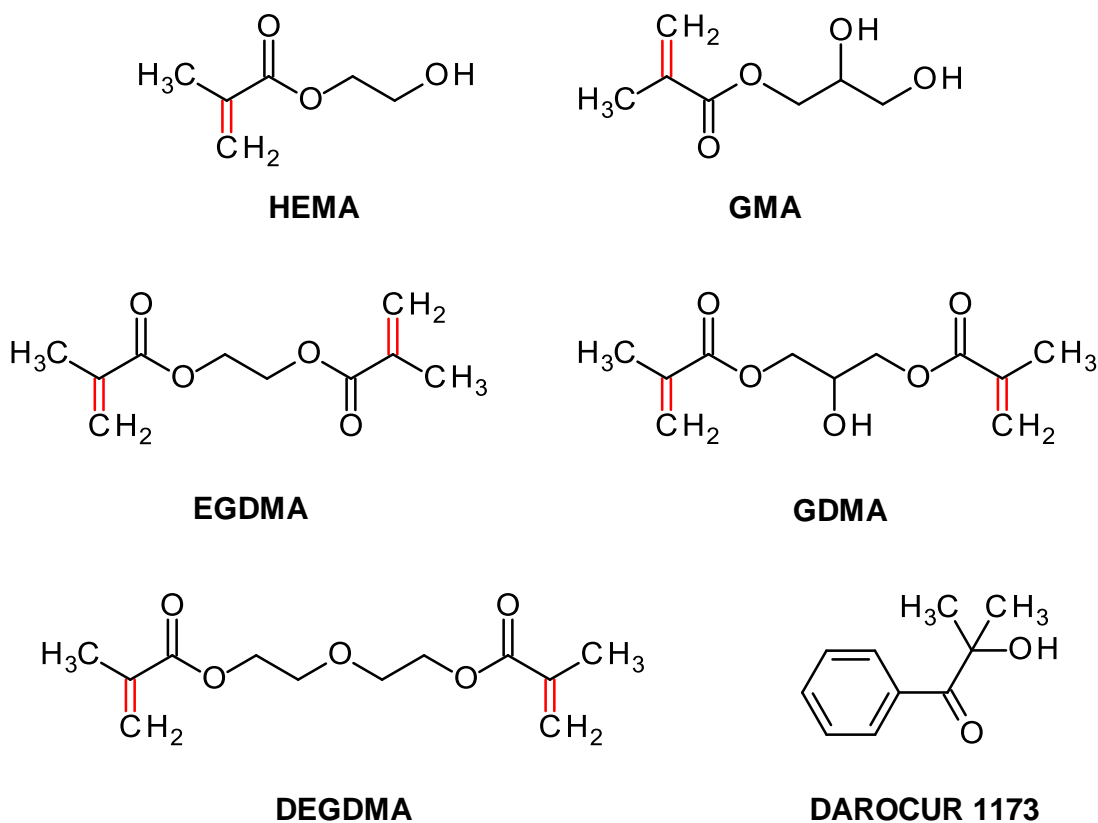
Figure 17. Structure of monomers.

Each monomer contained defined amount of bifunctional species leading to crosslinking polymerization even when the additional crosslinker was not added. According to the gas chromatography data, HEMA monomer of the source used here contained 0.14 wt.-% of ethylene glycol dimethacrylate (EGDMA), while GMA contained 0.03 wt.-% of glycerol dimethacrylate (GDMA). This fact was taken into account in calculations. The code of each sample represents only the amount of added for synthesis of covalent networks crosslinker. For instance, in the code "H80/1" the first letter (H) means the HEMA monomer used for polymerization, the number "80" defines the concentration of water in wt.-% used as diluent at polymerization and the number "1" following the slash means that 1 mol-% of crosslinker was added into the reaction mixture besides the amount of crosslinker irremovable from HEMA monomer. More details on sample coding are available in Experimental part (paragraph 2.4).

1.2. Types of PHEMA network 1

The single network hydrogels prepared as matrices for interpenetration by the second network were of various microstructures due to the different compositions of reaction mixtures and polymerization conditions. The network 1 microstructure variety is shown in Figure 18. When the amount of water in the reaction mixture is below the miscibility threshold (40 wt.-%), the polymerization within the entire volume leads to homogenous swollen gel without pores. High dilution of monomers (80 wt.-% of water) leads to the reaction induced phase separation, so called microsyneresis[148], which causes the formation of macroporous system. When the latter is polymerized under cryo-conditions, i.e., at temperatures below zero, the macropores are formed due to the formation of ice crystals acting as templates, while the walls of the hydrogels are non-porous. The polymerization of the same system under cryo-conditions in the presence of salt solution results in an interesting structure with large and small pores, that we call "double-porous cryogel". The pore formation was caused by ice crystals formation and by microsyneresis.
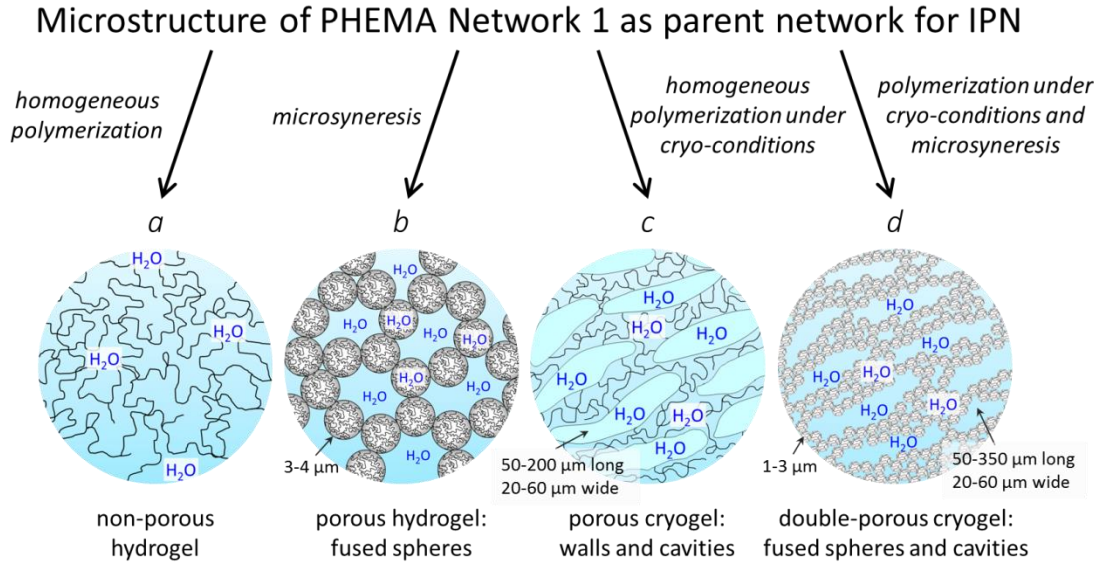
Figure 18. Types of PHEMA network 1 studied in the thesis used as parent networks for interpenetrating network (IPN) hydrogels.

1.3. Map of IPN hydrogels studied in thesis

The swollen network 1/network 2 IPN hydrogels were obtained by a four-step sequential process schematically shown in Figure 19. The details of synthesis were described in Experimental part (paragraph 2.3). Here, only some important features of IPN preparation will be briefly pointed out.
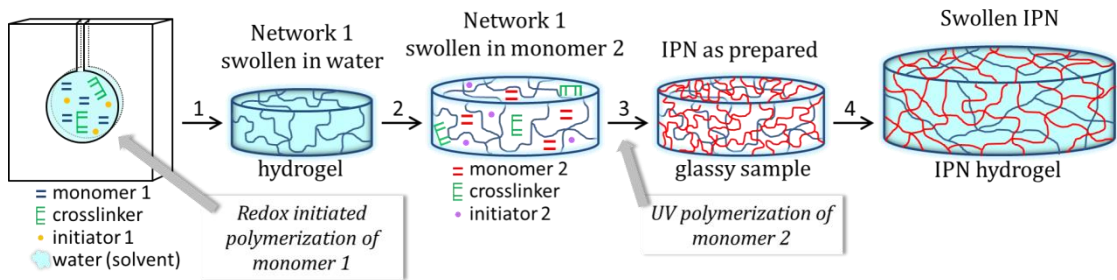
Figure 19. Scheme of sequential formation of IPN hydrogels: (1) preparation of network 1 by redox initiated crosslinking polymerization of HEMA monomer 1 followed by swelling in water, (2) swelling of the network 1 in the monomer 2 with crosslinking agent, (3) UV-initiated crosslinking polymerization of monomer 2, and (4) swelling of IPN in water.

The sol, i.e., unreacted monomers, remained after the formation of network 1 was removed by washing in distilled water to prevent its participation in formation of network 2. The network 1 gels were immersed into the reaction mixture of network 2

in the water-swollen state, because drying of network 1 might be accompanied by transition to glassy state as well as might cause some structure changes such as irreversible collapse of pores. Another reason for it is a long time diffusion of reaction mixture into the matrix of dry network. A complete replacement of water for monomers mixture of the network 2 was controlled indirectly by refractive index analysis of surrounding liquid containing the monomers mixture and water released from network 1, and directly by the ATR FTIR measurements of parent PHEMA network swollen in reaction mixture of network 2. The disc-shape of hydrogels was chosen in terms of suitability for further manipulation and measurements.

The IPN hydrogels studied in this thesis were summarized in scheme with four sections (Figure 20). The PHEMA-PHEMA IPN gels were collected in section A, the PHEMA-PGMA IPN gels in section B, the PGMA-PHEMA IPN gels in section C, and the PGMA-PGMA IPN gels in section D. For each IPN hydrogel, swelling in water and dimethyl sulfoxide (DMSO), deformation measurements in shear and tensile mode were carried out. The scope of all these experiments was represented by magenta color circles. The porous networks 1 were represented by blue circles.

The preparation of IPN gels based on PHEMA parent network 1 (sections A and B) was accompanied by the expansion of the network 1, whereas the IPN gels based on PGMA parent network 1 (sections C and D) revealed a phase separation accompanied by the sample shrinkage, when the network 1 was swollen in GMA or HEMA monomer 2. Because of such peculiarities of the PGMA-based IPNs, the PGMA-PHEMA IPN hydrogels were briefly discussed in terms of their specific morphology, while the results on the PGMA-PGMA IPN hydrogels were not included in this work. Thus, the main focus of this work is on PHEMA-based IPN hydrogels, i.e., the samples collected in sections A and B.
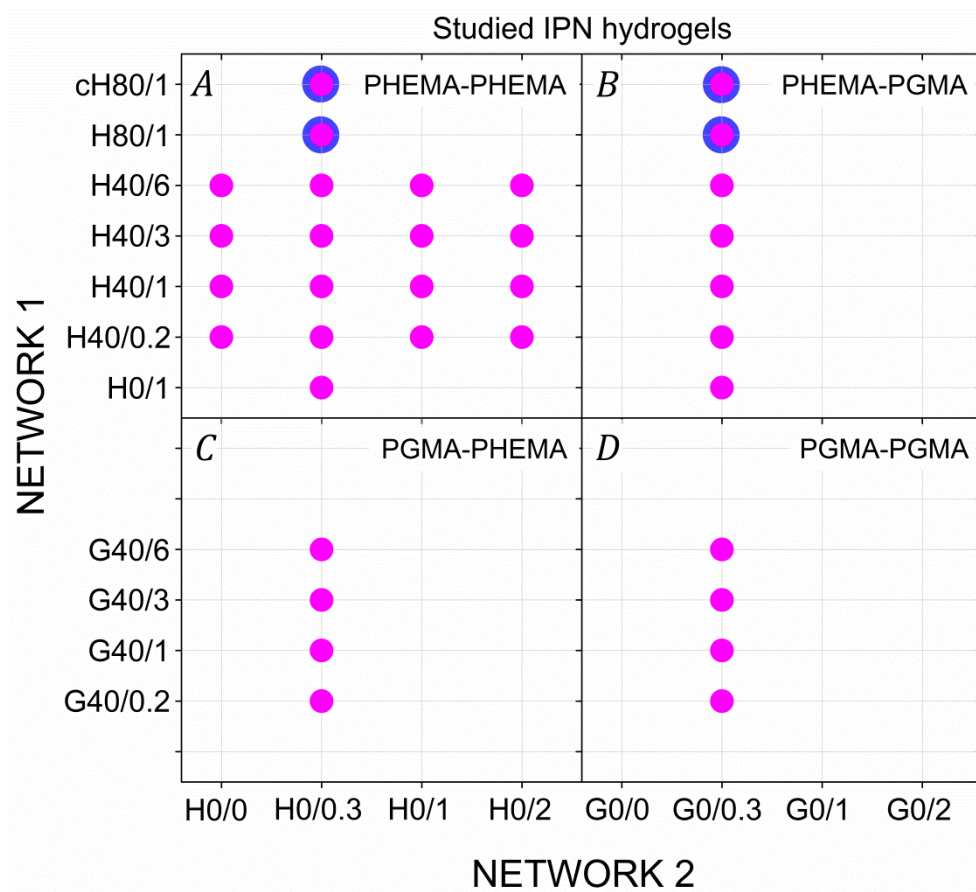
Figure 20. Overview of IPN hydrogels studied in terms of tensile test, rheological measurements, and swelling in water and dimethyl sulfoxide (DMSO) (magenta). The porous networks 1 are represented by blue circles.

2. Formation of IPN hydrogels

2.1. Rate of reference poly(glycerol methacrylate) formation

Kinetics of radical polymerization of PHEMA networks were thoroughly studied and described in literature.[111,123,112] Therefore, we focused on formation of the second PGMA network within the PHEMA matrix of various morphologies. As a reference, we studied the polymerization kinetics of the PGMA network separately. The course of crosslinking polymerization of reaction mixture of GMA and DEGDMA initiated by UV irradiation is shown in Figure 21a. The induction period of reaction lasted 20 – 25 minutes and followed by moderate increase of reaction rate. The reaction was finished after 90 – 100 minutes of irradiation, but the conversion of C=C double bonds was not complete and the sample contained about 15 % of sol fraction. The reaction mixture of monomers was not diluted with water in this case and was slightly viscous already at the beginning of the reaction. Corresponding ATR FTIR spectrum of reaction mixture is shown in Figure 21b (spectrum a). Incomplete conversion was caused by vitrification of the sample restricting the mobility of reactive species (Figure 21a and 21b (spectrum b)). Annealing at 120 °C caused the transition to rubbery state and the conversion of double bonds increased up to 99 % (Figure 21b, spectrum c).

Figure 21. Conversion of C=C bonds of GMA monomer as quantified by ATR FTIR spectroscopy during crosslinking polymerization with no diluent present at polymerization (a). Spectra of polymerizable mixture (b) before UV-irradiation (1), after 90 minutes of UV-irradiation (2), and after 90 minutes of UV-irradiation followed by heating (3).

The change of optical density during the crosslinking polymerization of PGMA was followed in the range of wavelengths from 300 to 420 nm (Figure 22). The GMA reaction mixture was a clear solution with low optical density, which increased with the network formation indicating its structuring. The final network was visually clear as well. In the range of visible light (from 400 nm), the values of optical density were low indicating the transparency of the sample. The region from approximately 310 to 360 nm revealed higher values of optical density due to the absorption of UV light by photoinitiator.
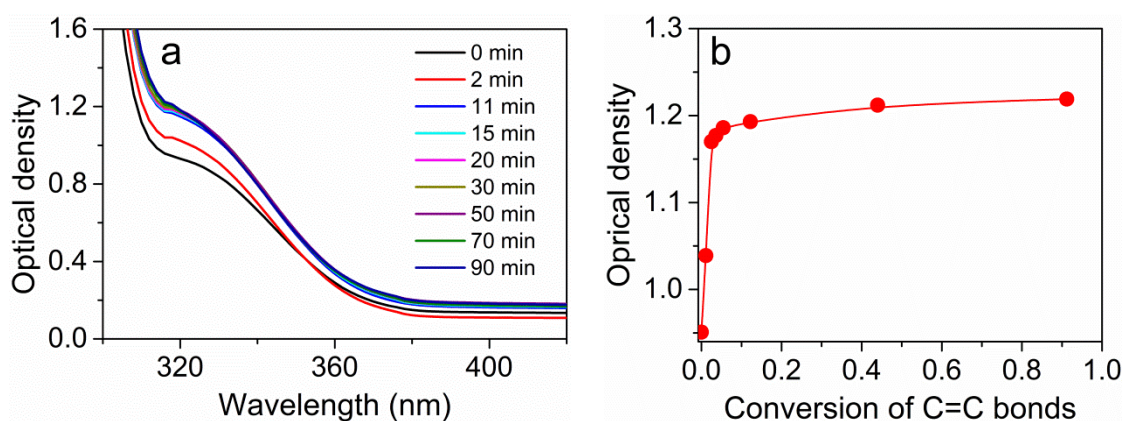
Figure 22. Optical density of GMA reaction mixture as a function of wavelength during the crosslinking polymerization with no diluent present at polymerization (a). Optical density of GMA reaction mixture at 317 nm wavelength as a function of conversion of C=C bonds (b).

2.2. Formation of IPN hydrogels

2.2.1. UV initiated photopolymerization – ATR FTIR spectroscopy

When looking for optimal conditions for preparation of the PGMA network, the kinetics of UV-polymerization of GMA was studied in the environment of PHEMA network by ATR FTIR spectroscopy. The spectra of PHEMA network and GMA monomer are shown in Figure 23 (curves a, b). The PHEMA network was swollen in water and no absorbance at 1637 cm^{-1} (dotted line) representing C=C bonds from unreacted monomers was detected (spectrum a). The GMA reaction mixture (spectrum b) did show the band at 1637 cm^{-1} clearly documenting the presence of C=C bonds. When the PHEMA network was swollen in GMA reaction mixture, the same peak appeared in spectrum c. After the photopolymerization (spectrum d), the intensity of this band decreased in intensity but did not disappear

completely indicating presence of unreacted monomers or pendant double bonds. The transition of the system into glassy state may have prevented their complete conversion. Heating up to 80 °C was sufficient to make the gel rubbery and promote further polymerization (spectrum e).
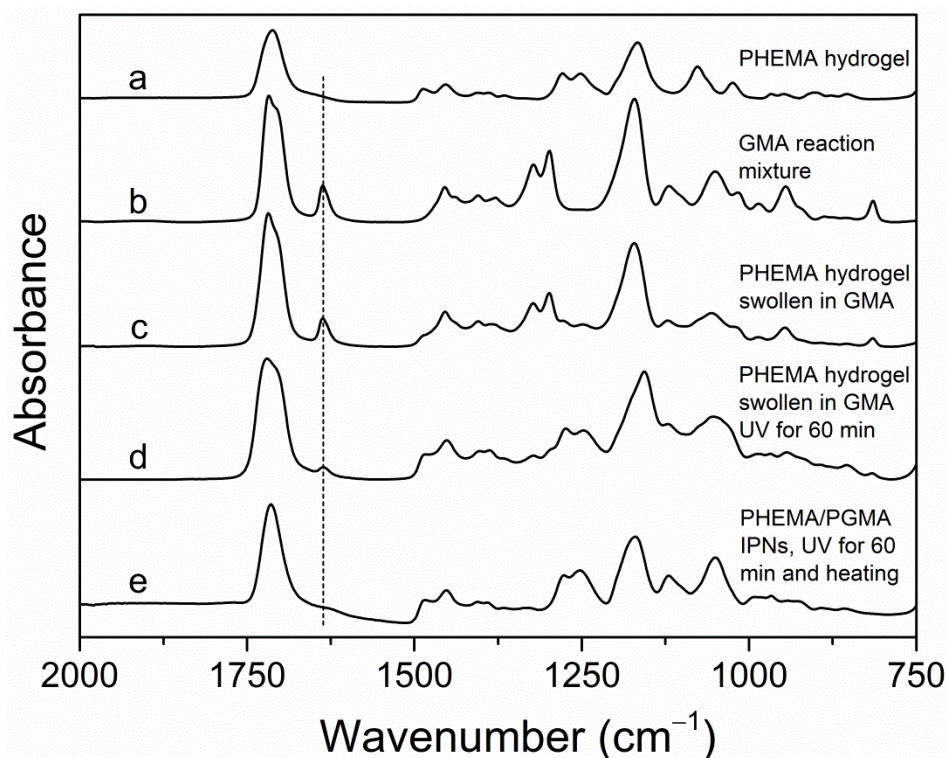
Figure 23. ATR FTIR spectra of (a) H80/1 single network; (b) GMA reaction mixture; (c) H80/1 single network swollen in the GMA reaction mixture; (d) H80/1–G0/0.3 IPNs after UV-polymerization; (e) H80/1–G0/0.3 IPNs after UV-polymerization and heating.

2.2.2. Rate of interpenetrating networks formation

ATR FTIR spectroscopy. To elucidate the mechanism of the second network formation, the kinetics of polymerization of GMA entrapped in the macroporous matrix (heterogeneous environment) and the non-porous matrix (homogeneous environment) was studied. The kinetics of the single PGMA network formation, serving as a reference system, was examined under the same reaction conditions.

The kinetic dependencies were typical for free-radical polymerizations accelerated by Trommsdorff effect with induction period. While the acceleration was caused by diffusion control of termination by recombination and assisted by increased viscosity (including gelation), the extent of the induction period was

68

largely dependent of the content of free-radical scavenging impurities. Different slopes of the curves in Figure 24 indicated that the conversion of C=C bonds was the most rapid when GMA was polymerized within the macroporous matrix, while the rate of GMA double-bond conversion was the lowest when GMA was polymerized in bulk. Another difference between the three systems was the duration of the respective induction periods. Polymerization of GMA in the matrix of macroporous PHEMA network started immediately after the irradiation and at room temperature, the maximal conversion of 85 % was reached in 15 minutes. The longest induction period was observed in the case of the single GMA network. In this case, the induction period lasted around 30 minutes after which the conversion sharply increased and the polymerization was completed in about 100 minutes.

To verify that no part of monomer was converted prior to monitoring the reaction kinetics by ATR FTIR spectroscopy, the total reaction heat associated with polymerization for each system was determined calorimetrically (Table 3). The values of reaction enthalpy released per mole of consumed C=C bonds were calculated for each system and were almost equal (within experimental scatter). This confirmed that no double bonds were lost by reaction prior to the UV irradiation.

In photopolymerization, a sufficient light penetration depth in the cured material is crucial for avoiding gradient polymerization in the sample.[188] The heterogeneous structure of IPN hydrogels causes light scattering, which influences the pathway of light inside the sample and, hence, affects the kinetics of the photopolymerization.[189]

Table 3. Reaction enthalpy released during network formation per mole of polymerizable monomer as determined by differential scanning calorimetry.

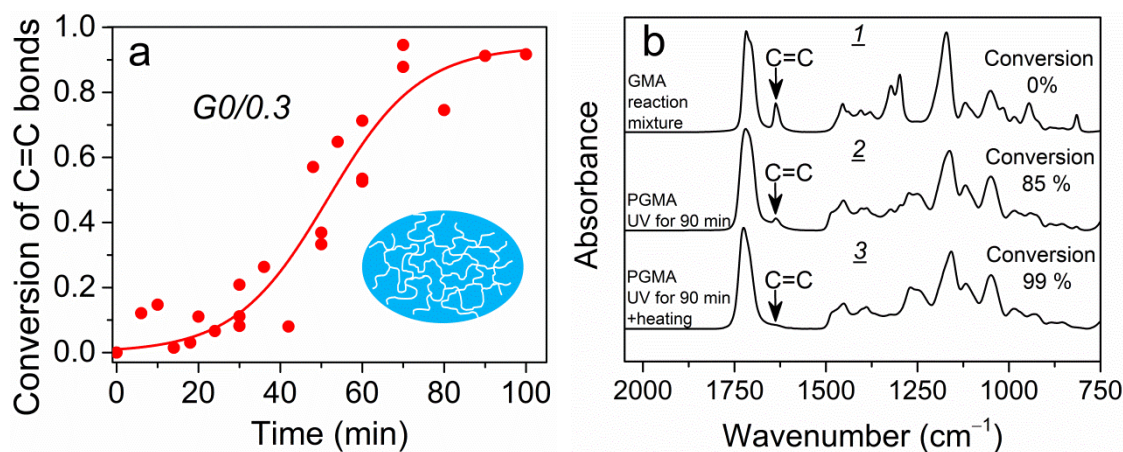| Sample	ΔH_{react} [kJ/mol]
G0/0.3	-58.3
H40/1–G0/0.3	-56.7
H80/1–G0/0.3	-53.8
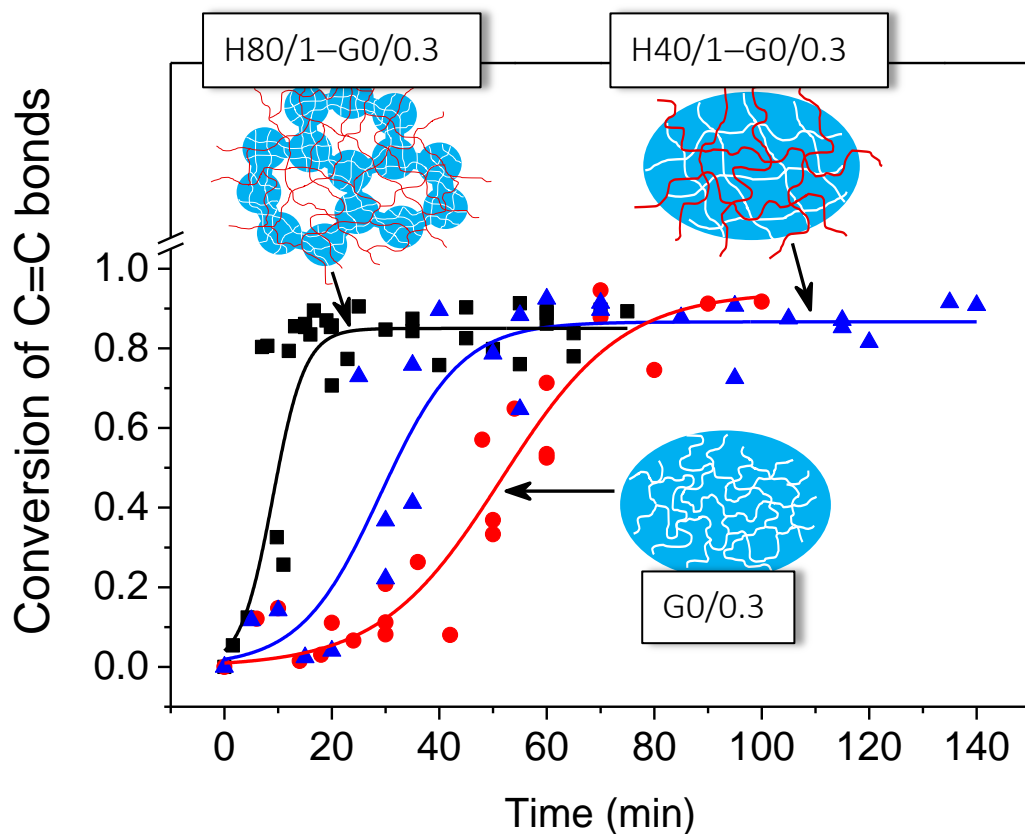
Figure 24. Conversion of C=C bonds of GMA monomer as quantified by ATR FTIR spectroscopy during crosslinking polymerization within PHEMA–PGMA IPN environments: curve H80/1–G0/0.3 shows conversion of GMA with time in macroporous IPN, curve H40/1–G0/0.3 shows conversion of GMA in homogenous IPN, and the curve G0/0.3 shows conversion of GMA monomer during formation of single homogenous PGMA network with no diluent present at polymerization.

Independent experiment on sol extraction was performed in order to confirm the formation of the second network (Figure 25). After the photopolymerization, the hydrogels were glassy, but in a good solvent dimethyl sulfoxide (DMSO) became soft due to the high degree of swelling of PHEMA–PGMA IPN hydrogel in DMSO. Sol was releasing from the network with the swelling of the hydrogel, when network chains were stretched. Gravimetric analysis showed that 15 % of unreacted monomers (sol) were extracted with DMSO from the as prepared PHEMA–PGMA IPN, and, in turn, only 85 % of GMA monomer was transformed into a PGMA network. Obtained data are in a good agreement with ATR FTIR experiments.
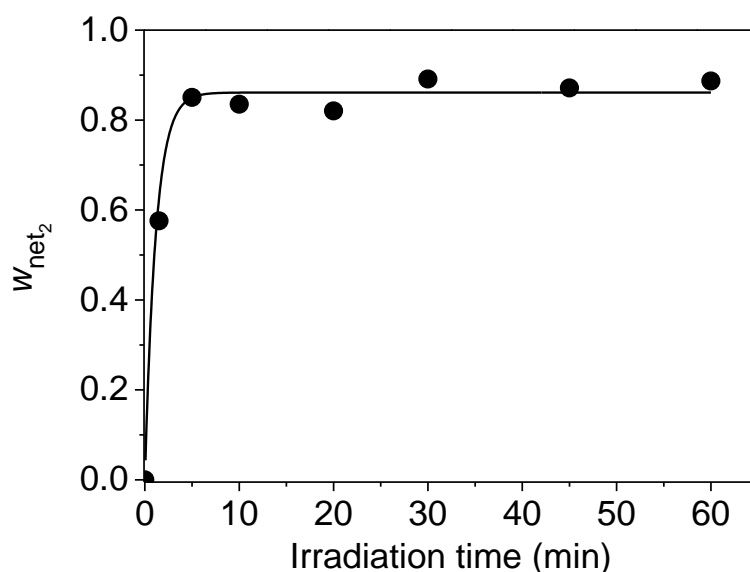
Figure 25. Weight fraction (w_{net2}) of PGMA network 2 forming in PHEMA–PGMA IPNs as a function of irradiation time followed by sol-extraction method.

UV light scattering. To understand the influence of the pre-formed environment of the first poly(2-hydroxyethyl methacrylate) (PHEMA) network on the kinetics of the second network formation, change of the optical properties of polymerizing systems was monitored during the polymerization by UV light scattering. The macroporous matrix PHEMA 80/1 of the fused-sphere morphology swollen in glycerol methacrylate (GMA) reaction mixture observed in visible light was slightly opaque, while the other two systems, PHEMA 40/1 swollen in GMA and single GMA reaction mixture, were visually transparent. Optical extinction of these monomer-swollen gels, and of a reference homogeneous (clear) PHEMA hydrogel swollen in water was measured in a broad wavelength range from 190 to 800 nm. The results are displayed in Figure 26 where only the region below 400 nm relevant for the reaction is shown. The reference system did not absorb light above 250 nm and showed only negligible scattering (cf. Figure 26, magenta line). All the monomer-swollen systems displayed attenuation of transmitted light due to absorption, scattering, and reflection.
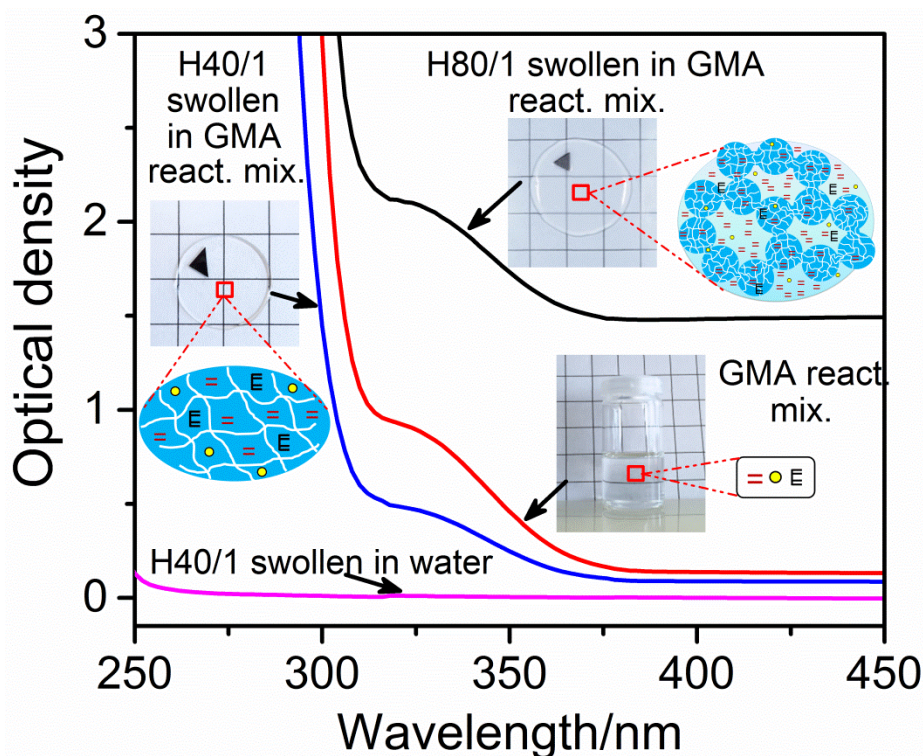
Figure 26. Optical density of macroporous PHEMA 80/1 (black curve) and non-porous PHEMA 40/1 (blue curve) hydrogels swollen in GMA reaction mixture, PHEMA matrix swollen in water (magenta curve), and reference GMA reaction mixture (red curve). Data obtained prior to polymerization, sample thickness was 1 mm in all cases.

All three systems revealed the absorption by the photoinitiator – 2-hydroxy-2-methyl-1-phenyl-propane-1-one (DAROCUR 1173) – seen as a broad extinction band centered at 325 nm. There is an apparent vertical shift of the otherwise similar spectra. Since the reaction mixtures were always the same, but were added to non-absorbing matrices of various morphologies, the difference in optical density (vertical shift) must be caused only by the light scattering effect. Indeed, when the diffusion transmission was measured using an integrating sphere (described in section 3.1.2 of Experimental part), the spectra were almost identical (Figure 27). It can be also seen from Figure 26 that the optical density due to scattering above 375 nm is almost wavelength independent. According to Mie theory it is a typical observation for scattering objects larger than the wavelength of the incident light.
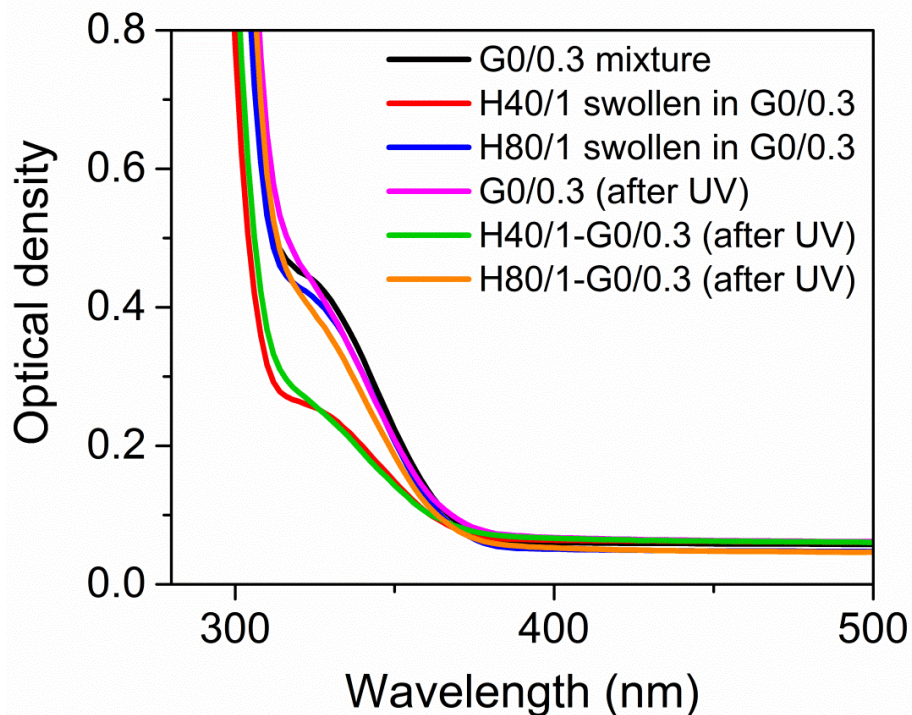
Figure 27. Optical density of gels measured prior and after the polymerization: H80/1-G0/0.3 (blue – prior, orange - after), H40/1-G0/0.3 (red – prior, green – after) and a reference G0/0.3 (black – prior, magenta – after). Measured using integrating sphere, sample thickness 1 mm in all cases.

Due to the light scattering in optically heterogeneous system, the UV beam travels via multiple reflection paths (Figure 28a, b). Through optically homogeneous system, the incident light passed straight forward with minimum scattering (Figure 28c). In the macroporous gel, the difference in the refractive index of swollen PHEMA matrix and GMA monomer mixture caused multiple scattering at the interfaces between the solid matrix and liquid mixture, made the optical path inside the sample longer and greater number of photoinitiator molecules were activated, thus the efficiency of initiation at a given intensity of the incident light was increased. As a result, the reaction run faster in the system with the greatest optical attenuation of the transmitted light. The above described differences in the optical transparency of gel matrices of various morphologies could explain the differences in the kinetics of IPN formation.
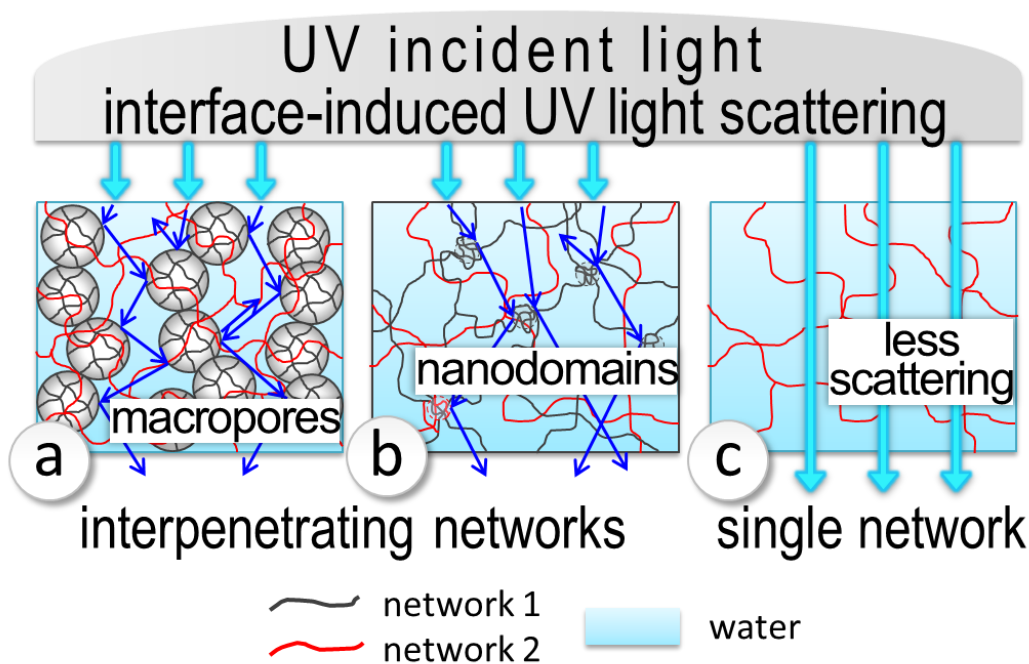
Figure 28. Optical path of UV-beam through the non-uniform (a and b) and uniform (c) polymer matrix.

Photopolymerization was shown to affect the optical density of the crosslinking systems in various ways (Figure 29). Formation of reference PGMA network and PGMA network within the H40/1 matrix was accompanied by an increase in optical density due to increased scattering particularly in the UV range which indicated structuring of the bulk of the samples and formation of inhomogeneities. In contrast, photopolymerization of GMA in the matrix of macroporous H80/1 network led to decrease in optical density implying homogenization of the entire system, as refractive indices of both components in the IPN became very similar. Indeed, the resulting H80/1–G0/0.3 IPN after UV polymerization (prior swelling in water) as well as the other two samples – H40/1–G0/0.3 and PGMA reference were both equally visually transparent and clear. After the polymerization, absorption in UV range in all three systems persists due to the presence of the photoinitiator. As it is known from ATR FTIR experiments that the conversion of C=C double bonds after the irradiation is not complete, some reactive molecules remain in the system.
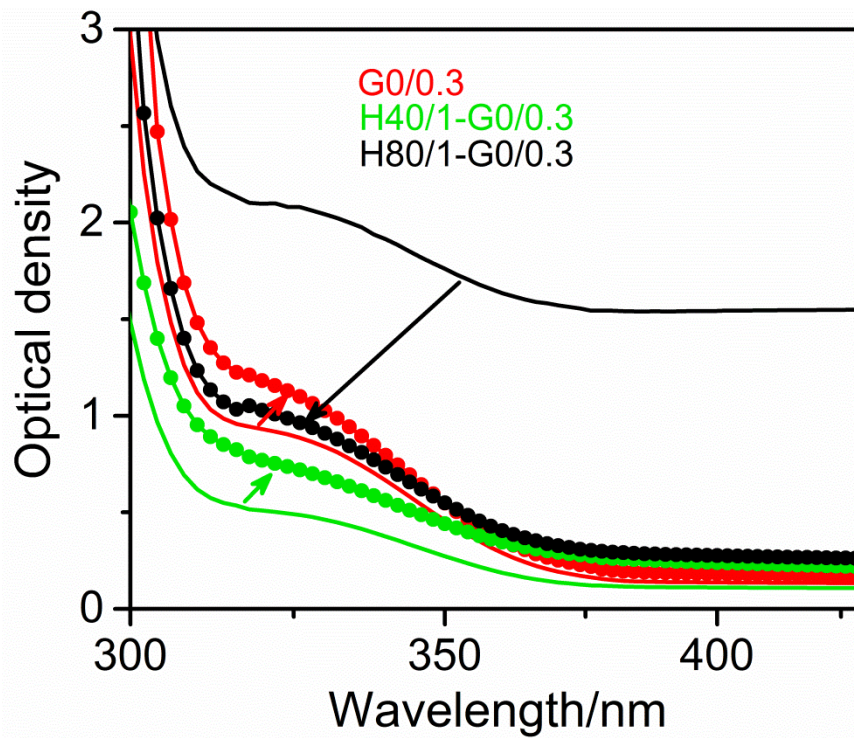
Figure 29. Optical density of the GMA reaction mixture (G0/0.3, red curves) and the same GMA reaction mixture G0/0.3 in the environments of macroporous H80/1 (black curves) and non-porous H40/1 (green curves) single networks before UV irradiation (solid lines) and after irradiation (connected full circles).

2.3. Gelation in single and in interpenetrating crosslinking systems

Formation of single PHEMA and PGMA networks and the second PGMA network structure within the heterogeneous environment of the first PHEMA network was detected by oscillatory shear measurement in dynamic oscillation mode. Since the available rheometer was not equipped with UV cell, the initiation of the polymerization was changed to redox type using the APS/TEMED initiating system and also to thermal type using the AIBN initiator.

The polymerization of HEMA monomer diluted with 40 and 80 wt.-% of water was initiated by the APS/TEMED system (Figure 30). The crosslinking polymerization of these systems under conditions we usually use in our experiments starts quite quickly, so that the manipulations including sample preparation, immersing it into the rheometer and launching the measurement takes somewhat longer time. To manage all the manipulations, record the entire gelation process and catch the gel point, the concentration of TEMED catalyst was reduced 10 times compared to our standard procedure. The gelation of polymers was studied at $T = 25$ °C and $f = 0.05$ Hz by monitoring the storage (G') and loss (G'') shear moduli changing with the reaction time. At the beginning of the reaction, when diluted HEMA reaction mixture formed a low-viscous liquid, the loss modulus characterizing the viscous properties of the sample was higher than the storage modulus characterizing its elastic properties. Each reaction mixture (H40/1 and H80/1) had its own induction period before the crosslinking polymerization started. For H40/1 sample, it was about 26 minutes, while for H80/1 sample − 42 minutes. The more the monomers mixture was diluted, the longer was the induction period. As reaction proceeded, both moduli started to increase sharply and, at a specific reaction time, the storage modulus became larger than the loss modulus indicating the liquid-solid transition. The crossover of both moduli was attributed to gel point previously[133,134]. The position of the gel point on time scale was delayed with the dilution. Both moduli did not reach the plateau by the time the measurement was stopped. Apparently, the gelation of PHEMA was not complete within the measurement time and more time was needed for this. In these gelation experiments, we did not aim to wait for the end of the reaction. However, in our standard synthesis procedures, first, we use higher concentrations of TEMED catalyst and, second, always leave the reaction overnight to achieve the complete conversion of monomers to polymer network.
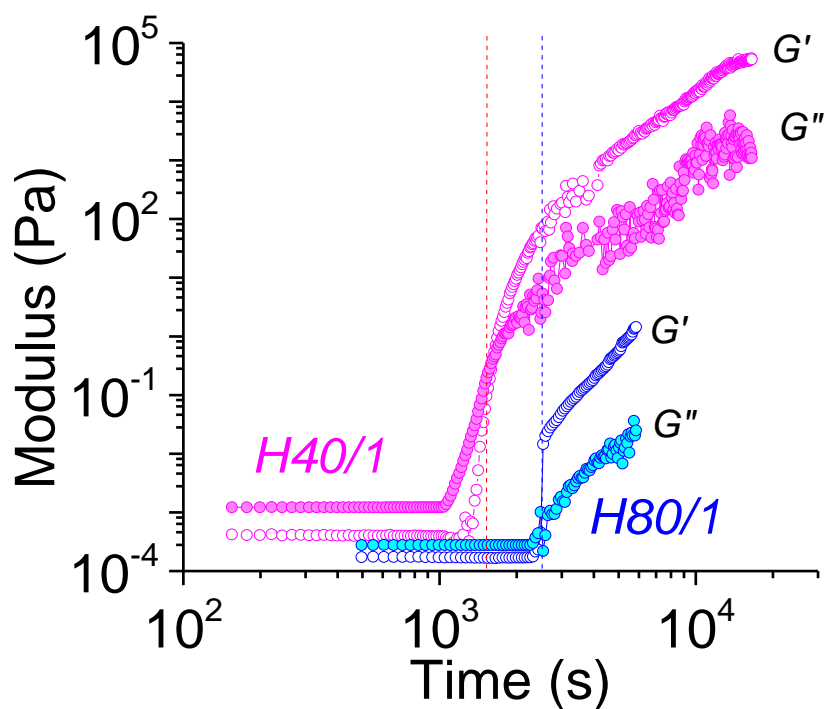
Figure 30. Gelation in water-diluted crosslinking PHEMA systems recorded at frequency of f = 0.05 Hz. The monomers mixtures were diluted with 40 wt.-% (H40/1, magenta curves) and 80 wt.-% (H80/1, blue curves) of water. Redox initiated polymerization with APS/TEMED system at T = 25 °C. Storage, G', (open) and loss, G'', (solid) moduli were recorded.

In-situ gelation of the PGMA in the environment of macroporous PHEMA (H80/1) network was followed by changes in both shear and loss moduli at f = 0.05 Hz (Figure 31). The reaction was initiated with thermal AIBN initiator at T = 70 °C, as it can be dissolved in non-aqueous media such as GMA and DEGDMA monomers mixture. The initial state of the system corresponding to PHEMA network swollen in GMA reaction mixture was "solid-liquid". That is probably the reason for the relatively high values of moduli already at the beginning of polymerization and that the shear modulus (G') exceeded the loss modulus (G''). After a quite long induction period, both moduli started to increase sharply and the system turned from "solid-liquid" to "solid-solid" state via crossover of G' and G'' indicating the gel point[133,134] and, thus, crosslinking of the second PGMA network. Crosslinking of the reference PGMA forming an individual single network was also accompanied with the increase of moduli. Since the reaction mixture was viscous, the G' was slightly higher than G'' at the beginning of the reaction. For both systems, the plateau region indicating

the completion of the reaction was achieved within the measurement time. PHEMA–PGMMA IPN hydrogel in its as prepared state revealed moduli above 1 MPa, which is significantly higher than the moduli of single PGMA and PHEMA networks.
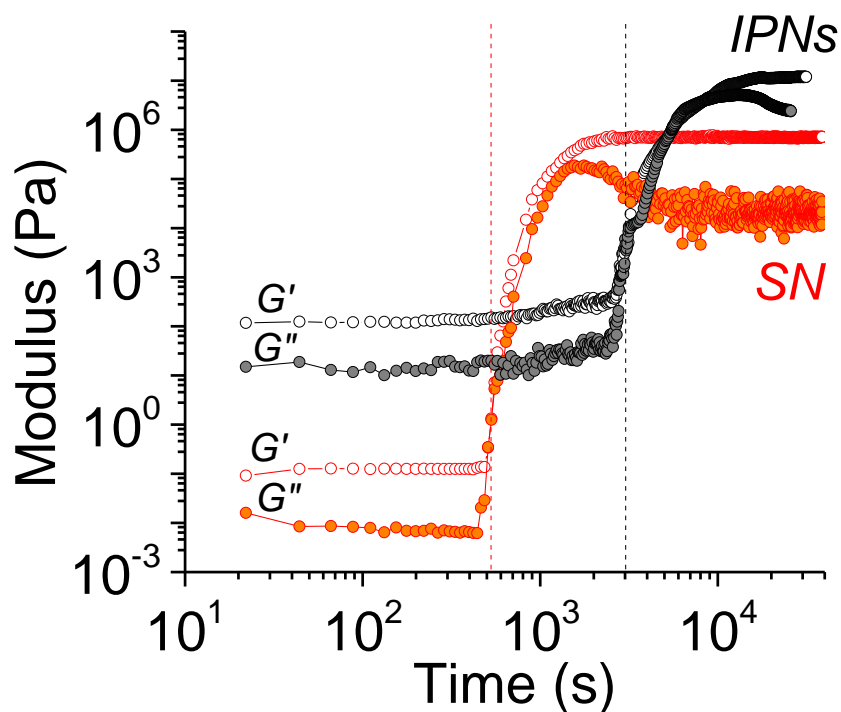
Figure 31. Gelation of PGMA while forming an individual single network (red curves) and while forming IPN in the environment of macroporous PHEMA (H80/1) network (black curves) recorded at frequency of $f = 0.05$ Hz. Thermally initiated polymerization with AIBN at $T = 70$ °C. Storage, G', (open) and loss, G'', (solid) moduli were recorded.

3. Morphology of single network and IPN hydrogels

3.1. Appearance of hydrogels

3.1.1. Single PHEMA networks

Phase separation in single PHEMA networks may occur depending on water content and crosslinker concentration in the initial reaction mixture. In Figure 32, the swollen hydrogels prepared with moderate amounts of water (up to 40 wt.-%) and crosslinker (up to 1 mol-%) are clear. The clarity of H30/3 hydrogel containing relatively high crosslinker concentration (3 mol-%) was achieved by reducing the initial water content in reaction mixture to 30 wt.-%. The transition from clear to fully phase separated white hydrogels passed through opalescent hydrogels lying on the diagonal line – H30/6, H40/3, and H50/1.
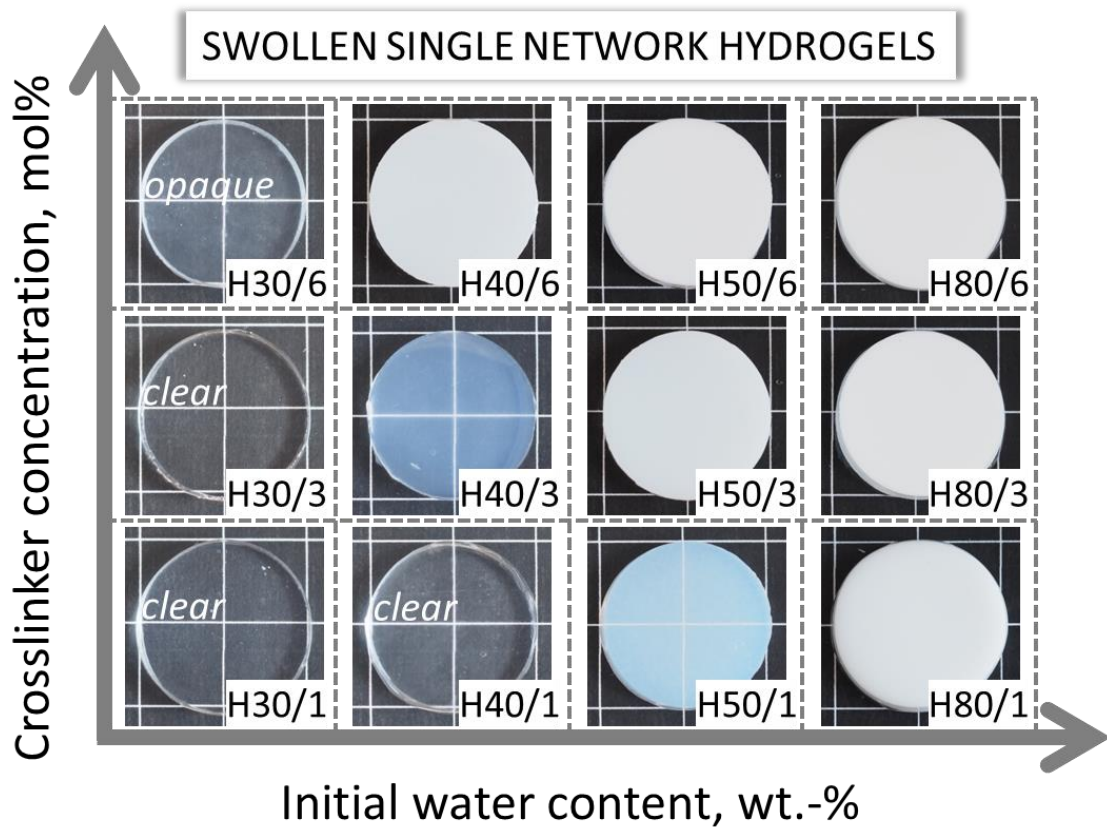
Figure 32. Visual appearance of swollen single network hydrogels: effect of initial water content and crosslinker concentration on the phase separation.

3.1.2. Interpenetrating polymer networks

3.1.2.1. Chemically homogeneous IPNs: PHEMA-PHEMA gels (H40/Y-H0/Z)

The appearance of swollen IPN hydrogels prepared from chemically identical poly(2-hydroxyethyl methacrylate) (PHEMA) networks differing in crosslinker concentration in both networks is presented in Figure 33.
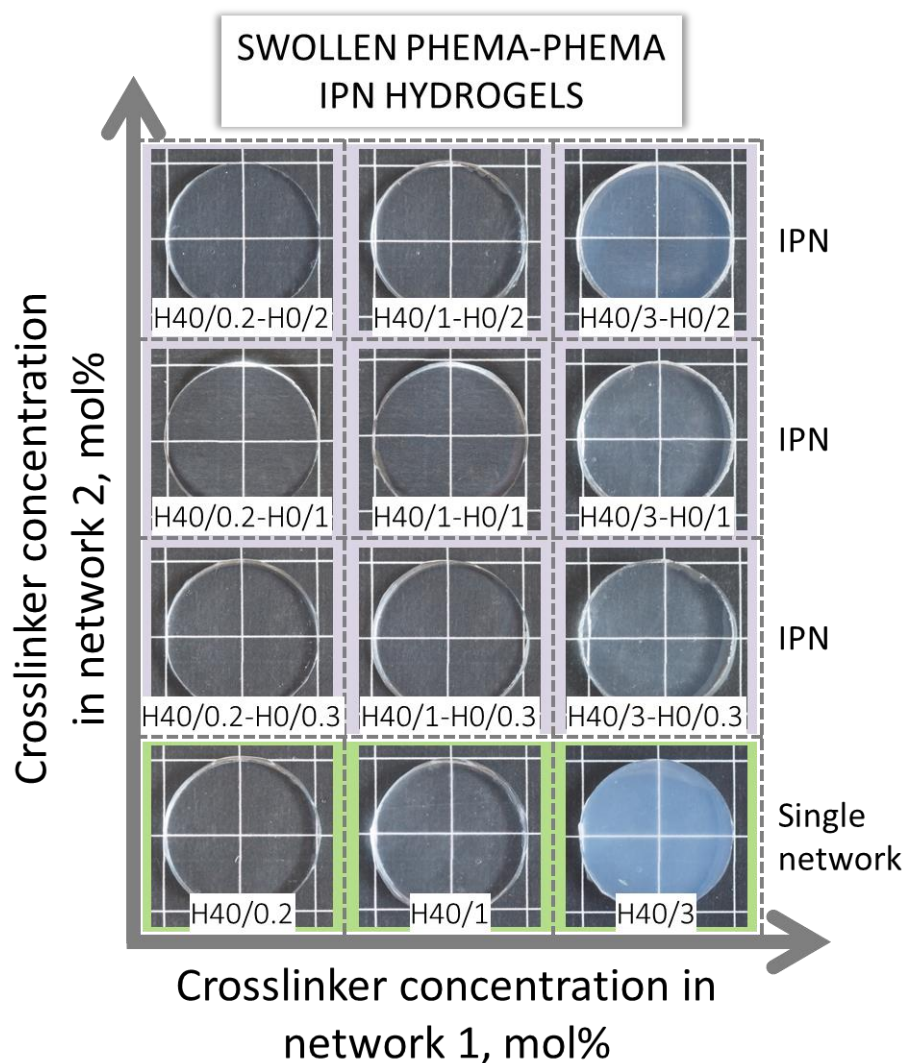
Figure 33. Visual appearance of swollen chemically homogeneous PHEMA-PHEMA IPN hydrogels. The first PHEMA networks were prepared with 40 wt.-% of water and various concentrations of crosslinkers (samples on green background), while the second PHEMA networks of various crosslinker concentrations formed in IPNs structure contained no water at preparation.

The lowest raw of the scheme was occupied by single PHEMA networks 1 prepared with 40 wt.-% of water and three different concentrations of crosslinker

(0.2 mol-%, 1 mol-%, and 3 mol-%). The PHEMA-PHEMA IPN hydrogels were prepared based on these H40/Y networks 1; the crosslinker concentration in network 2 increased in each column. The H40/0.2 and H40/1 based IPN hydrogels were optically clear independently on the crosslinker concentration in network 2. For instance, the H40/1-based IPN hydrogels had almost the same refractive index (RI 1.429-1.430). Introduction of the second network into the matrix of opalescent H40/3 hydrogel led to formation of less opalescent IPN hydrogels. Apparently, the hydrophobic domains of the heterogeneous H40/3 hydrogel became expanded by chains of the network 2 causing the optical transparency of material. Further increase of concentration of hydrophobic crosslinker in network 2 (H40/3-H0/2) led to its accumulation around the expanded due to the swelling hydrophobic domains of network 1. The opalescence in IPNs was occurring only in water indicating the expelling of water from domains due to the aggregation of hydrophobic groups and/or polymer chain segments.

3.1.2.2. Chemically heterogeneous IPNs: PGMA-PHEMA gels (G40/Y-H0/0.3)

Two hydroxyl groups in the structure of glycerol methacrylate monomer (GMA) make the corresponding PGMA network capable to absorb large amounts of water. Water-swollen single network PGMA hydrogels prepared with 40 wt.-% of water and with $0.2 - 6$ mol% of crosslinker were optically clear gels (Figure 34a). Gradual replacement of water with HEMA monomer led to the shrinkage of PGMA gels and change of the appearance of loosely crosslinked PGMA networks from clear to white (Figure 34b). Apparently, the HEMA monomer for PGMA network was thermodynamically worse solvent than water, therefore the polymer-polymer interaction was preferred over the polymer-solvent interaction. The chains of loosely crosslinked G40/0.2 hydrogel had more freedom to fold due to the fewer amounts of crosslinks in network, and therefore, the latter shrank more than tightly crosslinked G40/6 hydrogel.

The folding of polymer chains between crosslinks resulted in heterogeneous network structure with areas of higher polymer density and areas of lower polymer density. Therefore, the optical path of visible light through such network was longer due to the light scattering, and, as a result, we observed a white hydrogel. Due to the higher crosslink density limiting the folding of polymer chains and, hence, the

polymer-polymer interaction, the G40/3 and G40/6 hydrogels remained clear after the swelling in monomer 2 and after the crosslinking polymerization. When the PGMA-PHEMA IPN hydrogels were swollen in water (right column), the phase separation of various extents detectable by eye was observed in all four cases.
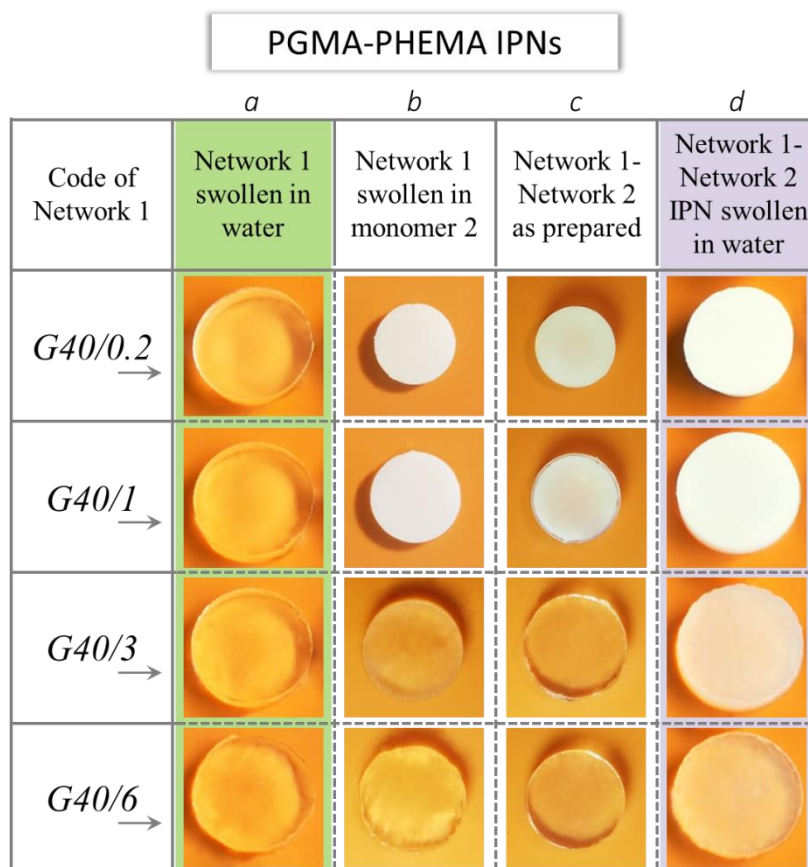
Figure 34. Visual appearance of PGMA-PHEMA IPN hydrogels at each stage of their formation: (a) PGMA network 1 swollen in water, (b) PGMA network 1 swollen in reaction mixture of HEMA monomer 2, (c) PGMA-PHEMA IPN as prepared after crosslinking polymerization, and (d) PGMA-PHEMA IPN hydrogel swollen in water. Single network PGMA hydrogel was prepared with 40 wt.-% of water and various crosslinker concentrations (left column). The second PHEMA network was prepared with no diluent and 0.3 mol-% of DEGDMA crosslinker.

Cryo-SEM micrographs of swollen in water G40/0.2-H0/0.3 and G40/1-H0/0.3 IPN hydrogels showed the existence of pores and polymeric fused-spheres (Figure 35), which are typical for single network PHEMA hydrogels prepared at certain water and crosslinker contents (see Figure 18b).[190] Apparently, pre-formed PGMA network acted as a solvent for the PHEMA second network and caused its

demixing into a separate phase and its separation was easier from the most loosely crosslinked PGMA network (G40/0.2) (Figure 35a).
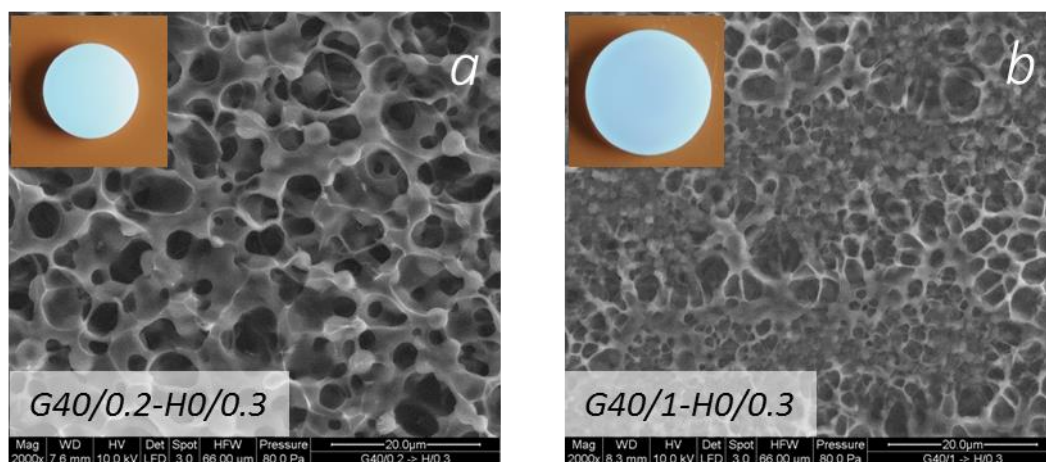
Figure 35. Cryo-SEM micrographs of swollen (a) G40/0.2-H0/0.3 and (b) G40/1-H0/0.3 IPN hydrogels.

3.1.2.3. Microstructured chemically homogeneous and chemically heterogeneous IPN hydrogels

The IPN hydrogels were microstructured because they were prepared within the matrix of macroporous phase-separated H80/1 hydrogel or macroporous cH80/1 cryogel. The process of IPNs formation in both cases is similar. As an example, in this paragraph we describe the entire procedure for fused-sphere morphology H80/1-based IPN hydrogels. Each step is represented by a sketch describing the morphology of gels and the states of networks, and by a photograph exhibiting the appearance of gels (Figure 36).

The macroporosity of the PHEMA network 1 was achieved by phase separation of excess water (poor solvent) occurring during polymerization (Figure 36a). The type of macroporosity is determined by the amount of water and by the cosolvency of HEMA–water mixtures.[148] As a result, for the H80/1 composition, a soft and opaque (white appearance) PHEMA network of low elastic modulus was obtained while the gels Hx/1 ($x = 0 - 40$) were fully transparent. Being polar and hydrogen-bonding, the HEMA and GMA easily permeated the pre-formed PHEMA hydrogel. The sample volume increased by factors 10 and 12 for HEMA and GMA, respectively, (see section on swelling properties) and the network chains in the pore walls were stretched accordingly.
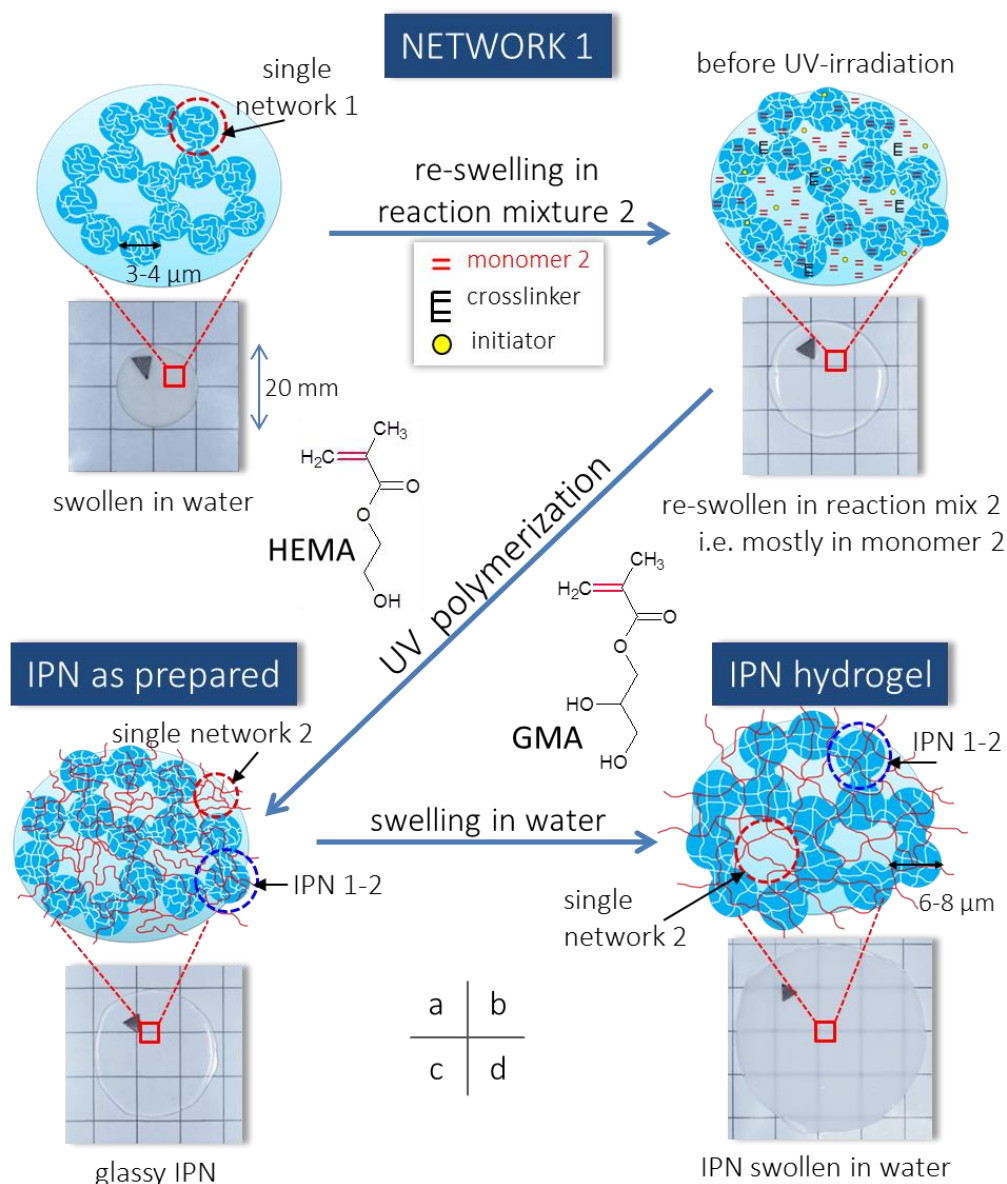
Figure 36. Evolution of macroporous PHEMA–PGMA IPN (H80/1–G0/0.3) morphology and transparency of hydrogels: (a) macroporous PHEMA network 1 (H80/1) swollen in water; (b) PHEMA network 1 swollen in GMA monomer 2; (c) loosely crosslinked PGMA network 2 formed in the matrix of tightly crosslinked PHEMA network 1 as well as in pores of the hydrogel; (d) PHEMA–PGMA IPN hydrogel swollen in water.

When macroporous and white PHEMA hydrogel was swollen by HEMA or GMA monomer, the "white" system became translucent but optically not fully clear (Figure 36b) and turned transparent again after UV-polymerization – the non-swollen

(glassy) IPN was fully transparent irrespective of whether the network 2 was PHEMA or PGMA (Figure 36c). The homogeneous IPNs were formed only in the PHEMA polymer matrix, whereas the pores of hydrogel were filled with the single PHEMA or PGMA network. The chains of PHEMA network 1 in the pore walls were stretched due to the swelling in the monomers, while the chains of the second network remained in their unperturbed state. When immersed in water, the IPNs swelled: the initially glassy IPNs turned soft and flexible. The swollen PHEMA–PHEMA IPN hydrogel remained transparent up to the content of water at first network polymerization 40 %, while the PHEMA–PGMA hydrogel became opaque. The differences in transparency of the swollen IPNs can be explained by match or mismatch of refractive indices between both phases caused primarily by different content of water. In the case of PHEMA–PHEMA IPN, the swelling degree of PHEMA matrix and PHEMA in pores is almost the same whereas the PGMA polymer in pores swells in water much more than in the interpenetrating matrix. The morphology of IPN gels influenced substantially their mechanical strength and swelling.

3.2.   Microscopy of single network hydrogels and cryogels

3.2.1. *Non-porous and single-porous gels*

The morphological structure in hydrogel "native", equilibrium swollen state, of the reference single H80/1 network and the H80/1–G0/0.3 IPN hydrogel was visualized by the laser scanning confocal microscopy (LSCM) and the images are shown in Figure 37. LSCM has the advantage that it can focus on thin parallel layers within the object and see the structure in the range of wavelengths of visible light although the object is non-transparent in transmitting visible light. PHEMA is non-fluorescent, but it can be labeled with dyes. For visualization of the morphology of single network PHEMA hydrogel, soaking it in 0.01 wt.-% PBS solution of fluorescein was the most straightforward way of sample visualization that worked. LSCM micrograph of swollen H80/1 hydrogel depicted the fused-sphere structure formed due to the reaction-induced phase separation with macropores between the sphere clusters, a structure ensuring bicontinuous topology (image a). Pore size varied in the range 10–15 μm, while the average size of spheres was approximately 2–4 μm. The cH80/1 cryogel consisted of large elongated and partially interconnected cell-like pores of characteristic dimensions: 50-200 μm long and 20-

60 μm wide (image b). While the G0/0.3 hydrogel prepared without dilution of monomers mixture was non-porous (image c). All considered samples were also observed in their swollen state by means of cryo-SEM technique. As seen from Figure 37 (images d, e and f), cryo-SEM and LSCM data are in a good agreement.
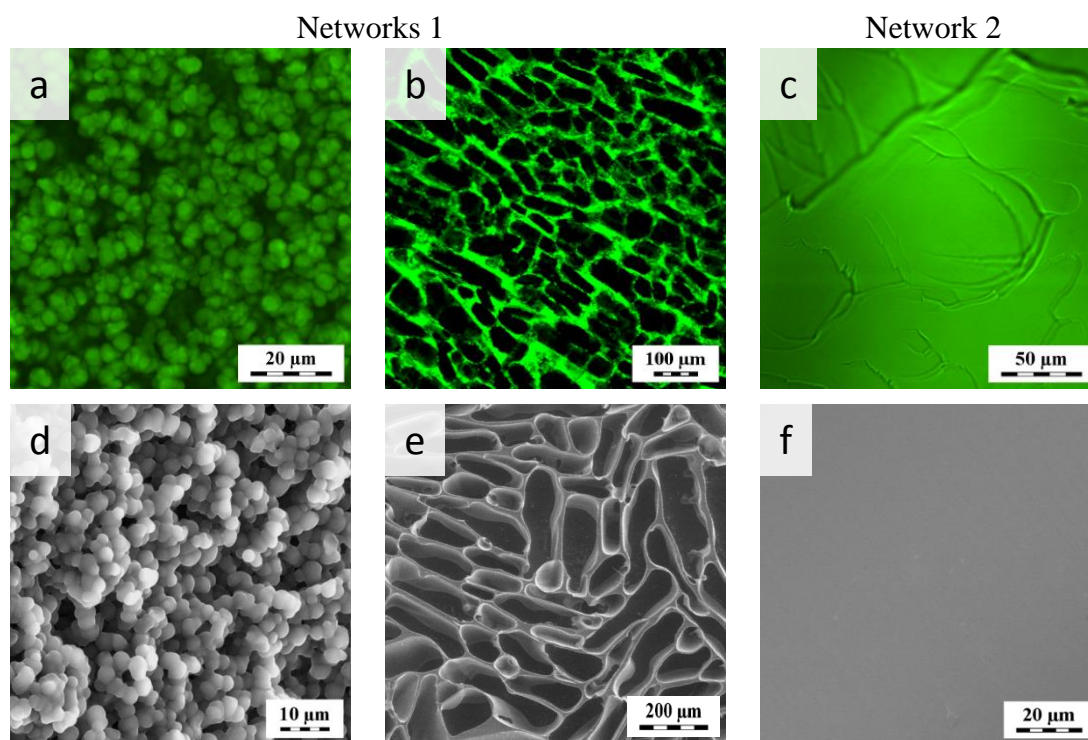
Figure 37. Laser scanning confocal microscopy (a, b, c) and cryo-SEM (d, e, f) micrographs of single network hydrogels swollen in water: H80/1 network 1 (a and d) and cH80/1 network 1 (b and e), and G0/0.3 network 2 (c and f).

3.2.2. Double-porous cryogels

In this work, we present an alternative route for synthesis of double-porous cryogels implying a parallel formation of large and small pores (Figure 38). Large pores were caused by ice crystals forming during the crosslinking polymerization of diluted with water reaction mixture under cryo-conditions (T = -14 °C). This method was described by Lozinsky[191,192] et al. Small pores in the walls of cryogel were caused by reaction-induced phase-separation due to the presence of aqueous solution of sodium chloride acting as the "salting-out" agent. The existence of pores of both types made them interconnected. Such procedure has not been reported before.

Cryogelation is practically feasible as requires only a low temperature. But not always the pores of single-porous cryogels obtained by such way are completely

interconnected. Mutual connections between pores are important in terms of proliferation of cells within the entire sample. Such highly porous morphology of PHEMA cryogels is supposed to be a perfect biocompatible substrate for cell growth. Figure 38 reveals the morphology of PHEMA cryogels prepared at very high dilution (95 wt.-% of diluent and only 5 wt.-% of monomers in the reaction mixture). One gel was prepared in the presence of pure water only, while the second gel was prepared in the presence of 0.5 M NaCl solution. The morphology of both cryogels was studied using light microscopy (images a and b) and cryo-SEM (images c and d). In pure water, the cryogel exhibited a single-porous structure (images a and c), while the "salting-out" effect of 0.5 M NaCl solution caused a double-porous structure (images b and d).
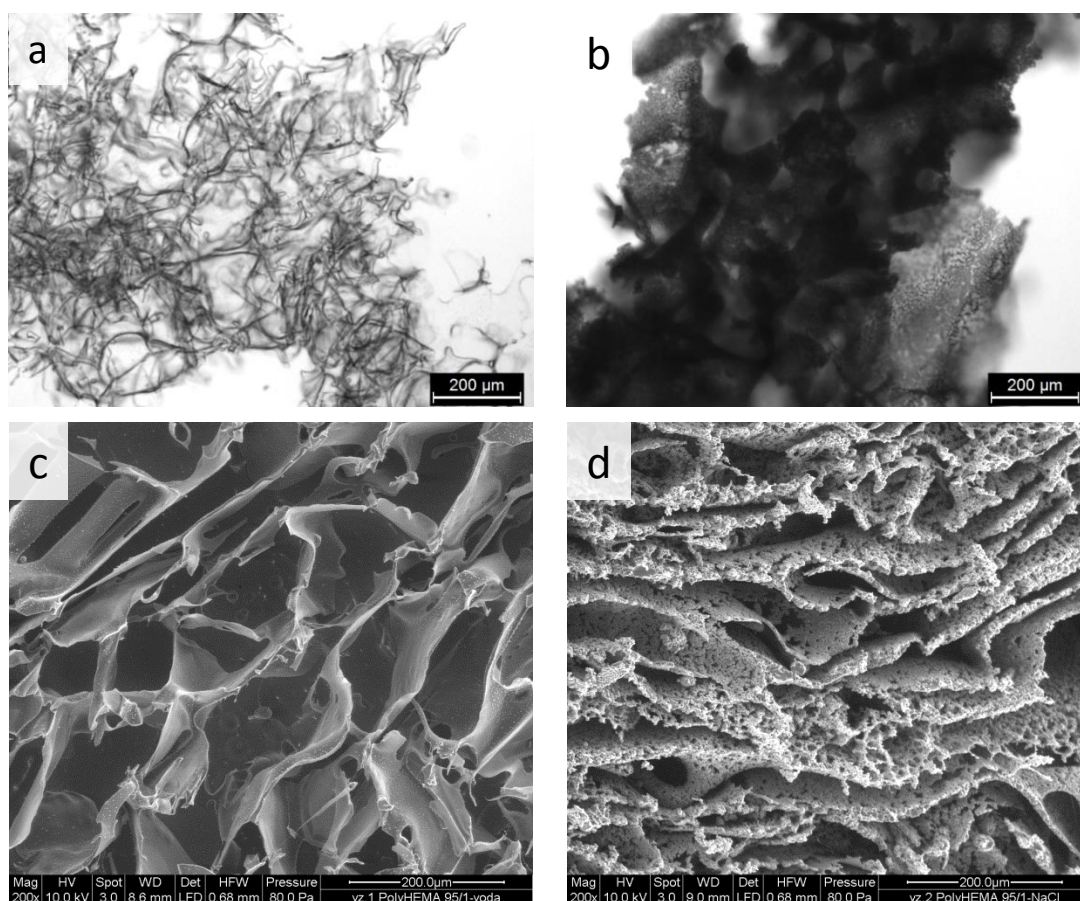
Figure 38. Single-porous and double-porous PHEMA cryogels prepared at dilution of 95 wt.-% of pure water (a, c) and 95 wt.-% of 0.5 M NaCl solution (b, d). Light (a and b) and cryo-SEM (c and d) microscopes were used to observe the morphology of swollen cryogels.

3.3. Interpenetrating network hydrogels

In the case of swollen IPN hydrogel, to observe the two distinct network phases, swelling in fluorescein or other dye solution would not be an appropriate method, since the dyes are not selective towards the studied networks. Therefore, each network was chemically labeled by incorporating the fluorescein and DY-677 dye molecules modified before with functional double bonds (C=C) groups able to copolymerize with network structure. Single network H80/1 was modified with functionalized fluorescein while the second network copolymerized with traces of functionalized DY-677. Excitation wavelengths of the dyes were different (495 nm and 673 nm), so that distribution of networks within the IPN could be visualized using the multi-staining mode of the LSCM. Thus, the darker greenish color on the micrograph a of Figure 39 represents the areas with the highest amount of initial PHEMA network interpenetrated with the second network, while a brownish color spots show the location of the neat second PGMA network. The mixing of color channels revealed blending of the both networks within the spheres as well as continuous transitions between the double network spheres and single network interstices. As the result of addition of the second network, size of spheres in swollen IPN hydrogel as well as size of pores (Figure 39) increased compared with H80/1 hydrogel (Figure 37a).
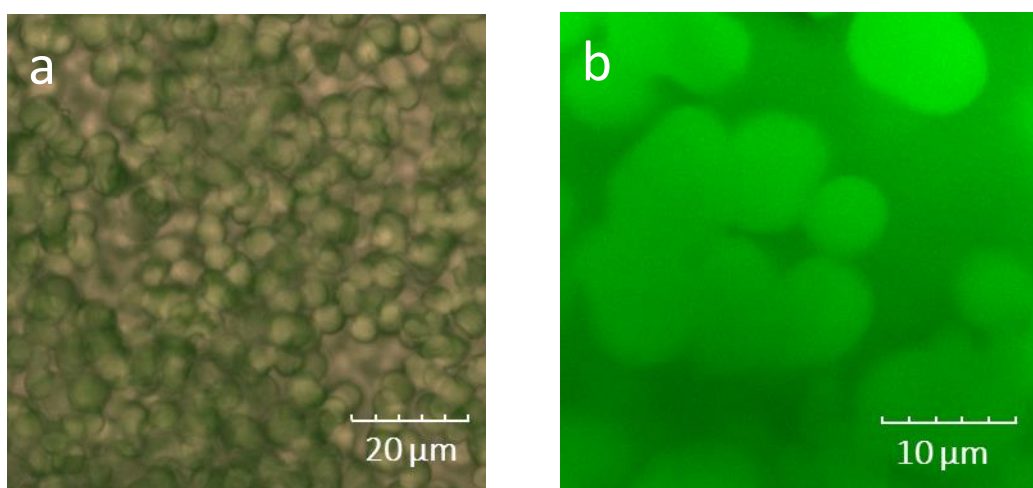
Figure 39. LCSM of H80/1-G0/0.3 IPN hydrogels: (a) network 1 (H80/1) and network 2 (G0/0.3) labeled with fluorescein and DY-677 dye, respectively, and (b) non-labeled network 1 (H80/1) and network 2 (G0/0.3) labeled with fluorescein.

In Figure 39b, there is the same kind of PHEMA-PGMA hydrogel, but differently stained. The first PHEMA polymer network was not labeled, while the modified fluorescein with C=C double bonds was added into the reaction mixture of the second PGMA network. Molecules of fluorescein are low molecular weight, quite mobile and can be differently distributed between fused polymer spheres and pores upon swelling of the first PHEMA gel in the reaction mixture of the second PGMA network. Once the equilibrium swelling is achieved and the system is polymerized, the double bonds of fluorescein get covalently bonded within the polymer chains and become irreversibly embedded in the structure of the second network. All the unreacted molecules of fluorescein and GMA/DEGDMA monomers were washed out from the hydrogel before the observation of its morphology by confocal microscopy. Such method was used to label the second network with the purpose to see the pores and to confirm the formation of the second network in the spheres of the matrix. It was shown, that the PGMA network was formed in the fused spheres of the first network as well as in pores; and no new pores were formed upon polymerization.

The intensity of fluorescein in spheres was higher than in pores. This could be explained by different swelling of polymer chains. Hydrophilic chains of PGMA network in pores are able to absorb large amount of water, while the unfolding of chains of PGMA network in fused spheres is restricted due to the interpenetration with the polymer chains of PHEMA.

3.4. Microstructure of hydrogels and its formation determined by x-ray scattering

3.4.1. PHEMA H40/1 hydrogel

The inhomogeneities developing during formation of single and interpenetrating networks and in swollen gels were characterized by Small-Wide Angle X-Ray Scattering (SWAXS). Figure 40 shows the development of inhomogeneities during PHEMA polymerization in the range of $q = 0.05 - 1$ Å^{-1}, which corresponds to distances $d \sim 10 - 0.5$ nm. The presence of diluents can be an important source of inhomogeneities.[193] If polymerization takes place in the presence of water (Figure 40), the scattering intensity increases in this region with increasing conversion of monomer to polymer and flat maxima develop at $d \approx 1$ nm and $d \approx 5$ nm. The first one may indicate intramolecular association of a few methyl groups of

the monomer units. The maximum in the region $d \approx 5$ nm seems to reflect (intermolecular) association of several network chains assisted by strengthening of iceberg structures of water. The formation of hydrophobic moieties invokes the existence of regions more dilute in polymer segments; since the polymer segments occupy a larger volume at these subcritical concentrations than the diluent molecules do, it is conceivable that the "organic" associates are continuous. SWAXS data are in a good agreement with dynamic light scattering measurements performed for monomers diluted by water (cf. Figure 47, paragraph 3.4.4).
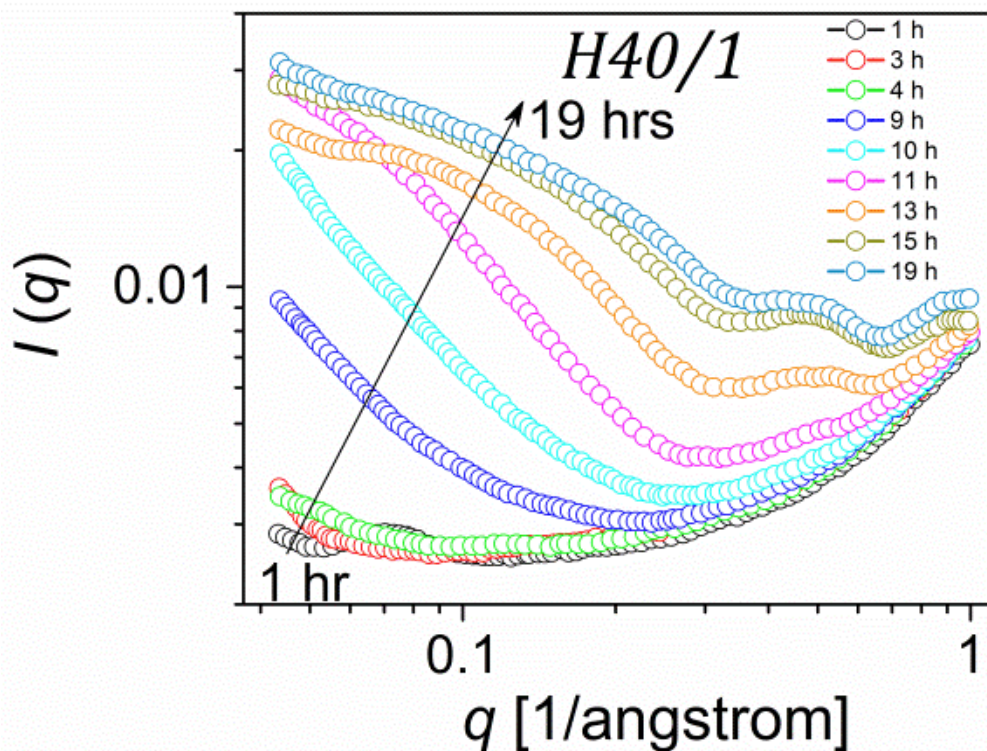
Figure 40. SWAXS dependencies for crosslinking polymerization of H40/1 gel in pure water. The polymerization was initiated with ammonium persulfate without adding TEMED to slow down the reaction to be able to record the SWAXS spectra as they develop in time.

To better understand the character of density fluctuations in H40/1 hydrogel, the spatial distribution of molecules in the network should be characterized by the type of structure growth and their fractal dimensions. For this purpose, we used a power law to analyze the SAXS curves within the small-q-region:

$$I(q) = I(0)q^{-p} \qquad \text{(Equation 4.1)}$$

where p is related to the fractal dimensions (D) and $I(0)$ is the prefactor. p is related to either the mass (D_m) or the surface (D_s) dimension of the structures:

$$p = D_m \ (p < 3)$$

$$p = 6 - D_s \ (3 < p < 4) \qquad \text{(Equation 4.2)}$$

The mass fractal dimension (D_m) is the characteristic of the "openness" of the fractal object containing branching and connecting structure. D_m equals to 1 for loosely connected aggregates with indistinct interfaces and to 3 for dense aggregates. The surface fractal dimension (D_s) is the characteristic of the surface of fractal object, which equals to 3 for fractals of rough surface and to 2 for fractals of smooth surface. The power law exponent p was calculated from the slope of $I(q) - q$ graph presented in logarithmic scales (Figure 40). As the crosslinking polymerization of H40/1 hydrogel preceded, the values of p changed from 0.46 up to the maximum at 1.18 and then decreased to 0.9 after 19 hours of reaction (Figure 41). Generally, H40/1 hydrogel prepared in the presence of water has a p value below 3, which corresponds to mass fractals represented by loosely connected domains with indistinct interface structure. The characteristic size of these physically crosslinked domains can be represented by the radius of gyration (R_g) determined from the slope of $\ln I(q) - q^2$ graph in the low-q-range. The size of domains (R_g) in structure was about 1.1–1.2 nm.
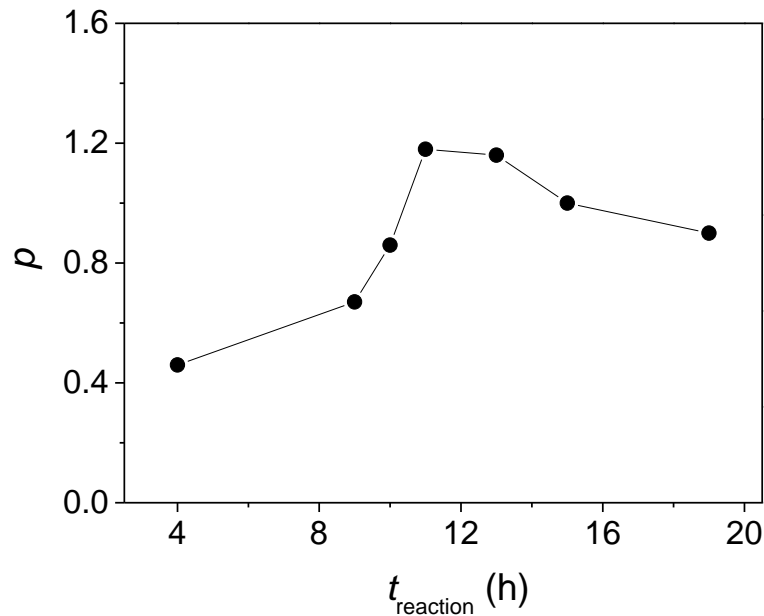
Figure 41. Power law exponent p at H40/1 crosslinking polymerization time $t_{reaction}$.

When instead of water a diluent was used that is thermodynamically better than water, the scattering behavior was quite different. Figure 42 shows the situation when 40 wt.-% of 0.5 M aqueous solution of magnesium perchlorate, which is a salting-in environment for PHEMA[194] polymer, was used as diluent. The HEMA can be diluted by such solutions without any limits and all resulting gels are clear unless $Mg(ClO_4)_2$ solution[190] is replaced by water or polymer solution is formed below critical dilution. In the q-range of $0.07 - 1$ Å^{-1}, the scattering intensity did not increase and the gel appeared as structure-less. Apparently, the presence of $Mg(ClO_4)_2$ in water prevented the iceberg structuring of water molecules, and thus, association of monomers forming small domains. The scattering in the q-range of $0.01 - 0.07$ Å^{-1} was caused by larger objects. An important observation was that all curves refracted at the same $q = 0.033$ Å^{-1} ($d \approx 19$ nm), having two slopes, indicating the parallel development of two types of inhomogeneities – smaller ($d < 19$ nm) and larger ($d > 19$ nm) objects of different fractal structures.
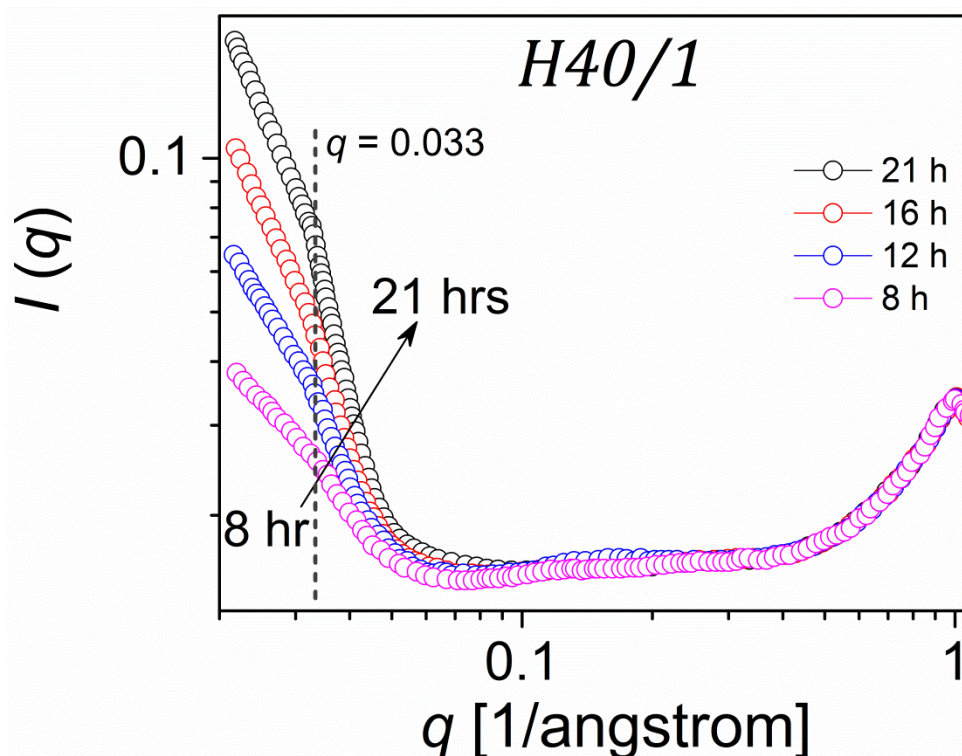
Figure 42. SWAXS dependencies for crosslinking polymerization of H40/1 gel in the aqueous solution of 0.5 M $Mg(ClO_4)_2$. The polymerization was initiated with ammonium persulfate without adding TEMED to slow down the reaction in order to be able to record the SWAXS spectra as they develop in time.

The part of the curve lower the refracting point $q = 0.033$ Å^{-1} corresponded to mass fractals with D_m between 0.9 and 2.1, while the part higher the refracting point corresponded to fractals, which at the beginning of reaction had mass dimensions and at the end of reaction had surface dimensions (Figure 43a). The latter indicated that the loose mass fractals with indistinct surface ($p = 1.1$) became dense surface fractals with smooth surface ($p = 3.9$). The R_g of mass fractals increased from 2.6 nm to 4.3 nm, while of mass-surface fractals increased from 2.3 nm to 4.6 nm (Figure 43b).
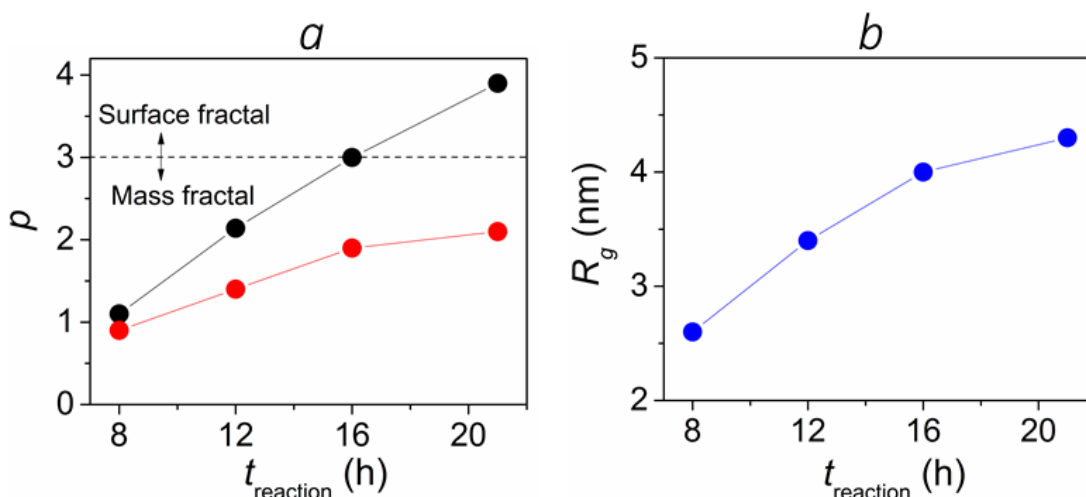
Figure 43. Power law exponent p (a) and the radius of gyration R_g (b) at H40/1 crosslinking polymerization time $t_{reaction}$. Hydrogel was polymerized in the salting-in aqueous solution of 0.5 M Mg(ClO$_4$)$_2$.

3.4.2. Formation of PHEMA-PHEMA IPN hydrogel

In this part, we will discuss the SWAXS data for interpenetrating networks and analyze the structure changes during the IPNs formation. Now, the difference is in that the "diluent" is initially HEMA monomer (plus small amount of crosslinker) and the monomer is converted into polymer, in contrast to preparation of H40/1 network 1 (Figure 44), where the initial diluent was HEMA-water mixture which was depleted by the monomer until water remained at the end of polymerization. While the small-scale association maximum at $q = 0.5$ Å^{-1} has disappeared completely, the scattering intensity at $q = 0.05$ Å^{-1} remained still high but the shape of the curve changed (Figure 44). We think that it means that the transient part of the hydrophobic effect has disappeared – in fact there is no reason for its existence because HEMA is a UCST solvent and does not form icebergs. However, the relatively high intensity at $q = 0.05$ Å^{-1} suggests that the largest inhomogeneities have been fixed by the meshes

of network 1 and have survived the structural reorganization. Apparent is the overall decrease of scattering with increasing conversion but the explanation is prosaic: by transforming the HEMA monomer 2 into the same polymer as is PHEMA network 1, the electron density difference (contrast between domains) decreases and eventually vanishes. After 30 minutes of irradiation no structural changes in network formation were observed.
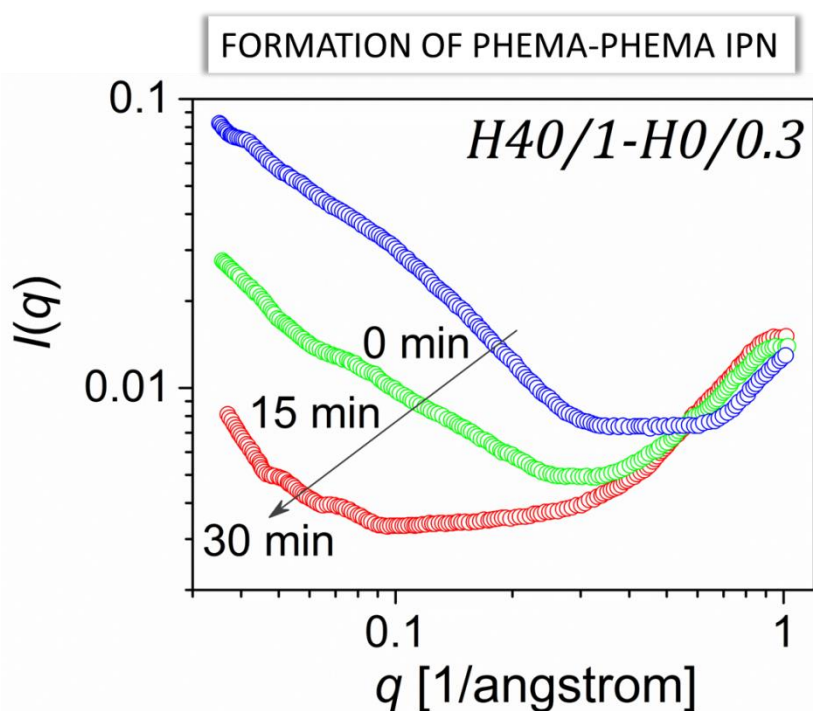
Figure 44. Changes of structure during the UV-initiated crosslinking polymerization of the H0/0.3 network 2 in the matrix of the H40/1 network 1 followed by SWAXS. Irradiation times: 0 min (blue), 15 min (green), 30 min (red).

The effect of crosslinker concentration in the second network is shown in Figure 45. The qualitative composition of both IPNs was identical; the only difference was in the amount of crosslinker (diethylene glycol dimethacrylate, DEGDMA) added into the reaction mixture of the second network. Two cases were considered: (1) when the second H0/0.3 network was loosely crosslinked as compared with the first H40/1 network, and (2) when the second H0/2 network was highly crosslinked as compared with the first H40/1 network. A general character of H40/1-H0/2 network formation was similar to that shown in Figure 45, but the electron density fluctuations in it were even less.
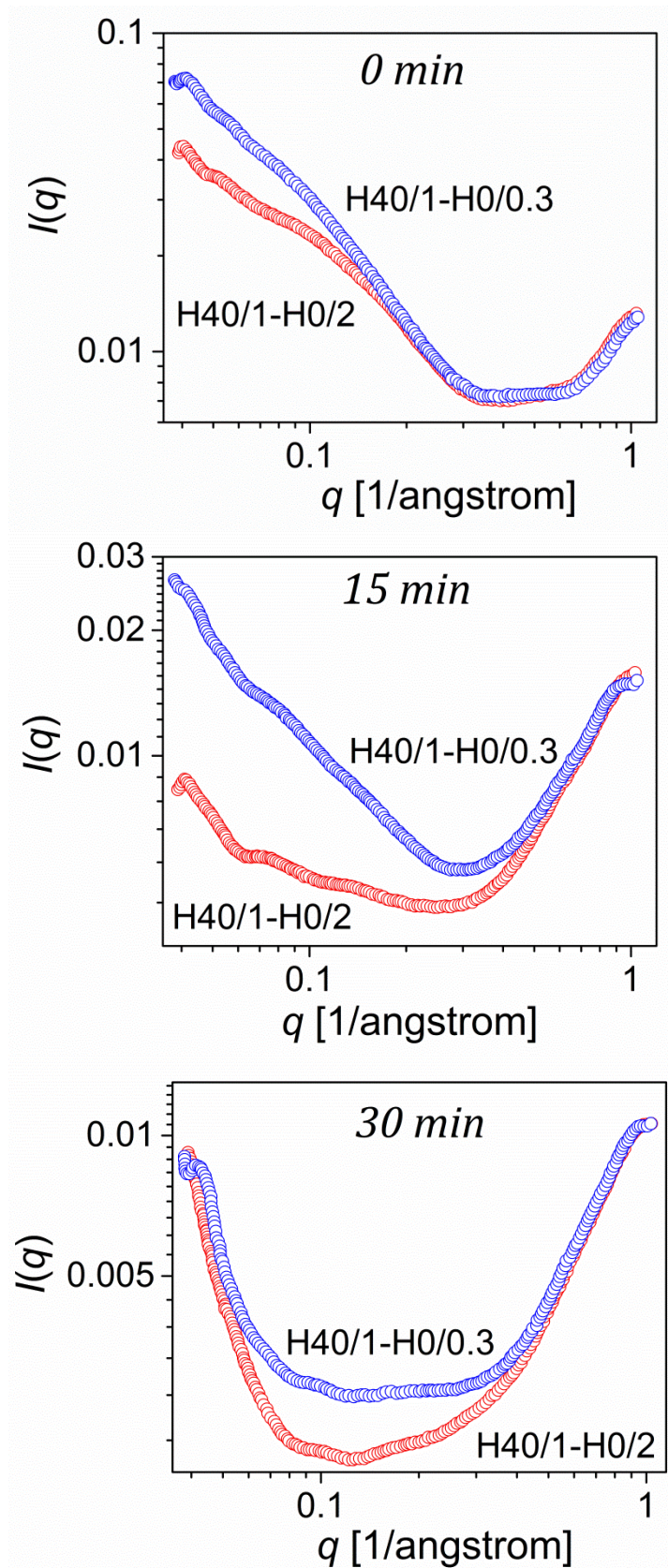
Figure 45. Changes of structure during the UV-initiated crosslinking polymerization of the H0/0.3 (blue curves) and H0/2 (red curves) networks 2 in the matrix of the H40/1 network 1 followed by SWAXS.

3.4.3. Comparison of H40/1 single network and H40/1-H0/0.3 IPN hydrogel

The differences in structures of H40/1 single network and H40/1-H0/0.3 IPN in as prepared state and in equilibrium swollen state are compared in Figure 46. Inhomogeneities increased with networks swelling and became more pronounced.[45]
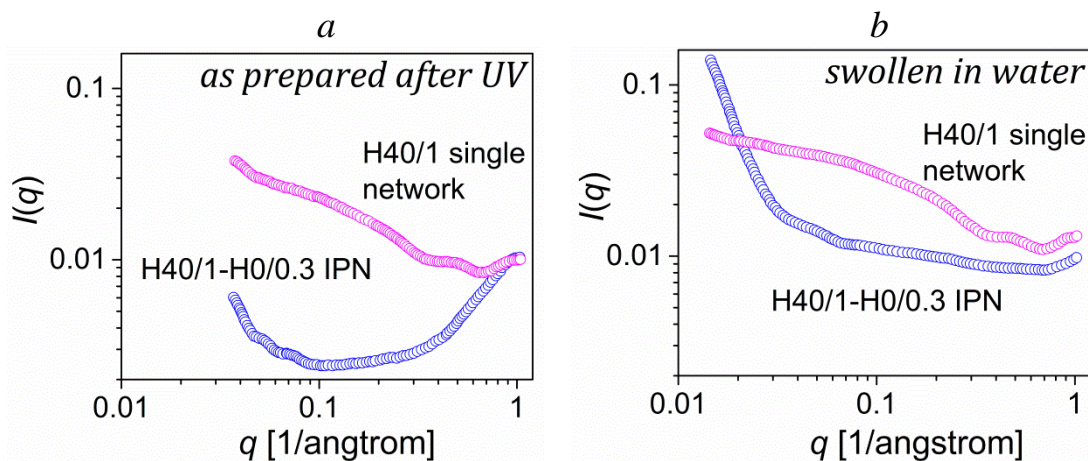
Figure 46. Comparison of structure changes by SWAXS. Single network H40/1 (magenta curves) vs. H40/1-H0/0.3 IPN (blue curves) in (a) as prepared state and (b) equilibrium swollen state.

Figure 46b shows that the inhomogeneity at $q > 0.02$ Å^{-1} remained intact even when the structure-forming solvent (water) penetrated the network. Apparently, the intermeshed structure of the IPN prevented the chains or their parts from reorganization. Also, the expansion of chains of H40/1 network 1 in the IPN made the small scale intramolecular segmental association as well as the larger-scale intermolecular chain association difficult. On the other hand, the small-angle scattering at $q < 0.02$ Å^{-1} has increased indicating the presence of large size aggregates. The scattering intensity for swollen single H40/1 network was only slightly increased compared to its as prepared state. In both states, the networks were soft and contained similar amounts of water corresponding to similar networks structure. While after the water-free crosslinking polymerization of PHEMA network 2 (H0/0.3) within the matrix of PHEMA network 1 (H40/1), the obtained H40/1-H0/0.3 IPN system was in a glassy state. After its swelling in water, the size of all inhomogeneities increased, and the overall intensity and the intensity of small-angle scattering due to large aggregates increased as well.

Concluding this section, we can say we have solid indications that in the

presence of water as diluent, the inhomogeneities were formed due to different concentrations of polymer segments in volume caused by intramolecular association of methyl groups of the monomer units and intermolecular association of several network chains assisted by strengthening of iceberg structures of water. Utilization of thermodynamically better diluent such as aqueous solution of $Mg(ClO_4)_2$ prevented the association of monomers into small domains due to the inability of water molecules to form iceberg structures. Small scale domains also disappeared when the HEMA monomer was swollen to network 1, but a part of domains of larger size remained in system and was fixed by the network 2. These fixed inhomogeneities reappeared in the water swollen interpenetrating network, whereas the smaller associates were prevented from reforming apparently due to internetwork perturbations and expansion of chains of network 1.

3.4.4. Dynamic light scattering measurements

The organization of molecules of both monomers (HEMA or GMA) into clusters (hydrophobic domains) when diluted with water was observed by dynamic light scattering technique (Figure 47a). The concentration of monomers was varied in the range from 0.5 wt.-% up to 98 wt.-%. Figure 47a shows that mixing of monomer with water was accompanied by the formation of aggregates, the size of which depended on concentration. Mixtures poor of monomer (< 10 wt.-%) or water (< 2 wt.-%) contained small aggregates (up to 1.7 nm). When the concentration of monomers was in the range of $10 - 80$ wt.-%, the formed aggregates were of larger size: $2 - 4.2$ nm for GMA and $3.6 - 5.6$ nm for HEMA. Both curves passed through the maximum at monomer concentrations: 30 wt.-% of HEMA and 80 wt.-% of GMA. Dilution of HEMA molecules with water resulted in continuous increase of size of aggregates, as poor affinity of monomer molecules to water made the monomer-monomer interaction more preferable than that between monomer and water. However, too high dilution of HEMA monomer (90 wt.-% of water) characterized by increase of entropy led to the fact, that diluent pulled the monomer molecules away from each other evenly distributing them in the bulk and preventing the formation of too large aggregates, i.e., the entropy factor prevailed over the energy of monomer-monomer interaction. In the same time, dilution of GMA monomer ($20 - 99.5$ wt.-% of water) caused the homogenization of mixtures by forming considerably smaller aggregates. Indeed, the hydrophilic GMA molecules

with two hydroxyl groups are very well interacting with water molecules, so that increase of entropy with dilution of monomer easily obstructs the aggregation of monomer molecules. There must be already some organization of molecules in GMA monomer, since, on the one hand, it contains hydrophilic hydroxyl groups and hydrophobic methacrylate fragments, and on the other hand, it always contains traces of isomers and water, which may affect the organization of GMA molecules. Addition of 2 wt.-% of water into the otherwise viscous GMA monomer was so insignificant, that the entropy factor caused by such low dilution became negligible and almost did not affect the size of aggregates.
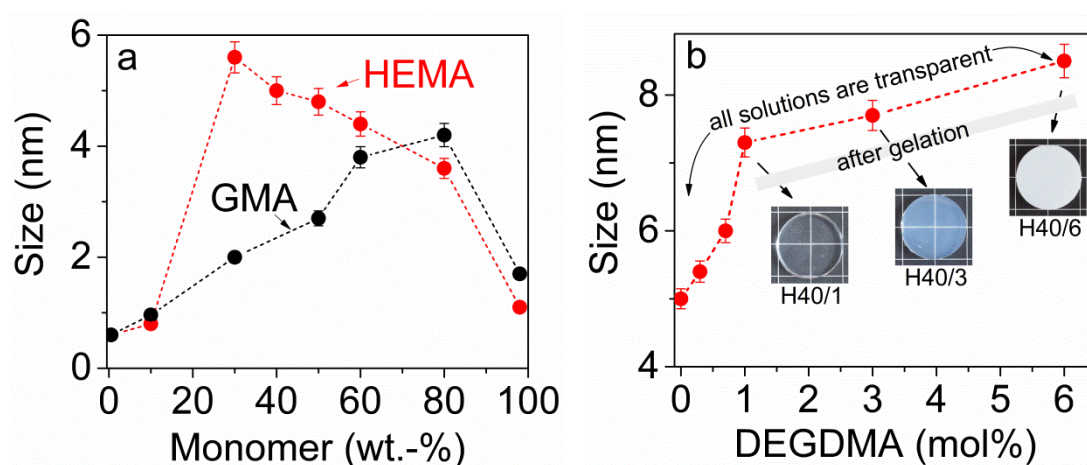
Figure 47. Size of aggregates in aqueous solutions of monomers determined by dynamic light scattering method: (a) HEMA or GMA monomers mixed with water at various ratios, (b) HEMA monomer (60 wt.-%) mixed with water (40 wt.-%) and DEGDMA crosslinker (0 – 6 mol-%).

Addition of more hydrophobic diethylene glycol dimethacrylate (DEGDMA) crosslinker with two double bonds at the ends of the molecule into the HEMA:Water = 60:40 mixture led to increase of aggregates size from 5.0 nm to 8.5 nm with the increase of crosslinker concentration (Figure 47b). The size of aggregates at 1 mol-% of DEGDMA crosslinker was about 7.3 nm, which is in a good agreement with the SWAXS data. All solutions within the investigated range of crosslinker concentrations were optically transparent, though at submicroscopic level they were inhomogeneous. After crosslinking polymerization, the heterogeneity of gels structure containing 3 and 6 mol-% of DEGDMA appeared already at macroscopic level for gels (bluish and white gels on photo).

4. Swelling properties of hydrogels

4.1. Swelling effect on gel vitrification

Thermal and viscoelastic properties of gels are governed by swelling change. PHEMA hydrogels prepared without dilution are hard and glassy materials already at room temperature, while the dilution of monomers at preparation prevents the vitrification at room temperature and shifts the glass transition temperature (T_g) to lower values making the gel viscoelastic and soft. Generally, T_g decreases as the weight fraction of low molecular additives acting as plasticizers increases. In Table 4, experimentally determined glass transition temperatures for gels and temperatures found in the literature are shown. The values of T_g are affected by method of measurement, but, in general, our experimental data are in consistent with literature data. Crosslinking polymerization of the reference single GMA network and the GMA network polymerized within the PHEMA matrices without water revealed almost the same T_g (85 – 86 °C). The values of T_g after the polymerization, when unreacted monomers were still present in network, were lower than after sol extraction because sol acted as a plasticizer for network and shifted the T_g to lower values. The final T_g of xerogels (dried gels) was in the range of 108 – 112 °C. The T_g of reference PHEMA and PGMA single networks were very similar, therefore in PHEMA–PGMA IPN gels constituent networks were indistinguishable in terms of segmental mobility.

Table 4. DSC determination of glass transition temperature (T_g) of as prepared networks after the polymerization and dried network after the extraction of sol-fraction by washing in distilled.

Sample	T_g after polymerization (^{0}C)	T_g after sol extraction (^{0}C)	T_g from literature (^{0}C)
	as prepared gels	*dried gels*	
H40/1-G0/0.3	84	112	n/a
H80/1-G0/0.3	85	111	n/a
PGMA 0/0.3	85	108	84.4 [195], 105 [196,197]
PHEMA 80/1	86	113	113 [198]

4.2. Swelling of single networks

4.2.1. Hydrogels and cryogels

Swelling values of polymer networks are governed by the effect of initial water content, crosslinker concentration and morphology. Water is infinitely miscible with a neat HEMA monomer, but it is a poor solvent for PHEMA. Therefore, as crosslinking polymerization proceeds, the reaction mixture, containing HEMA monomer and water as major components, gets richer in water and phase separation ("microsyneresis") occurs at critical conversion of C=C double bonds[148]. Indeed, different dilution of HEMA monomer contributes to different morphology of gels – non-porous and porous.[190] Swelling values of such hydrogels prepared at different dilutions and at constant crosslinker concentration (1 mol-% of DEGDMA) are plotted in Figure 48 as the reciprocal volume fraction of polymer in swollen hydrogel ($1/\phi_2$) and the reciprocal volume fraction of the monomer in the initial reaction mixture ($1/\phi_2^0$). The diagonal line on the graph corresponds to the situation when ϕ_2 = ϕ_2^0, which means that the volumes of samples after the polymerization and at equilibrium swelling after sol extraction remain constant. The field above this line points out to samples, which are gaining additional water from the surroundings and expand in volume. This was the case of PGMA hydrogels. In case of PHEMA hydrogels, all points were either on line (water content at gel preparation < 80 wt.-%) or below it (water content at gel preparation > 80 wt.-%) regardless of crosslinker concentration (1 mol-% or 6 mol-%). The former indicated the shrinkage of hydrogel after the polymerization due to the separation of the excess liquid from a bulk phase, so-called "macrosyneresis". Thus, the samples with high initial water content reveal both "macro-" and "microsyneresis".
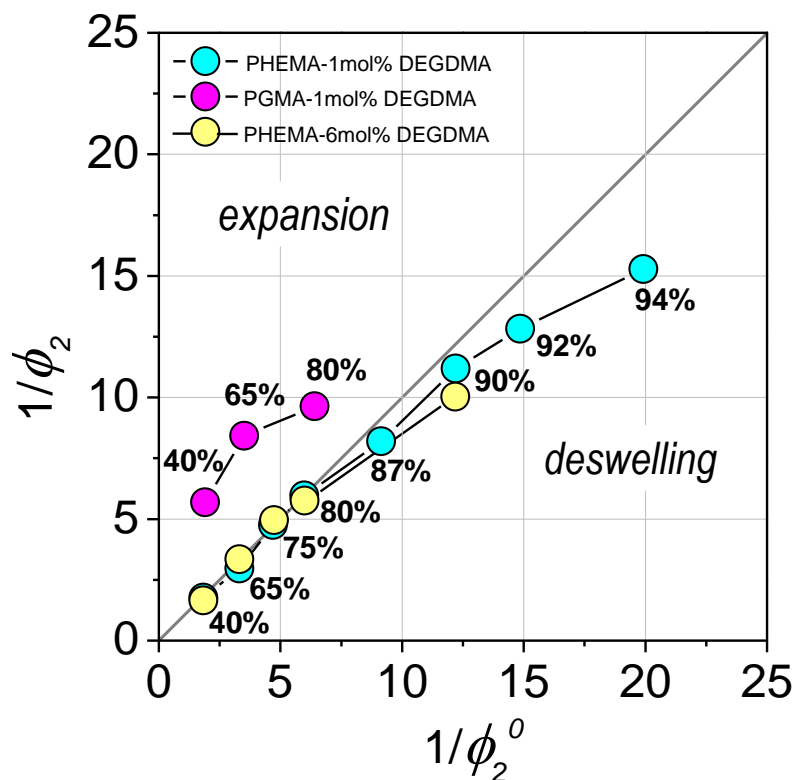
Figure 48. Equilibrium volume of swollen gel per volume of the dry polymer versus reciprocal volume fraction of the monomer in the initial mixture corrected for polymerization contraction. PHEMA hydrogels contained various amounts of water (30 – 94 wt.-%) and concentration of DEGDMA crosslinker (1 mol-% and 6 mol-%) at preparation. PGMA hydrogels contained various amounts of water (40 – 80 wt.-%) and constant concentration of DEGDMA crosslinker (1 mol-%) at preparation.

In Figure 49, similar graph is plotted for HEMA and GMA hydrogels prepared at constant dilution (40 wt.-%), while the DEGDMA crosslinker concentrations varied (0.2 – 6 mol-%). At first, one should note that two series of samples are on opposite sides from the line – PGMA gels gained additional water after polymerization, while the volumes of PHEMA gels remained the same or slightly decreased at high crosslinker concentration indicating the expelling of water from the hydrogel. More densely crosslinked PHEMA hydrogel tend to expel more water than loosely crosslinked hydrogel, but the difference within the series was not significant. Whereas the swelling of PGMA hydrogels after polymerization was enormous, especially for loosely crosslinked networks.
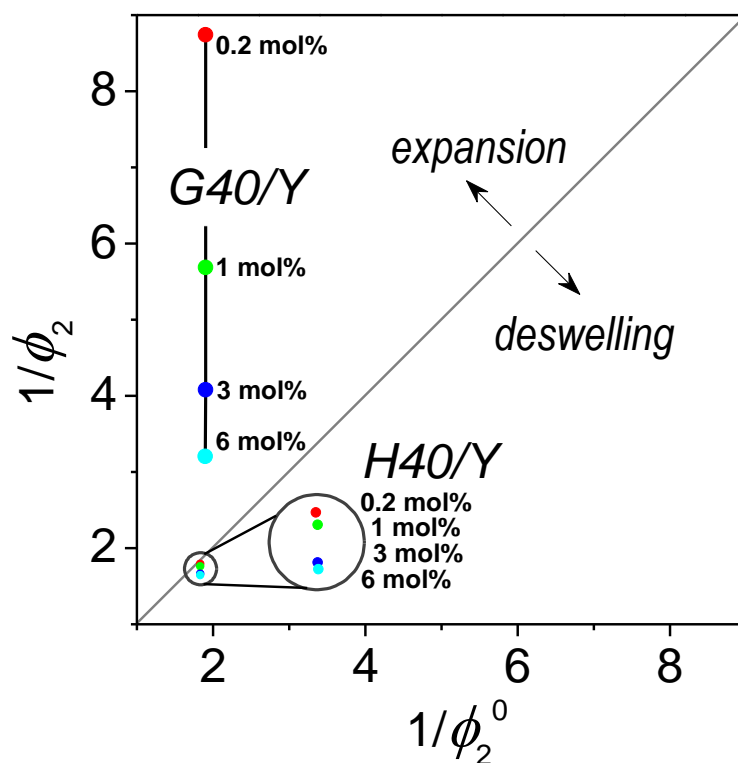
Figure 49. Effect of DEGDMA crosslinker concentration (0.2 − 6 mol-%) in single H40/1 or G40/1 network hydrogels on swelling properties. Equilibrium volume of swollen gel per volume of the dry polymer versus the reciprocal volume fraction of the monomer in the initial mixture corrected for polymerization contraction.

Swelling behavior of single network hydrogels polymerized under different conditions was studied in water, HEMA and GMA monomers, and dimethyl sulfoxide (DMSO). Degrees of swelling (Q_v and Q_m) determined from volume and mass changes of swollen and dry gels as well as equilibrium solvent content (ESC) values are summarized in Table 5. The swelling of macroporous gels compared to non-porous ones in all four solvents was obviously better. In the case of macroporous gels, the weight degree of swelling was always higher than their volume swelling because the pores were filled in with solvents. DMSO is shown to be the best solvent for all single network gels studied here, as it can suppress the physical interactions caused by association of hydrophobic parts of methacrylate polymer chains and enormously stretch the network, which is held together only by chemical crosslinks.[190]

The influence of polymerization conditions on swelling properties of porous gels was very clearly demonstrated for H80/1 hydrogel versus cH80/1 cryogel. The chemical composition of both gels was absolutely the same. The only difference was

in temperature of polymerization (room temperature vs. $T = -14$ °C). Nevertheless, it was shown that the total water content in cryogel was lower than that in hydrogel. The explanation of such behavior implied the consideration of networks morphology, namely, the spatial distribution of polymer matrix as well as pores in the same volume. In contrast to prepared at room temperature H80/1 hydrogel, the phase separation in which occurred due to the immiscibility of polymer with diluent, the pores in cH80/1 cryogel were caused by formation of large ice crystals pushing the monomers reaction mixture away. The LSCM micrographs revealed that H80/1 hydrogel consisted of large number of small pores, while the cH80/1 cryogels − of small number of large pores (Figure 37). Such morphology certainly affects the total fraction of pores in macroporous gels, which was confirmed by direct and indirect porosity (P) determination tests (Table 6). *Direct* tests included:

(a) equilibrium swelling of polymer matrix of preliminary lyophilized sample in water vapor followed by application of Equation 3.8 (see experimental part):

$$P = \frac{m_{sw} - m_{sw}^{V}}{m_{sw}}$$

where (m_{sw}) is the weight of sample fully swollen in water and (m_{sw}^{V}) is the weight of sample, the gel phase of which is swollen in water vapor.

(b) filling in the pores of macroporous samples with indifferent to polymer matrix cyclohexane followed by application of Equation 3.9 (see experimental part):

$$P = \frac{m_{sw}^{CH} - m_{d}^{L}}{m_{sw}^{CH}}$$

where (m_{sw}^{CH}) is the weight of sample, the pores of which are filled with cyclohexane, and (m_{d}^{L}) is the weight of dried by lyophilization sample.

Whereas *indirect* way of porosity estimation included the assumption, that the swelling of polymer matrix is similar to that of non-porous H40/1 hydrogel, and the porosity can be calculated from equilibrium swelling of samples in water and HEMA monomer (cf. Appendix 2). Comparing the porosity of both samples, one can find that it was approximately 6–10 % higher for H80/1 hydrogel (Table 6), while the swelling degree (SD) of polymer matrices in water for both hydrogel and cryogel determined using Equation 3.6 was almost the same (32 vs. 34 wt.-%) and corresponded to swelling of non-porous PHEMA hydrogel in water. The swelling

behavior of H80/1 hydrogel and cH80/1 cryogel differed in water as well as in monomers (HEMA and GMA), but it was very similar in DMSO (Table 5).

Table 5. Swelling parameters of single network hydrogels prepared in different ways: volume degree of swelling (Q_V), mass degree of swelling (Q_m), and equilibrium solvent content (ESC).

Sample	Polymerization conditions	Swelling parameters[a]		
		Q_v	Q_m	ESC
Swelling in WATER				
H0/0.3	UV (DAROCUR 1173) at RT	1.53	1.56	0.56
G0/0.3	UV (DAROCUR 1173) at RT	4.42	3.79	2.79
H0/1	Thermal (AIBN) at T = 70 °C	1.65	1.59	0.59
H40/1	Redox (APS/TEMED) at RT	1.61	1.66	0.66
H80/1	Redox (APS/TEMED) at RT	3.71	5.40	4.40
cH80/1	Redox (APS/TEMED) at T = -14 °C	3.51	4.84	3.84
Swelling in HEMA monomer				
H0/0.3	UV (DAROCUR 1173) at RT	2.99	2.74	1.74
G0/0.3	UV (DAROCUR 1173) at RT	1.34	1.24	0.24
H0/1	Thermal (AIBN) at T = 70 °C	2.77	2.77	1.77
H40/1	Redox (APS/TEMED) at RT	4.60	3.57	2.57
H80/1	Redox (APS/TEMED) at RT	10.05	11.24	10.24
cH80/1	Redox (APS/TEMED) at T = -14 °C	6.28	10.46	9.46
Swelling in GMA monomer				
H0/0.3	UV (DAROCUR 1173) at RT	2.78	3.42	2.42
G0/0.3	UV (DAROCUR 1173) at RT	3.02	2.71	1.71
H0/1	Thermal (AIBN) at T = 70 °C	3.30	3.35	2.35
H40/1	Redox (APS/TEMED) at RT	4.80	4.33	3.33
H80/1	Redox (APS/TEMED) at RT	11.59	13.97	12.97
cH80/1	Redox (APS/TEMED) at T = -14 °C	6.64	13.47	12.47
Swelling in DMSO				
H0/0.3	UV (DAROCUR 1173) at RT	5.14	5.15	4.15
G0/0.3	UV (DAROCUR 1173) at RT	7.79	6.57	5.57
H0/1	Thermal (AIBN) at T = 70 °C	6.30	5.10	4.10
H40/1	Redox (APS/TEMED) at RT	6.42	7.11	6.11
H80/1	Redox (APS/TEMED) at RT	14.72	20.84	19.84
cH80/1	Redox (APS/TEMED) at T = -14 °C	14.69	20.83	19.83

[a]swelling parameters expressed for volumes: $Q_v = V_{sw}/V_d$ and for weights: $Q_m = m_{sw}/m_d$ and ESC = $(m_{sw} - m_d)/m_d$, while the sample dry volume, V_d, was determined by drying the sample to its constant weight at 100 °C under pressure reduced using the oil pump.

Another observation was that the swelling in water vapor of lyophilized dry polymer matrices results in shrinkage accompanied by transition from rigid to soft

and elastic state (cf. Table 6, inserted photographs). The most significant volume shrinkage of 58 % was observed for H80/1 hydrogel against 21 % for cH80/1 cryogel. Lyophilization is based on the fixation of macroporous structure of gels preventing the collapse of pores. Also this method may cause permanent changes in structure and cracks depending on sample preparation conditions. Quick freezing of swollen samples led to prompt formation of ice crystals not only in pores, but also in polymer matrix. Sublimation of ice from the entire sample resulted in dry macroporous gel with "frozen" structure of stretched polymer chains of network, in which residual stress was retained. Subsequent swelling of polymer matrix in water vapor increased the mobility of network chains and the entropy; stretched chains tend to release the residual stress and take up energetically favorable conformations. As during the swelling in vapor pores were not filled in with solvent, but water may be condensed on walls, the total volume of gel decreased because of chain relaxation compared to its initial dry state. The less shrinkage of cryogel was caused by lower pore fraction.

Table 6. Porosity of H80/1 hydrogel and cH80/1 cryogel calculated and determined experimentally by swelling of polymer matrix in H_2O vapor and filling in the pores by cyclohexane. Photographs on the right hand side demonstrate the volume transitions of H80/1 and cH80/1 polymer matrices from lyophilized dry state to swollen in water vapor state.

GEL	Porosity				Swelling degree
	Calculated		Experimental		
	H_2O	HEMA	H_2O vapor	Cyclohexane	H_2O vapor
H80/1	0.71	0.73	0.70	0.73	0.32
cH80/1	0.62	0.63	0.64	0.62	0.34

H80/1 hydrogel — rigid (dry), soft (swollen), Porosity ≈ 0.72, 10 µm

cH80/1 cryogel — rigid (dry), soft (swollen), Porosity ≈ 0.63, 200 µm
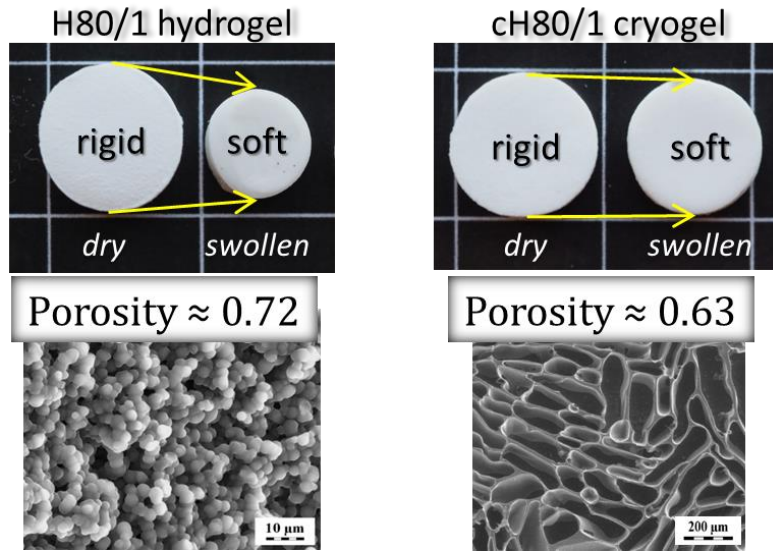
The macroscopic gel volume changes are important for space filling issues and are relevant for characterization of state of coiling of network chains. Adopting the usual assumption that network chains are in their reference states at network formation (nf), the dilation factor of network chains α is defined by the ratio of actual volume V to the volume at network formation V_{nf}

$$\alpha = \sqrt[3]{V/V_{nf}}$$

(Equation 4.3)

The data in Table 7 represent the expansion of polymer chains in non-porous and macroporous single network gels when they are swollen in water, HEMA and GMA monomers, and dimethyl sulfoxide (DMSO). The polymer chains of single network gels prepared with no water are in their non-stretched state-of-ease (H0/0.3, H0/1, G0/0.3), i.e., $\alpha = 1$. In water, the expansion of chains of H0/0.3 and H0/1 networks was about 15 % and 18 %, while in DMSO, it was 73 % and 85 %, respectively. The polymer chains of PHEMA gels prepared in the presence of water are already pre-stretched. The extent of stretching increases with the dilution of monomers reaction mixture. Chain expansion in initially non-stretched H0/1 network and initially pre-stretched H40/1 network after the swelling in water was almost identical and equal to 17-18 % ($\alpha = 1.18$ for H0/1 and $\alpha = 1.17$ for H40/1). As shown in Figure 46, the H40/1 and H80/1 hydrogels neither gain additional water after the polymerization when immersed into water nor shrink, which means that equilibrium swelling of hydrogel corresponds to initial water content. Hence, the expansion of chains of both as-prepared and equilibrium-swollen gels is the same.

106

The macroporous H80/1 hydrogel and cH80/1 cryogel have similar expansion of polymer chains in water and DMSO. Water is the worst solvent in this series of solvents and, therefore, not able to stretch chains of both gels significantly. DMSO, on the contrary, stretches chains to high extent while disturbing the physical hydrophobic interactions. The dilation factor of cryogel becomes lower than of hydrogel only when gels are swollen in monomers, which are solvents of moderate power in this series.

Table 7. A complete set of dilation factor (α) values for networks 1 and networks 2: calculated for equilibrium swollen single networks in water, monomers, and dimethyl sulfoxide (DMSO).

Hydrogel		Dilation factor, α			
		in water	in HEMA	in GMA	in DMSO
networks 1	H0/1	1.18	1.40	1.49	1.85
	H40/1	1.17	1.66	1.69	1.86
	H80/1	1.55	2.16	2.26	2.45
	cH80/1	1.52	1.84	1.88	2.45
networks 2	H0/0.3	1.15	1.44	1.41	1.73
	G0/0.3	1.64	1.10	1.45	1.98

4.2.2. Swelling of single network PHEMA gels in monomer–water cosolvents

Swelling of single PHEMA networks in monomers can be improved by employing water as a cosolvent. Considerable expanding of polymer chains in such monomer–water mixture attributed to the so called "cosolvency phenomenon" provoked by co-existence of molecules interacting with both hydrophilic and hydrophobic groups of polymer chains and making the polymer-polymer interaction less preferable. Indeed, monomer molecules interact with hydrophobic groups, while water molecules interact with hydroxyl groups of network. Swelling of PHEMA hydrogels in pure monomers (HEMA or GMA) was higher than that in pure water. But the highest swelling of hydrogels regardless of their morphology was observed in mixtures with equal amounts of monomer and water (Figure 50). When the concentration of one of the components increased, the swelling parameter shifted to lower values. The presence of two hydroxyl groups in GMA molecule made it self-

sufficient to interact with both hydrophobic and hydrophilic groups of polymer chains, so that the addition of water had no significant effect on swelling values.
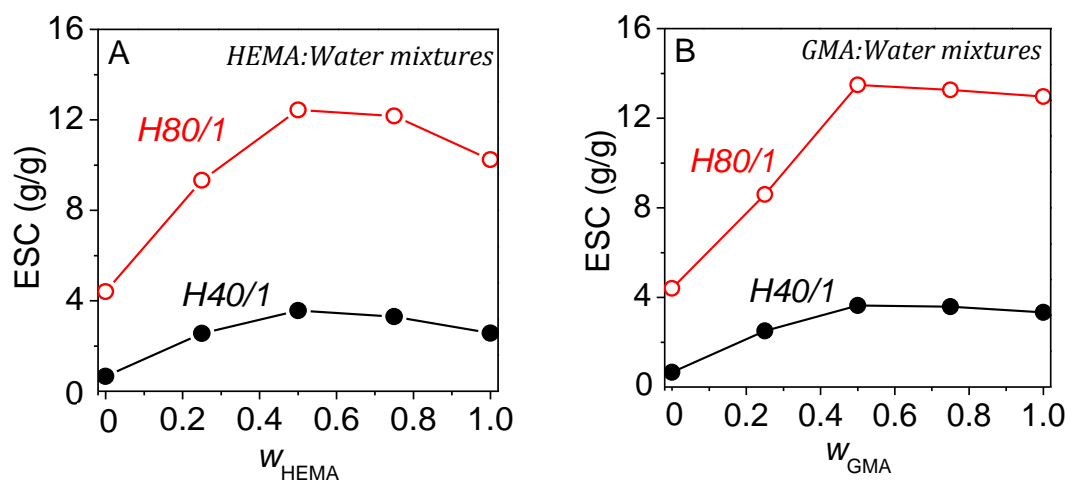
Figure 50. Equilibrium swelling of non-porous H40/1 and porous H80/1 single network hydrogels in (a) HEMA:water and (b) GMA:water mixtures as a function of weight fraction of monomer.

4.3. Swelling of IPN hydrogels

Equilibrium water content (EWC) in IPN hydrogels consisting of two chemically identical PHEMA networks, the first network of which was prepared in the presence of 40 wt.-% of water, decreased with the increase of crosslinker concentration in both networks (Table 8). H0/0 means that no additional crosslinker was used at network preparation, but the crosslinking polymerization took place due to the traces of irremovable crosslinker in HEMA monomer (0.14 mol-% of EGDMA, see the structure in Figure 17).

Table 8. Equilibrium water content (EWC) in chemically homogeneous PHEMA-PHEMA IPN hydrogels.

EWC of chemically homogeneous IPN hydrogels, g/g					
Network 1		Network 2			
		H0/0	H0/0.3	H0/1	H0/2
H40/0.2	0.721	0.643	0.623	0.563	0.553
H40/1	0.658	0.627	0.620	0.556	0.546
H40/3	0.592	0.584	0.538	0.518	0.507
H40/6	0.586	0.542	0.493	0.439	0.434

Swelling parameters of IPNs in water and DMSO are collected in Table 9 and they will serve as reference data for further calculation of parameters characterizing the networks chain extension. It is impressive how the already expanded by the second network chains of the first PHEMA network can be stretched further within the IPN gel when the latter is swollen in solvents, especially in DMSO. We introduced α_1 parameter as a criterion of extension of network 1 chains embedded into the IPN structure.

Table 9. Swelling parameters of IPN hydrogels: volume degree of swelling (Q_V), mass degree of swelling (Q_m), and equilibrium solvent content (ESC).

Sample	Polymerization conditions	Q_v	Q_m	ESC
Swollen in WATER				
H0/1-G0/0.3	1st net: thermal (AIBN) 2nd net: UV (DAROCUR 1173)	2.67	2.13	1.13
H0/1-H0/0.3	1st net: thermal (AIBN) 2nd net: UV (DAROCUR 1173)	1.60	1.57	0.57
H40/1-G0/0.3	1st net: redox (APS/TEMED) 2nd net: UV (DAROCUR 1173)	2.04	2.11	1.11
H40/1-H0/0.3	1st net: redox (APS/TEMED) 2nd net: UV (DAROCUR 1173)	1.56	1.62	0.62
H80/1-G0/0.3	1st net: redox (APS/TEMED) 2nd net: UV (DAROCUR 1173)	4.27	3.16	2.16
H80/1-H0/0.3	1st net: redox (APS/TEMED) 2nd net: UV (DAROCUR 1173)	1.45	1.58	0.58
cH80/1-G0/0.3	1st net: redox (APS/TEMED), T = -14 ^{0}C 2nd net: UV (DAROCUR 1173)	3.62	3.26	2.26
cH80/1-H0/0.3	1st net: redox (APS/TEMED), T = -14 ^{0}C 2nd net: UV (DAROCUR 1173)	1.69	1.69	0.69
Swollen in DMSO				
H0/1-G0/0.3	1st net: thermal (AIBN) 2nd net: UV (DAROCUR 1173)	4.86	4.46	3.46
H0/1-H0/0.3	1st net: thermal (AIBN) 2nd net: UV (DAROCUR 1173)	3.26	3.85	2.85
H40/1-G0/0.3	1st net: redox (APS/TEMED) 2nd net: UV (DAROCUR 1173)	5.63	5.73	4.73
H40/1-H0/0.3	1st net: redox (APS/TEMED) 2nd net: UV (DAROCUR 1173)	4.62	4.78	3.78
H80/1-G0/0.3	1st net: redox (APS/TEMED) 2nd net: UV (DAROCUR 1173)	8.19	5.67	4.67
H80/1-H0/0.3	1st net: redox (APS/TEMED) 2nd net: UV (DAROCUR 1173)	3.51	4.29	3.29
cH80/1-G0/0.3	1st net: redox (APS/TEMED), T = -14 ^{0}C 2nd net: UV (DAROCUR 1173)	6.02	5.94	4.94
cH80/1-H0/0.3	1st net: redox (APS/TEMED), T = -14 ^{0}C 2nd net: UV (DAROCUR 1173)	4.61	4.96	3.96

Figure 51 shows the dilation factor α for chains of network 1 (α_1) at various stages of IPN formation and after final swelling in water or DMSO. The numerical values of α_1 for chains of network 1 in IPNs (Table 10) can be compared with α values of single networks in the Table 7.

The inspection of α-values for chains of network 1 discovers their large extension in the swollen IPN especially when swollen in DMSO ($\alpha_1 = 2.95$) for HEMA-GMA IPN made from macroporous parent network which in the current case corresponds to about 47% of their contour lengths; in the case of H80/1-H0/0.3 swollen in DMSO ($\alpha_1 = 2.11$), it makes about 33%.[1] This fact tells us that the theoretical model based on Gaussian chains is no longer applicable when analyzing the elasticity and swelling data. This conclusions is also valid for the PHEMA-PHEMA IPN made from homogeneous parent network ($\alpha_1 = 2.36$).

The second − even more important − observation is that the extension of network 1 chains under working conditions of the IPN (swollen in water) was much higher when macroporous PHEMA gel H80/1 was used as network 1 for H80/1-G0/0.3; $\alpha_1^3 = 13.4$ compared to $\alpha_1^3 = 6.08$ for the homogeneous H40/1-G0/0.3 (cf. Figure 51). This is, however, not so in the case of H80/1-H0/0.3, on contrary, α_1^3 for homogeneous matrix is somewhat higher.

---

[1] The number of monomer units, n_m, in a network 1 chain ≈ 100, number of monomer units in a statistical segment ≈ 2.5, number of statistical segments $n_s \approx n_m/2.5$, contour length $\approx n_s l_s$, unperturbed length $\approx n_s^{1/2} l_s$, l_s length of statistical segment

Volume expansion of chains of network 1 by swelling:
Example sketched for IPN gel H80/1–G0/0.3

parent single network H80/1

$$V_{rel1} = (\alpha_1)^3 = \frac{V}{V_{nf1}}$$

as prepared in water

swollen in monomer 2

reswelling

polymerization

IPN

$V_{rel1} = 1$

$V_{rel1} = 3.1$

$V_{rel1} \sim 3.1$

swelling in water

IPN

in water
$V_{rel1} = 13.4$

swelling in DMSO

IPN

in DMSO
$V_{rel1} = 26$

...volume occupied initially – after its preparation – by network 1

...volume occupied by network 1 gel sample

...volume occupied by the whole IPN sample, i.e. spanned by extended chains of network 1

IPN gel	$(\alpha_1)^3$		
	in non-swollen IPN	in IPN swollen in water	in IPN swollen in DMSO
H0/1-H	2.77	4.43	9.03
H40/1-H	2.86	4.46	13.21
H80/1-H	2.71	3.93	9.51
cH80/1-H	1.79	3.02	8.25
H0/1-G	3.30	8.81	16.04
H40/1-G	2.98	6.08	16.80
H80/1-G	3.13	13.40	25.65
cH80/1-G	1.89	6.85	11.39

Figure 51. A sketch illustrating expansion of chains of **network 1** in a single network and in an IPN H80/1–G0/0.3 due to swelling: volume change shown as relative volume of the network 1, V_{rel1}, which is expressed as a ratio of swollen sample volume, V_{sw}, to the reference volume of the network 1, V_{nf}. The parent network H80/1 swells in the monomer 2, GMA, and swelling of prepared IPN H80/1–G0/0.3 in water and in dimethyl sulfoxide (DMSO) is shown. Volume occupied initially by network 1 is drawn to offer a mind image to the reader. Data shows dilation factor $(\alpha_1)^3$ of network 1 chains in homogeneous and microstructured IPNs.

The osmotic expansion of network 1 by swelling of network 2 depends primarily on the swelling power of the polymer 2, but also on the compatibility of chains 1 and 2 which is poorer when chains are chemically different. Network 1 phase within IPN of pore walls is then more crosslinked in the PHEMA-PHEMA case by additional entanglements than in the PHEMA-PGMA case. A complete set of

values of α_1 is available in the Table 10. Comparing the dilation factors of chains of network 2 in IPNs and in freely swelling gels, one can find that the expansions of network 1 is counterbalanced by compression of network 2, i.e., the network 2 swells less than under unconstrained conditions.

In good solvent dimethyl sulfoxide (DMSO), the values of the factor α were considerably higher. For instance, for H80/1 network in H80/1–G0/0.3 IPN swollen in DMSO, the factor α reached the value 4.2 compared to α about 1.8 in the non-swollen IPN (i.e., the H80/1 in GMA). The chains of non-porous PHEMA gels can be significantly stretched ($\alpha = 1.5$ in a single H40/1 network vs. $\alpha = 2.8$ in H40/1–G0/0.3 IPN).
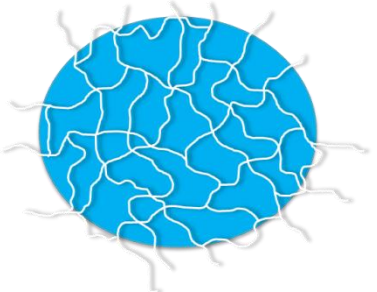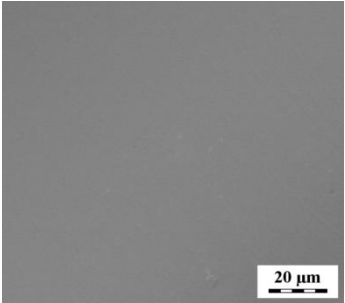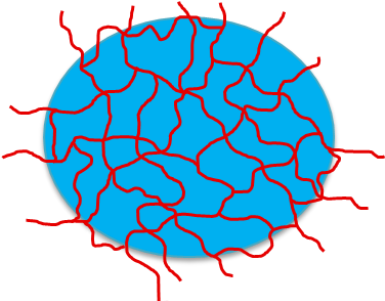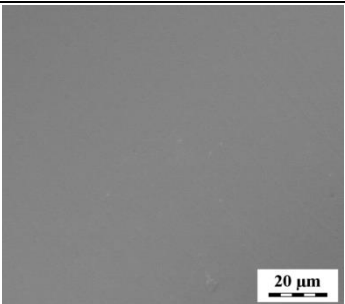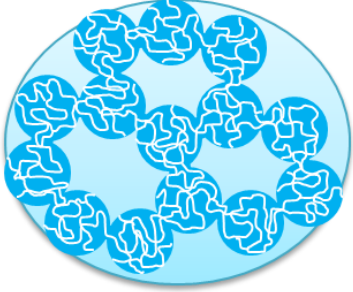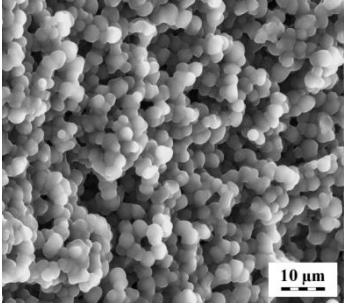
Table 10. A complete set of chain extension factor α_1 values for network 1 calculated for equilibrium swollen IPNs in water and DMSO.

Hydrogel		Dilation factor, α_1	
		in water	in DMSO
IPNs	H0/1-H0/0.3	1.64	2.08
	H40/1-H0/0.3	1.93	2.77
	H80/1-H0/0.3	2.44	3.28
	cH80/1-H0/0.3	2.20	3.07
	H0/1-G0/0.3	2.07	2.52
	H40/1-G0/0.3	2.14	3.00
	H80/1-G0/0.3	3.67	4.56
	cH80/1-G0/0.3	2.89	3.42
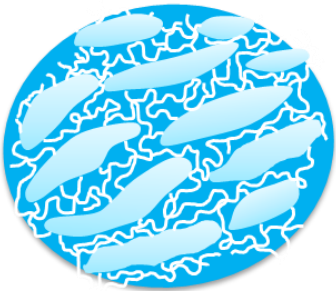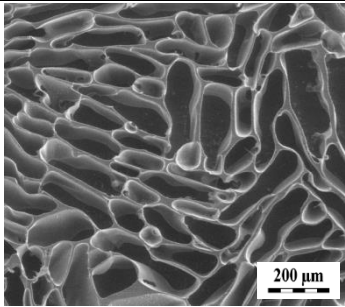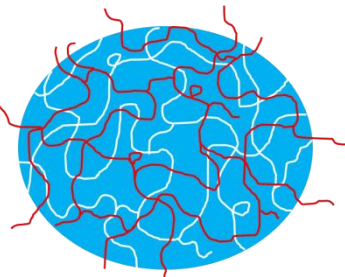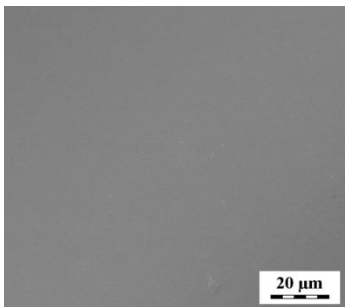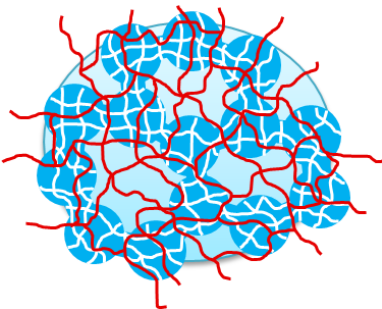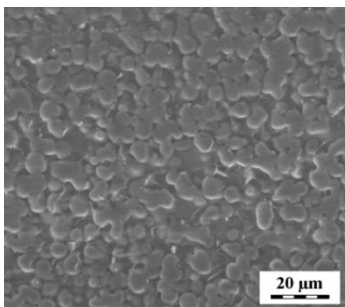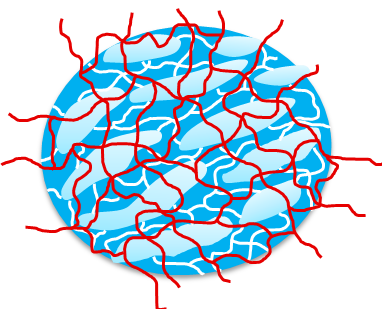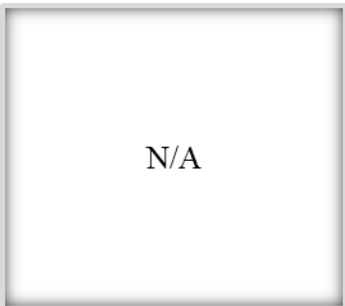
5. Deformation behavior of hydrogels

For better orientation in this part of the thesis and better understanding the correlation between the morphology of gels and their mechanical properties, the overview of hydrogels of various morphology and corresponding cartoons and micrographs is presented in Table 11. The left column represents the coding of single network and IPN gels, the following column contains the cartoons depicting the coiling states of networks 1 and 2 in swollen gels, and the right column reveals the morphology of swollen gels observed by cryo-SEM method.

Table 11. Overview of hydrogels of various morphology and corresponding cartoons and micrographs.

Sample code	Cartoon	Micrograph
SWOLLEN SINGLE NETWORKS		
H0/1 H40/Y (Y<3) network 1		Non-porous
H0/0 H0/0.3 H0/1 H0/2 G0/0.3 network 2		Non-porous
H80/1 hydrogel		Macroporous with fused spheres

cH80/1 cryogel		 **200 μm** Macroporous with cell-like pores
SWOLLEN INTERPENETRATING POLYMER NETWORKS		
H0/1-H(G) H40/1-H(G) IPNs		 **20 μm** Non-porous
H80/1-H(G) IPN		 **20 μm** Microstructured IPN
cH80/1-H(G) IPN		N/A Microstructured IPN

5.1. Tensile deformation behavior

5.1.1. Constituent single network hydrogels H40/Y: effect of crosslinker concentration

Tensile deformation behavior of a series of swollen non-porous PHEMA-PHEMA IPN hydrogels consisting of non-porous H40/Y first networks and non-porous H0/Z second networks are discussed in this paragraph. Some of these systems may serve as model samples for fundamental studies of relationship between the structural, swelling and mechanical properties, since they consist of chemically identical constituent PHEMA networks and there are no complications caused by the morphology as constituent networks are non-porous (H40/0.2 and H40/1 based IPNs).

Mechanical performances of single H40/Y first networks were studies as a reference data. Figure 52 shows stress-strain dependencies for single PHEMA networks 1 prepared at 40 wt.-% of water and various amounts of DEGDMA crosslinker (0.2 – 6 mol-%). In this work, the strength of gels was defined as a force (F) divided by constant area (S) and attributed to "engineering stress" (σ) further called just "stress". The increase of crosslinker concentration in gels resulted in increase of stress at break and Young's modulus (Figure 52, inserted table), and in decrease of strain at break. Generally, crosslinked PHEMA networks can be considered as hybrid materials as they contain both chemical and physical crosslinks. The latter was observed by scattering experiments and explained by hydrophobic interactions between polymer chain segments. The ratio between chemical and physical crosslinks may determine eventual mechanical properties of the material. For instance, the amount of added chemical crosslinker in H40/0.2 sample is very low, and therefore the effects from chemical and physical crosslinks may be comparable. Low density of chemical crosslinks provides for relatively long length flexible polymer chains, which can be highly stretched under the deformation of hydrogel. Physical crosslinks are generally weaker than chemical crosslinks, but their presence in networks increases the overall crosslinking density. Reversible decrosslinking of physical crosslinks under large deformation causes the energy dissipation due to the dissociation of hydrophobic interactions, which is a general principle for the design of tough hydrogels. Fabrication of hybrid-crosslinked hydrogels is a way to maintain high elasticity of tough hydrogels.[199] Thus, H40/0.2 gel overcome large expansion and ruptured at high deformation of 340 % (λ_b = 4.4),

and at the same time exhibited relatively high stress at break (340 kPa), which was not significantly lower than strengths of other samples within the series. The effect of physical crosslinks becomes suppressed with increase of concentration of added crosslinker, and the mechanical properties of single PHEMA networks become driven by chemical crosslinks only. So, highly crosslinked hydrogels have high strengths, but rupture at low strains.
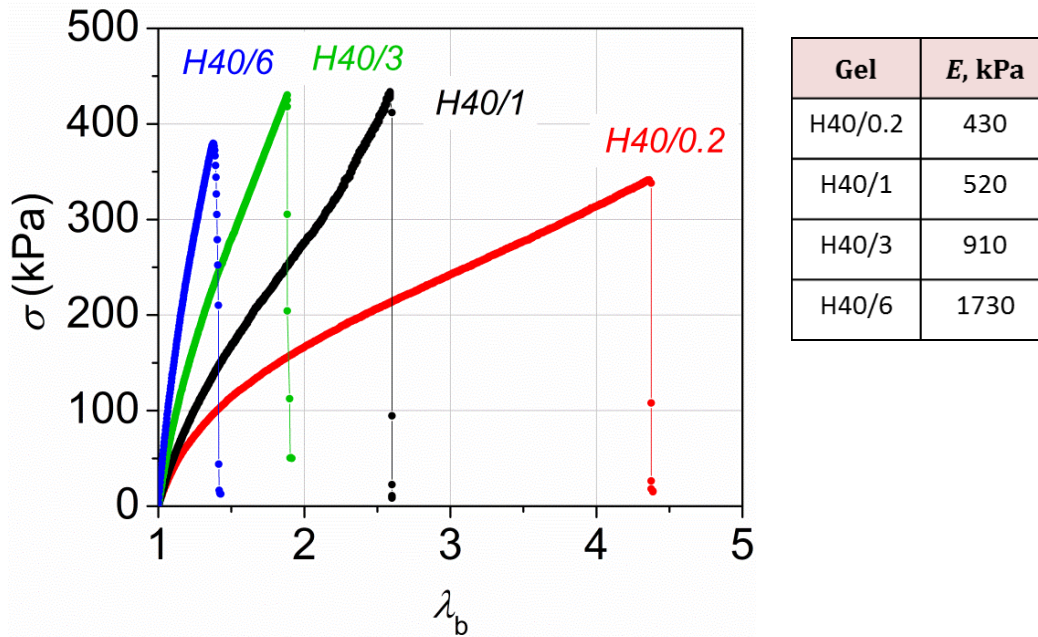
Gel	E, kPa
H40/0.2	430
H40/1	520
H40/3	910
H40/6	1730

Figure 52. Stress-strain dependencies at extension for single PHEMA networks prepared at 40 wt.-% of water and various concentrations (mol-%) of DEGDMA crosslinker.

The Young's moduli (E) of swollen hydrogels are defined phenomenologically as $E = \sigma/(\lambda - 1)$ and determined at fairly small uniaxial deformations of few percents ($\lambda < 1.05$). The Young's moduli of single network PHEMA hydrogels prepared at 40 wt.-% of water were in the range of 430 – 1730 kPa. If only homogenous PHEMA hydrogels containing up to 1 mol-% of crosslinker are considered, then their Young's moduli were 430 and 520 kPa. Obtained values are in consistent with those given in literature (300 – 800 kPa) for manufactured PHEMA contact lenses[200,201] as well as for PHEMA hydrogels.[202,203]

5.1.2. Chemically homogeneous PHEMA-PHEMA IPN hydrogels

Chemically homogeneous PHEMA-PHEMA IPN hydrogels were stiffer than their parent H40/Y first networks (Figure 53). Stress-strain dependencies of IPNs were sensitive to change of crosslinker concentration in both networks. IPNs were strengthened with increase of crosslinker amount in the second network. Lower strain values of IPNs were compensated by high stresses at break as well as high Young's moduli. Interlocking of loosely crosslinked H0/0 or H0/0.3 second network with loosely crosslinked H0/0.2 first network resulted in more or less homogeneous IPN hydrogel since the crosslink density in both networks was similar. But the higher strength of these IPNs is explained by the higher total chain density in them (Figure 53a). Interlocking of H0/0.2 parent network with notably denser networks such as H0/1 or H0/2 made the IPN stiff but incapable to overcome large extensions due to the fact that the extension of chains in IPN is driven by short chains of the second network. Tightly crosslinked H40/3 and H40/6 networks are not able to absorb large amounts of second network monomers mixture, therefore the IPNs revealed high stresses and broke at low strains (Figure 53c and 53d). The amount of crosslinker in the second network had no big influence of the mechanical performance of the IPNs, because the second networks were less crosslinked than their parent networks (H40/3 or H40/6). The best IPN hydrogels with high both stresses and strains were obtained on the basis of H40/1 networks (Figure 53b). Among the series, the best parameters were obtained for H40/1-H0/0.3 hydrogel – 820 kPa of stress at break and 140 % of strain ($\lambda_b = 2.4$).
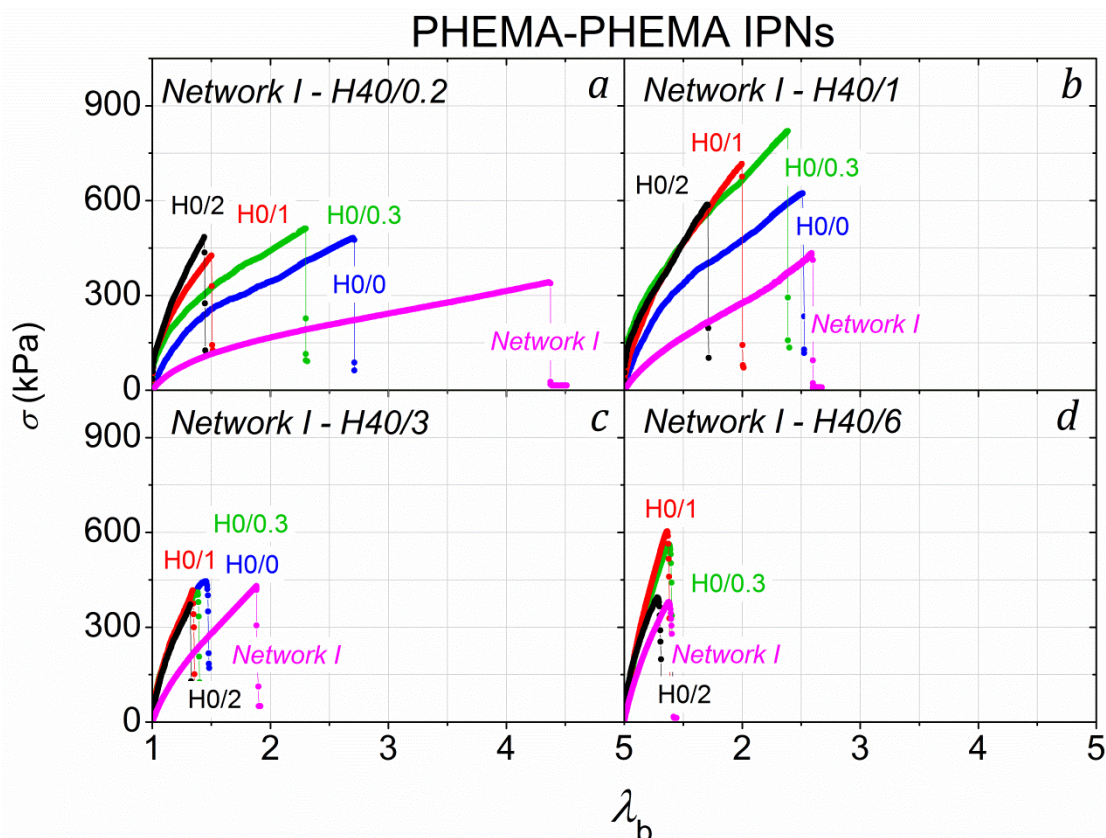
Figure 53. Stress-strain dependencies at extension for different PHEMA-PHEMA homo-IPN hydrogels: H0/Y second network interlocked with (a) H40/0.2, (b) H40/1, (c) H40/3, and (d) H40/6 first networks.

The different crosslinker concentration in each constituent network influenced the values of Young's modulus (E), which were increasing with the increase of crosslinker amount in both networks (Figure 54a). The crosslinker concentration in networks are represented as follows: (a) in network 1 – by differently colored curves, each of which is related to one of H40/Y based IPN series, (b) in network 2 – by values on x axis related to "Z" in H40/Y-H0/Z gels. Embedding of second networks of various crosslinker concentrations into the IPN structure led only to stiffening of the single network PHEMA hydrogel. To estimate the extent of stiffening, the modulus of the IPN (E_{IPN}) was related to the modulus of the reference single network 1 (E_{SN1}). The Figure 54b shows the dependence of E_{IPN}/E_{SN1} ratio on the concentration of the crosslinker in network 2. In all cases, the E_{IPN}/E_{SN1} ratio was above 1 ($E_{IPN}/E_{SN1} > 1$), but the most significant improvement of modulus was achieved for H40/1-based IPNs. This was apparently due to the fact that the total crosslink density in H40/1 network 1 based IPNs was higher than in IPNs prepared from H40/0.2 network 1. Additionally, the PHEMA networks 1

118

prepared at 3 and 6 mol-% of crosslinker concentration are already strong gels with high Young's modulus, therefore the values of E_{IPN}/E_{SN1} ratio for them were not as high as for H40/0.2 and H40/1 network 1 based IPNs.
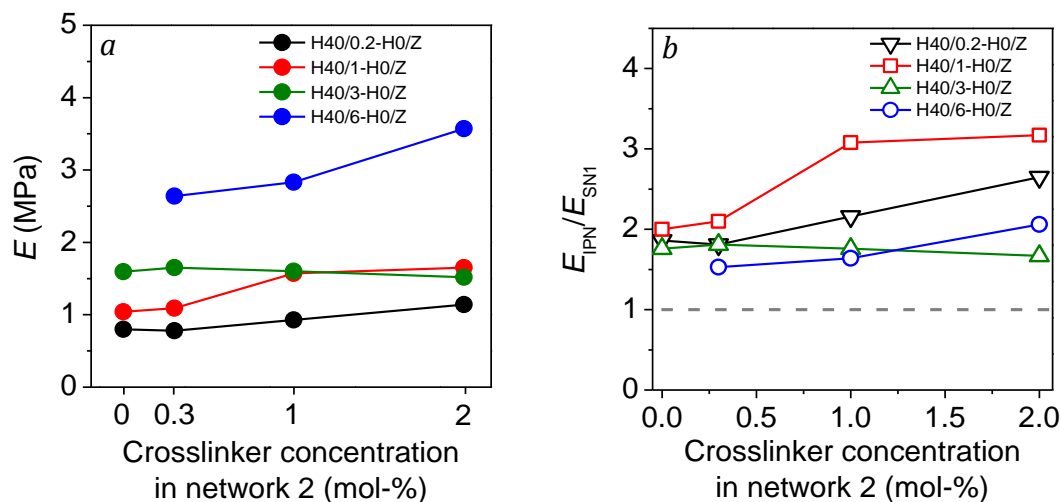
Figure 54. Young's modulus (E) of swollen H40/Y-H0/Z IPN hydrogels (a). Effect of crosslinker concentration (mol-%) in the second network on Young's moduli of the IPN hydrogels (b). Young's moduli of IPN hydrogels (E_{IPN}) were related to Young's moduli of single network 1 hydrogels (E_{SN1}).

The capacity of IPN hydrogels to absorb water is expectably worse than of single network hydrogels due to the higher density of crosslinked polymer chains. Furthermore, increase of crosslinker concentration in both constituent networks (Y mol-% and Z mol-%) reduces the total swelling of H40/Y-H0/Z IPN (Table 5). To assess how much the IPNs swelling properties were deteriorated regarding their reference single networks, we used EWC_{IPN}/EWC_{SN1} ratio (Figure 55). Notable drop of swelling values was observed for loosely crosslinked H40/0.2 based IPN and tightly crosslinked heterogeneous H40/6 based IPN hydrogels. Apparently, larger amount of second network monomers mixture penetrated the loosely crosslinked H40/0.2 matrix eventually creating a dense network with low degree of swelling. Whereas the swelling of H40/6 based IPNs was restricted by the tightly crosslinked H40/6 matrix. It is worth to emphasize, that for IPNs without crosslinker in the second network or very small amount of it (0.3 mol-%) the deterioration of swelling properties (EWC_{IPN}/EWC_{SN1}) was insignificant in comparison with considerable enhancement of mechanical properties (E_{IPN}/E_{SN1}) of IPNs.
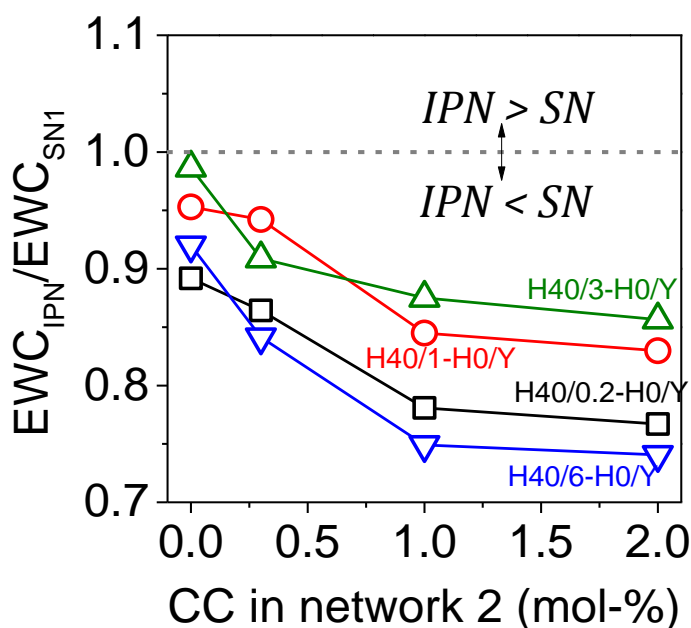
Figure 55. Effect of crosslinker concentration (CC, mol%) in the second networks on the swelling properties of the IPN hydrogels. Equilibrium water content in the IPN hydrogels (EWC_{IPN}) was related to the equilibrium water content in the single network (EWC_{SN}) hydrogels.

Comparison of refractive index, degree of strengthening E_{IPN}/E_{SN1}, and EWC_{IPN}/EWC_{SN1} ratio is shown for H40/1 based IPN hydrogels in Table 12. The EWC_{IPN}/EWC_{SN1} ratios were below 1, but the reduction was relatively small – about 5-17 %. While the Young's moduli of swollen IPN hydrogels enhanced by more than 100 %. For H40/1-H0/0 IPN, for instance, increase in modulus E by 100 % cost it a reduction in EWC only by 5 %. For H40/1-H0/2 IPN, increase in modulus E by 220 % cost it a reduction in EWC by 17 %. Refractive indices of IPNs (RI 1.429 – 1.430) were very similar to that of single PHEMA network (RI 1.433). Decrease in values was negligible (less than 0.3 %). This result is important in terms of possible application of PHEMA-based IPN hydrogels in ophthalmology, as values are in the range of indices, which are typical for real PHEMA-based contact lenses (RI 1.380-1.440).[204]

Table 12. Effect of crosslinker concentration in the second network on refractive index (RI), degree of strengthening (E_{IPN}/E_{SN1}), and (EWC_{IPN}/EWC_{SN1}) ratio of PHEMA-PHEMA hydrogels. Selected data for H40/1-based IPNs are summarized in Table. Crosslinker concentration (CC, mol-%) in network 2 indicates the concentration of added crosslinker.

Hydrogel	CC in Network 2, mol-%	RI	E_{IPN}/E_{SN1}	EWC_{IPN}/EWC_{SN1}
H40/1	-	1.433	1	1
H40/1-H0/0	0	1.429	2.0	0.95
H40/1-H0/0.3	0.3	1.429	2.1	0.89
H40/1-H0/1	1	1.430	3.0	0.84
H40/1-H0/2	2	1.429	3.2	0.83

5.1.3. *PHEMA-PHEMA* versus *PHEMA-PGMA IPN hydrogels*

The tensile behavior of constituent single network hydrogels (networks 1, 2) used to build up interpenetrating networks was studied. Figure 56 shows the portfolio of deformation responses to elongation of mostly HEMA-based gels covering a wide range of strain at break, strength and Young's modulus values. It should be noted that the networks H0/0.3, H0/1, H40/1 and G0/0.3 do not contain any pores whereas the gels H80/1 and cH80/1 have distinct macroporous morphologies (see inserts in the Figure 56). However, even the gels H40/1 formed in presence of water as diluent (40 wt.-%) contain weak nanosized inhomogeneities – fluctuations in polymer segment concentrations (cf. paragraph 3.4, page 98). The three non-porous HEMA-based gels which contained between 36 and 40 wt.-% of water at equilibrium provided the highest values of moduli while the sample H40/1 shows somewhat lower modulus and increased strain at break. This is related to the effect of diluent on concentration of elastically active network chains: the presence of diluent promotes formation of cyclic structures and thus a decrease of crosslink density.
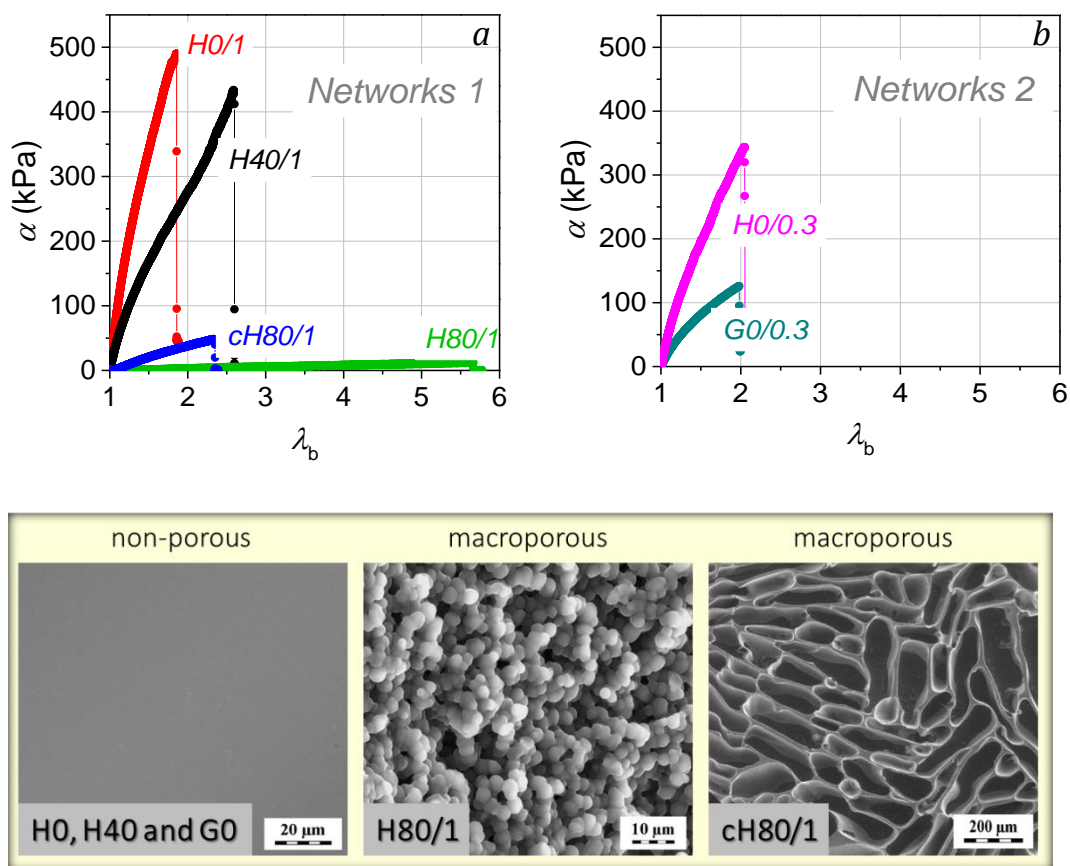
Figure 56. Stress-strain dependencies at extension for single networks 1 and 2.

The ultimate strain of gels is directly related to material performance at application and provides quantitative comparison of how much of elongation can the structures withstand before it ruptures. The sample H80/1 shows remarkably large capacity of straining, almost 500 % of deformation. Interestingly, the macroporous cH80/1 cryogel that contains somewhat less water at testing state breaks down at much lower strain. Both macroporous gels: the phase separated structure characterized by chemically fused spheres (H80/1) and the cryogel containing large cells of a characteristic dimension of 50-80 μm (cH80/1) provided low moduli. The modulus of poly(glycerol methacrylate) gel G0/0.3 was lower than that of the PHEMA gels that are not macroporous and also their ultimate extensions were comparable. The G0/0.3 swelling degree in water was, however, much higher.

The tensile properties of neat PHEMA and PGMA networks, and PHEMA–PGMA and PHEMA–PHEMA IPNs are shown in Figure 57, Figure 58 and Figure 59.
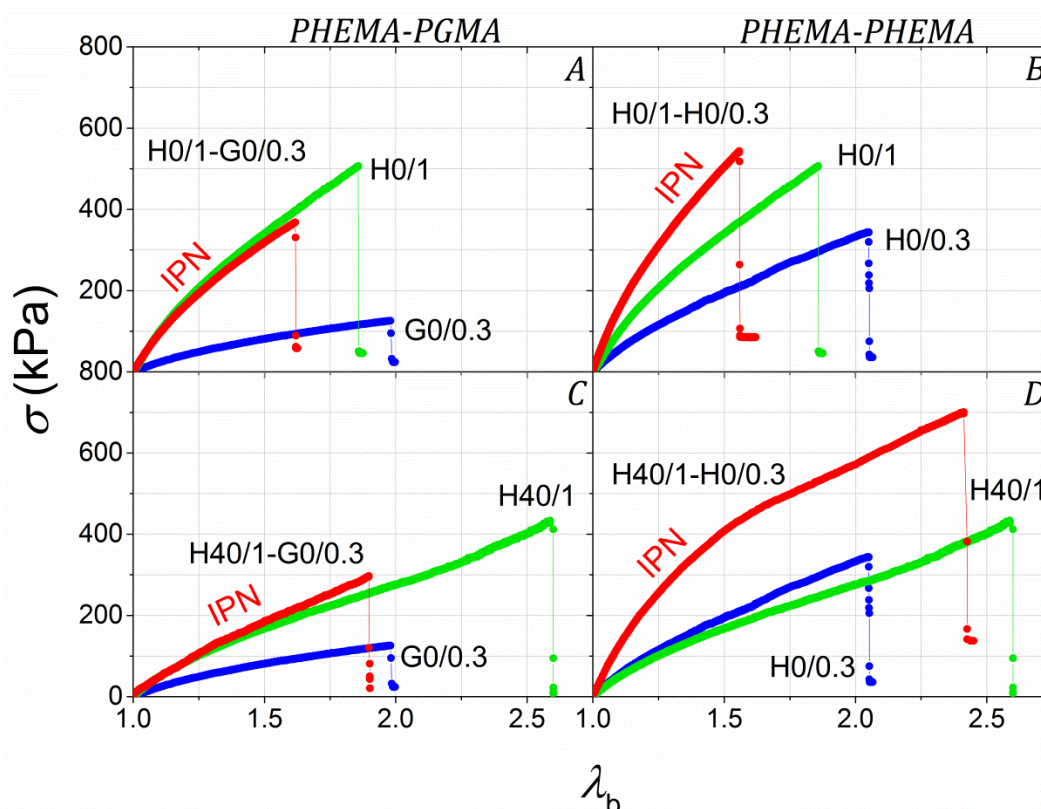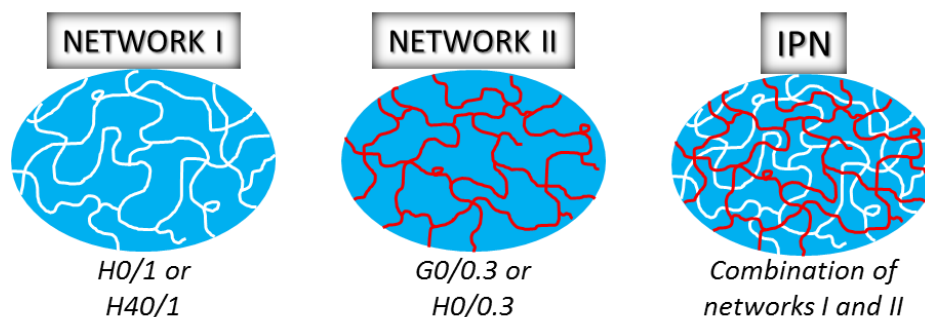
Figure 57. Stress-strain dependencies at extension for PHEMA-PGMA and PHEMA-PHEMA IPN hydrogels: the G0/0.3 second network interlocked with the (a) H0/1 and (c) H40/1 first network; the H0/0.3 second network interlocked with the (b) H0/1 and (d) H40/1 first network.

The factors affecting the mechanical properties of hydrogels are very complex and include the chemical nature of both networks and their interactions, morphology of the first network, crosslink densities, etc. In extension, neither yielding nor brittle fracture were observed. Dilution at preparation of the first network led to the formation of gels of lower stiffness. Dilution 40 % of water

123

decreased the modulus of these non-porous gels more than would be predicted by the factor $(\phi_2^0)^{2/3} = (V_d/V_{nf})^{2/3}$ very likely due to increased cyclization. For non-porous gels, dilution improved the value of strain at break of the PHEMA gels without impairing their strength (H0/0.3 vs. H40/1); its true strength (cf. data of Table 13) was greatly improved (H40/1 vs. H0/1). The PHEMA–PHEMA IPN gels were stronger than PHEMA–PGMA IPNs, the Young's modulus of the former exceeded 1 MPa.
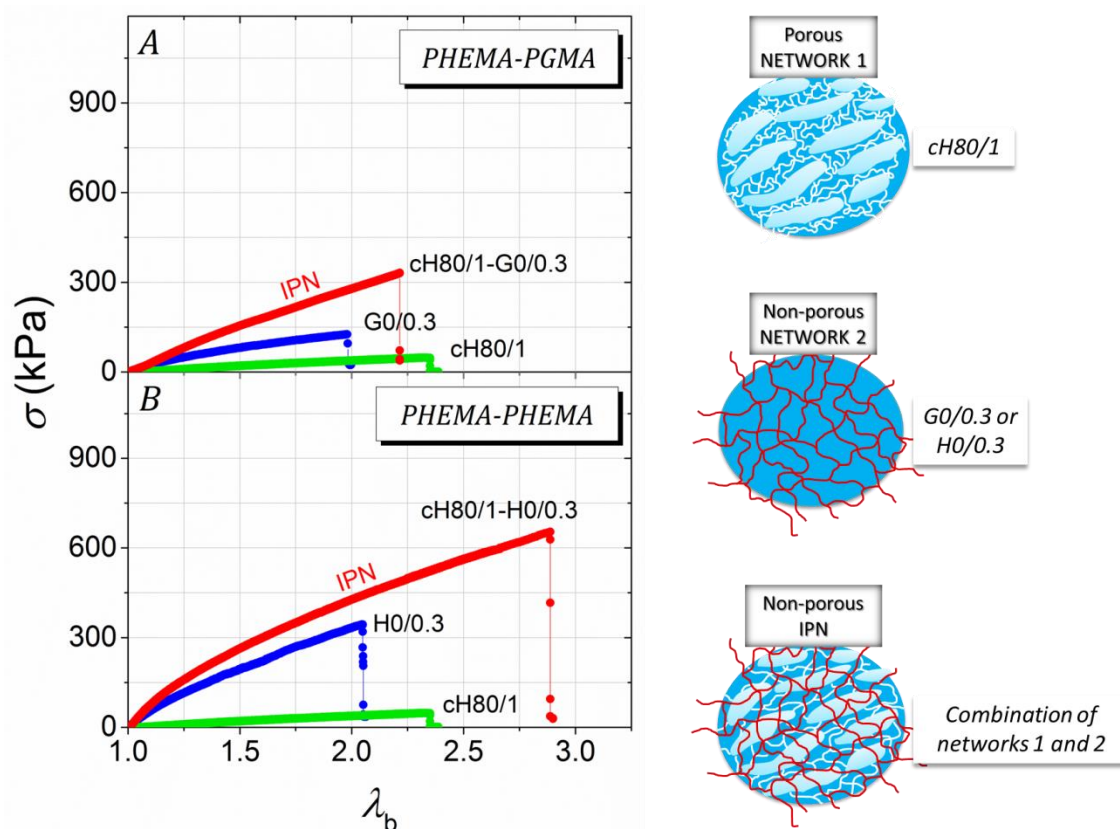
Figure 58. Stress-strain dependencies at extension for the cH80/1 first network cryogel interlocked with the (a) G0/0.3 and (b) H0/0.3 second networks.
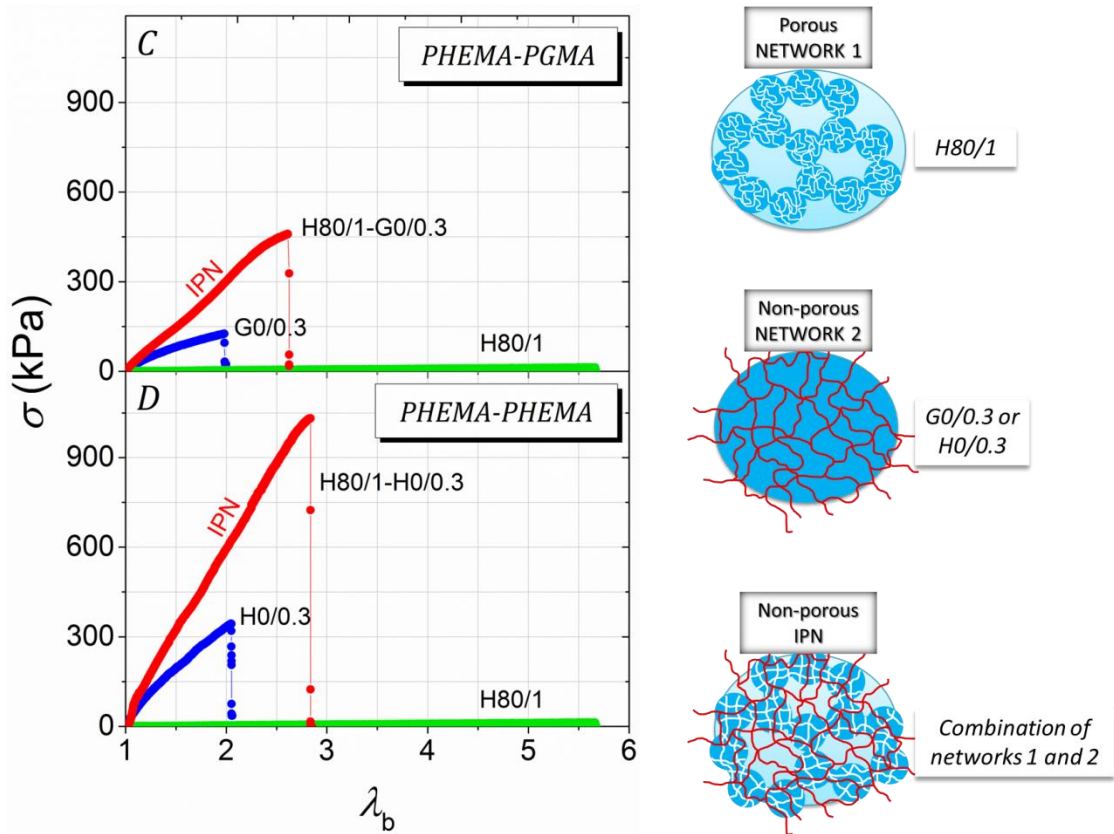
Figure 59. Stress-strain dependencies at extension for the H80/1 first network hydrogel interlocked with the (c) G0/0.3 and (d) H0/0.3 second networks.

Swollen interpenetrating networks based on the mechanically weak macroporous H80/1 gel showed the best mechanical performance (H80/1–H0/0.3, H80/1–G0/0.3, cf. Table 13). This macroporous network absorbs large amounts of the monomer of the second network. H80/1-based IPNs reveal better tensile strength and strain at break than H40/1-based IPNs. The H80/1–H0/0.3 was very tough with the true strength $S_b = \sigma_b(\lambda_b - 1)$ close to 2 MPa, and stress at break of 1 MPa and elongation at break almost 300 %. The reasons for this extreme improvement are not yet fully clear and will be the object of further studies. It is possible that GMA monomer is transferred continuously into the network phase during GMA polymerization and makes the necks between spheres of H80/1 softer and more oriented. The soft and compressed network 2 "phase" in former pores may block crack spreading, a phenomenon utilized in rubber toughened thermosets.[205]

Table 13. Tensile and swelling properties of hydrogels. Measuring conditions: swollen state, ambient temperature, λ_b = length at break/undeformed length, Q_V related to volume of dry sample annealed at 100 °C.

Sample		Stress at break σ_b [kPa]	Strain at break λ_b	True strength $S_b = \sigma_b(\lambda_b - 1)$ [kPa]	Young's modulus E [kPa]	Q_V^*	$S_b Q_V$ [kPa]
single network 1	H0/1	488	1.85	415	1060	1.65	685
	H40/1	433	2.59	688	520	1.61	1108
	H80/1	13	5.65	60	4	3.71	222
	cH80/1	60	2.45	87	720	3.51	305
single network 2	H0/0.3	344	2.05	361	590	1.53	563
	G0/0.3	125	1.98	122	250	4.42	539
inter penetrating networks	H0/1–G0/0.3	367	1.62	227	1010	2.67	606
	H40/1–G0/0.3	300	1.90	270	460	2.04	551
	H80/1–G0/0.3	460	2.63	750	380	4.27	3164
	cH80/1–G0/0.3	330	2.25	413	280	3.62	1495
	H0/1–H0/0.3	540	1.56	302	1720	1.60	483
	H40/1–H0/0.3	700	2.41	987	1330	1.56	1540
	H80/1–H0/0.3	1032	2.84	1899	980	1.45	2753
	cH80/1–H0/0.3	650	2.82	1183	900	1.69	2000

For certain ophthalmologic applications, good mechanical properties of highly swellable hydrogels are needed. From this point of view, the product $S_b Q_V$ can serve as the criterion. Table 13 shows that H80/1–G0/0.3 is a clear winner. This IPN is followed by H80/1–H0/0.3, which is a certain surprise. Its second place is due to its high modulus and true strength but its swelling degree is relatively low. The high values of E and S_b can be due to approaching the glass transition region and if so, the properties may be sensitive to temperature variations.

126

5.2. Elastically active network chains concentration in single PHEMA networks

According to the rubber-elasticity theory, the equilibrium Young's modulus of Gaussian networks is proportional to the concentration of elastically active network chains (EANC) and is a function of solvent content and dilution at network formation:[206]

$$E = 3RTA\nu_e\phi_2^{1/3}(\phi_2^0)^{2/3}$$

(Equation 4.4)

where R is universal gas constant, T is the temperature in K, A is a dimensionless factor in the Flory-Erman rubber elasticity theory, ν_e is the concentration of elastically active network chains (EANC) in moles per volume, ϕ_2 is the volume fraction of polymer at swelling equilibrium and $\phi_2^0 = V_d/V_{nf}$ is related to dilution at network formation.

Figure 60 represents the correlation between the real concentrations of EANC calculated from the experimentally measured Young's moduli (E) and the concentrations of EANC determined from the composition of network (ideal), i.e., the concentration of the crosslinker at preparation, assuming that each consumed double bond of crosslinker contributed to one EANC. The concentration of EANC was calculated for transparent homogeneous H40/0.2 and H40/1, translucent intermediate H40/3 and white phase-separated H40/6 hydrogels. The concentration of the EGDMA crosslinker present in commercial HEMA monomer was also considered. The dependence between real and ideal EANC concentrations was close to linear with slope of 0.3. Such deviation from the diagonal was due to incomplete utilization of crosslinker molecules forming EANC and very likely intramolecular reactions causing the cyclization. Formally, this theory cannot be applied to heterogeneous H40/3 and H40/6 gels, as it does not contain any parameters taking into account the inhomogeneous structure of networks. The low position of real EANC values on the graph for these samples supported this precaution. The real concentration of EANC in loosely crosslinked H40/0.2 hydrogel was slightly higher than that determined from its composition. Possible explanation is the presence of physical hydrophobic interactions becoming important at low concentration of chemical crosslinks and contributing to total crosslink density in network.
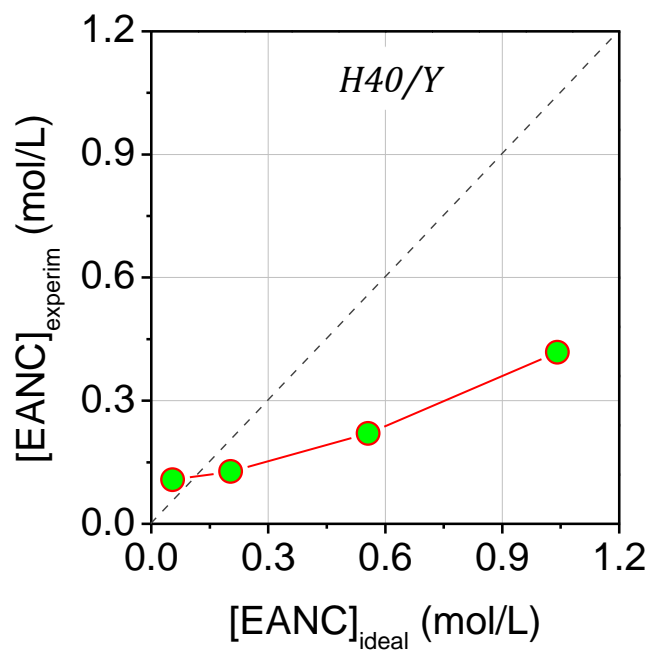
Figure 60. Concentration of elastically active network chains (EANC) in single network H40/Y hydrogels determined from the composition of reaction mixture (ideal) and calculated from the experimentally measured modulus (experimental). The values of "Y" corresponding to the concentration of DEGDMA crosslinker in the H40/Y hydrogels were 0.2, 1, 3, and 6 mol-%.

5.3. Theoretical treatment of swelling and elasticity of swollen IPN hydrogels

For interpenetrating networks, the situation is much more complicated when segment-segment interaction parameters are different, unless the interactions between segments of the two polymers are attractive or the attraction is mediated by the solvent. According to Dušek[207] [ref. to oral communication and derivation of physical model of IPN swelling and deformation, unpublished work], the consideration of mixing in IPNs as mixing of two networks or even two uncrosslinked polymers of infinite molecular weight in the classical way would lead to exclusion of one network from the other because of very large entropic penalty. One should have to consider mixing conditions at the scale of network meshes. The situation is much simpler in the case of sequential IPNs of the same chemical composition, since then the segments of one network do not recognize whether their partners belong to "network a" or "network b" and have no reason for separating at the mesh level. Only the network chains of "network a" are at different state of strain: not those of "network b" (Figure 61).
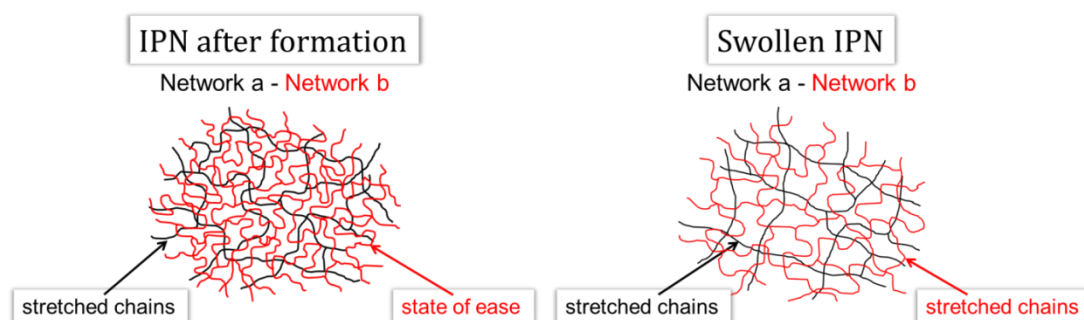
Figure 61. Different coiling states of "network a" and "network b" in the IPN structure after its formation and after swelling.

At hand is the "Two-Networks" theory of Andrews, Tobolsky and, Hanson in which the contribution by the two networks differing in the states of strain of network chains are considered additive.[3] As Dušek pointed out, the "Two-Networks" theory has been more or less successfully applied to networks additionally crosslinked in different states of strain, where the chains in one state are grafted to chains in another state. However, when the external stress is removed, the structure relaxes to a state of ease corresponding to minimum of free energy. So, the TNT is conceptually not the best model to be used. The TNT model suits much better the

class of homogeneous (sequential) IPNs, and in this work it has been formulated and tested. One of the questions to be made clear in these studies is the possible contributions by extra entanglements made by intermeshing of the two networks. Time-to-time, it has been debated the literature. So far, no theoretical approach is available but work is under way. Testing of conformity of experiments with TNT model will tell us whether such amendment is in agreement with experiments.

5.3.1. Two-networks theory applied to homogeneous IPNs of the same composition[207] [ref. to unpublished work of Dušek]

The modification concerns the elastic term of Helmholtz energy. For interpenetrating networks:

$$\frac{\Delta F_{el}}{kT} = \frac{AN_{ea}}{2}\left(\lambda_{ax}^2 + \lambda_{ay}^2 + \lambda_{az}^2 - 3\right) + \frac{AN_{eb}}{2}\left(\lambda_{bx}^2 + \lambda_{by}^2 + \lambda_{bz}^2 - 3\right)$$
$$- B\left(N_{ea}\ln\left(\frac{V}{V_a}\right) + N_{eb}\ln\left(\frac{V}{V_b}\right)\right)$$

(Equation 4.5)

The subscript "a" and "b" are related to "network a" and "network b". The reference volumes V_a and V_b relate to volumes after the first stage and second (final) stage, respectively. The meaning of other symbols is analogous to the case of single networks; N_{ea} and N_{eb} are numbers of elastically active network chain in a and b network, respectively. Complete list of symbols and their meaning is given at the end of this paragraph, see Table 14.

Definitions of quantities used (all symbols V mean extensive quantities – real volumes):

$$\phi_2 = \frac{V_{ap} + V_{bp}}{V_{ap} + V_{bp} + V_s}$$

$$\phi_{2a}^0 = \frac{V_{ap}}{V_{ap} + V_{ad}}$$

$$\phi_{2b}^0 = \frac{V_{ap} + V_{bp}}{V_{ap} + V_{bp} + V_{bd}}$$

$$\varphi_a = \frac{V_{ap}}{V_{ap} + V_{bp}}$$

$$\varphi_b = \frac{V_{bp}}{V_{ap} + V_{bp}}$$

<div align="right">(Equation 4.6)</div>

V_{ap} and V_{bp} are volumes of polymer a and polymer b, respectively, V_s is volume of solvent, and V_{ad} and V_{bd} are volumes of diluents added with monomer a and monomer b, respectively.

Swelling of interpenetrating networks

$$\lambda_{ax} = \lambda_{ay} = \lambda_{az} = \lambda_a; \quad \lambda_{ax}\lambda_{ay}\lambda_{az} = V/V_a$$

<div align="right">(Equation 4.7)</div>

$$\frac{\Delta F_{el}}{kT} = \frac{AN_{ea}}{2}(3\lambda_a^2 - 3) + \frac{AN_{eb}}{2}(3\lambda_b^2 - 3) - B\left(N_{ea}\ln\left(\frac{V}{V_0}\right) + N_{eb}\ln\left(\frac{V}{V_0}\right)\right)$$

<div align="right">(Equation 4.8)</div>

$$\lambda_a^2 = \left(\frac{V_{ap} + V_{bp} + V_{1m}N_1}{V_{ap} + V_{ad}}\right)^{2/3} \quad \lambda_b^2 = \left(\frac{V_{ap} + V_{bp} + V_{1m}N_1}{V_{ap} + V_{bp} + V_{bd}}\right)^{2/3}$$

<div align="right">(Equation 4.9)</div>

$$\frac{\partial \lambda_a^2}{\partial N_1} = \frac{2}{3}\frac{V_{1m}}{V_{ap} + V_{ad}}\left(\frac{V_{ap} + V_{bp} + V_s}{V_{ap} + V_{ad}}\right)^{-1/3}$$

<div align="right">(Equation 4.10)</div>

$$\frac{\partial \lambda_b^2}{\partial N_1} = \frac{2}{3}\frac{V_{1m}}{V_{ap} + V_{bp} + V_{bd}}\left(\frac{V_{ap} + V_{bp} + V_s}{V_{ap} + V_{bp} + V_{bd}}\right)^{-1/3}$$

<div align="right">(Equation 4.11)</div>

$$\frac{\Delta \mu_{1,el}}{RT} = A\frac{N_{ea}}{V_{ap}}\frac{\partial \lambda_a^2}{\partial N_1}V_{ap} + A\frac{N_{eb}}{V_{bp}}\frac{\partial \lambda_b^2}{\partial N_1}V_{bp}$$

$$= AV_{1m}\nu_{ea}\frac{V_{ap}}{V_{ap} + V_{ad}}\left(\frac{V_{ap} + V_{bp} + V_s}{V_{ap} + V_{ad}}\right)^{-1/3}$$

$$+ AV_{1m}\nu_{ea}\frac{V_{bp}}{V_{ap} + V_{bp} + V_{bd}}\left(\frac{V_{ap} + V_{bp} + V_s}{V_{ap} + V_{bp} + V_{bd}}\right)^{-1/3}$$

<div align="right">(Equation 4.12)</div>

$$V_{1m}\nu_{ea}\frac{V_{ap}}{V_{ap}+V_{ad}}\left(\frac{V_{ap}+V_{bp}+V_s}{V_{ap}+V_{ad}}\right)^{-1/3}$$

$$+AV_{1m}\nu_{ea}\frac{V_{bp}}{V_{ap}+V_{bp}+V_{bd}}\left(\frac{V_{ap}+V_{bp}+V_s}{V_{ap}+V_{bp}+V_{bd}}\right)^{-1/3}$$

(Equation 4.13)

$$V_{1m}\nu_{ea}\frac{V_{ap}}{V_{ap}+V_{ad}}\left(\frac{V_{ap}+V_{bp}+V_s}{V_{ap}+V_{ad}}\right)^{-1/3}=V_{1m}\nu_{ea}\phi_{2a}^0\phi_2^{1/3}\varphi_a^{1/3}(\phi_{2a}^0)^{-1/3}$$

$$=V_{1m}\nu_{ea}\phi_2^{1/3}\varphi_a^{1/3}(\phi_{2a}^0)^{2/3}$$

(Equation 4.14)

$$AV_{1m}\nu_{ea}\frac{V_{bp}}{V_{ap}+V_{bp}+V_{bd}}\left(\frac{V_{ap}+V_{bp}+V_s}{V_{ap}+V_{bp}+V_{bd}}\right)^{-1/3}$$

$$=AV_{1m}\nu_{ea}\frac{V_{bp}^{2/3}}{\left(V_{ap}+V_{bp}+V_{bd}\right)^{2/3}}\frac{V_{bp}^{1/3}}{\left(V_{ap}+V_{bp}+V_s\right)^{1/3}}$$

(Equation 4.15)

$$\left(\frac{V_{bp}}{V_{ap}+V_{bp}+V_{bd}}\right)^{2/3}=\left(\frac{V_{ap}+V_{bp}}{V_{ap}+V_{bp}+V_{bd}}\frac{V_{bp}}{V_{ap}+V_{bp}}\right)^{2/3}=\left(\phi_{2b}^0\right)^{2/3}\varphi_b^{2/3}$$

(Equation 4.16)

$$\frac{V_{bp}^{1/3}}{\left(V_{ap}+V_{bp}+V_s\right)^{1/3}}=\left(\frac{V_{ap}+V_{bp}}{V_{ap}+V_{bp}+V_s}\frac{V_{bp}}{V_{ap}+V_{bp}}\right)^{1/3}=\phi_2^{1/3}\varphi_b^{1/3}$$

(Equation 4.17)

$$\frac{\Delta\mu_{1,el}}{RT}=A\frac{N_{ea}}{V_{ap}}\frac{\partial\lambda_a^2}{\partial N_1}V_{ap}+A\frac{N_{eb}}{V_{bp}}\frac{\partial\lambda_b^2}{\partial N_1}V_{bp}$$

$$=AV_{1m}\phi_2^{1/3}\left(\nu_{ea}\varphi_a^{1/3}\phi_{0a}^{2/3}+\nu_{eb}\varphi_b(\phi_{2b}^0)^{2/3}\right)$$

$$+B\phi_2(\nu_{ea}\varphi_a+\nu_{eb}\varphi_b)$$

(Equation 4.18)

Thus, the contribution to the swelling equation due to elasticity is given by the equation:

$$\frac{\Delta\mu_{1,\text{el}}}{RT} = AV_{1\text{m}}\phi_2^{1/3}\left(\nu_{\text{ea}}\varphi_{\text{a}}^{1/3}(\phi_{2\text{a}}^0)^{2/3} + \nu_{\text{eb}}\varphi_{\text{b}}(\phi_{2\text{b}}^0)^{2/3}\right) + B\phi_2(\nu_{\text{ea}}\varphi_{\text{a}} + \nu_{\text{eb}}\varphi_{\text{b}})$$

(Equation 4.19)

The mixing contribution involves equally all segments of network a and network b. Therefore it remains the same and is a function of ϕ_2.

$$\frac{\Delta\mu_1}{RT} = \ln(1 - \phi_2) + \phi_2 + \chi\phi_2^2 + AV_{1\text{m}}\phi_2^{1/3}\left(\nu_{\text{ea}}\varphi_{\text{a}}^{1/3}(\phi_{2\text{a}}^0)^{2/3} + \nu_{\text{eb}}\varphi_{\text{b}}(\phi_{2\text{b}}^0)^{2/3}\right)$$
$$+ B\phi_2(\nu_{\text{ea}}\varphi_{\text{a}} + \nu_{\text{eb}}\varphi_{\text{b}}) = 0$$

(Equation 4.20)

Deformation

Recalling the equation:

$$\frac{\Delta F_{\text{el}}}{kT} = \frac{AN_{\text{ea}}}{2}\left(\lambda_{\text{a}x}^2 + \lambda_{\text{a}y}^2 + \lambda_{\text{a}z}^2 - 3\right) + \frac{AN_{\text{eb}}}{2}\left(\lambda_{\text{b}x}^2 + \lambda_{\text{b}y}^2 + \lambda_{\text{b}z}^2 - 3\right)$$
$$- B\left(N_{\text{ea}}\ln\left(\frac{V}{V_{\text{a}}}\right) + N_{\text{eb}}\ln\left(\frac{V}{V_{\text{b}}}\right)\right)$$

(Equation 4.21)

passing from deformation ratios relative to reference state to deformation ratios relative to the swollen isotropic state (used in experiments), we employ the relations (L is dimension (length) in arbitrary units):

$$\lambda_{\text{a}j} = \frac{L_{\text{a}j}}{L_{\text{a}j0}} = \frac{L_{\text{a}j}}{\left(L_{\text{a}j}\right)_{\text{iso}}}\frac{\left(L_{\text{a}j}\right)_{\text{iso}}}{L_{\text{a}j0}} = \Lambda_{\text{a}j}\frac{\left(L_{\text{a}j}\right)_{\text{iso}}}{L_{\text{a}j0}}$$

$$\lambda_{\text{b}j} = \frac{L_{\text{b}j}}{L_{\text{b}j0}} = \frac{L_{\text{b}j}}{\left(L_{\text{b}j}\right)_{\text{iso}}}\frac{\left(L_{\text{b}j}\right)_{\text{iso}}}{L_{\text{b}j0}} = \Lambda_{\text{b}j}\frac{\left(L_{\text{b}j}\right)_{\text{iso}}}{L_{\text{b}j0}}$$

(Equation 4.22)

where L_{iso} refers to isotropic swollen state and L_0 refers to the reference state taken here as state at network formation.

Inserting these relations, one obtains:

$$\frac{\Delta F_{el}}{kT} = \frac{AN_{ea}}{2} \phi_2^{-2/3} \varphi_a^{-2/3} (\phi_{2a}^0)^{2/3} \left(\Lambda_x^2 + \Lambda_y^2 + \Lambda_z^2 - 3\right)$$

$$+ \frac{AN_{eb}}{2} \phi_2^{-2/3} (\phi_{2b}^0)^{2/3} \left(\Lambda_x^2 + \Lambda_y^2 + \Lambda_z^2 - 3\right)$$

$$- B\left(N_{ea} \ln\left(\frac{V}{V_a}\right) + N_{eb} \ln\left(\frac{V}{V_b}\right)\right)$$

(Equation 4.23)

which gives:

$$\frac{\Delta F_{el}}{kT} = A\phi_2^{-2/3} \left(\frac{N_{ea}\varphi_a^{-2/3}(\phi_{2a}^0)^{2/3} + (\phi_{2b}^0)^{2/3}N_{eb}}{2}\right) \left(\Lambda_x^2 + \Lambda_y^2 + \Lambda_z^2 - 3\right)$$

$$- B\left(N_{ea} \ln\left(\frac{V}{V_a}\right) + N_{eb} \ln\left(\frac{V}{V_b}\right)\right)$$

(Equation 4.24)

Simple shear:

$$\Lambda_x = \Lambda, \Lambda_y = 1, \Lambda_x\Lambda_y\Lambda_z = V/V_{iso}, \Lambda_z = (V/V_{iso})\Lambda^{-1} \approx \Lambda^{-1}$$

(Equation 4.25)

gives:

$$\frac{\Delta F_{el}}{kT} = A\phi_2^{-2/3} \left(\frac{N_{ea}\varphi_a^{-2/3}(\phi_{2a}^0)^{2/3} + (\phi_{2b}^0)^{2/3}N_{eb}}{2}\right) \left(\Lambda^2 + \Lambda^{-2} - 2\right)$$

$$- B\left(N_{ea} \ln\left(\frac{V}{V_a}\right) + N_{eb} \ln\left(\frac{V}{V_b}\right)\right)$$

(Equation 4.26)

Transforming $\gamma = \Lambda - \Lambda^{-1}$ and differentiating:

$$\left(\frac{\partial \Delta F_{el}}{\partial \gamma}\right)_{T,V} = AkT\phi_2^{-2/3} \left(N_{ea}\varphi_a^{-2/3}(\phi_{2a}^0)^{2/3} + N_{eb}(\phi_{2b}^0)^{2/3}\right)\gamma$$

(Equation 4.27)

per swollen cross-section and passing from molecules to moles of EANCs per volume (ν_{ea}, ν_{eb}) and expressing the concentration in moles per unit dry volume instead of swollen volume:

$$\sigma_{sw} = AkT\phi_2^{1/3} \left(\nu_{ea}\varphi_a^{1/3}(\phi_{2a}^0)^{2/3} + \nu_{eb}(\phi_{2b}^0)^{2/3}\varphi_b\right)\gamma$$

(Equation 4.28)

134

Passing from molecules to moles of EANCs per volume (ν_{ea}, ν_{eb}) and expressing the concentration in moles per unit dry volume instead of swollen volume (factor V_d/V):

$$G_{sw} = RTA\phi_2^{1/3}\left(\nu_{ea}\varphi_a^{1/3}(\phi_{2a}^0)^{2/3} + \nu_{eb}(\phi_{2b}^0)^{2/3}\varphi_b\right)$$

(Equation 4.29)

Extension/Compression

$\Lambda_x = \Lambda, \qquad \Lambda_y = \Lambda_z, \qquad \Lambda_x\Lambda_y\Lambda_z = V/V_{iso}, \qquad \Lambda_y^2 = \Lambda_z^2 = (V/V_{iso})\Lambda^{-1} = (\phi_{2,iso}/\phi_2)\Lambda^{-1} \approx \Lambda^{-1}$

$$\frac{\Delta F_{el}}{kT} = A\phi_2^{-2/3}\left(\frac{N_{ea}\varphi_a^{-2/3}(\phi_{2a}^0)^{2/3} + (\phi_{2b}^0)^{2/3}N_{eb}}{2}\right)(\Lambda^2 + 2\Lambda^{-1} - 3)$$

$$- B\left(N_{ea}\ln\left(\frac{V}{V_a}\right) + N_{eb}\ln\left(\frac{V}{V_b}\right)\right)$$

(Equation 4.30)

The uniaxial force, f_{ec} causing deformation Λ (subscript "ec" stands for extension/compression is equal to:

$$\left(\frac{\partial\Delta F_{el}}{\partial L_x}\right)_{T,V} = f_{ec}$$

$$= AkT\phi_2^{-2/3}\left(N_{ea}\varphi_a^{-2/3}(\phi_{2a}^0)^{2/3} + (\phi_{2b}^0)^{2/3}N_{eb}\right)(\Lambda$$

$$- (\phi_{2,iso}/\phi_2)\Lambda^{-2})$$

$$\approx AkT\phi_2^{-2/3}\left(N_{ea}\varphi_a^{-2/3}(\phi_{2a}^0)^{2/3} + (\phi_{2b}^0)^{2/3}N_{eb}\right)(\Lambda - \Lambda^{-2})$$

(Equation 4.31)

Passing to concentrations and stress, f_{ec}, per unit cross-section area of undeformed, isotropic sample, one gets:

$$\sigma_{ec} = ART\phi_2^{1/3}\left(\nu_{ea}\varphi_a^{1/3}(\phi_{2a}^0)^{2/3} + \nu_{eb}\varphi_b(\phi_{2b}^0)^{2/3}\right)(\Lambda - (\phi_{2,iso}/\phi_2)\Lambda^{-2})$$

$$\approx ART\phi_2^{1/3}\left(\nu_{ea}\varphi_a^{1/3}(\phi_{2a}^0)^{2/3} + \nu_{eb}\varphi_b(\phi_{2b}^0)^{2/3}\right)(\Lambda - \Lambda^{-2})$$

(Equation 4.32)

The final relation:

$$\sigma_{ec} = ART\phi_2^{1/3}\left(\nu_{ea}\varphi_a^{1/3}(\phi_{2a}^0)^{2/3} + \nu_{eb}\varphi_b(\phi_{2b}^0)^{2/3}\right)(\Lambda - \Lambda^{-2})$$

(Equation 4.33)

has the same factor in front of the deformation function as in shear, but the deformation function is different.

Table 14. List of symbols and their meaning used in this paragraph 5.3.

A and B	front factors in the Flory-Erman junction-fluctuation theory
E	Young's modulus
f_e	elastically effective crosslinker functionality
f_{ec}	uniaxial force (subscript "ec" stands for extension/compression)
ΔF_{mix}	Helmholtz energy change of mixing of polymer and solvent
ΔF_{el}	Helmholtz energy change of elastic deformation
ΔG_{sw}	Gibbs energy change of swelling
ΔG_{mix}	Gibbs energy change of mixing of polymer and solvent
ΔG_{el}	Gibbs energy change of elastic deformation
k	Boltzmann constant
L_j	actual length of sample in the i-th direction
$\left(L_j\right)_{iso}$	length of sample in the i-th direction in the isotropic (swollen) network
L_{j0}	length of sample in the reference state ($\approx$ state at network formation)
N_1	number of moles of solvent molecules
N_e	number of EANC
N_{ea}	number of EANC in network a
N_{eb}	number of EANC in network b
R	universal gas constant
S_{iso}	cross-sectional area of undeformed, isotropic sample
T	temperature
V_0	reference volume
V_{1m}	molar volume of the solvent
V_a	volume of network a
V_b	volume of network b
V_{ap} and V_{bp}	volume of polymer a and polymer b
V_{ad} and V_{bd}	volumes of diluents added with monomer a and monomer b
V_s	volume of solvent in the swollen IPN
γ	shear deformation

ε	strain in uniaxial deformation
λ_{b}	deformation at break
$\lambda_{\mathrm{ix}}, \lambda_{\mathrm{iy}}, \lambda_{\mathrm{iz}}$	deformation ratios with respect to the reference state along the l coordinate axes of network i
Λ_{j}	deformation ratio with respect to the isotropic (swollen) state
$\Delta\mu_{1,\mathrm{mix}}$	solvent chemical potential change
ν_{e}	concentration of EANC
σ	deformation stress
$\varphi_{\mathrm{a}}, \varphi_{\mathrm{b}}$	volume fractions of polymer network a and polymer network b in dry IPN
χ	Flory-Huggins interaction parameter
ϕ_1	volume fraction of solvent
ϕ_2	volume fraction of polymer in swollen single network
ϕ_2^0	volume fraction of all polymerizable substances at preparation
$\phi_{2\mathrm{a}}^0, \phi_{2\mathrm{b}}^0$	volume fraction of polymer a, and polymer b, respectively, in the mixtures with their diluents; for definitions, cf. eqs. (4.6)

5.3.2. Comparison of experiment vs. theory applied to PHEMA-PHEMA IPN hydrogels

For estimation of correlation between the concentration of EANC, swelling ratio and Young's modulus of IPN hydrogels, we formulated a model for the cases, when:

- hydrogels are non-porous and homogeneous;
- both networks are formed from chemically identical monomers;
- networks differ in crosslink density;
- coiling states of network chains is different.

When formulating this model, the following assumptions were made:

- additivity of contribution by two networks;
- no extra contribution by mutual interactions;
- isotropic swelling.

According to the model, the relation between the Young's modulus of IPNs and their crosslink densities was derived from the Helmholtz energy of deformation of a network of Gaussian chains:

$$E = 3RTA\phi_2^{1/3} \left(\nu_{ea}\varphi_a^{1/3}(\phi_{2a}^0)^{2/3} + \nu_{eb}\varphi_b(\phi_{2b}^0)^{2/3} \right)$$

<div align="right">(Equation 4.34)</div>

where R is universal gas constant, T is the temperature in K, A is a dimensionless factor in the Flory-Erman rubber elasticity theory (equal to 1 here), ϕ_2 is the total volume fraction of polymer (network 1 (or called "network a") and network 2 (or called "network b")) at swelling equilibrium, ν_{ea} and ν_{eb} are the concentrations of elastically active network chains (EANC) in networks 1 and 2 in moles per volume, φ_a and φ_b are volume fractions of networks 1 and 2, ϕ_{2a}^0 is the volume fraction of network 1 in IPN and ϕ_{2b}^0 is the volume fraction of networks 1 and 2 in swollen IPN.

This model was applied to PHEMA-PHEMA IPN hydrogels, the first network of which was prepared at 40 wt.-% of water and various crosslinker concentrations (Y = 0.2 − 6 mol-%), whereas the second network was prepared without diluent and at constant amount of crosslinker (0.3 mol-%) (Figure 62). The values of $E_{experim}$ were obtained by equilibrium tensile measurements, the E_{calc} was calculated according to the Equation 4.34.
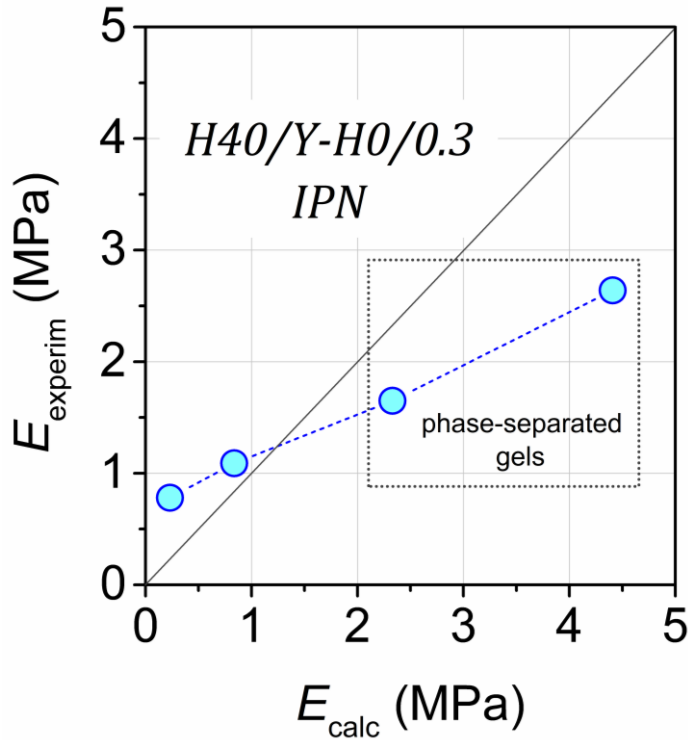
Figure 62. Young's moduli of swollen H40/Y-H0/0.3 IPN hydrogels determined by tensile tests (experimental) and calculated from the composition and swelling of

networks according to Equation 4.34. The values of "Y" corresponding to the concentration of DEGDMA crosslinker in the H40/Y parent network were 0.2, 1, 3, and 6 mol-%.

The dependence between moduli was close to linear with slope of 0.44. The deviation from the diagonal line observed for H40/3 and H40/6 based IPNs can be explained similarly to the previous graph in Figure 60 – lower values of experimentally determined moduli (E_{experim}) were caused by lower concentration of EANC due to incomplete utilization of crosslinker molecules. For less crosslinked PHEMA networks with 0.2 and 1 mol-% concentration of added crosslinker, the E_{experim} was somewhat higher than E_{calc}. The reason for this could be extra entanglements between interpenetrating networks of IPN hydrogels.

5.4. Oscillatory shear deformation of hydrogels

5.4.1. Finding gap for swollen hydrogels

The mechanical properties of swollen hydrogels subjected to oscillatory shear deformation using the rheometer will be discussed in this part. The measurements included several important precautions: the ensuring the parallelism and smoothness of sample surfaces as well as the absence of defects (bubbles, scratches, etc.) on sample surfaces by careful preparation of the sample, finding a correct gap between the plates, and prevention of solvent evaporation during the deformation. The parallelism of sample surfaces was controlled by using a spacer of precise thickness in the polymerization mold. The most crucial and arduous part in measurement of soft hydrogels was ensuring the perfect contact of sample with the measuring shear geometry. Finding a "correct" gap between (Figure 16 in Experimental part) the measuring plates of the shear geometry prevents the sample slippage and water squeezing due to overpressing of the sample. To achieve the optimal contact, the auto-tension mode with a target normal force set to 1.5 – 3 % of maximum possible compression weight (which is 2 kg for Gemini HR Nano) and corresponding to 30 – 60 g was used. In the "auto-tension" regime, the geometry gradually approached the disc sample upper surface until full contact. The entire process from "no contact" to "full contact" was monitored by the change of storage (G') and loss (G'') moduli, thrust and gap size. As an example, the Figure 63 shows the dynamic change of the mentioned parameters upon searching a contact with sample for the case of swollen PHEMA hydrogel (H40/1). Low values of moduli and thrust at the beginning of measurement indicated the absence of contact of geometry with the sample. The G', G'' and thrust values increased with the decrease of gap size (i.e., with force on sample). At a certain gap size, the values of moduli and thrust sharply increased and passed to the plateau region. This plateau had a certain length for each sample. The gap size at the beginning of the plateau region (further remaining constant) was considered as the appropriate distance between measuring plates providing minimum normal force acting on the sample and related to full sample surface contact with the measuring geometry. The measurements were thus carried out at this gap size determined for each sample type. The absence of slippage between the sample and geometry was controlled by smooth output signal in the force oscillation mode without or with only low harmonic distortion (close to 0 %).
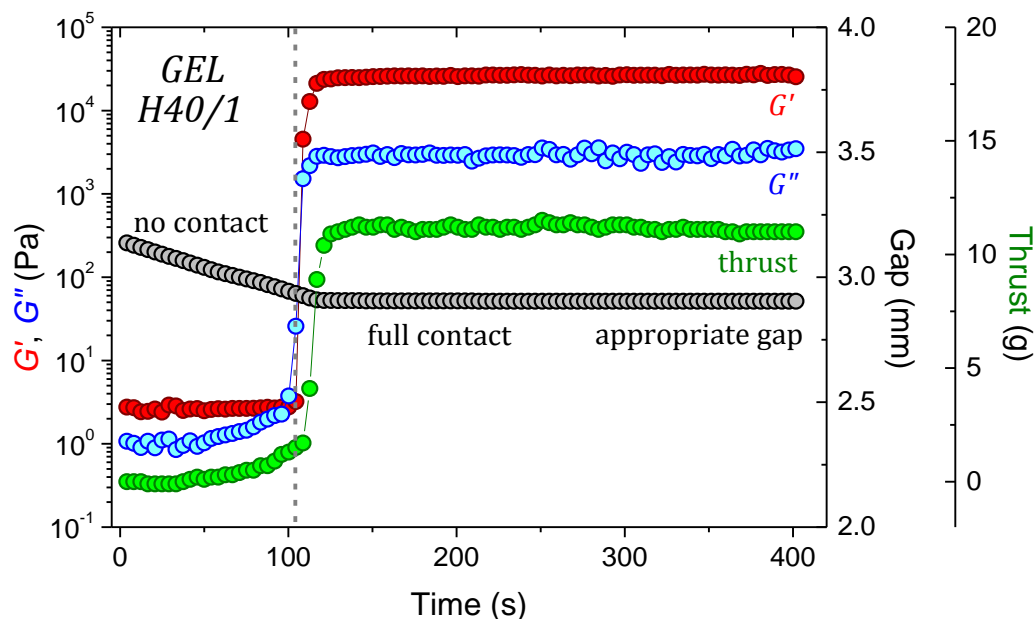
Figure 63. Experimental method for finding a "correct gap" between the measuring plates in auto-tension mode with a target normal force set to 2 % at frequency of 1 Hz. The example is given for swollen H40/1 hydrogel.

Once the appropriate gap was found, the deformation strain ensuring measurement in linear viscoelastic region (LVR) is to be determined. In LVR, the viscoelastic properties of materials are independent of applied strain or stress. The LVR was determined from so called amplitude sweep upon which the storage modulus, G', was measured at various strains. An example of amplitude sweep measurement for non-porous H40/1 and macroporous H80/1 hydrogels is shown in Figure 64. The linear region for non-porous PHEMA gel was relatively broad, that within the applied range of strains the non-linear region was not reached. The deformation of macroporous PHEMA hydrogel revealed both linear and non-linear regions. The linear region was in the range of strains from $2 \cdot 10^{-4}$ to $4 \cdot 10^{-3}$. The deformation of hydrogels at various strains in amplitude sweep test disturbs the network polymer chains and puts them out of the equilibrium state; therefore, the swollen gels are supposed to be equilibrated in a single frequency mode before the final measurement. This implied the tracking of mechanical responses of sample to stress oscillations at 1 Hz in time. Once the parameters have stopped changing for at least 15-20 minutes indicating the fully relaxed state of gel, the next step can be started.
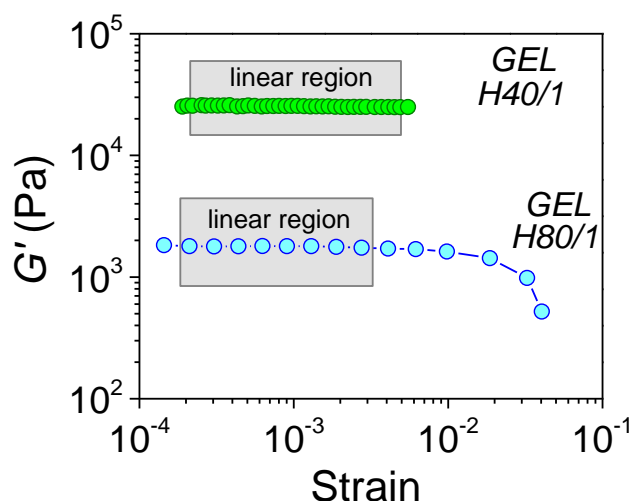
141

Figure 64. Storage modulus of hydrogels as a function of strain. Amplitude sweep test for swollen non-porous (H40/1) hydrogel deformed at strains from $1.9 \cdot 10^{-4}$ to $5.5 \cdot 10^{-3}$ and for macroporous (H80/1) PHEMA hydrogel deformed at strains from $1.4 \cdot 10^{-4}$ to $4 \cdot 10^{-2}$: determination of linear viscoelastic region.

The next step of the experimental examination of linear shear oscillatory behavior of the gels was the measurement of dynamic frequency dependent values of G', G''. This was done as so called frequency sweep test, which can be also an indicator of the correctness of the found gap size, as allows following the stability of thrust upon the measurement. Theoretically, thrust should be close to zero, but small deviations ($\pm$ 5 g) are acceptable in our measurements. The details of thrust measurement are available in Appendix 3.

5.4.2. Constituent single network hydrogels H40/Y: effect of crosslinker concentration

A typical graph with spectra of dynamic mechanical parameters for swollen PHEMA hydrogels is presented in Figure 65. Both moduli representing the elastic (storage modulus, G') and viscous (loss modulus, G'') constituents of viscoelastic properties of swollen H40/1 hydrogel decreased with decrease of frequencies. As expected for chemically crosslinked elastic hydrogels, the storage modulus (G') of the sample was higher than the loss modulus (G''). At slow dynamic loading, the difference in moduli was more than one order of magnitude; at fast dynamic loading, the difference was around three times. The slope of G''-curve was sharper, while the G'-curve revealed broad nearly frequency-independent plateau region corresponding to rubbery state of hydrogel. The gradual increase of G' at frequencies above 1 Hz

142

suggests the onset of the main transition region also referred to as α-relaxation that suggests the transition of sample to the state of "vitrification". The growth of G'' was significantly faster, so that the crossover of curves (corresponding to tan δ maximum, i.e., the state of transition) is likely to appear at higher frequencies out of studied region.

The loss factor (tan δ), which is the ratio of moduli G'/G'', also decreased towards low frequencies and was close to zero, which is typical for covalently crosslinked polymer networks in their rubbery state. The Figure 65 shows an example of dynamic-mechanical properties measurement performed for all studied hydrogels (single networks and IPNs), but in the frame of this work we will focus only on storage moduli (G') of materials.
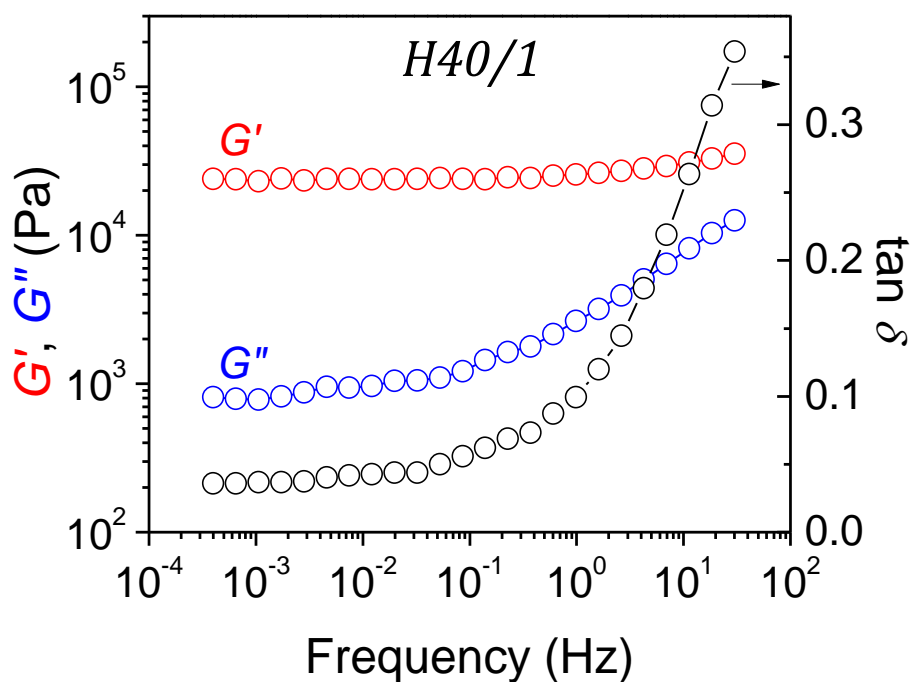
Figure 65. Storage (G') and loss (G'') shear moduli, and loss factor (tan δ) of water-swollen non-porous single network H40/1 hydrogel as a function of frequency.

Dynamic mechanical properties of swollen PHEMA hydrogels (H40/Y) crosslinked to various extents (0.2 – 6 mol-% of crosslinker) and prepared at 40 wt.-% of water as diluent were measured in the frequency range from $4 \cdot 10^{-4}$ to 40 Hz and at strain of 10^{-3} chosen from linear viscoelastic region (LVR) (see Figure 64). The storage modulus (G') of swollen gels increased from less to more crosslinked networks in the range from approximately 10^4 to 10^5 Pa (Figure 66). Indeed, the

stronger hydrogels were formed in samples with more elastically active network chains (EANC) per sample volume. The *G'* of loosely crosslinked H40/0.2 hydrogel gradually decreased at slow dynamic loading all the time and the frequency-independent plateau region corresponding to equilibrium state was not observed. Apparently, the relaxation process of network chains in this hydrogel is slow, and their full relaxation will occur later at even lower frequencies hardly achievable by the standard method. For the rest of hydrogels, the nearly frequency-independent plateau regions were observed, although the length of region shortened with the increase of crosslinker concentration. As the network chains of heterogeneous H40/6 hydrogel were shorter and rigid compared to other hydrogels, this sample showed earlier onset of transition to glassy region. However, this sample is going through incipient microphase separation during its preparation, so its homogeneity is lost.
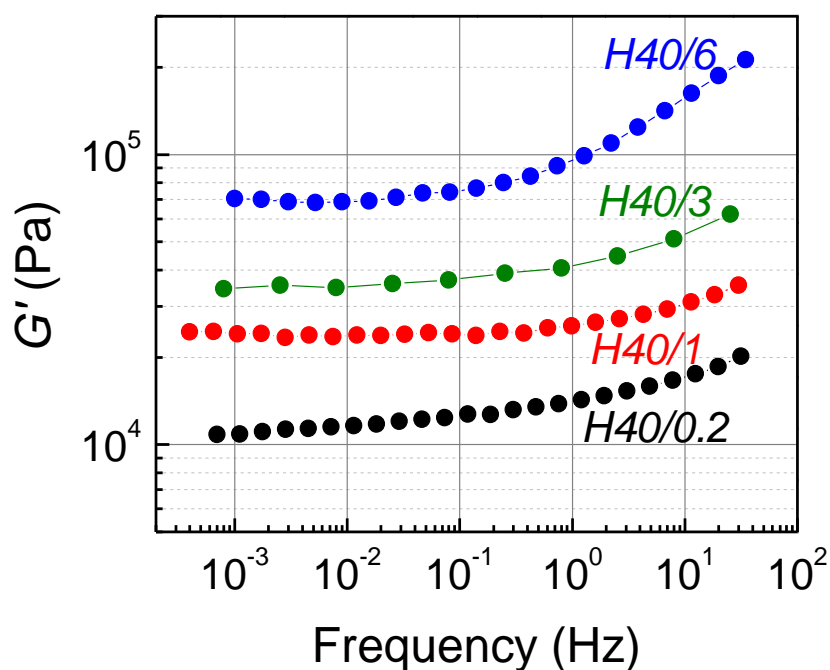
Figure 66. Storage modulus (*G'*) of water-swollen single network PHEMA hydrogels prepared at 40 wt.-% of water as diluent and various crosslinker concentrations (0.2, 1, 3, and 6 mol.%) as a function of frequency.

5.4.3. Chemically homogeneous PHEMA-PHEMA IPN hydrogels

Interpenetration of the described above single PHEMA networks with the second PHEMA network of low crosslinker concentration (0.3 mol-%) led to formation of stronger hydrogels (Figure 67). The *G'* of IPNs increased with the

increase of crosslinker concentration in network 1 (Figure 67a). The general dynamics of moduli for IPNs was similar to that for reference single networks, however, in the case of IPNs, all curves were more or less parallel just shifted up and down. The embedding of the second network into the loosely crosslinked H40/0.2 network did not contribute to faster relaxation of polymer chains in considered frequency range, perhaps, due to additional topological constraints. Despite the reinforcement of all hydrogels, the increase of G'_{IPN}/G'_{SN1} ratio was non-linear (Figure 67b). Two IPN hydrogels with the least concentration of crosslinker in network 1 (0.2 and 1 mol-%) drop out from the linearity. For the network 1 prepared at 0.2 mol-% of crosslinker, the embedding of network 2 contained comparable amount of crosslinker (0.3 mol-%) was significant and resulted in considerable reinforcement of IPN hydrogel compared to reference single network. Whereas for the network 1 contained 5 times more crosslinker (1 mol-%), the embedding of network contained 0.3 mol-% of crosslinker did not contribute to excellent mechanical properties of IPN. Although the 0.3 mol-% of crosslinker in network 2 is almost nothing for tightly crosslinked H40/3 and H40/6 networks 1, the great reinforcement of hydrogels was seemingly related to intermediate (H40/3) and heterogeneous (H40/6) morphology of reference network 1 gels. Thereby, the resulting IPNs can be considered as heterogeneous hybrid hydrogels with uneven distribution of crosslink density.
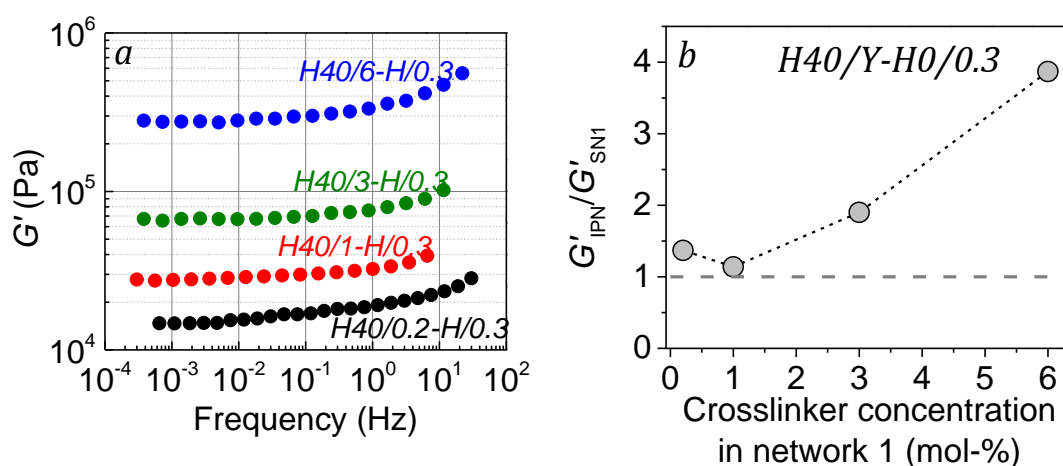
Figure 67. Storage modulus (G') of water-swollen H40/Y-H0/0.3 IPN hydrogels as a function of frequency (a). At preparation, the network 1 (H40/Y) contained 40 wt.-% of water and various crosslinker concentrations (0.2, 1, 3, and 6 mol-%), while the network 2 was not diluted and contained 0.3 mol-% of crosslinker (H0/0.3). The

reinforcement ratio (G'_{IPN}/G'_{SN1}) of IPN hydrogels was estimated as a relation of storage moduli of IPNs (G'_{IPN}) and of reference single networks 1 (G'_{SN1}) (b).

5.4.4. PHEMA-PHEMA versus PHEMA-PGMA IPN hydrogels

Dynamic storage moduli measured in a wide range of frequencies for non-porous and porous constituent PHEMA networks 1 and PHEMA or PGMA networks 2 are shown in Figure 68 (a and b). The modulus G' decreased: (1) with dilution of monomers mixture with water at preparation and (2) with reduction of crosslinker concentration. Dilution of monomers mixture affected the morphology of hydrogels, which was discussed earlier in paragraphs 3.1 (page 88) and 3.2 (94). To recall, at certain dilution of HEMA monomer (above 40 wt.-% of water), the PHEMA becomes immiscible with water and the reaction-induced phase separation causes the formation of inhomogeneities, even pores, in the gel matrix. When the crosslinking polymerization of the same reaction mixture took place at low temperature ($T = -14$ °C), the pores of cryogels were formed due to ice crystals (cf. details of morphology in paragraph 3.2, Figure 37). The "phase-separated" macroporous hydrogel and macroporous cryogel formed at high diluent content (80 wt.-% of water) were mechanically weaker than non-porous hydrogels prepared at moderate dilution (below 40 wt.-% of water) (Figure 68a). The different morphology and porosity (0.72 for H80/1 vs 0.63 for cH80/1) of gels of the same composition (80/1) caused the difference in their mechanical properties: the modulus of cH80/1 cryogel of lower porosity was higher than of H80/1 hydrogel.

Also, it is worth to mention, how significantly the moduli of two non-porous hydrogels (H0/1 and H40/1) of similar degree of swelling (SD: 37 % and 39.8 %, respectively) differed. The G' in near-equilibrium region for H0/1 was 48.8 kPa versus 24.5 kPa for H40/1. Being a poor solvent for PHEMA network, water molecules stretch the polymer chains of PHEMA networks prepared without dilution or at moderate dilution (0 – 40 wt.-%) only up to swelling degree of SD = 37 - 40 % . So, if 40 wt.-% of diluent was already present during the crosslinking polymerization, then almost no additional water can be swollen to network at swelling equilibrium. But the mechanical response of these networks to deformation was sensitive to the extent of dilution at networks preparation due to different states of polymerizing HEMA-chains. Preparation of a network without diluent led to formation of homogeneous network structure, which swelled in water to the same

extent as e.g., H40/1 hydrogel. A moderate dilution of monomers with water as shown by SWAXS and DLS methods resulted in material of inhomogeneous distribution of network chains in space and the mechanical loading of such network resulted in somewhat lower modulus response. This needs to be studied/explained in future.

As for crosslinker concentration, the more crosslinked H0/1 hydrogel was stronger than the H0/0.3 hydrogel of lower crosslink density. If one compares the moduli of reference swollen in water H0/0.3 and G0/0.3 networks 2, the modulus of the latter was approximately 6 times lower, although the compositions of both networks were identical (Figure 68b). The difference in mechanical properties ($G'_{(H0/0.3)}/G'_{(G0/0.3)}$ = 6.2) was caused by different content of water at equilibrium swollen state. Thus, G0/0.3 hydrogel contained almost 5 times more water than H0/0.3 hydrogel (2.79 g of water per 1 g of dry G0/0.3 network versus 0.56 g of water per 1 g of dry H0/0.3 network).
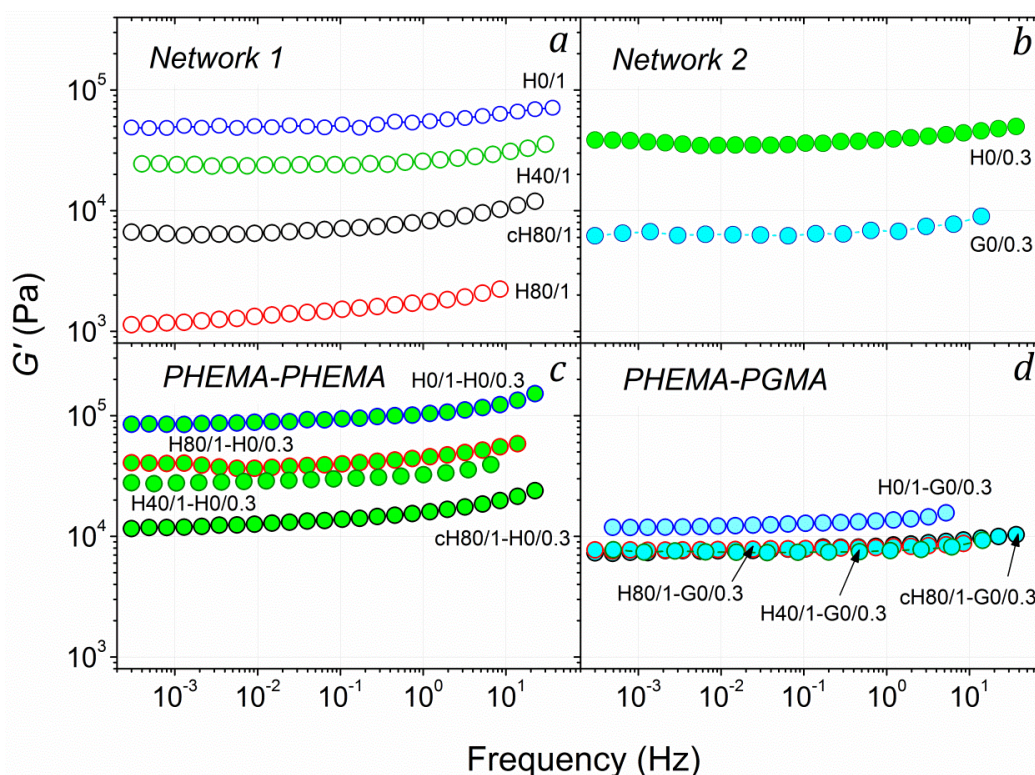
Figure 68. Storage moduli (G') of water-swollen single and IPN hydrogels measured in a frequency range from $4 \cdot 10^{-4}$ to 40 Hz: (a) constituent single PHEMA networks 1, (b) constituent single PHEMA and PGMA networks 2, (c) PHEMA-PHEMA IPNs, and (d) PHEMA-PGMA IPNs.

The IPN hydrogels containing poly(glycerol methacrylate) (PGMA) as a second network were mechanically weaker than PHEMA-PHEMA IPN hydrogels (Figure 68, c and d). This was caused by two factors: first, the swelling of PHEMA network 1 in GMA monomer was higher than that in HEMA monomer (Table 5) so, the resulting IPN differ in the overall content of the second network structure. Second, the PGMA containing IPNs absorbed more water than IPNs formed from two identical less hydrophilic HEMA monomers (Table 10). The storage moduli of PHEMA-PGMA IPNs were very similar except for slightly higher G' of H0/1-G0/0.3 IPN gel (Figure 68d). The swelling of H0/1 network in GMA monomer was slightly less than of other single PHEMA networks, therefore, its increase of modulus can be explained by lower amount of water. Another important parameter affecting the mechanical behavior of PGMA containing IPNs was the microstructure of parent PHEMA network 1. Embedding of hydrophilic PGMA network into the non-porous PHEMA network 1 (H0/1 and H40/1) reduced the moduli of the latter. On the contrary, macroporous PHEMA networks 1 (H80/1 and cH80/1) were reinforced by PGMA network. However, this reinforcement was perhaps mostly caused by changing the morphology from porous to non-porous one. The volume degree of swelling (Q_v) of porous gels swollen in GMA monomer compared to their reference dry state increased approximately 11.6 times (!) for H80/1 hydrogel and 6.6 times for cH80/1 cryogel (Table 5). Or in terms of weights, 1 g of dry H80/1 network contained 12.97 g of GMA monomer, while1 g of dry cH80/1 cryogel contained 12.47 g of GMA monomer. Obviously, the mechanical properties of these IPNs were driven by swelling and mechanical properties of the second PGMA network constituting a great proportion of the IPN. However, due to the presence of network 1 matrix, the moduli of both IPNs exceeded the modulus of reference G0/0.3 hydrogel by 20 %. A huge influence of morphology on apparent storage modulus was revealed on the example of H80/1 hydrogel and cH80/1 cryogel. In principle, the amount of GMA monomer swollen to both networks was relatively similar, but its distribution between the pores and gel matrix was apparently different and not even. For the macroporous H80/1 hydrogel with fused-spheres structure, the enhancement in final modulus was superior. The G' of cH80/1-G0/0.3 IPN was 1.2 times higher than that of reference cH80/1 cryogel network with cell-like structure, while the G' of H80/1-G0/0.3 IPN was 6.7 times higher than that of reference H80/1 network.

The IPNs with embedded PHEMA as a second network were all reinforced mostly in accordance with the amount of HEMA monomer penetrated the volume of the first network (Figure 68c). The IPNs prepared on the base of non-porous H0/1 network and macroporous H80/1 network were significantly reinforced exhibiting the moduli surpassing the moduli of their constituent networks. At the same time, the moduli (G'_{IPN}) of non-porous H40/1-based and macroporous cH80/1-based IPNs were between $G'_{network1} < G'_{IPN} < G'_{network2}$. This phenomenon was mostly caused by the morphology of network 1, the features of which were already discussed above.

Thus, the excellent enhancement of mechanical properties ($G'_{IPN}/G'_{SN1} = 37$) was observed for H80/1-H0/0.3 IPN hydrogel. For other PHEMA-PHEMA IPNs, the G'_{IPN}/G'_{SN1} ratios were 1.13 for H40/1-H0/0.3, 1.74 for H0/1-H0/0.3 and 1.81 for cH80/1-H0/0.3. To conclude, the mechanical response of hydrogels to tensile, oscillation shear or other types of deformation should be always considered in relation to their microstructure.

Chapter 5. Conclusions

Preparation and microstructure of single network and IPN hydrogels

1. Interpenetrating polymer network (IPN) hydrogels were prepared by sequential process of redox-initiated radical polymerization of the first network prepared from 2-hydroxyethyl methacrylate (HEMA), and UV-initiated radical polymerization of the second network prepared from 2-hydroxyethyl methacrylate (HEMA) or glycerol methacrylate (GMA).

2. The variously microstructured first poly(HEMA) networks were obtained by varying the composition of reaction mixtures (dilution with water to various extents, presence of aqueous salt solutions, crosslinker concentration) or the polymerization conditions (temperature) and served as parent matrices for IPN hydrogels. Thus, the non-porous, single-porous hydrogels and cryogels, and double-porous cryogels were studied.
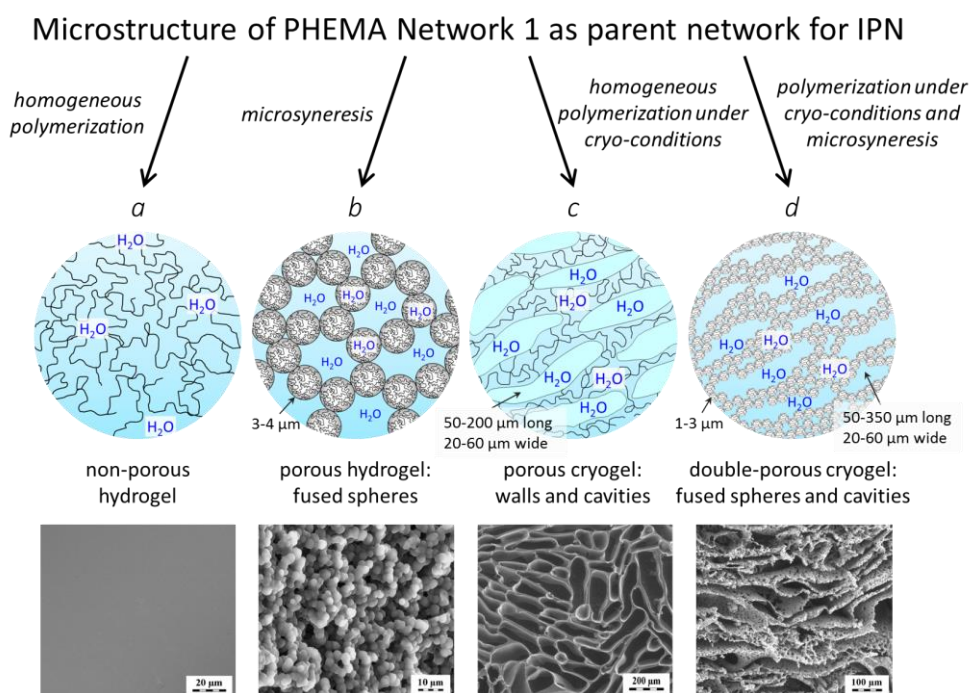
3. A novel route for *one-step* synthesis of double-porous PHEMA network cryogels with interconnected pores was proposed. These materials were obtained by simultaneous formation of large pores due to the ice crystals formed under cryogelation conditions and small pores on walls of cryogel caused by reaction

induced phase separation due to the presence of NaCl solution. The potential of these cryogels to host cells was demonstrated.

Double-porous cryogel

pores formed due to ice crystals (50-350 μm long, 20-60 μm wide)

pores formed due to the reaction-induced phase separation (fused-spheres of size of 1-3 μm)

mouse mesenchymal stem cells
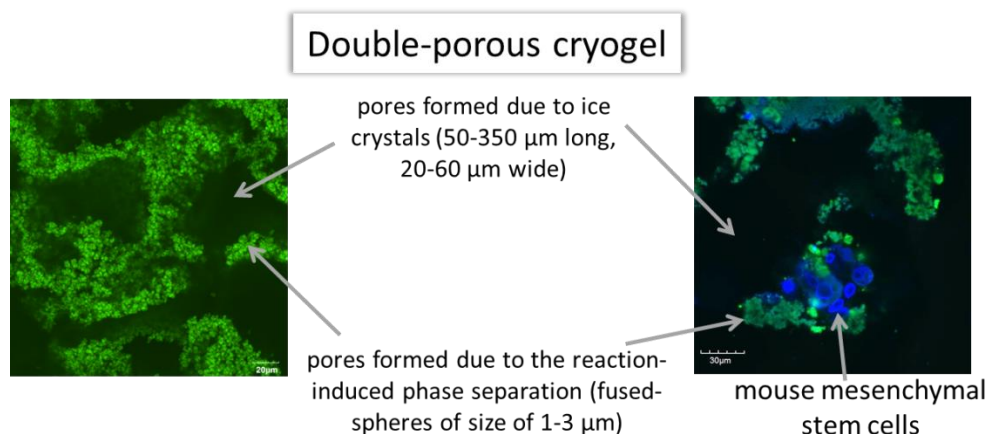
4. The space distrubution of networks within the IPN hydrogel was visualized by laser scanning confocal microscopy (LSCM). Two distinct network phases were observed due to the chemical labeling of each network by incorporating fluorescent dyes of different excitation wavelengths. The distribution of the second network in the pores and gel phase of the parent network was visualized by labeling of the second netowork only.

IPN hydrogel: PHEMA network 1-PGMA network 2

double staining of IPN: PHEMA (green) and PGMA (brownish)

single staining of IPN: PGMA (green)
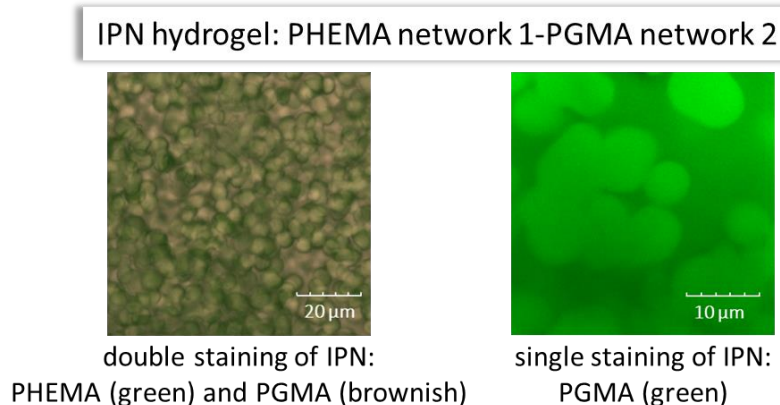
Mechanism, rate and structuring in forming IPN system

1. Investigation of polymetization rate of the second network by the ATR FTIR method revealed its dependence on the microstructure of the parent PHEMA network. It was shown that the polymerization of the second network is faster in microstructured parent networks (non-porous and macroporous) rather than the independent polymerization of the second network. The reaction of the second network polymerization was faster when it was conducted in macroporous parent network than in non-porous parent network. Careful optical analysis of samples

151

suggested that the acceleration in microstrucutred matrices was caused by the multiple UV-light scattering from the interface of the embedded macroporous matrix in the course of preparation of microstructure IPNs (MIPNs) hydrogel. This knowledge may improve the technology of MIPN hydrogels fabrication *in situ* − such as, for example, 3D print methods.
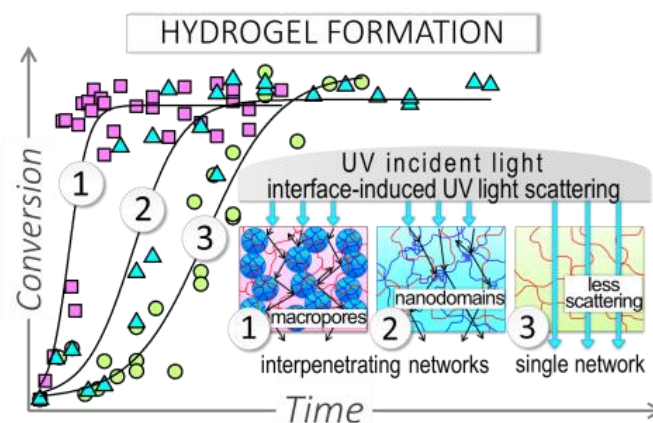
2. The crosslinking of the second network in the matrix of the parent PHEMA network was confirmed by *in situ* monitoring the gelation using the rheometer. The gelation of the second network was manifested by *G'* and *G''* that consented with the semiempirical theory of Winter and Chambon.

3. The SWAXS studies of the crosslinking polymerization of water-diluted HEMA monomer showed the development of structure inhomogeneities (hydrophobic nanosized domains) caused by intramolecular associations of hydrophobic groups of the monomer units and intermolecular associations of several network chains assisted by strengthening of iceberg structures of water. The utilization of aqueous solution of $Mg(ClO_4)_2$ acting as a salting-in additive instead of pure water for network formation led to suppression of association of monomers into small hydrophobic domains. When resulting PHEMA single network with nanosized domains was swollen in HEMA monomer, which is not UCST solvent and does not form icebergs, the small-scale associations disappeared, while the largest inhomogeneities have been fixed by the meshes of network 1 and have survived the structural reorganizations. The overall decrease of scattering in the course of crosslinking polymerization of the HEMA monomer corresponded to a decrease in the contrast of electron densities between the two PHEMA networks.

Formation of PHEMA single network		Formation of PHEMA-PHEMA IPN
in water	*in 0.5 M aqueous solution of Mg(ClO₄)₂*	
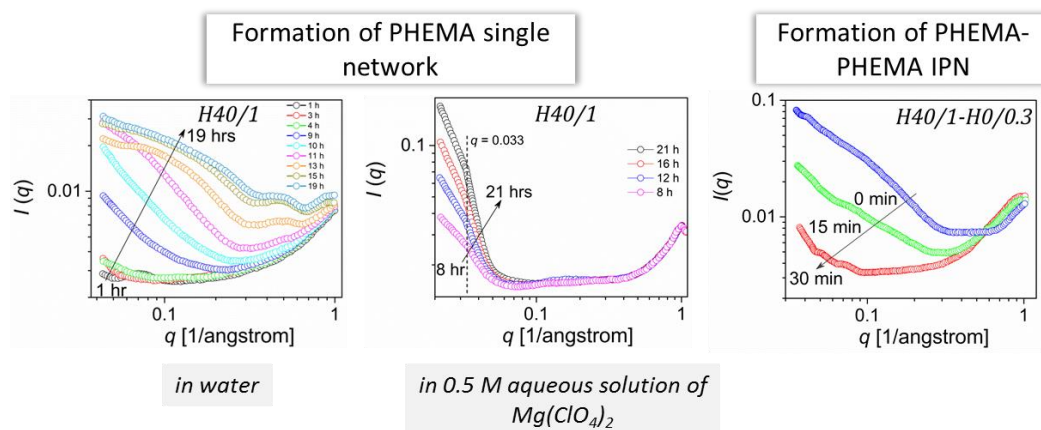
Swelling of IPN hydrogels

1. The effect of initial water and crosslinker contents in the reaction mixture on the microstructure and, thus, swelling of single network hydrogels was demonstrated. High dilution of monomers and low crosslinker concentration at network preparation led to formation of hydrogels of high swelling. The PHEMA single networks prepared at high water dilution (> 80 wt.-%) revealed the separation of the excess liquid from a bulk phase during and after polymerization ("micro-" and "macrosyneresis" phenomenon). The PGMA single networks regardless of their composition (dilution, crosslinker concentration) gained additional water from the surroundings after polymerization and significantly expanded in volume.

2. The effect of polymerization conditions on swelling properties of samples was demonstrated for single network PHEMA gels, which were identical in terms of their chemical composition, but were polymerized at different temperatures. The polymerization at room temperature led to formation of macroporous hydrogel of fused-spheres structure, while at $T = -14$ °C the macroporous cryogel with cell-like pores was formed. The porosity of the fused-spheres structure hydrogel was 10 % higher than that of the cryogel.

3. Poly(glycerol methacrylate), PGMA, as a second network increased the swelling capacity of parent PHEMA network. The swelling of the PHEMA-PGMA IPNs was higher than that of the PHEMA-PHEMA IPNs. The PHEMA parent network in IPNs exhibited surprisingly high swelling capacity when incorporated into the IPN with more hydrophilic PGMA. The PHEMA network chains in hydrogel structured into heterogeneous-spherical morphology were stretched upon swelling in water linearly by a factor of up to $\alpha_1 = 2.4$ that corresponded to almost 140 %

153

extension compared to their state at preparation, while in DMSO – by a factor of up to $\alpha_1 = 2.95$ that corresponded to almost 200 % extension compared to their state at preparation.

Volume expansion of chains of network 1 by swelling:
Example sketched for IPN gel H80/1–G0/0.3

$$V_{\text{rel1}} = (\alpha_1)^3 = \frac{V}{V_{\text{nf1}}}$$

IPN gel	$(\alpha_1)^3$		
	in non-swollen IPN	in IPN swollen in water	in IPN swollen in DMSO
H0/1-H	2.77	4.43	9.03
H40/1-H	2.86	4.46	13.21
H80/1-H	2.71	3.93	9.51
cH80/1-H	1.79	3.02	8.25
H0/1-G	3.30	8.81	16.04
H40/1-G	2.98	6.08	16.80
H80/1-G	3.13	13.40	25.65
cH80/1-G	1.89	6.85	11.39

Deformation behavior of IPNs

1. Deformation behavior of all IPNs and their constituent single networks were characterized in extension by the experimentally obtained Young's modulus (E), ultimate stress and strain, and in shear by the storage modulus (G'). Relatively poor mechanical properties (E, G', σ) were observed for single network gels prepared at high dilution or at low crosslinker concentrations, macroporous gels (H80/1 and cH80/1), and highly swollen gels.

2. The non-porous PHEMA parent networks prepared at moderate dilution with water (40 wt.-%) were reinforced when another PHEMA network was incorporated into their network structures. The elastic moduli of the IPN hydrogels H40/1-H0/Z (Z: 0, 0.3, 1, and 2 mol-% of crosslinker) were enhanced by 100 – 220 %, while the equilibrium water content was reduced only by 5 – 17 % and the refractive index remained similar to that of single PHEMA hydrogel (1.429 – 1.430

for IPNs versus 1.433 for single PHEMA). Such characteristics make these materials promising in ophthalmology.

3. Concentration of elastically active network chains (EANC) in macroscopically homogeneous non-porous PHEMA gels prepared at moderate amount of diluent and various crosslinker concentrations (H40/Y) was calculated from the experimentally determined Young's modulus according to the rubber-elasticity theory and compared with ideal EANC concentration calculated from the composition of networks. The correlation between real and ideal EANC concentrations was close to linear with slope of 0.3. The deviation from the diagonal line with slope 1 was due to incomplete utilization of crosslinker molecules forming EANC and intramolecular reactions causing the cyclization. The contribution of physical hydrophobic interactions to mechanical performance could be distinguished in networks of low concentration of chemical crosslinks.

4. The rubber-elasticity theory has been adapted to homogeneous non-porous PHEMA-PHEMA interpenetrating polymer networks (H40/Y-H0/0.3). Experimental values of the Young's modulus ($E_{experim}$) taken from tensile measurements were compared with the Young's modulus (E_{calc}) calculated according to the physical model derived based on Flory, Erman, Stockmayer, and Dušek approach. The deviation from the diagonal line observed for H40/3 and H40/6 based IPNs could be explained by lower concentration of EANC due to incomplete utilization of crosslinker molecules and somewhat heterogeneous structures – due to onset of syneresis – of their constituent single networks 1. For loosely crosslinked PHEMA networks 1 with 0.2 and 1 mol-% concentration of added crosslinker, the $E_{experim}$ was larger than E_{calc}. The reason for this could be explained by extra entanglements between interpenetrating networks of IPN hydrogels.
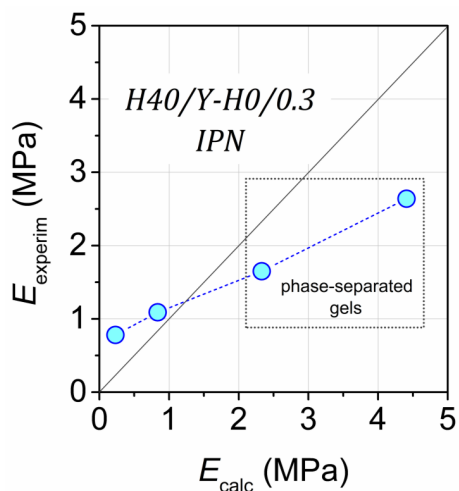
5. As the IPNs concept implies the creation of highly swellable materials with good mechanical properties, we introduced the product "$S_b Q_V$" serving as a criterion of successful combination of polymer networks. The most important result of this study is the finding that combination of macroporous PHEMA as the first network, which by itself is mechanically rather poor, with PGMA or PHEMA as the second network offers interpenetrating networks (IPNs) of superior mechanical properties compared to the properties of their constituents. Despite considerably improved mechanical properties of these "microstructured" PHEMA–PGMA IPNs, their degree of swelling in water remains reasonably high which is important for certain medical applications. This favorable result gives an impetus to investigate the reinforcing ability of other macroporous morphologies such as double-porous cryogels or patterned structures obtained, e.g., by 3D printing.

156

Chapter 6. Appendices

Appendix 1.

Application of macroporous double-porous cryogels

1.1. 2D images of double-porous cryogels

The cells can sense and respond to mechanical stimuli and topography of the microenvironment.[46,47,48,49] In addition to other parameters, the fate of cells strongly depends on mechanical characteristics of polymer matrices correlating to their microstructure, which can be tuned simply by changing the composition of the reaction mixture. For instance, double-porosity of cryogels can be achieved in both cases – when the reaction mixture is diluted at 80 wt.-% (Figure S1a) or at 95 wt.-% of NaCl solution (Figure S1b).
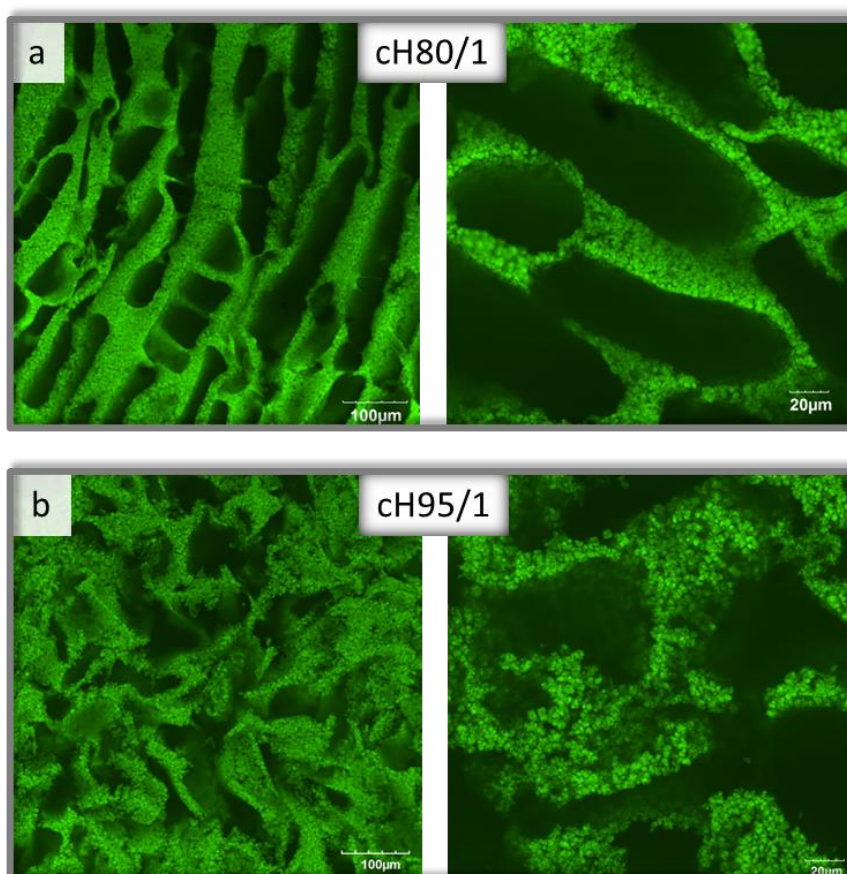
Figure S1. LSCM micrographs of swollen PHEMA cryogels prepared at different dilution with 0.5 M NaCl solution: (a) cH80/1 cryogel prepared at 80 wt.-% of dilution (left – 100 μm and right – 20 μm) and (b) cH95/1 cryogel prepared at 95 wt.-% of dilution (left – 100 μm and right – 20 μm).

According to LSCM micrographs, besides large pores formed due to the ice crystals, the small pores also exist on walls of both cryogels. The dimensional characteristics of both cryogels are given in Table S1. The main difference between these two gels, which might create obstacles for cells, is in the thickness of walls. Perhaps, the proliferation of cells through the thicker walls of double-porous cH80/1 cryogel can be more complicated. On the other hand, the mechanical properties of double-porous cH80/1 substrate are better, which could be an advantage in some cases.

Table S1. Dimensional characteristics of cryogels obtained by LSCM micrographs analysis.

Cryogel	Large pores due to ice crystals, μm		Small pores on walls due to phase separation, μm	Fused spheres on walls, μm	Thickness of walls, μm
	length	width			
cH80/1	40-350	10-60	2-15	1-2	10-20
cH95/1	50-300	20-70	5-15	1-2	3-6

1.2. 3D-reconstruction of volume double-porous cryogel phase

The LSCM method allows making z-stacks of swollen gels, which can be reconstructed into the volume gel phase of certain thickness. Such 3D structure was obtained for double-porous H95/1 cryogel prepared in the presence of 0.5 M NaCl using the Mimics 8.13 software (Figure S2). The structure was reconstructed from the set of z-stacks (approximately 200) of the total depth of 89.76 μm, and the distance between stacks was 0.44 μm. The analysis of 3D image implied the calculation of pixels representing the gel matrix (violet areas, $Pixels_{gel}$) and the pixels representing the pores (white areas, $Pixels_{pores}$). The ratio of these values resulted in the porosity (P) of cH95/1 cryogel and equaled to 0.72:

$$P = \frac{Pixels_{pores}}{Pixels_{gel} + Pixels_{pores}}$$

(Equation S1)

To estimate the total volume of water in cryogel from the 3D image, we assumed that the amount of water in gel matrix is similar to PHEMA hydrogel prepared at 40 wt.-% of water, i.e., swelling degree (SD_{40}) $\approx$ 0.4 (Equation 3.6).

Hence, knowing the number of pixels related to gel matrix, we could calculate the amount of water kept in it. The total amount of water in cryogel can be calculated as the sum of water in pores and water in gel matrix and equaled to 0.905. One should note that the data obtained from 3D image analysis are in a good agreement with experimental values (porosity was 73 % (Equation 3.10), total volume of water in cryogel was 0.895 (Equation 3.6)).
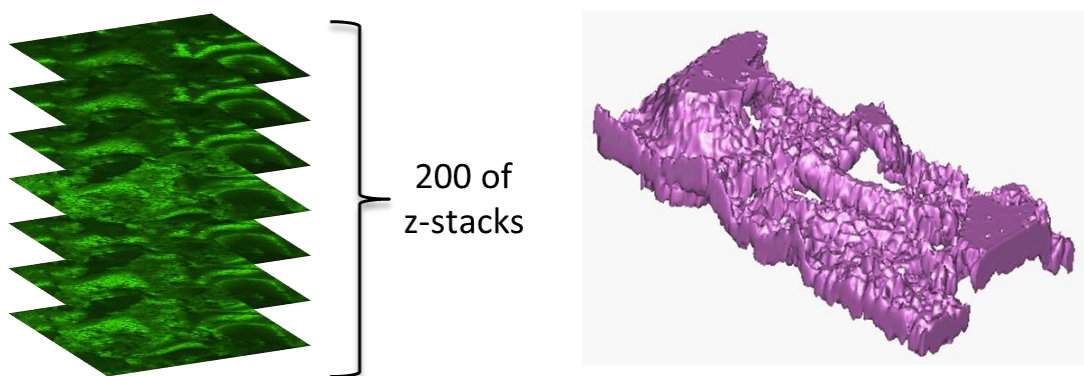
Figure S2. 3D structure of double-porous cH95/1 cryogel reconstructed by Mimics 8.13 software from 200 z-stacks obtained by LSCM.

The reconstructed volume gel phase (Figure S2) was then transferred to STL (STereoLithography) format using ANSYS software (Figure S3). This format is suitable for 3D printers as can be directly used for printing and for finite element analysis (FEM) solver as represents the 3D object as a mesh of tetrahedron non-linear elements suitable for simulations. As a first experiment, the FEM solver was used for simulation of uniaxial tensile deformation of swollen gel (Figure S4).
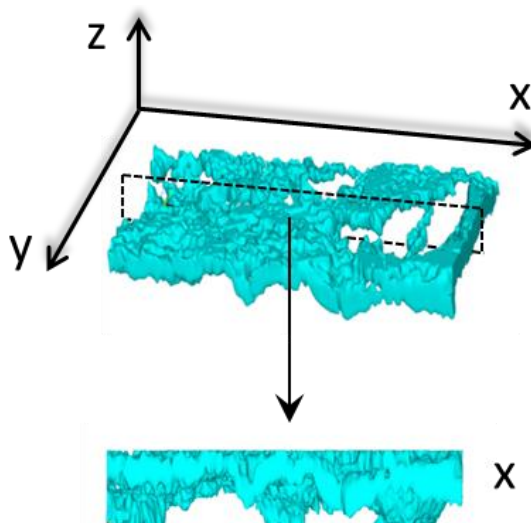
Figure S3. 3D structure of double-porous cH95/1 cryogel in STL format obtained by

ANSYS software.

The Figure S4 shows the distribution of deformation (a) and stresses (b) in cryogel under tensile loading. The model describes the situation, when the one side of the sample was fixed in a clamp, and the sample underwent the stretching from the other side. Each color corresponded to certain deformation or stress values defined on the scale. The areas close to the fixed side of cryogel revealed the smallest deformation, whereas the largest deformation was observed for areas close to the side subjected to stretching. The red area indicating the maximum deformation was observed in the thin gel wall. As for distribution of stresses, their values also increased towards the stretched side.
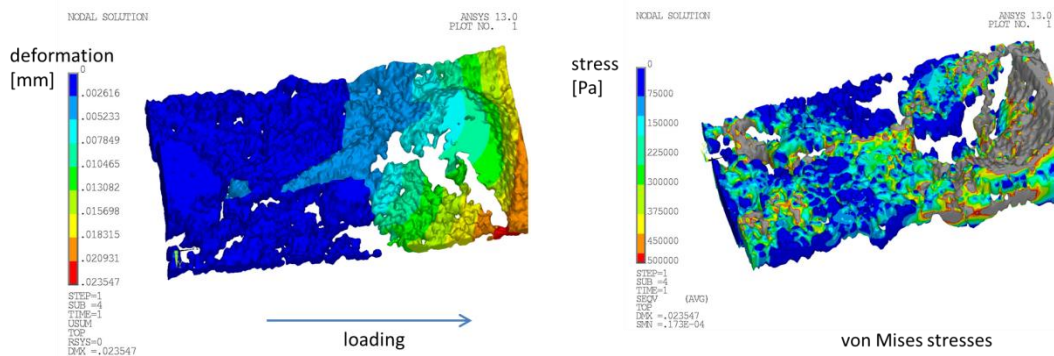
Figure S4. Distribution of deformation and stresses in cH95/1 cryogel under tensile loading.

To conclude this small paragraph, one should note, that this work is still in progress, but the preliminary experiments included the synthesis of macroporous material, visualization of its 3D-structure, and processing this information using Finite Element Method (FEM) algorithms in combination with statistical-mechanical models of hydrogels behavior showed the promising results. In principle, the model is able to examine the response of the macroporous elements to various kinds of external mechanical stimuli and provide structural network parameters needed to synthetize optimized scaffold. The simulating model and the mathematical apparatus will be further developed and improved.

1.3. Cells growth on double-porous cryogel scaffolds

1.3.1. Evaluation of the number of cells growing on the gel

The cultivation and seeding of cells in the double-porous PHEMA cryogel scaffolds were carried out similarly as described in the work of Přádný[208] *et.al*. Briefly, the cryogels were sterilized by autoclaving (30 min, 120 °C, 120 kPa), cut into several pieces and then placed into the wells of flat-bottom plates containing 500 µL of Dulbecco's Modified Eagle Medium (DMEM) (without cells), which was gradually diffusing into the cryogel during two hours. After the aspiration of swelling media around the swollen cryogel, the rMSC – mouse mesenchymal stem cells (kindly provided by Dr. Jendelova of IEM AS CR, v. v. i) resuspended in fresh DMEM media (5×10^4 cells per 1 mL) were added to the well with scaffolds and cultivated for five days. The evaluation of cells growth and viability on the cryogel scaffolds were done in triplicates. The number and viability of cells on the scaffolds were evaluated on the 1st, 3rd and 5th day. During the cultivation period, the media was replaced with a fresh portion of media containing 10-times diluted cell viability reagent – Alamar Blue (Thermo Scientific, Czech Republic), and after that the system was incubated for 4 hours at 37°C. Only in the viable cells, the active component of the Alamar Blue – resazurin – was reduced to a highly fluorescent resorufin. The fluorescence of resorufin with the excitation spectrum peak at 570 nm was detected by the Synergy Neo plate reader (Bio-Tek, Czech Republic). This is how the amount of growing/viable cells can be evaluated. The intensity of fluorescence of viable cells was correlated with the calibration curve plotted for various defined amounts of cells growing in the 96-well plates.

1.3.2. Laser scanning confocal microscopy for observation of cells on the cryogel scaffold

The cells attached to cryogel were labeled on the 5th day with 5 µg/mL Hoechst 33258 dsDNA binding dye, while the cryogel scaffold was labeled with Cell Mask Green dye (Thermo scientific, Czech Republic) originally intended for labeling of cell membranes. Better affinity of Cell Mask Green dye for the cryogel was observed. The samples were visualized using the Olympus multiphoton laser scanning confocal microscope (LSCM) with FV10-ASW viewer software (Olympus, Japan). The details of LSCM studies were described in Experimental part (section 3.4.3).

1.3.3. Results

The double-porous structure of cryogels might be attractive for cells, as large pores might provide space for cells proliferation, while small pores help diffusion of nutrients. However, in these preliminary experiments, there were found examples, when large pores of single-porous scaffolds became blocked with cells hindering thus diffusion of nutrients towards the cells and thus maintain their viability.[209] The efficacy of differently microstructured double-porous PHEMA hydrogels in cells growth was shown in the work of Přádný[208] *et.al*. The large pores of such hydrogels were generated by incorporation of sacrificed templates: solid particles of sodium chloride that were washed out after the gel formation, while the small pores were formed by the reaction-induced phase-separation caused by addition of a certain diluent. The viability of cells after 4 days in the case of these templated double-porous gels was consistently between 90 and 100 %, whereas almost no cell growth or their low amount was detected on single-porous scaffolds.

In current work, we tested a cryogel-like microstructure of two-size pores (experimental part, paragraph 2.1.3), but perhaps with a low number of sufficiently large channels throughout the structure. The survival of rMSC on the matrix of double-porous PHEMA cryogel (cH95/1) as a function of incubation period is shown on graph in Figure S5. The number of cells adhered to scaffold after one incubation day was around 1×10^4 per 1 mL of media. The numbers of grown cells on the days three and five were reduced approximately by half. Again, this could be explained by low permeability of this particular "porous architecture" typical to cryogel. The pores are structured rather as cavities separated with gel porous walls and proliferation is hindered due to lack of connection between the pores and possibly also by lack of signals stimulating the growth of this type of cells.

Eventually, the rMSC cells grown on the double-porous cH95/1 cryogel scaffold were visualized on the sixth day of the cultivation using the cell nuclei fluorescence (Figure S5). Bright blue spots on the LSCM micrograph corresponded to cells nuclei, the green color on the micrograph corresponded to cryogel scaffold labeled with the Cell Mask Green dye.
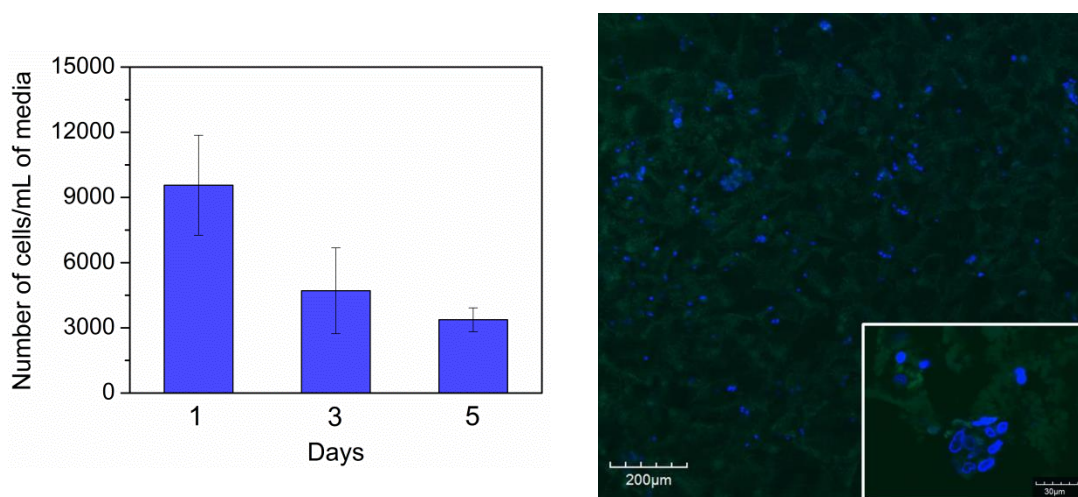
Figure S5. Cells growth in the matrix of neat double-porous cH95/1cryogel prepared in the presence of 0.5 M NaCl solution.

Besides the limits set by hydrogel microstructure, the ability to host cells of neat macroporous PHEMA gels (hydrogels, cryogels) should be investigated further. Although the significant cells growth was detected on double-porous *templated* PHEMA hydrogel,[208] the cells behavior on double-porous PHEMA *cryogels* was different most likely due to the different topology. Here, we present a preliminary experiment showing the possibility of cells growth on our material. But it is clear, that further modification of gels is needed. Further treatments of cryogels may include: different conditions set at cryogelation process leading to more open pores, the surface modification of gel walls, for example, by poly(ornithine) and laminin layers, the surface modification of walls with low-molecular oligopeptides (RGD, IKVAV amino acid sequences), or the modification of cryogel chemical composition with comonomers containing positive or negative charges. This work motivates our incentive to continue in this direction in the frame of future research projects.

Appendix 2.

Derivation of equation assessing the fraction of pores in macroporous swollen gels

Model system: macroporous gel swollen in water (or monomers, or other solvents). The total volume (V_{total}) of the system is the sum of volumes of polymer matrix ($V_{polymer}$) and of pores (V_{pores}).

Macroporous swollen gel

$$V_{total} = V_{polymer} + V_{pores}$$
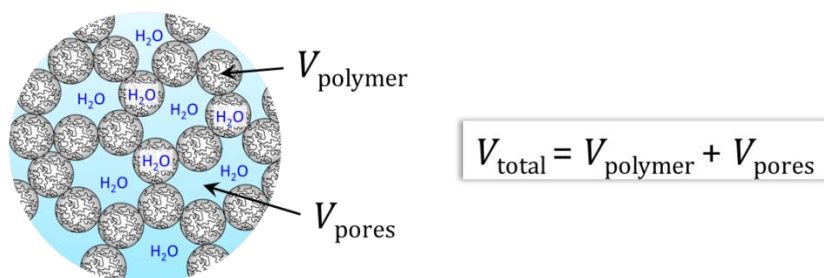
Assumption:

We assume, that the swelling of polymer matrix of macroporous swollen gel is similar to swelling of non-porous PHEMA hydrogel prepared at 40 wt.-% of water or less (Figure S6).
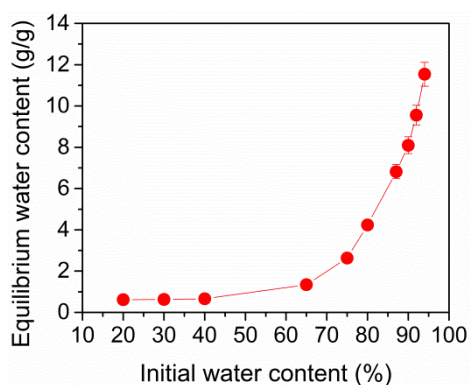
Figure S6. Equilibrium water content in poly(2-hydroxyethyl methacrylate) (PHEMA) hydrogels prepared at various initial water content (20 – 94 wt.-%) and 1 mol-% of diethylene glycol dimethacrylate (DEGDMA) crosslinker.

Table S2. Symbols used in derivation and their description.

Symbol	Description
$m_{solvent}^{gel}$	weight of solvent in gel phase
$m_{solvent}^{pores}$	weight of solvent in pores

m_{dry}	weight of dry gel
$m_{\text{solvent}}^{\text{total}}$	total weight of solvent in gel
m_{total}	total weight of swollen gel
ESC_{40}	equilibrium water content in PHEMA network prepared at 40 wt.-% of water
ESC_{x}	equilibrium water content in macroporous PHEMA network prepared at X wt.-% of water
V_{pores}	volume of pores
V_{polymer}	volume of polymer matrix
V_{total}	total volume of swollen gel
φ_{pores}	volume fraction of pores
φ_{polymer}	volume fraction of polymer matrix
ρ_{d}	density of dry PHEMA gel, 1.2338 g/mL
ρ_{solvent}	density of solvent, 0.99707 g/mL for water, 1.073 g/mL for HEMA monomer
$\rho_{\text{sw.gel}}$	density of swollen PHEMA gel

1. $\varphi_{\text{pores}} = \dfrac{V_{\text{pores}}}{V_{\text{total}}}$

2. $\varphi_{\text{polymer}} = 1 - \varphi_{\text{pores}}$

3. $V_{\text{pores}} = \dfrac{m_{\text{pores}}}{\rho_{\text{pores}}} = \dfrac{m_{\text{solvent}}^{\text{pores}}}{\rho_{\text{solvent}}}$

4. $ESC_{40} = \dfrac{m_{\text{solvent}}^{\text{gel}}}{m_{\text{dry}}}$

5. $ESC_{\text{x}} = \dfrac{m_{\text{solvent}}^{\text{total}}}{m_{\text{dry}}} = \dfrac{m_{\text{solvent}}^{\text{gel}} + m_{\text{solvent}}^{\text{pores}}}{m_{\text{dry}}}$

6. $ESC_{\text{x}} = \dfrac{m_{\text{solvent}}^{\text{gel}}}{m_{\text{dry}}} + \dfrac{m_{\text{solvent}}^{\text{pores}}}{m_{\text{dry}}} = EWC_{40} + \dfrac{m_{\text{solvent}}^{\text{pores}}}{m_{\text{dry}}}$

7. $m_{\text{solvent}}^{\text{pores}} = (EWC_{\text{x}} - EWC_{40}) \cdot m_{\text{dry}}$

8. $V_{\text{pores}} = \dfrac{(EWC_{\text{x}} - EWC_{40}) \cdot m_{\text{dry}}}{\rho_{\text{solvent}}}$

9. $V_{\text{total}} = \dfrac{m_{\text{total}}}{\rho_{\text{total}}} = \dfrac{m_{\text{dry}} + m_{\text{solvent}}^{\text{total}}}{\rho_{\text{total}}} = \dfrac{m_{\text{dry}} + EWC_{\text{x}} \cdot m_{\text{dry}}}{\rho_{\text{total}}} = \dfrac{m_{\text{dry}} \cdot (1 + EWC_{\text{x}})}{\rho_{\text{total}}}$

10. $\varphi_{\text{pores}} = \dfrac{(EWC_{\text{x}} - EWC_{40}) \cdot m_{\text{dry}} \cdot \rho_{\text{total}}}{\rho_{\text{solvent}} \cdot (1 + EWC_{\text{x}}) \cdot m_{\text{dry}}} = \dfrac{(EWC_{\text{x}} - EWC_{40}) \cdot \rho_{\text{total}}}{\rho_{\text{solvent}} \cdot (1 + EWC_{\text{x}})}$

Determination of density of swollen gel:

a) in water

1. $V_{\text{sw.gel}} = V_{\text{d}} + V_{\text{H}_2\text{O}}$

2. $\dfrac{m_{\text{sw.gel}}}{\rho_{\text{sw.gel}}} = \dfrac{m_{\text{dry}}}{\rho_{\text{dry}}} + \dfrac{m_{\text{H}_2\text{O}}}{\rho_{\text{H}_2\text{O}}}$

3. $\text{EWC} = \dfrac{m_{\text{sw.gel}} - m_{\text{dry}}}{m_{\text{dry}}} = \dfrac{m_{\text{H}_2\text{O}}}{m_{\text{dry}}}$

4. $m_{\text{sw.gel}} = m_{\text{dry}} \cdot (1 + \text{EWC})$

5. If $m_{\text{sw.gel}} = 1$ g and EWC_{40} (H40/1 in water) $= 0.66$, $1 = m_{\text{dry}} \cdot (1 + 0.66)$

6. $m_{\text{dry}} = 0.61$ g, $m_{\text{sw.gel}} = 1$ g, $m_{\text{H2O}} = 0.39$ g

7. $\dfrac{1}{x} = \dfrac{0.61}{1.2338} + \dfrac{0.39}{0.99707}$

8. $x = 1.129\,\dfrac{\text{g}}{\text{mL}}$, $\rho_{\text{sw.gel}}(in\ water)$

b) in HEMA monomer

1. EWC_{40} (H40/1 in HEMA monomer) $= 2.57$

2. $m_{\text{dry}} = 0.28$ g, $m_{\text{sw.gel}} = 1$ g, $m_{\text{HEMA}} = 0.72$ g

3. $\dfrac{1}{x} = \dfrac{0.28}{1.2338} + \dfrac{0.72}{1.073}$

$x = 1.114\,\dfrac{\text{g}}{\text{mL}}$, $\rho_{\text{sw.gel}}(in\ HEMA\ monomer)$

Appendix 3.

The stability of thrust upon frequency sweep test

The control of stability of thrust during the frequency sweep test is important as its frequency-independent behavior indicates the correct gap size. Ideally, the thrust should be close to zero and remain constant in the entire range of frequencies. Significant deviation of thrust to negative values indicates the existence of a high stress in sample due to high compression. As measurement proceeds from higher frequencies to lower frequencies, the highly compressed polymer chains relax and total stress in sample reduces causing the reduction of thrust. Increase of thrust to positive values was rarely observed for our systems. Apparently, such situation may occur, for instance, when the sample uptakes additional water upon measurement to reach the equilibrium if water was somehow squeezed or evaporated from it (e.g., during the manipulations with the sample). As a result, the volume of hydrogel changes due to the swelling pushing the upper geometry and causing the increase of thrust. A slight increase of thrust was sometimes observed just before its drop (Figure S7b, black curve), which was possibly caused by slight volume changes of sample before the relaxation of polymer chains. In Figure S7, the parallel tracking of storage modulus (a) and thrust (b) as a function of frequency at three different levels of sample compression (2, 5, and 7 %) is shown for swollen non-porous H40/1 hydrogel. High compression of sample resulted in high storage modulus: 103 kPa at 5 % of compression and 146 kPa at 10 % of compression; data is given for $f = 1$ Hz. But the thrust was not stable during the whole measurement range of frequencies and at lower frequencies deviated towards the negative values indicating the relaxation of polymer chains and, hence, too high sample compression. Higher was the compression, earlier dropped the thrust. Whereas the gap size found using an auto-tension mode revealed lower storage modulus (33 kPa at 1 Hz), but a stable thrust in the whole range of frequencies. There is a vast literature on oscillatory shear deformation of swollen hydrogels, but in the majority of them detailed instructions on gap finding or important precautions concerning the features of measurement are missing. Therefore, sometimes the storage moduli of swollen hydrogels of similar composition and similar swelling degree differ significantly, which forces us to doubt the accuracy of the obtained data. For instance, the swollen H40/1 hydrogel is a traditional material for soft contact lenses. In our experiments, its equilibrium water

content (EWC) was 0.66 g/g ($\approx$ 39 % of water), and the storage modulus determined according to the described above method was 24.5 kPa at low frequency of $4 \cdot 10^{-4}$ Hz. Moreover, the independent measurement of this swollen sample carried out on another available rheometer (Ares-G2 rheometer, TA Instruments) by a colleague specialist also showed a similar value of storage modulus, $G' = 26$ kPa at $f = 3 \cdot 10^{-3}$ Hz. In literature, quite a broad range of storage moduli determined by various techniques for PHEMA hydrogels of similar water content (36 – 40 % of water) was reported: from tens of kPa to tens of MPa[68,210,172,211]. Or, for instance, PHEMA hydrogel prepared without diluent – H0/1 – exhibited in our case EWC = 0.56 g/g ($\approx$ 36 % of water) and $G' = 48.8$ kPa at frequency $f = 3 \cdot 10^{-4}$ Hz. In literature, the storage modulus of such bulk hydrogels with similar water uptake was also different, for example, 70 kPa[212] or 250 kPa[213]. It is not excluded, that the proposed method of performing the oscillatory shear deformation of hydrogels is still needed to be improved and thoroughly developed and that some other parameters are worth to be considered. But for now each step of the analysis seems reasonable.
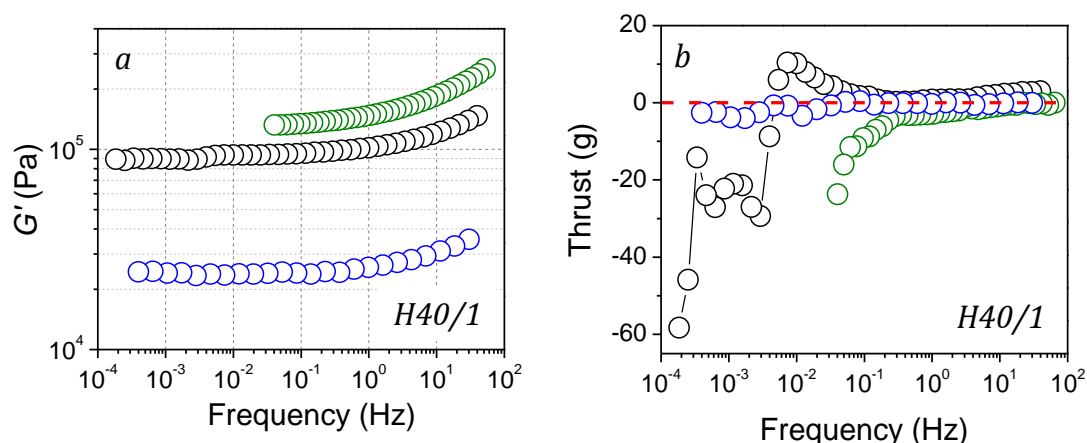

Figure S7. Dynamic storage modulus (G') (a) and thrust (b) measured for swollen non-porous H40/1 hydrogel at various compressions: 2 % (auto-tension mode), 5 % and 7 %.

Chapter 7. Bibliography

(1)   McNaught, A. D.; Wilkinson, A. *IUPAC. Compendium of Chemical Terminology, 2nd Ed. (the "Gold Book")*; Blackwell Scientific Publications, Oxford, 1997.

(2)   Aylsworth, J. W. Plastic Composition. U.S. Pat. 1,111,284, 1914.

(3)   Andrews, R. D.; Tobolsky, A. V; Hanson, E. E. The Theory of Permanent Set at Elevated Temperatures in Natural and Synthetic Rubber Vulcanizates The Theory of Permanent Set at Elevated Temperatures in Natural and Synthetic Rubber Vulcanizates. *J. Appl. Phys.* **1946**, *17* (1946), 352–361 DOI: 10.1063/1.1707724.

(4)   Millar J. R. Interpenetrating Polymer Networks. Styrene-Divinylbenzene Copolymers with Two and Three Interpenetrating Networks, and Their Sulphonates. *J. Chem. Soc.* **1960**, 1311–1317.

(5)   Sperling, L. H. Recent Advances in Interpenetrating Polymer Networks. *Polym. Eng. Sci.* **1985**, *25* (9), 517–520.

(6)   Frisch, H. L.; Klempner, D.; Frisch, K. C. A Topologically Interpenetrating Elastomeric Network. *Rubber Chem. Technol.* **1970**, *43* (4), 883–886 DOI: 10.5254/1.3547298.

(7)   Lipatov, Y. S.; Sergeyeva, L. M.; Mozzhukhina, L. V.; Apukhtina, N. P. Some Physico-Chemical Properties of Filled Interpenetrating Networks. *Polym. Sci. U.S.S.R.* **1974**, *16* (10), 2658–2666 DOI: 10.1016/0032-3950(74)90460-2.

(8)   Gong, J. P.; Katsuyama, Y.; Kurokawa, T.; Osada, Y. Double-Network Hydrogels with Extremely High Mechanical Strength. *Adv. Mater.* **2003**, *15* (14), 1155–1158 DOI: 10.1002/adma.200304907.

(9)   Shams Es-haghi, S.; Leonov, A. I.; Weiss, R. A. Deconstructing the Double-Network Hydrogels: The Importance of Grafted Chains for Achieving Toughness. *Macromolecules* **2014**, *47* (14), 4769–4777 DOI: 10.1021/ma500815d.

(10)   Chirila, T. V.; Vijayasekaran, S.; Home, R.; Crawfor, G. J. Interpenetrating Polymer Network (IPN) as a Permanent Joint between the Elements of a New Type of Artificial Cornea. *J. Biomed. Mater. Res.* **1994**, *28*, 745–753 DOI: 10.1007/978-1-62703-432-6_2.

(11)   Chirila, T. V.; Hill, A. J.; Richens, D. T. Effect of Redundant Chain Packing on the Uptake of Calcium Phosphate in Poly(2-hydroxyethyl methacrylate) Hydrogels. *Aust. J. Chem.* **2007**, *60* (6), 439 DOI: 10.1071/CH07111.

(12)   Chirila, T. V.; George, K. A.; Abdul Ghafor, W. A.; Pas, S. J.; Hill, A. J. Sequential Homo-Interpenetrating Polymer Networks of Poly(2-hydroxyethyl methacrylate): Synthesis, Characterization, and Calcium Uptake. *J. Appl. Polym. Sci.* **2012**, *126* (S2), 455–466 DOI: 10.1002/app.36824.

(13) Lou, X.; Vijayasekaran, S.; Chirila, T. V.; Maley, M. A. L.; Hicks, C. R.; Constable, I. J. Synthesis, Physical Characterization, and Biological Performance of Sequential Homointerpenetrating Polymer Network Sponges Based on Poly(2-hydroxyethyl methacrylate). *J. Biomed. Mater. Res.* **1999**, *47* (3), 404–411 DOI: 10.1002/(SICI)1097-4636(19991205)47:3<404::AID-JBM16>3.0.CO;2-F.

(14) Parke-Houben, R. Topological Constraints in Interpenetrating Polymer Network Hydrogels, Stanford University, 2012.

(15) Miyata, T.; Asami, N.; Okawa, K.; Uragami, T. Rapid Response of a Poly(acrylamide) Hydrogel Having a Semi-Interpenetrating Polymer Network Structure. *Polym. Adv. Technol.* **2006**, *17*, 794–797 DOI: 10.1002/pat.818.

(16) Argun, A.; Can, V.; Altun, U.; Okay, O. Nonionic Double and Triple Network Hydrogels of High Mechanical Strength. *Macromolecules* **2014**, *47* (18), 6430–6440 DOI: 10.1021/ma5014176.

(17) Hoffman, A. S. Hydrogels for Biomedical Applications. *Adv. Drug Deliv. Rev.* **2002**, *54*, 3–12 DOI: 10.1016/j.addr.2012.09.010.

(18) Ferrer, G. G.; Pradas, M. M.; Ribelles, J. L. G.; Colomer, F. R.; Castilla-Cortázar, I.; Vidaurre, A. Influence of the Nature of the Porous Confining Network on the Sorption, Diffusion and Mechanical Properties of Hydrogel IPNs. *Eur. Polym. J.* **2010**, *46* (4), 774–782 DOI: 10.1016/j.eurpolymj.2009.12.018.

(19) Weng, L.; Gouldstone, A.; Wu, Y.; Chen, W. Mechanically Strong Double Network Photocrosslinked Hydrogels from N,N-dimethylacrylamide and Glycidyl Methacrylated Hyaluronan. *Biomaterials* **2008**, *29* (14), 2153–2163 DOI: 10.1016/j.biomaterials.2008.01.012.

(20) Tang, Q.; Yu, J.-R.; Chen, L.; Zhu, J.; Hu, Z.-M. Porous Silicone Hydrogel Interpenetrating Polymer Networks Prepared Using a Template Method for Biomedical Use. *Polym. Int.* **2011**, *60* (7), 1136–1141 DOI: 10.1002/pi.3053.

(21) Dragan, E. S.; Lazar, M. M.; Dinu, M. V.; Doroftei, F. Macroporous Composite IPN Hydrogels Based on Poly(acrylamide) and Chitosan with Tuned Swelling and Sorption of Cationic Dyes. *Chem. Eng. J.* **2012**, *204–205*, 198–209 DOI: 10.1016/j.cej.2012.07.126.

(22) Buwalda, S. J.; Boere, K. W. M.; Dijkstra, P. J.; Feijen, J.; Vermonden, T.; Hennink, W. E. Hydrogels in a Historical Perspective: From Simple Networks to Smart Materials. *Journal of Controlled Release*. 2014.

(23) Zhang, J.; Peppas, N. a. Synthesis and Characterization of pH- and Temperature-Sensitive Poly(methacrylic acid)/Poly(N-isopropylacrylamide) Interpenetrating Polymeric Networks. *Macromolecules* **2000**, *33* (1), 102–107 DOI: 10.1021/ma991398q.

(24) Nizam El-Din, H. M.; Abd Alla, S. G.; El-Naggar, A. W. M. Radiation Synthesis and Characterization of Hydrogels Composed of Poly(vinyl alcohol) and Acrylamide Mixtures. *J. Macromol. Sci. Part A* **2007**, *44* (1), 47–54 DOI:

10.1080/10601320601044450.

(25)   Gong, J. P. Why Are Double Network Hydrogels so Tough? *Soft Matter* **2010**, *6* (12), 2583 DOI: 10.1039/b924290b.

(26)   Na, Y. H.; Kurokawa, T.; Katsuyama, Y.; Tsukeshiba, H.; Gong, J. P.; Osada, Y.; Okabe, S.; Karino, T.; Shibayama, M. Structural Characteristics of Double Network Gels with Extremely High Mechanical Strength. *Macromolecules* **2004**, *37* (14), 5370–5374 DOI: 10.1021/ma049506i.

(27)   Tsukeshiba, H.; Huang, M.; Na, Y. H.; Kurokawa, T.; Kuwabara, R.; Tanaka, Y.; Furukawa, H.; Osada, Y.; Gong, J. P. Effect of Polymer Entanglement on the Toughening of Double Network Hydrogels. *J. Phys. Chem. B* **2005**, *109* (34), 16304–16309 DOI: 10.1021/jp052419n.

(28)   Wu, C.; Zuo, J.; Chu, B. Laser Light Scattering Studies of Epoxy Polymerization of 1,4-butanediol diglycidyl ether with cis-1,2-cyclohexanedicarboxylic anhydride. *Macromolecules* **1989**, *22*, 838–842.

(29)   Zhao, Y.; Zhang, G.; Wu, C. Nonergodic Dynamics of a Novel Thermally Sensitive Hybrid Gel. *Macromolecules* **2001**, *34* (22), 7804–7808 DOI: 10.1021/ma010672p.

(30)   Ngai, T.; Wu, C. Effect of Cross-Linking on Dynamics of Semidilute Copolymer Solutions: Poly(methyl methacrylate-co-7-acryloyloxy-4-methylcoumarin) in Chloroform. *Macromolecules* **2003**, *36* (3), 848–854 DOI: 10.1021/ma021580i.

(31)   Myung, D.; Koh, W.; Ko, J.; Hu, Y.; Carrasco, M.; Noolandi, J.; Ta, C. N.; Frank, C. W. Biomimetic Strain Hardening in Interpenetrating Polymer Network Hydrogels. *Polymer (Guildf).* **2007**, *48* (18), 5376–5387 DOI: 10.1016/j.polymer.2007.06.070.

(32)   Myung, D.; Koh, W.; Bakri, A.; Zhang, F.; Marshall, A.; Ko, J.; Noolandi, J.; Carrasco, M.; Cochran, J. R.; Frank, C. W.; Ta, C. N. Design and Fabrication of an Artificial Cornea Based on a Photolithographically Patterned Hydrogel Construct. *Biomed. Microdevices* **2007**, *9* (6), 911–922 DOI: 10.1007/s10544-006-9040-4.

(33)   Myung, D.; Waters, D.; Wiseman, M.; Duhamel, P.; Noolandi, J.; Ta, C. N.; Frank, C. W. Progress in the Development of Interpenetrating Polymer Network Hydrogels. *Polym. Adv. Technol.* **2008**, *19* (6), 647–657 DOI: 10.1002/pat.1134.

(34)   Waters, D. J.; Engberg, K.; Parke-Houben, R.; Ta, C. N.; Jackson, A. J.; Toney, M. F.; Frank, C. W. Structure and Mechanism of Strength Enhancement in Interpenetrating Polymer Network Hydrogels. *Macromolecules* **2011**, *44* (14), 5776–5787 DOI: 10.1021/ma200693e.

(35)   Waters, D. J.; Engberg, K.; Parke-Houben, R.; Hartmann, L.; Ta, C. N.; Toney, M. F.; Frank, C. W. Morphology of Photopolymerized End-Linked Poly(ethylene glycol) Hydrogels by Small-Angle X-Ray Scattering. *Macromolecules* **2010**, *43* (16), 6861–6870 DOI: 10.1021/ma101070s.

(36) Nishi, S.; Kotaka, T. Complex-Forming Poly(oxyethylene):poly(acrylic acid) Interpenetrating Polymer Networks. 1. Preparation, Structure, and Viscoelastic Properties. *Macromolecules* **1985**, *18* (8), 1519–1525 DOI: 10.1021/ma00150a001.

(37) Nishi, S.; Kotaka, T. Complex-Forming Poly(oxyethylene)/Poly(acrylic acid) Interpenetrating Polymer Networks. 2. Function as a Chemical Valve. *Macromolecules* **1986**, *19* (4), 978–984 DOI: 10.1021/ma00158a007.

(38) Nishi, S.; Kotaka, T. Complex-Forming Polyoxyethylene: Poly(acrylic acid) Interpenetrating Polymer Networks III. Swelling and Mechanochemical Behavior. *Polym. J.* **1989**, *21* (5), 393–402 DOI: 10.1295/polymj.21.393.

(39) Shams Es-haghi, S.; Weiss, R. A. Fabrication of Tough Hydrogels from Chemically Cross-Linked Multiple Neutral Networks. *Macromolecules* **2016**, *49* (23), 8980–8987 DOI: 10.1021/acs.macromol.6b02264.

(40) Chen, Q.; Zhu, L.; Huang, L.; Chen, H.; Xu, K.; Tan, Y.; Wang, P.; Zheng, J. Fracture of the Physically Cross-Linked First Network in Hybrid Double Network Hydrogels. *Macromolecules* **2014**, *47* (6), 2140–2148 DOI: 10.1021/ma402542r.

(41) Chen, Q.; Zhu, L.; Chen, H.; Yan, H.; Huang, L.; Yang, J.; Zheng, J. A Novel Design Strategy for Fully Physically Linked Double Network Hydrogels with Tough, Fatigue Resistant, and Self- Healing Properties. *Adv. Funct. Mater.* **2015**, *25* (10), 1598–1607 DOI: 10.1002/adfm.201404357.

(42) Kaneko, D.; Tada, T.; Kurokawa, T.; Gong, J. P.; Osada, Y. Mechanically Strong Hydrogels with Ultra-Low Frictional Coefficients. *Adv. Mater.* **2005**, *17* (5), 535–538 DOI: 10.1002/adma.200400739.

(43) Shams Es-haghi, S.; Weiss, R. A. Finite Strain Damage-Elastoplasticity in Double-Network Hydrogels. *Polymer (Guildf).* **2016**, *103*, 277–287 DOI: 10.1016/j.polymer.2016.09.054.

(44) Tavsanli, B.; Can, V.; Okay, O. Mechanically Strong Triple Network Hydrogels Based on Hyaluronan and poly(N,N-dimethylacrylamide). *Soft Matter* **2015**, *11* (43), 8517–8524 DOI: 10.1039/C5SM01941A.

(45) Furukawa, H.; Horie, K.; Nozaki, R.; Okada, M. Swelling-Induced Modulation of Static and Dynamic Fluctuations in Polyacrylamide Gels Observed by Scanning Microscopic Light Scattering. *Phys. Rev. E* **2003**, *68* (3), 31406 DOI: 10.1103/PhysRevE.68.031406.

(46) Engler, A. J.; Sen, S.; Sweeney, H. L.; Discher, D. E. Matrix Elasticity Directs Stem Cell Lineage Specification. *Cell* **2006**, *126* (4), 677–689 DOI: 10.1016/j.cell.2006.06.044.

(47) Banerjee, A.; Arha, M.; Choudhary, S.; Ashton, R. S.; Bhatia, S. R.; Schaffer, D. V.; Kane, R. S. The Influence of Hydrogel Modulus on the Proliferation and Differentiation of Encapsulated Neural Stem Cells. *Biomaterials* **2009**, *30* (27), 4695–4699 DOI: 10.1016/j.biomaterials.2009.05.050.

(48) Kshitiz; Park, J.; Kim, P.; Helen, W.; Engler, A. J.; Levchenko, A.; Kim, D.-

H. Control of Stem Cell Fate and Function by Engineering Physical Microenvironments. *Integr. Biol.* **2012**, *4* (9), 1008–1018 DOI: 10.1039/c2ib20080e.

(49) Roeder, B. A.; Kokini, K.; Sturgis, J. E.; Robinson, J. P.; Voytik-Harbin, S. L. Tensile Mechanical Properties of Three-Dimensional Type I Collagen Extracellular Matrices With Varied Microstructure. *J. Biomech. Eng.* **2002**, *124* (2), 214 DOI: 10.1115/1.1449904.

(50) Mansour J.M. Biomechanics of Cartilage. *Kinesiol. Mech. Pathomechanics Hum. Mov.* **2003**, 66–79 DOI: 10.1002/art.23548.

(51) Kempson, G. E.; Freeman, M. A. R.; Swanson, S. A. V. Tensile Properties of Articular Cartilage. *Nature* **1968**, *220* (5172), 1127–1128 DOI: 10.1038/2201127b0.

(52) Corkhill, P. H.; Trevett, A. S.; Tighe, B. J. The Potential of Hydrogels as Synthetic Articular Cartilage. *Proc. Inst. Mech. Eng. H.* **1990**, *204*, 147–155 DOI: 10.1243/PIME.

(53) Kerin, A. J.; Wisnom, M. R.; Adams, M. A. The Compressive Strength of Articular Cartilage. *Proc. Inst. Mech. Eng. H.* **1998**, *212*, 273–280 DOI: 10.1243/0954411981534051.

(54) Hunziker, E. B. Articular Cartilage Repair: Basic Science and Clinical Progress. A Review of the Current Status and Prospects. *Osteoarthr. Cartil.* **2002**, *10*, 432–463 DOI: 10.1053/joca.2002.0801.

(55) Buckley, M. R.; Gleghorn, J. P.; Bonassar, L. J.; Cohen, I. Mapping the Depth Dependence of Shear Properties in Articular Cartilage. *J. Biomech.* **2008**, *41*, 2430–2437 DOI: 10.1016/j.jbiomech.2008.05.021.

(56) Wang, H.; Ateshian, G. A. The Normal Stress Effect and Equilibrium Friction Coefficient of Articular Cartilage under Steady Frictional Shear. *J. Biomech.* **1997**, *30* (8), 771–776 DOI: 10.1016/S0021-9290(97)00031-6.

(57) Doulabi, A.; Mequanint, K.; Mohammadi, H. Blends and Nanocomposite Biomaterials for Articular Cartilage Tissue Engineering. *Materials (Basel).* **2014**, *7* (7), 5327–5355 DOI: 10.3390/ma7075327.

(58) Yasuda, K.; Ping, J.; Katsuyama, Y.; Nakayama, A. Biomechanical Properties of High-Toughness Double Network Hydrogels. **2005**, *26*, 4468–4475 DOI: 10.1016/j.biomaterials.2004.11.021.

(59) Nakayama, A.; Kakugo, A.; Gong, J. P.; Osada, Y.; Takai, M.; Erata, T.; Kawano, S. High Mechanical Strength Double-Network Hydrogel with Bacterial Cellulose. *Adv. Funct. Mater.* **2004**, *14* (11), 1124–1128 DOI: 10.1002/adfm.200305197.

(60) Shin, H.; Olsen, B. D.; Khademhosseini, A. The Mechanical Properties and Cytotoxicity of Cell-Laden Double-Network Hydrogels Based on Photocrosslinkable Gelatin and Gellan Gum Biomacromolecules. *Biomaterials* **2012**, *33* (11), 3143–3152 DOI: 10.1016/j.biomaterials.2011.12.050.

(61) Fan, C.; Liao, L.; Zhang, C.; Liu, L. A Tough Double Network Hydrogel for Cartilage Tissue Engineering. *J. Mater. Chem. B* **2013**, *1* (34), 4251 DOI: 10.1039/c3tb20600a.

(62) Yasuda, K.; Kitamura, N.; Gong, J. P.; Arakaki, K.; Kwon, H. J.; Onodera, S.; Chen, Y. M.; Kurokawa, T.; Kanaya, F.; Ohmiya, Y.; Osada, Y. A Novel Double-Network Hydrogel Induces Spontaneous Articular Cartilage Regeneration in Vivo in a Large Osteochondral Defect. *Macromol. Biosci.* **2009**, *9* (4), 307–316 DOI: 10.1002/mabi.200800223.

(63) Bobyn, J. D.; Wilson, G. J.; MacGregor, D. C.; Pilliar, R. M.; Weatherly, G. C. Effect of Pore Size on the Peel Strength of Attachment of Fibrous Tissue to Porous-Surfaced Implants. *J. Biomed. Mater. Res.* **1982**, *16* (5), 571–584 DOI: 10.1002/jbm.820160505.

(64) Moretti, M.; Wendt, D.; Schaefer, D.; Jakob, M.; Hunziker, E. B.; Heberer, M.; Martin, I. Structural Characterization and Reliable Biomechanical Assessment of Integrative Cartilage Repair. *J. Biomech.* **2005**, *38* (9), 1846–1854 DOI: 10.1016/j.jbiomech.2004.08.021.

(65) Kurokawa, T.; Furukawa, H.; Wang, W.; Tanaka, Y.; Gong, J. P. Formation of a Strong Hydrogel-Porous Solid Interface via the Double-Network Principle. *Acta Biomater.* **2010**, *6* (4), 1353–1359 DOI: 10.1016/j.actbio.2009.10.046.

(66) Yuk, H.; Zhang, T.; Lin, S.; Parada, G. A.; Zhao, X. Tough Bonding of Hydrogels to Diverse Non-Porous Surfaces. *Nat. Mater.* **2015**, *15* (2), 190–196 DOI: 10.1038/nmat4463.

(67) Wichterle, O.; Lím, D. Hydrophilic Gels for Biological Use. *Nature* **1960**, *185* (4706), 117–118 DOI: 10.1038/185117a0.

(68) Wang, L.; Lu, C.; Liu, H.; Lin, S.; Nan, K.; Chen, H.; Li, L. A Double Network Strategy to Improve Epithelization of a poly(2-hydroxyethyl methacrylate) Hydrogel for Corneal Repair Application. *RSC Adv.* **2016**, *6* (2), 1194–1202 DOI: 10.1039/C5RA17726J.

(69) González-Chomón, C.; Braga, M. E. M.; De Sousa, H. C.; Concheiro, A.; Alvarez-Lorenzo, C. Antifouling Foldable Acrylic IOLs Loaded with Norfloxacin by Aqueous Soaking and by Supercritical Carbon Dioxide Technology. *Eur. J. Pharm. Biopharm.* **2012**, *82* (2), 383–391 DOI: 10.1016/j.ejpb.2012.07.007.

(70) Refojo, M. F. Polymers in Ophthalmic Surgery. *J. Biomed. Mater. Res.* **1971**, *5* (1), 113–119 DOI: 10.1002/jbm.820050108.

(71) Ismail, M. M. Correction of Hyperopia with Intracorneal Implants. *J. Cataract Refract. Surg.* **2002**, *28* (3), 527–530 DOI: 10.1016/S0886-3350(01)01128-2.

(72) Zeng, Y.; Yang, J.; Huang, K.; Lee, Z.; Lee, X. A Comparison of Biomechanical Properties between Human and Porcine Cornea. *J. Biomech.* **2001**, *34* (4), 533–537 DOI: 10.1016/S0021-9290(00)00219-0.

(73) Elsheikh, A.; Wang, D.; Brown, M.; Rama, P.; Campanelli, M.; Pye, D. Assessment of Corneal Biomechanical Properties and Their Variation with

Age. *Curr. Eye Res.* **2007**, *32* (1), 11–19 DOI: 10.1080/02713680601077145.

(74) Jiang, H.; Zuo, Y.; Zhang, L.; Li, J.; Zhang, A.; Li, Y.; Yang, X. Property-Based Design: Optimization and Characterization of Poly(vinyl alcohol) (PVA) Hydrogel and PVA-Matrix Composite for Artificial Cornea. *J. Mater. Sci. Mater. Med.* **2014**, *25* (3), 941–952 DOI: 10.1007/s10856-013-5121-0.

(75) Liu, W.; Deng, C.; McLaughlin, C. R.; Fagerholm, P.; Lagali, N. S.; Heyne, B.; Scaiano, J. C.; Watsky, M. A.; Kato, Y.; Munger, R.; Shinozaki, N.; Li, F.; Griffith, M. Collagen-Phosphorylcholine Interpenetrating Network Hydrogels as Corneal Substitutes. *Biomaterials* **2009**, *30* (8), 1551–1559 DOI: 10.1016/j.biomaterials.2008.11.022.

(76) Costa, A. M. S.; Mano, J. F. Extremely Strong and Tough Hydrogels as Prospective Candidates for Tissue Repair − A Review. *Eur. Polym. J.* **2015**, *72*, 344–364 DOI: 10.1016/j.eurpolymj.2015.07.053.

(77) Parke-Houben, R.; Fox, C. H.; Zheng, L. L.; Waters, D. J.; Cochran, J. R.; Ta, C. N.; Frank, C. W. Interpenetrating Polymer Network Hydrogel Scaffolds for Artificial Cornea Periphery. *J. Mater. Sci. Mater. Med.* **2015**, *26* (2), 107–119 DOI: 10.1007/s10856-015-5442-2.

(78) Cardona, H. Keratoprosthesis: Acrylic Optical Cylinder with Supporting Intralamellar Plate. *Am. J. Ophthalmol.* **1962**, *54* (2), 284–294 DOI: 10.1016/0002-9394(62)93291-9.

(79) Arica, M. Y.; Hasirci, V. N. Permeability of PHEMA Membranes Prepared by Photoinitiation. *Polym. Int.* **1993**, *32* (2), 177–182 DOI: 10.1002/pi.4990320211.

(80) Zhang, Q.; Fang, Z.; Cao, Y.; Du, H.; Wu, H.; Beuerman, R.; Chan-Park, M. B.; Duan, H.; Xu, R. High Refractive Index Inorganic-Organic Interpenetrating Polymer Network (IPN) Hydrogel Nanocomposite toward Artificial Cornea Implants. *ACS Macro Lett.* **2012**, *1* (7), 876–881 DOI: 10.1021/mz300078y.

(81) Park, S.; Nam, S. H.; Koh, W. G. Preparation of Collagen-Immobilized Poly(ethylene glycol)/poly(2-hydroxyethyl methacrylate) Interpenetrating Network Hydrogels for Potential Application of Artificial Cornea. *J. Appl. Polym. Sci.* **2012** DOI: 10.1002/app.34532.

(82) Lei, J.; Mayer, C.; Freger, V.; Ulbricht, M. Synthesis and Characterization of Poly(ethylene glycol) Methacrylate Based Hydrogel Networks for Anti-Biofouling Applications. *Macromol. Mater. Eng.* **2013**, *298* (9), 967–980 DOI: 10.1002/mame.201200297.

(83) Carr, L. R.; Xue, H.; Jiang, S. Functionalizable and Nonfouling Zwitterionic Carboxybetaine Hydrogels with a Carboxybetaine Dimethacrylate Crosslinker. *Biomaterials* **2011**, *32* (4), 961–968 DOI: 10.1016/j.biomaterials.2010.09.067.

(84) Yin, H.; Akasaki, T.; Lin Sun, T.; Nakajima, T.; Kurokawa, T.; Nonoyama, T.; Taira, T.; Saruwatari, Y.; Ping Gong, J. Double Network Hydrogels from Polyzwitterions: High Mechanical Strength and Excellent Anti-Biofouling

Properties. *J. Mater. Chem. B* **2013**, *1* (30), 3685–3693 DOI: 10.1039/C3TB20324G.

(85)   Chen, H.; Chen, Q.; Hu, R.; Wang, H.; Zhang Newby, B.; Chang, Y.; Zheng, J. Mechanically Strong Hybrid Double Network Hydrogels with Antifouling Property. *J. Mater. Chem. B* **2015**, *3*, 5426–5435 DOI: 10.1039/C5TB00681C.

(86)   Ajiro, H.; Watanabe, J.; Akashi, M. Cell Adhesion and Proliferation on Poly(N-vinylacetamide) Hydrogels and Double Network Approaches for Changing Cellular Affinities. *Biomacromolecules* **2008**, *9*, 426–430 DOI: 10.1021/bm701221c.

(87)   Murosaki, T.; Noguchi, T.; Hashimoto, K.; Kakugo, A.; Kurokawa, T.; Saito, J.; Chen, Y. M.; Furukawa, H.; Gong, J. P. Antifouling Properties of Tough Gels against Barnacles in a Long-Term Marine Environment Experiment. *Biofouling* **2009**, *25* (7), 657–666 DOI: 10.1080/08927010903082628.

(88)   Chen, P.; Wang, X.; Wang, G. Y.; Duo, Y. R.; Zhang, X. Y.; Hu, X. H.; Zhang, X. J. Double Network Self-Healing Graphene Hydrogel by Two Step Method for Anticancer Drug Delivery. *Mater. Technol.* **2014**, *29* (4), 210–213 DOI: 10.1179/1753555714Y.0000000128.

(89)   Pacelli, S.; Paolicelli, P.; Pepi, F.; Garzoli, S.; Polini, A.; Tita, B.; Vitalone, A.; Casadei, M. A. Gellan Gum and Poly(ethylene glycol) dimethacrylate Double Network Hydrogels with Improved Mechanical Properties. *J. Polym. Res.* **2014**, *21* (5) DOI: 10.1007/s10965-014-0409-4.

(90)   Kato, M.; Shoda, N.; Yamamoto, T.; Shiratori, R.; Toyoʹoka, T. Development of a Silica-Based Double-Network Hydrogel for High-Throughput Screening of Encapsulated Enzymes. *Analyst* **2009**, *134* (3), 577–581 DOI: 10.1039/B813936A.

(91)   Zhang, Y.; Chen, Q.; Ge, J.; Liu, Z. Controlled Display of Enzyme Activity with a Stretchable Hydrogel. *Chem. Commun.* **2013**, *49* (84), 9815–9817 DOI: 10.1039/C3CC45837G.

(92)   Luo, R.; Cao, Y.; Shi, P.; Chen, C. H. Near-Infrared Light Responsive Multi-Compartmental Hydrogel Particles Synthesized through Droplets Assembly Induced by Superhydrophobic Surface. *Small* **2014**, *10* (23), 4886–4894 DOI: 10.1002/smll.201401312.

(93)   Chen, S. C.; Wu, Y. C.; Mi, F. L.; Lin, Y. H.; Yu, L. C.; Sung, H. W. A Novel pH-Sensitive Hydrogel Composed of N,O-carboxymethyl Chitosan and Alginate Cross-Linked by Genipin for Protein Drug Delivery. *J. Control. Release* **2004**, *96* (2), 285–300 DOI: 10.1016/j.jconrel.2004.02.002.

(94)   Thimma Reddy, T.; Takahara, A. Simultaneous and Sequential Micro-Porous Semi-Interpenetrating Polymer Network Hydrogel Films for Drug Delivery and Wound Dressing Applications. *Polymer (Guildf).* **2009**, *50* (15), 3537–3546 DOI: 10.1016/j.polymer.2009.05.062.

(95)   Yin, L.; Fei, L.; Cui, F.; Tang, C.; Yin, C. Superporous Hydrogels Containing Poly(acrylic acid-co-acrylamide)/O-carboxymethyl Chitosan Interpenetrating

Polymer Networks. *Biomaterials* **2007**, *28* (6), 1258–1266 DOI: 10.1016/j.biomaterials.2006.11.008.

(96)   Wang, J.; Zhou, X.; Xiao, H. Structure and Properties of cellulose/poly(N-isopropylacrylamide) Hydrogels Prepared by SIPN Strategy. *Carbohydr. Polym.* **2013**, *94* (2), 749–754 DOI: 10.1016/j.carbpol.2013.01.036.

(97)   Matricardi, P.; Di Meo, C.; Coviello, T.; Hennink, W. E.; Alhaique, F. Interpenetrating Polymer Networks Polysaccharide Hydrogels for Drug Delivery and Tissue Engineering. *Adv. Drug Deliv. Rev.* **2013**, *65* (9), 1172–1187 DOI: 10.1016/j.addr.2013.04.002.

(98)   Wang, J.; Li, X. Enhancing Protein Resistance of Hydrogels Based on poly(2-Hydroxyethyl Methacrylate) and poly(2-methacryloyloxyethyl phosphorylcholine) with Interpenetrating Network Structure. *J. Appl. Polym. Sci.* **2011**, *121* (6), 3347–3352 DOI: 10.1002/app.33960.

(99)   Bera, R.; Dey, A.; Datta sarma, A.; Chakrabarty, D. Synthesis and Characterization of acrylic acid-2-hydroxyethyl methacrylate IPN Hydrogels. *RSC Adv.* **2015**, *5* (93), 75870–75880 DOI: 10.1039/C5RA12110H.

(100)   Bajpai, A. K.; Shrivastava, M. Enhanced Water Sorption of a Semi-Interpenetrating Polymer Network (IPN) of Poly(2-hydroxyethyl methacrylate) (PHEMA) and Poly(ethylene glycol) (PEG). *J. Macromol. Sci. Part A* **2002**, *39* (7), 667–692 DOI: 10.1081/MA-120004511.

(101)   Tang, Q.; Yu, J. R.; Chen, L.; Zhu, J.; Hu, Z. M. Preparation and Properties of Morphology Controlled poly(2-hydroxyethyl methacrylate)/poly(N-vinyl pyrrolidone) Double Networks for Biomedical Use. *Curr. Appl. Phys.* **2010**, *10* (3), 766–770 DOI: 10.1016/j.cap.2009.09.012.

(102)   Domingues, J. A. L.; Bonelli, N.; Giorgi, R.; Fratini, E.; Gorel, F.; Baglioni, P. Innovative Hydrogels Based on Semi-Interpenetrating p(HEMA)/PVP Networks for the Cleaning of Water-Sensitive Cultural Heritage Artifacts. *Langmuir* **2013**, *29* (8), 2746–2755 DOI: 10.1021/la3048664.

(103)   Ramaraj, B.; Radhakrishnan, G. Modification of the Dynamic Swelling Behaviour of poly(2-hydroxyethyl methacrylate) Hydrogels in Water through Interpenetrating Polymer Networks (IPNs). *Polymer (Guildf).* **1994**, *35* (10), 2167–2173 DOI: 10.1016/0032-3861(94)90245-3.

(104)   Santin, M.; Huang, S.; Iannace, S.; Ambrosio, L. Synthesis and Characterization of a New Interpenetrated poly(2-hydroxyethyl methacrylate)-Gelatin Composite Polymer. *Biomaterials* **1996**, *17* (15), 1459–1467.

(105)   Krezović, B. D.; Dimitrijević, S. I.; Filipović, J. M.; Nikolić, R. R.; Tomić, S. L. Antimicrobial P(HEMA/IA)/PVP Semi-Interpenetrating Network Hydrogels. *Polym. Bull.* **2013**, *70* (3), 809–819 DOI: 10.1007/s00289-012-0830-y.

(106)   Lim, H.-L.; Kim, H.-J.; Jun, J. Development of Hydrogel Lenses Functionalized with an Interpenetrating Chitosan Network for Reduction of Protein Adsorption. *J. Nanosci. Nanotechnol.* **2016**, *16* (11), 11952–11956

DOI: 10.1166/jnn.2016.13624.

(107) Elbarbary, A. M.; Ghobashy, M. M. Phosphorylation of chitosan/HEMA Interpenetrating Polymer Network Prepared by γ-Radiation for Metal Ions Removal from Aqueous Solutions. *Carbohydr. Polym.* **2017**, *162*, 16–27 DOI: 10.1016/j.carbpol.2017.01.013.

(108) Lipatov, Y. S.; Alekseeva, T. *Phase-Separated Interpenetrating Polymer Networks*; 2007; Vol. 208.

(109) Young, J. S.; Bowman, C. N. Effect of Polymerization Temperature and Cross-Linker Concentration on Reaction Diffusion Controlled Termination. *Macromolecules* **1999**, *32* (19), 6073–6081 DOI: 10.1021/ma9902955.

(110) Goodner, M. D.; Lee, H. R.; Bowman, C. N. Method for Determining the Kinetic Parameters in Diffusion-Controlled Free-Radical Homopolymerizations. *Ind. Eng. Chem. Res.* **1997**, *36* (1), 1247–1252 DOI: 10.1021/ie9605387.

(111) Hacioğlu, B.; Berchtold, K. A.; Lovell, L. G.; Nie, J.; Bowman, C. N. Polymerization Kinetics of HEMA/DEGDMA: Using Changes in Initiation and Chain Transfer Rates to Explore the Effects of Chain-Length-Dependent Termination. *Biomaterials* **2002**, *23* (20), 4057–4064 DOI: 10.1016/S0142-9612(02)00138-2.

(112) Huang, C.-W.; Sun, Y.-M.; Huang, W.-F. Curing Kinetics of the Synthesis of poly(2-hydroxyethyl methacrylate) (PHEMA) with Ethylene glycol dimethacrylate (EGDMA) as a Crosslinking Agent. *J. Polym. Sci. Part A Polym. Chem.* **1997**, *35* (10), 1873–1889 DOI: 10.1002/(SICI)1099-0518(19970730)35:10<1873::AID-POLA2>3.0.CO;2-P.

(113) Elliott, J. E.; Bowman, C. N. Monomer Functionality and Polymer Network Formation. *Macromolecules* **2001**, *34* (13), 4642–4649 DOI: 10.1021/ma010153m.

(114) Dušek, K.; Ilavský, M. Cyclization in Crosslinking Polymerization. I. Chain Polymerization of a Bis Unsaturated Monomer (Monodisperse Case). *J. Polym. Sci.* **1975**, *73* (53), 57–73.

(115) Okay, O.; Naghash, H. J.; Pekcan, Ö. Critical Properties for Gelation in Free-Radical Crosslinking Copolymerization. *Macromol. Theory Simulations* **1995**, *4* (5), 967–981 DOI: 10.1002/mats.1995.040040509.

(116) Elliott, J. E.; Bowman, C. N. Kinetics of Primary Cyclization Reactions in Cross-Linked Polymers: An Analytical and Numerical Approach to Heterogeneity in Network Formation. *Macromolecules* **1999**, *32* (25), 8621–8628 DOI: 10.1021/ma990797i.

(117) Elliott, J. E.; Anseth, J. W.; Bowman, C. N. Kinetic Modeling of the Effect of Solvent Concentration on Primary Cyclization during Polymerization of Multifunctional Monomers. *Chem. Eng. Sci.* **2001**, *56* (10), 3173–3184 DOI: 10.1016/S0009-2509(00)00547-9.

(118) Elliott, J. E.; Bowman, C. N. Effects of Solvent Quality during Polymerization

on Network Structure of Cross-Linked Methacrylate Copolymers. *J. Phys. Chem. B* **2002**, *106* (11), 2843–2847 DOI: 10.1021/jp012845i.

(119) Matsumoto, A. Free-Radical Crosslinking Polymerization and Copolymerization of Multivinyl Compounds. In *Advances in polymer science*; 1995; Vol. 123, pp 41–80.

(120) Matsumoto, A.; Matsuo, H.; Ando, H.; Oiwa, M. Solvent Effect in the Copolymerization of Methyl methacrylate with Oligoglycol dimethacrylate. *Eur. Polym. J.* **1989**, *25* (3), 237–239 DOI: 10.1016/0014-3057(89)90224-3.

(121) Graham, N. B.; Hayes, C. M. G. Microgels 1: Solution Polymerization Using Vinyl Monomers. *Macromol. Symp.* **1995**, *93* (1), 293–300 DOI: 10.1002/masy.19950930135.

(122) Graham, N. B.; Cameron, A. Nanogels and Microgels: The New Polymeric Materials Playground. *Pure Appl. Chem.* **1998**, *70* (6), 1271–1275 DOI: 10.1351/pac199870061271.

(123) Li, L.; Lee, L. J. Photopolymerization of HEMA/DEGDMA Hydrogels in Solution. *Polymer (Guildf).* **2005**, *46* (25), 11540–11547 DOI: 10.1016/j.polymer.2005.10.051.

(124) Suthar, B.; Xiao, H. X.; Klempner, D.; Frisch, K. C. A Review of Kinetic Studies on the Formation of Interpenetrating Polymer Networks. *Polym. Adv. Technol.* **1995**, *7*, 221–233.

(125) Touhsaent, R. E.; Thomas, D. A.; Sperling, L. H. Epoxy/Acrylic Simultaneous Interpenetrating Networks. *J. Polym. Sci.* **1974**, *190* (46), 175–190.

(126) Lipatov, Y. S.; Semenovitch, G. M.; Skiba, S. I.; Karabanova, L. V.; Sergeeva, L. M. The Kinetic Peculiarities of Interpenetrating Polymer Network Formation. *Polymer (Guildf).* **1992**, *33* (2), 361–364 DOI: 10.1016/0032-3861(92)90994-8.

(127) Lipatov, Y. S.; Alekseeva, T. T.; Rosovitskii, V. F.; Babkina, N. V. Microphase Separation in Interpenetrating Polymer Networks as Affected by the Kinetics of Their Formation. *Polym. Sci. Ser. A* **1993**, *35* (6), 652–657.

(128) Flory, P. J. Molecular Size Distribution in Three Dimensional Polymers. I. Gelation. *J. Am. Chem. Soc.* **1941**, *63* (11), 3083–3090 DOI: 10.1021/ja01856a061.

(129) Stauffer, D.; Coniglio, A.; Adam, M. Gelation and Critical Phenomena. *Adv. Polym. Sci.* **1982**, *44*, 103–158 DOI: 10.1007/3-540-11471-8_4.

(130) Almdal, K.; Dyre, J.; Hvidt, S.; Kramer, O. Towards a Phenomenological Definition of the Term "Gel." *Polym. Gels Networks* **1993**, *1* (1), 5–17 DOI: 10.1016/0966-7822(93)90020-I.

(131) Ďuračková, A.; Valentová, H.; Dušková-Smrčková, M.; Dušek, K. Effect of Diluent on the Gel Point and Mechanical Properties of Polyurethane Networks. *Polym. Bull.* **2007**, *58* (1), 201–211 DOI: 10.1007/s00289-006-0589-0.

(132) Dušková-Smrčková, M.; Valentová, H.; Ďuračková, A.; Dušek, K. Effect of Dilution on Structure and Properties of Polyurethane Networks. Pregel and Postgel Cyclization and Phase Separation. *Macromolecules* **2010**, *43* (15), 6450–6462 DOI: 10.1021/ma100626d.

(133) Tung, C.-Y. M.; Dynes, P. J. Relationship between Viscoelastic Properties and Gelation in Thermosetting Systems. *J. Appl. Polym. Sci.* **1982**, *27* (2), 569–574 DOI: 10.1002/app.1982.070270220.

(134) Winter, H. H.; Chambon, F. Analysis of Linear Viscoelasticity of a Crosslinking Polymer at the Gel Point. *J. Rheol. (N. Y. N. Y).* **1986**, *30* (2), 367 DOI: 10.1122/1.549853.

(135) Han, Y. A.; Lee, E. M.; Ji, B. C. Mechanical Properties of Semi-Interpenetrating Polymer Network Hydrogels Based on poly(2-hydroxyethyl methacrylate) Copolymer and Chitosan. *Fibers Polym.* **2008**, *9* (4), 393–399 DOI: 10.1007/s12221-008-0063-8.

(136) Zhang, J. T.; Bhat, R.; Jandt, K. D. Temperature-Sensitive PVA/PNIPAAm Semi-IPN Hydrogels with Enhanced Responsive Properties. *Acta Biomater.* **2009**, *5* (1), 488–497 DOI: 10.1016/j.actbio.2008.06.012.

(137) Hernández, R.; Mijangos, C.; López, D. Study of the Effect of Poly(vinyl alcohol) Concentration on the Gelation Point of Poly(vinyl alcohol) Poly(acrylic acid) Semi-IPN Systems as Determined by Viscoelastic Measurements. *J. Polym. Sci. Part B Polym. Phys.* **2005**, *43* (15), 1944–1949 DOI: 10.1002/polb.20486.

(138) Zhang, H.; Qadeer, A.; Chen, W. In Situ Gelable Interpenetrating Double Network Hydrogel Formulated from Binary Components: Thiolated Chitosan and Oxidized Dextran. *Biomacromolecules* **2011**, *12* (5), 1428–1437 DOI: 10.1021/bm101192b.

(139) Shikanov, A.; Xu, M.; Woodruff, T. K.; Shea, L. D. Interpenetrating Fibrin-Alginate Matrices for in Vitro Ovarian Follicle Development. *Biomaterials* **2009**, *30* (29), 5476–5485 DOI: 10.1016/j.biomaterials.2009.06.054.

(140) Klempner, D.; Wang, C. L.; Ashtiani, M.; Frisch, K. C. Sound Attenuation of Interpenetrating Polymer Network Foams. *J. Appl. Polym. Sci.* **1986**, *32* (3), 4197–4208 DOI: 10.1002/app.1986.070320332.

(141) Dragan, E. S. Advances in Interpenetrating Polymer Network Hydrogels and Their Applications. *Pure Appl. Chem.* **2014**, *86* (11), 1707–1721 DOI: 10.1515/pac-2014-0713.

(142) Siegfried, D. L.; Manson, J. A.; Sperling, L. H. Viscoelastic Behavior and Phase Domain Formation in Millar Interpenetrating Polymer Networks of Polystyrene. *J. Polym. Sci. Polym. Phys. Ed.* **1978**, *16* (4), 583–597 DOI: 10.1002/pol.1978.180160402.

(143) Siegfried, D. L.; Thomas, D. A.; Sperling, L. H. A Reexamination of Polystyrene/Polystyrene Homo Interpenetrating Polymer Networks: Aspects of Relative Network Continuity and Internetwork Coupling. *Macromolecules*

1979, *12* (4), 586–589 DOI: 10.1021/ma60070a009.

(144) Thiele, J. L.; Cohen, R. E. Synthesis, Characterization, and Viscoelastic Behavior of Single-phase Interpenetrating Polystyrene Networks. *Polym. Eng. Sci.* **1979**, *19* (4), 284–293 DOI: 10.1002/pen.760190410.

(145) Zheng, B.; Li, H.; Wang, G.; Liu, K.; Wang, L.; Pan, G. Visualizing Phase Separation in Polystyrene/Polystyrene Homo-IPNs via Sulfonation. *Polym. Int.* **2009**, *58* (4), 343–347 DOI: 10.1002/pi.2552.

(146) Dušek, K. Phase Separation during the Formation of Three-Dimensional Polymers. *Polym. Lett.* **1965**, *3*, 209–212.

(147) Dušek, K.; Dušková-Smrčková, M. Network Structure Formation during Crosslinking of Organic Coating Systems. *Prog. Polym. Sci.* **2000**, *25* (9), 1215–1260 DOI: 10.1016/S0079-6700(00)00028-9.

(148) Dušek, K.; Sedláček, B. Phase Separation in poly(2-hydroxyethyl methacrylate) Gels in the Presence of Water. *Eur. Polym. J.* **1971**, *7* (9), 1275–1285 DOI: 10.1016/0014-3057(71)90118-2.

(149) Kovačič, S.; Štefanec, D.; Krajnc, P. Highly Porous Open-Cellular Monoliths from 2-hydroxyethyl methacrylate Based High Internal Phase Emulsions (HIPEs): Preparation and Void Size Tuning. *Macromolecules* **2007**, *40* (22), 8056–8060 DOI: 10.1021/ma071380c.

(150) Donatelli, A. A.; Sperling, L. H.; Thomas, D. A. A Semiempirical Derivation of Phase Domain Size in Interpenetrating Polymer Networks. *J. Appl. Polym. Sci.* **1977**, *21* (5), 1189–1197 DOI: 10.1002/app.1977.070210503.

(151) Donatelli, A. A.; Sperling, L. H.; Thomas, D. A. Interpenetrating Polymer Networks Based on SBR/PS. 1. Control of Morphology by Level of Cross-Linking. *Macromolecules* **1976**, *9* (4), 671–675 DOI: 10.1021/ma60052a029.

(152) Yeo, J. K.; Sperling, L. H.; Thomas, D. A. Theoretical Prediction of Domain Sizes in IPN's and Related Materials. *Polymer (Guildf).* **1983**, *24* (3), 307–313 DOI: 10.1016/0032-3861(83)90268-9.

(153) Sperling, L. H. Interpenetrating Polymer Networks. *Encycl. Polym. Sci. Technol.* **2004**, *10* (6), 272–311.

(154) Williams, R. J. J.; Borrajo, J.; Adabbo, H. E.; Rojas, A. J. A Model for Phase Separation During a Thermoset Polymerization. **1984**, 195–213 DOI: 10.1021/ba-1984-0208.ch013.

(155) Vazquez, A.; Rojas, A. J.; Adabbo, H. E.; Borrajo, J.; Williams, R. J. J. Rubber-Modified Thermosets: Prediction of the Particle Size Distribution of Dispersed Domains. *Polymer (Guildf).* **1987**, *28* (7), 1156–1164 DOI: 10.1016/0032-3861(87)90259-X.

(156) Cahn John E., J. W. H. Free Energy of a Nonuniform System. I. Interfacial Free Energy. *J. Chem. Phys.* **1958**, *28* (2), 258–267 DOI: 10.1063/1.1744102.

(157) Lipatov, Y. S. Interfacial Regions in the Phase-Separated Interpenetrating

Networks. *Polym. Bull.* **2007**, *58* (1), 105–118 DOI: 10.1007/s00289-006-0632-1.

(158) Zhang, J.; Wang, J.; Zhang, H.; Lin, J.; Ge, Z.; Zou, X. Macroporous Interpenetrating Network of Polyethylene glycol (PEG) and Gelatin for Cartilage Regeneration. *Biomed. Mater.* **2016**, *11* (3), 35014 DOI: 10.1088/1748-6041/11/3/035014.

(159) Zhao, Q.; Sun, J.; Wu, X.; Lin, Y. Macroporous Double-Network Cryogels: Formation Mechanism, Enhanced Mechanical Strength and temperature/pH Dual Sensitivity. *Soft Matter* **2011**, *7* (9), 4284 DOI: 10.1039/c0sm01407a.

(160) Paterson, S. M.; Casadio, Y. S.; Brown, D. H.; Shaw, J. A.; Chirila, T. V.; Baker, M. V. Laser Scanning Confocal Microscopy versus Scanning Electron Microscopy for Characterization of Polymer Morphology: Sample Preparation Drastically Distorts Morphologies of poly(2-hydroxyethyl methacrylate)-Based Hydrogels. *J. Appl. Polym. Sci.* **2013**, *127* (6), 4296–4304 DOI: 10.1002/app.38034.

(161) Trieu, H. H.; Qutubuddin, S. Polyvinyl Alcohol Hydrogels I. Microscopic Structure by Freeze-Etching and Critical Point Drying Techniques. *Colloid Polym. Sci.* **1994**, *272* (3), 301–309 DOI: 10.1007/BF00655501.

(162) Miller, D. R.; Peppas, N. A. Bulk Characterization and Scanning Electron Microscopy of Hydrogels of P(VA-Co-NVP). *Biomaterials* **1986**, *7* (5), 329–339 DOI: 10.1016/0142-9612(86)90003-7.

(163) Aston, R.; Sewell, K.; Klein, T.; Lawrie, G.; Grondahl, L. Evaluation of the Impact of Freezing Preparation Techniques on the Characterisation of Alginate Hydrogels by Cryo-SEM. *Eur. Polym. J.* **2016**, *82*, 1–15 DOI: 10.1016/j.eurpolymj.2016.06.025.

(164) Giesche, H. Mercury Porosimetry: A General (Practical) Overview. *Part. Part. Syst. Charact.* **2006**, *23* (1), 9–19 DOI: 10.1002/ppsc.200601009.

(165) Hecht, A. M.; Duplessix, R.; Geissler, E. Structural Inhomogeneities in the Range 2.5-2500 a in Polyacrylamide Gels. *Macromolecules* **1985**, *18* (11), 2167–2173 DOI: DOI 10.1021/ma00153a018.

(166) Tominaga, T.; Tirumala, V. R.; Lin, E. K.; Gong, J. P.; Furukawa, H.; Osada, Y.; Wu, W. L. The Molecular Origin of Enhanced Toughness in Double-Network Hydrogels: A Neutron Scattering Study. *Polymer (Guildf).* **2007**, *48* (26), 7449–7454 DOI: 10.1016/j.polymer.2007.10.016.

(167) Wang, L.; Shan, G.; Pan, P. A Strong and Tough Interpenetrating Network Hydrogel with Ultrahigh Compression Resistance. *Soft Matter* **2014**, *10* (21), 3850–3856 DOI: 10.1039/c4sm00206g.

(168) Dušek, K.; Dušková-Smrčková, M.; Šomvársky, J. Effect of Constraints on Swelling of Polymer Networks. *Macromol. Symp.* **2015**, *358* (1), 120–127 DOI: 10.1002/masy.201500025.

(169) Zhao, X.; Hong, W.; Suo, Z. Inhomogeneous and Anisotropic Equilibrium State of a Swollen Hydrogel Containing a Hard Core. *Appl. Phys. Lett.* **2008**,

92 (5), 17–20 DOI: 10.1063/1.2840158.

(170) Hong, W.; Liu, Z.; Suo, Z. Inhomogeneous Swelling of a Gel in Equilibrium with a Solvent and Mechanical Load. *Int. J. Solids Struct.* **2009**, *46* (17), 3282–3289 DOI: 10.1016/j.ijsolstr.2009.04.022.

(171) Clayton, A. B.; Chirila, T. V.; Dalton, P. D. Hydrophilic Sponges Based on 2-hydroxyethyl methacrylate. III. Effect of Incorporating a Hydrophilic Crosslinking Agent on the Equilibrium Water Content and Pore Structure. *Polym. Int.* **1997**, *42* (1), 45–56 DOI: 10.1002/(SICI)1097-0126(199701)42:1<45::AID-PI658>3.0.CO;2-W.

(172) Karpushkin, E.; Dušková-Smrčková, M.; Remmler, T.; Lapčíková, M.; Dušek, K. Rheological Properties of Homogeneous and Heterogeneous poly(2-hydroxyethyl methacrylate) Hydrogels. *Polym. Int.* **2012**, *61* (2), 328–336 DOI: 10.1002/pi.3194.

(173) Refojo, M. F. Glyceryl methacrylate Hydrogels. *J. Appl. Polym. Sci.* **1965**, *9*, 3161–3170 DOI: 10.1002/app.1965.070090920.

(174) Refojo, M. F. Permeation of Water Through Some Hydrogels. *J. Appl. Polym. Sci.* **1965**, *9* (10), 3417–3426 DOI: 10.1002/app.1965.070091019.

(175) Šprincl, L.; Kopeček, J.; Lím, D. Effect of Porosity of Heterogeneous Poly(glycol monomethacrylate) Gels on the Healing-in of Test Implants. *J. Biomed. Mater. Res.* **1971**, *5* (5), 447–458 DOI: 10.1002/jbm.820050503.

(176) Gates, G.; Harmon, J. P.; Ors, J.; Benz, P. 2,3-dihydroxypropyl methacrylate and 2-hydroxyethyl methacrylate Hydrogels: Gel Structure and Transport Properties. *Polymer (Guildf).* **2002**, *44* (1), 215–222 DOI: 10.1016/S0032-3861(02)00723-1.

(177) Passos, M. F.; Fernández-Gutiérrez, M.; Vázquez-Lasa, B.; Román, J. S.; Filho, R. M. PHEMA-PLLA Semi-Interpenetrating Polymer Networks: A Study of Their Swelling Kinetics, Mechanical Properties and Cellular Behavior. *Eur. Polym. J.* **2016**, *85*, 150–163 DOI: 10.1016/j.eurpolymj.2016.10.023.

(178) Anseth, K. S.; Bowman, C. N.; Brannon-Peppas, L. Mechanical Properties of Hydrogels and Their Experimental Determination. *Biomaterials* **1996**, *17* (17), 1647–1657 DOI: 10.1016/0142-9612(96)87644-7.

(179) Murata Hiroshi. Rheology - Theory and Application to Biomaterials. In *Polymerization*; Ailton De Souza Gomes, Ed.; InTech, 2012; pp 403–426.

(180) Julian Vincent. Basic Ealsticity and Viscoelasticity. In *Structural Biomaterials*; Princeton University Press, 2012; pp 1–28.

(181) Davis, J. R. Introduction to Tensile Testing. In *Tensile testing*; Davis, J. R., Ed.; ASM International, 2004; pp 1–13.

(182) Ahearne, M.; Yang, Y.; Liu, K. Mechanical Characterisation of Hydrogels for Tissue Engineering Applications. In *Tissue Engineering*; Ashammakhi, N., Reis, R., Chiellini, F., Eds.; 2008; Vol. 4, pp 1–16.

(183) Shen, C.; Li, Y.; Wang, H.; Meng, Q.; Naito, Y.; Shinoka, T.; Breuer, C. K.; Khademhosseini, A.; Gong, J. P.; Yang, Y.; Khademhosseini, A.; Gong, J. P. Mechanically Strong Interpenetrating Network Hydrogels for Differential Cellular Adhesion. *RSC Adv.* **2017**, *7* (29), 18046–18053 DOI: 10.1039/C7RA01271C.

(184) Chen, Q.; Chen, H.; Zheng, J. Fundamentals of Double Network Hydrogels. *J. Mater. Chem. B* **2015**, *3* (18), 3654–3676 DOI: 10.1039/C5TB00123D.

(185) Hu, Y. Y.; Zhang, J.; Fang, Q. C.; Jiang, D. M.; Lin, C. C.; Zeng, Y.; Jiang, J. Sen. Salt and pH Sensitive Semi-Interpenetrating Polyelectrolyte Hydrogels poly(HEMA-Co-METAC)/PEG and Its BSA Adsorption Behavior. *J. Appl. Polym. Sci.* **2015**, *132* (9), 1–11 DOI: 10.1002/app.41537.

(186) L. R. G. Treloar. *The Physics of Rubber Elasticity*, Third Edit.; Clarendon Press, Oxford, 1975.

(187) Koningsveld, R.; Stockmayer, W.; Nies, E. *Polymer Phase Diagrams*; Oxford University Press, Oxford, 2001.

(188) Désilles, N.; Lecamp, L.; Lebaudy, P.; Bunel, C. Gradient Structure Materials from Homogeneous System Induced by UV Photopolymerization. *Polymer (Guildf).* **2003**, *44* (20), 6159–6167 DOI: 10.1016/S0032-3861(03)00664-5.

(189) Désilles, N.; Gautrelet, C.; Lecamp, L.; Lebaudy, P.; Bunel, C. Effect of UV Light Scattering during Photopolymerization on UV Spectroscopy Measurements. *Eur. Polym. J.* **2005**, *41* (6), 1296–1303 DOI: 10.1016/j.eurpolymj.2004.12.019.

(190) Karpushkin, E.; Dušková-Smrčková, M.; Šlouf, M.; Dušek, K. Rheology and Porosity Control of poly(2-hydroxyethyl methacrylate) Hydrogels. *Polymer (Guildf).* **2013**, *54*, 661–672 DOI: 10.1016/j.polymer.2012.11.055.

(191) Lozinsky, V. I. Cryogels on the Basis of Natural and Synthetic Polymers: Preparation, Properties and Application. *Russ. Chem. Rev.* **2002**, *71* (6), 489–511 DOI: 10.1070/RC2002v071n06ABEH000720.

(192) Lozinsky, V. I.; Galaev, I. Y.; Plieva, F. M.; Savina, I. N.; Jungvid, H.; Mattiasson, B. Polymeric Cryogels as Promising Materials of Biotechnological Interest. *Trends Biotechnol.* **2003**, *21* (10), 445–451 DOI: 10.1016/j.tibtech.2003.08.002.

(193) Dušek, K.; Šomvársky, J. Topological Nanoinhomogeneities in Polymer Networks. *Macromol. Symp.* **1996**, *106*, 119–136.

(194) Dušek, K.; Bohdanecký, M.; Vošický, V. Solubilization of Poly(2-hydroxyethyl methacrylate) with Aqueous Salt Solutions; Swelling of Gels. *Collect. Czech. Chem. Commun.* **1977**, *42*, 1599–1614.

(195) Mohomed, K.; Moussy, F.; Harmon, J. P. Dielectric Analyses of a Series of poly(2-hydroxyethyl methacrylate-co-2,3-dihydroxypropyl methacylate) Copolymers. *Polymer (Guildf).* **2006**, *47* (11), 3856–3865 DOI: 10.1016/j.polymer.2006.03.099.

(196) Gates, G.; Harmon, J.; Ors, J.; Benz, P. Intra and Intermolecular Relaxations 2,3-dihydroxypropyl methacrylate and 2-hydroxyethyl methacrylate Hydrogels. *Polymer (Guildf)*. **2003**, *44* (1), 207–214 DOI: 10.1016/S0032-3861(02)00725-5.

(197) Kyeremateng, S. O.; Amado, E.; Kressler, J. Synthesis and Characterization of Random Copolymers of (2,2-dimethyl-1,3-dioxolan-4-yl)methyl methacrylate and 2,3-dihydroxypropyl methacrylate. *Eur. Polym. J.* **2007**, *43* (8), 3380–3391 DOI: 10.1016/j.eurpolymj.2007.04.048.

(198) Meakin, J. R.; Hukins, D. W. L.; Imrie, C. T.; Aspden, R. M. Thermal Analysis of poly(2-hydroxyethyl methacrylate) (pHEMA) Hydrogels. *J. Mater. Sci. Mater. Med.* **2003**, *14* (1), 9–15 DOI: 10.1023/A:1021589017753.

(199) Zhao, X. Multi-Scale Multi-Mechanism Design of Tough Hydrogels: Building Dissipation into Stretchy Networks. *Soft Matter* **2014**, *10* (5), 672–687 DOI: 10.1039/C3SM52272E.

(200) Tranoudis, I.; Efron, N. Tensile Properties of Soft Contact Lens Materials. *Contact Lens Anterior Eye* **2004**, *27* (4), 177–191 DOI: 10.1016/j.clae.2004.08.002.

(201) Bhamra, T. S.; Tighe, B. J. Mechanical Properties of Contact Lenses: The Contribution of Measurement Techniques and Clinical Feedback to 50 Years of Materials Development. *Contact Lens Anterior Eye* **2017**, *40* (2), 70–81 DOI: 10.1016/j.clae.2016.11.005.

(202) Seo, E.; Kumar, S.; Lee, J.; Jang, J.; Park, J. H.; Chang, M. C.; Kwon, I.; Lee, J.-S.; Huh, Y. Modified Hydrogels Based on poly(2-hydroxyethyl methacrylate) (pHEMA) with Higher Surface Wettability and Mechanical Properties. *Macromol. Res.* **2017**, *25* (7), 704–711 DOI: 10.1007/s13233-017-5068-y.

(203) Lin, Z.; Wu, W.; Wang, J.; Jin, X. Studies on Swelling Behaviors, Mechanical Properties, Network Parameters and Thermodynamic Interaction of Water Sorption of 2-hydroxyethyl methacrylate/novolac epoxy vinyl ester resin Copolymeric Hydrogels. *React. Funct. Polym.* **2007**, *67* (9), 789–797 DOI: 10.1016/j.reactfunctpolym.2006.12.010.

(204) González-Méijome, J. M.; López-Alemany, A.; Lira, M.; Almeida, J. B.; Oliveira, M. E. C. D. R.; Parafita, M. A. Equivalences between Refractive Index and Equilibrium Water Content of Conventional and Silicone Hydrogel Soft Contact Lenses from Automated and Manual Refractometry. *J. Biomed. Mater. Res. Part B Appl. Biomater.* **2007**, *80B* (1), 184–191 DOI: 10.1002/jbm.b.30583.

(205) Kinloch, A. J. Relationships Between the Microstructure and Fracture Behavior of Rubber-Toughened Thermosetting Polymers. In *Rubber-Toughened Plastics*; 1989; pp 67–91.

(206) Dušková-Smrčková, M.; Valentová, H.; Ďuračková, A.; Dušek, K. Effect of Dilution on Structure and Properties of Polyurethane Networks. Pregel and Postgel Cyclization and Phase Separation. *Macromolecules* **2010**, *43* (15),

6450–6462 DOI: 10.1021/ma100626d.

(207) Dušek, K. Theoretical Treatment of Swelling and Elasticity of Swollen IPN Hydrogels (Unpublished Work).

(208) Přádný, M.; Dušková-Smrčková, M.; Dušek, K.; Janoušková, O.; Sadakbayeva, Z.; Šlouf, M.; Michálek, J. Macroporous 2-hydroxyethyl methacrylate Hydrogels of Dual Porosity for Cell Cultivation: Morphology, Swelling, Permeability, and Mechanical Behavior. *J. Polym. Res.* **2014**, *21* (579), 1–12 DOI: 10.1007/s10965-014-0579-0.

(209) Lesný, P.; Přádný, M.; Jendelová, P.; Michálek, J.; Vacík, J.; Syková, E. Macroporous Hydrogels Based on 2-hydroxyethyl methacrylate. Part 4: Growth of Rat Bone Marrow Stromal Cells in Three-Dimensional Hydrogels with Positive and Negative Surface Charges and in Polyelectrolyte Complexes. *J. Mater. Sci. Mater. Med.* **2006**, *17* (9), 829–833 DOI: 10.1007/s10856-006-9842-1.

(210) Meakin, J. R.; Hukins, D. W. L.; Aspden, R. M.; Imrie, C. T. Rheological Properties of poly(2-hydroxyethyl methacrylate) (pHEMA) as a Function of Water Content and Deformation Frequency. *J. Mater. Sci. Mater. Med.* **2003**, *14* (9), 783–787 DOI: 10.1023/A:1025088405674.

(211) Lindblad, M. S.; Albertsson, A. C.; Ranucci, E.; Laus, M.; Giani, E. Biodegradable Polymers from Renewable Sources: Rheological Characterization of Hemicellulose-Based Hydrogels. *Biomacromolecules* **2005**, *6* (2), 684–690 DOI: 10.1021/bm049515z.

(212) dos Santos, J.-F. R.; Couceiro, R.; Concheiro, A.; Torres-Labandeira, J.-J.; Alvarez-Lorenzo, C. Poly(hydroxyethyl methacrylate-co-methacrylated-β-cyclodextrin) Hydrogels: Synthesis, Cytocompatibility, Mechanical Properties and Drug Loading/release Properties. *Acta Biomater.* **2008**, *4* (3), 745–755 DOI: 10.1016/j.actbio.2007.12.008.

(213) Guvendiren, M.; Heiney, P. A.; Yang, S. Precipitated Calcium Carbonate Hybrid Hydrogels: Structural and Mechanical Properties. *Macromolecules* **2009**, *42* (17), 6606–6613 DOI: 10.1021/ma9012576.

List of figures

The porous networks 1 are represented by blue circles.

Figure 21. Conversion of C=C bonds of GMA monomer as quantified by ATR FTIR spectroscopy during crosslinking polymerization with no diluent present at polymerization (a). Spectra of polymerizable mixture (b) before UV-irradiation (1), after 90 minutes of UV-irradiation (2), and after 90 minutes of UV-irradiation followed by heating (3).

Figure 22. Optical density of GMA reaction mixture as a function of wavelength during the crosslinking polymerization with no diluent present at polymerization (a). Optical density of GMA reaction mixture at 317 nm wavelength as a function of conversion of C=C bonds (b).

Figure 23. ATR FTIR spectra of (a) H80/1 single network; (b) GMA reaction mixture; (c) H80/1 single network swollen in the GMA reaction mixture; (d) H80/1–G0/0.3 IPNs after UV-polymerization; (e) H80/1–G0/0.3 IPNs after UV-polymerization and heating.

Figure 24. Conversion of C=C bonds of GMA monomer as quantified by ATR FTIR spectroscopy during crosslinking polymerization within PHEMA–PGMA IPN environments: curve H80/1–G0/0.3 shows conversion of GMA with time in macroporous IPN, curve H40/1–G0/0.3 shows conversion of GMA in homogenous IPN, and the curve G0/0.3 shows conversion of GMA monomer during formation of single homogenous PGMA network with no diluent present at polymerization.

Figure 25. Weight fraction (w_{net2}) of PGMA network 2 forming in PHEMA–PGMA IPNs as a function of irradiation time followed by sol-extraction method.

Figure 26. Optical density of macroporous PHEMA 80/1 (black curve) and non-porous PHEMA 40/1 (blue curve) hydrogels swollen in GMA reaction mixture, PHEMA matrix swollen in water (magenta curve), and reference GMA reaction mixture (red curve). Data obtained prior to polymerization, sample thickness was 1 mm in all cases.

Figure 27. Optical density of gels measured prior and after the polymerization: H80/1-G0/0.3 (blue – prior, orange - after), H40/1-G0/0.3 (red – prior, green – after) and a reference G0/0.3 (black – prior, magenta – after). Measured using integrating sphere, sample thickness 1 mm in all cases.

Figure 28. Optical path of UV-beam through the non-uniform (a and b) and uniform (c) polymer matrix.

Figure 29. Optical density of the GMA reaction mixture (G0/0.3, red curves) and the same GMA reaction mixture G0/0.3 in the environments of macroporous H80/1 (black curves) and non-porous H40/1 (green curves) single networks before UV irradiation (solid lines) and after irradiation (connected full circles).

Figure 30. Gelation in water-diluted crosslinking PHEMA systems recorded at frequency of f = 0.05 Hz. The monomers mixtures were diluted with 40 wt.-% (H40/1, magenta curves) and 80 wt.-% (H80/1, blue curves) of water. Redox initiated polymerization with APS/TEMED system at T = 25 °C. Storage, G', (open) and loss, G'', (solid) moduli were recorded.

Figure 31. Gelation of PGMA while forming an individual single network (red curves) and while forming IPN in the environment of macroporous PHEMA (H80/1) network (black curves) recorded at frequency of f = 0.05 Hz. Thermally initiated polymerization with AIBN at T = 70 °C. Storage, G', (open) and loss, G'', (solid) moduli were recorded.

Figure 32. Visual appearance of swollen single network hydrogels: effect of initial water content and crosslinker concentration on the phase separation.

Figure 33. Visual appearance of swollen chemically homogeneous PHEMA-PHEMA IPN hydrogels. The first PHEMA networks were prepared with 40 wt.-% of water and various concentrations of crosslinkers (samples on green background), while the second PHEMA networks of various crosslinker concentrations formed in IPNs structure contained no water at preparation.

Figure 34. Visual appearance of PGMA-PHEMA IPN hydrogels at each stage of their formation: (a) PGMA network 1 swollen in water, (b) PGMA network 1 swollen in reaction mixture of HEMA monomer 2, (c) PGMA-PHEMA IPN as prepared after crosslinking polymerization, and (d) PGMA-PHEMA IPN hydrogel swollen in water. Single network PGMA hydrogel was prepared with 40 wt.-% of water and various crosslinker concentrations (left column). The second PHEMA network was prepared with no diluent and 0.3 mol-% of DEGDMA crosslinker.

Figure 35. Cryo-SEM micrographs of swollen (a) G40/0.2-H0/0.3 and (b) G40/1-H0/0.3 IPN hydrogels.

Figure 36. Evolution of macroporous PHEMA–PGMA IPN (H80/1–G0/0.3) morphology and transparency of hydrogels: (a) macroporous PHEMA network 1 (H80/1) swollen in water; (b) PHEMA network 1 swollen in GMA monomer 2; (c) loosely crosslinked PGMA network 2 formed in the matrix of tightly crosslinked PHEMA network 1 as well as in pores of the hydrogel; (d) PHEMA–PGMA IPN hydrogel swollen in water.

Figure 37. Laser scanning confocal microscopy (a, b, c) and cryo-SEM (d, e, f) micrographs of single network hydrogels swollen in water: H80/1 network 1 (a and d) and cH80/1 network 1 (b and e), and G0/0.3 network 2 (c and f).

Figure 38. Single-porous and double-porous PHEMA cryogels prepared at dilution of 95 wt.-% of pure water (a, c) and 95 wt.-% of 0.5 M NaCl solution (b, d). Light (a and b) and cryo-SEM (c and d) microscopes were used to observe the morphology of swollen cryogels.

Figure 39. LCSM of H80/1-G0/0.3 IPN hydrogels: (a) network 1 (H80/1) and network 2 (G0/0.3) labeled with fluorescein and DY-677 dye, respectively, and (b) non-labeled network 1 (H80/1) and network 2 (G0/0.3) labeled with fluorescein.

Figure 40. SWAXS dependencies for crosslinking polymerization of H40/1 gel in pure water. The polymerization was initiated with ammonium persulfate without adding TEMED to slow down the reaction to be able to record the SWAXS spectra as they develop in time.

Figure 41. Power law exponent p at H40/1 crosslinking polymerization time $t_{reaction}$.

Figure 42. SWAXS dependencies for crosslinking polymerization of H40/1 gel in the aqueous solution of 0.5 M $Mg(ClO_4)_2$. The polymerization was initiated with ammonium persulfate without adding TEMED to slow down the reaction in order to be able to record the SWAXS spectra as they develop in time.

Figure 43. Power law exponent p (a) and the radius of gyration R_g (b) at H40/1 crosslinking polymerization time $t_{reaction}$. Hydrogel was polymerized in the salting-in aqueous solution of 0.5 M $Mg(ClO_4)_2$.

Figure 44. Changes of structure during the UV-initiated crosslinking polymerization of the H0/0.3 network 2 in the matrix of the H40/1 network 1 followed by SWAXS.

Irradiation times: 0 min (blue), 15 min (green), 30 min (red).

Figure 45. Changes of structure during the UV-initiated crosslinking polymerization of the H0/0.3 (blue curves) and H0/2 (red curves) networks 2 in the matrix of the H40/1 network 1 followed by SWAXS.

Figure 46. Comparison of structure changes by SWAXS. Single network H40/1 (magenta curves) vs. H40/1-H0/0.3 IPN (blue curves) in (a) as prepared state and (b) equilibrium swollen state.

Figure 47. Size of aggregates in aqueous solutions of monomers determined by dynamic light scattering method: (a) HEMA or GMA monomers mixed with water at various ratios, (b) HEMA monomer (60 wt.-%) mixed with water (40 wt.-%) and DEGDMA crosslinker ($0 - 6$ mol-%).

Figure 48. Equilibrium volume of swollen gel per volume of the dry polymer versus reciprocal volume fraction of the monomer in the initial mixture corrected for polymerization contraction. PHEMA hydrogels contained various amounts of water ($30 - 94$ wt.-%) and concentration of DEGDMA crosslinker (1 mol-% and 6 mol-%) at preparation. PGMA hydrogels contained various amounts of water ($40 - 80$ wt.-%) and constant concentration of DEGDMA crosslinker (1 mol-%) at preparation.

Figure 49. Effect of DEGDMA crosslinker concentration ($0.2 - 6$ mol-%) in single H40/1 or G40/1 network hydrogels on swelling properties. Equilibrium volume of swollen gel per volume of the dry polymer versus the reciprocal volume fraction of the monomer in the initial mixture corrected for polymerization contraction.

Figure 50. Equilibrium swelling of non-porous H40/1 and porous H80/1 single network hydrogels in (a) HEMA:water and (b) GMA:water mixtures as a function of weight fraction of monomer.

Figure 51. A sketch illustrating expansion of chains of **network 1** in a single network and in an IPN H80/1–G0/0.3 due to swelling: volume change shown as relative volume of the network 1, V_{rel1}, which is expressed as a ratio of swollen sample volume, V_{sw}, to the reference volume of the network 1, V_{nf}. The parent network H80/1 swells in the monomer 2, GMA, and swelling of prepared IPN H80/1–G0/0.3 in water and in dimethyl sulfoxide (DMSO) is shown. Volume occupied initially by network 1 is drawn to offer a mind image to the reader. Data shows dilation factor $(\alpha_1)^3$ of network 1 chains in homogeneous and microstructured IPNs.

Figure 52. Stress-strain dependencies at extension for single PHEMA networks prepared at 40 wt.-% of water and various concentrations (mol-%) of DEGDMA crosslinker.

Figure 53. Stress-strain dependencies at extension for different PHEMA-PHEMA homo-IPN hydrogels: H0/Y second network interlocked with (a) H40/0.2, (b) H40/1, (c) H40/3, and (d) H40/6 first networks.

Figure 54. Young's modulus (E) of swollen H40/Y-H0/Z IPN hydrogels (a). Effect of crosslinker concentration (mol-%) in the second network on Young's moduli of the IPN hydrogels (b). Young's moduli of IPN hydrogels (E_{IPN}) were related to Young's moduli of single network 1 hydrogels (E_{SN1}).

Figure 55. Effect of crosslinker concentration (CC, mol%) in the second networks on the swelling properties of the IPN hydrogels. Equilibrium water content in the IPN hydrogels (EWC_{IPN}) was related to the equilibrium water content in the single network (EWC_{SN}) hydrogels.

Figure 56. Stress-strain dependencies at extension for single networks 1 and 2.

Figure 57. Stress-strain dependencies at extension for PHEMA-PGMA and PHEMA-PHEMA IPN hydrogels: the G0/0.3 second network interlocked with the (a) H0/1 and (c) H40/1 first network; the H0/0.3 second network interlocked with the (b) H0/1 and (d) H40/1 first network.

Figure 58. Stress-strain dependencies at extension for the cH80/1 first network cryogel interlocked with the (a) G0/0.3 and (b) H0/0.3 second networks.

Figure 59. Stress-strain dependencies at extension for the H80/1 first network hydrogel interlocked with the (c) G0/0.3 and (d) H0/0.3 second networks.

Figure 60. Concentration of elastically active network chains (EANC) in single network H40/Y hydrogels determined from the composition of reaction mixture (ideal) and calculated from the experimentally measured modulus (experimental). The values of "Y" corresponding to the concentration of DEGDMA crosslinker in the H40/Y hydrogels were 0.2, 1, 3, and 6 mol-%.

Figure 61. Different coiling states of "network a" and "network b" in the IPN structure after its formation and after swelling.

Figure 62. Young's moduli of swollen H40/Y-H0/0.3 IPN hydrogels determined by tensile tests (experimental) and calculated from the composition and swelling of networks according to Equation 4.43. The values of "Y" corresponding to the concentration of DEGDMA crosslinker in the H40/Y parent network were 0.2, 1, 3, and 6 mol-%.

Figure 63. Experimental method for finding a "correct gap" between the measuring plates in auto-tension mode with a target normal force set to 2 % at frequency of 1 Hz. The example is given for swollen H40/1 hydrogel.

Figure 64. . Storage modulus of hydrogels as a function of strain. Amplitude sweep test for swollen non-porous (H40/1) hydrogel deformed at strains from $1.9 \cdot 10^{-4}$ to $5.5 \cdot 10^{-3}$ and for macroporous (H80/1) PHEMA hydrogel deformed at strains from $1.4 \cdot 10^{-4}$ to $4 \cdot 10^{-2}$: determination of linear viscoelastic region.

Figure 65. Storage (G') and loss (G'') shear moduli, and loss factor (tan δ) of water-swollen non-porous single network H40/1 hydrogel as a function of frequency.

Figure 66. Storage modulus (G') of water-swollen single network PHEMA hydrogels prepared at 40 wt.-% of water as diluent and various crosslinker concentrations (0.2, 1, 3, and 6 mol.%) as a function of frequency.

Figure 67. Storage modulus (G') of water-swollen H40/Y-H0/0.3 IPN hydrogels as a function of frequency (a). At preparation, the network 1 (H40/Y) contained 40 wt.-% of water and various crosslinker concentrations (0.2, 1, 3, and 6 mol-%), while the network 2 was not diluted and contained 0.3 mol-% of crosslinker (H0/0.3). The reinforcement ratio (G'_{IPN}/G'_{SN1}) of IPN hydrogels was estimated as a relation of storage moduli of IPNs (G'_{IPN}) and of reference single networks 1 (G'_{SN1}) (b).

Figure 68. Storage moduli (G') of water-swollen single and IPN hydrogels measured in a frequency range from $4 \cdot 10^{-4}$ to 40 Hz: (a) constituent single PHEMA networks 1, (b) constituent single PHEMA and PGMA networks 2, (c) PHEMA-PHEMA IPNs, and (d) PHEMA-PGMA IPNs.

List of tables

List of abbreviations

AAm	acrylamide
AFM	atomic-force microscopy
AIBN	2,2′-azobis(2-methylpropionitrile)
APS	ammonium persulfate
ATR FTIR	attenuated total reflectance Fourier transform infrared spectroscopy
BAAm	*N,N'*-methylene-bis-acrylamide
Cryo-LVSEM	low-vacuum cryo-scanning electron microscopy
Cryo-SEM	cryo-scanning electron microscopy
DAAm	*N,N'*-dimethylacrylamide
DAROCUR 1173	2-hydroxy-2-methyl-1-phenyl-propane-1-one
DEGDMA	di(ethylene glycol) dimethacrylate
DLS	dynamic light scattering
DMSO	dimethyl sulfoxide
DN	double network
DPD-DA	oligo(2,2-dimethyltrimethylene carbonate)-poly(ethylene glycol)-oligo(2,2-dimethyltrimethylene carbonate)-diacrylate
DSC	differential scanning calorimeter
DY-677-NHS	amine coupling asymmetric cyanine ester
EANC	elastically active network chains
EDTA	ethylenediaminetetraacetic acid
EGDMA	ethylene glycol dimethacrylate
ESC	equilibrium solvent content
ESEM	environmental scanning electron microscopy
EWC	equilibrium water content
F-E	finite-extensibility models
FEM	finite element analysis
FITC	fluorescein isothiocyanate isomer I
GDMA	glycerol dimethacrylate
GelMA	gelatin methacrylamide
GGMA	gellan gum methacrylate
GMA	glycerol methacrylate
HA	hyaluronic acid
HA-GMA	methacrylated hyaluronic acid
HEMA	2-hydroxyethyl methacrylate
IPN	interpenetrating polymer network
LFD	large-field detector
LM	light microscopy
LSCM	laser scanning confocal microscopy
LVR	linear viscoelastic region

MBAA	*N*,*N'*-methylene-bis-acrylamide
MEHQ	4-methoxyphenol (hydroquinone monomethyl ether)
MEK	methyl ethyl ketone
MIPN	microstructured interpenetrating polymer network
PAA	poly(acrylic acid)
PAAm	polyacrylamide
PAMPS	poly(2-acrylamido-2-methyl-1-propanesulfonic acid)
PBS	phosphate-buffered saline
PCBMA	poly(carboxybetaine methacrylate)
PCDME	poly((*N*-carboxymethyl)-*N*,*N*-dimethyl-2-(methacryloyloxy) ethanaminium
PDMA	poly(*N*,*N*-dimethylacrylamide)
PDMAAm	poly(*N*,*N'*-dimethylacrylamide)
PDMS	poly(dimethylsiloxane)
PEA	poly(ethyl acrylate)
PEG	poly(ethylene glycol)
PEG-DM	poly(ethylene glycol) dimethacrylate
PGMA	poly(glycerol methacrylate)
PHEA	poly(2-hydroxyethyl acrylate)
PHEMA	poly(2-hydroxyethyl methacrylate)
PMMA	poly(methyl methacrylate)
PNIPAM	poly(*N*-isopropylacrylamide)
PNVA	poly(*N*-vinylacetamide)
PVA	poly(vinyl alcohol)
PVP	polyvinylpyrrolidone
RI	refractive index
SANS	small-angle neutron scattering
SAXS	small-angle X-ray scattering
SD	swelling degree
SEM	scanning electron microscopy
SN	single network
STL	STereoLithography
SWAXS	small and wide-angle X-ray scattering
TEMED	*N*,*N*,*N'*,*N'*-tetramethylethylenediamine
TMPTMA	trimethylolpropane trimethacylate
UCST	upper critical solution temperature
UV	ultraviolet
UV-VIS	ultraviolet–visible spectroscopy

List of frequently used symbols

A and B	front factors in the Flory-Erman junction-fluctuation theory
D_m	mass fractal dimension
D_s	surface fractal dimension
ESC	equilibrium solvent content
EWC	equilibrium water content
EWC_G	equilibrium water content in the gel phase
E	Young's modulus
f	frequency
f_e	elastically effective crosslinker functionality
f_ec	uniaxial force (subscript "ec" stands for extension/compression)
ΔF_mix	Helmholtz energy change of mixing of polymer and solvent
ΔF_el	Helmholtz energy change of elastic deformation
g	interaction function
G	equilibrium shear modulus
G'	storage modulus
G''	loss modulus
G^*	complex modulus
ΔG_sw	Gibbs energy change of swelling
ΔG_mix	Gibbs energy change of mixing of polymer and solvent
ΔG_el	Gibbs energy change of elastic deformation
k	Boltzmann constant
l_s	length of statistical segment
L_j	actual length of sample in the i-th direction
$\left(L_\mathrm{j}\right)_\mathrm{iso}$	length of sample in the i-th direction in the isotropic (swollen) network
L_j0	length of sample in the reference state ($\approx$ state at network formation)
m_d	weight dry network
m_d^L	weight of freeze-dried hydrogel
m_sw	weight of swollen network
m_sw^V	weight of hydrogel swollen in water vapor
n_m	number of monomer units

n_s	number of statistical segments
N_1	number of moles of solvent molecules
N_e	number of EANC
N_{ea}	number of EANC in network a
N_{eb}	number of EANC in network b
p	power low exponent related to fractal dimensions
P	porosity
q	scattering vector
Q_m	weight swelling ratio
Q_V	volume swelling ratio
R	universal gas constant
R_g	radius of gyration
S_b	true strength
SD	swelling degree
S_{iso}	cross-sectional area of undeformed, isotropic sample
$\tan \delta$	loss factor
T	temperature
T_g	glass transition temperature
$t_{reaction}$	polymerization time
V_0	reference volume
V_{1m}	molar volume of the solvent
V_a	volume of network a
V_b	volume of network b
V_{ap} and V_{bp}	volume of polymer a and polymer b
V_{ad} and V_{bd}	volumes of diluents added with monomer a and monomer b
V_s	volume of solvent in the swollen IPN
V_{sw}	volume of swollen network
V_d	volume of dry network
V_{nf}	volume at network formation
V_{rel1}	relative volume of the network 1
α	dilation factor,
α_1	dilation factor for chains of network 1
γ	shear deformation
δ	phase angle
ε	strain in uniaxial deformation

θ	scattering angle
λ	wavelength
λ_b	deformation at break
$\lambda_{ix}, \lambda_{iy}, \lambda_{iz}$	deformation ratios with respect to the reference state along the l coordinate axes of network i
Λ_j	deformation ratio with respect to the isotropic (swollen) state
$\Delta\mu_{1,mix}$	solvent chemical potential change
ν_e	concentration of EANC
ρ_{gel}	density of gel
ρ_{solv}	density of solvent
σ	deformation stress
σ_b	stress at break
σ_{true}	true strength
φ_a, φ_b	volume fractions of polymer network a and polymer network b in dry IPN
χ	Flory-Huggins interaction parameter
ϕ_1	volume fraction of solvent
ϕ_2	volume fraction of polymer in swollen single network
ϕ_2^0	volume fraction of all polymerizable substances at preparation
ϕ_{2a}^0, ϕ_{2b}^0	volume fraction of polymer a, and polymer b, respectively, in the mixtures with their diluents; for definitions, cf. eq. (4.6)
ϕ_{pores}	fraction of pores

List of publications

Articles related to this Thesis:

1. <u>Zhansaya Sadakbayeva</u>, Miroslava Dušková-Smrčková, Adriana Šturcová, Jiři Pfleger, Karel Dušek. Morphology effects on formation and enhancement of mechanical properties of poly(2-hydroxyethyl methacrylate) interpenetrating polymer network hydrogel materials // *Journal of Materials Chemistry B*. **2017**. (submitted)

2. Miroslava Dušková-Smrčková, <u>Zhansaya Sadakbayeva</u>, Miloš Steinhart, Karel Dušek "The manifold varieties of poly(2-hydroxyethyl methacrylate) (PHEMA) hydrogels – IPNs" // *Macromolecular Symposia*. Vol. 372. PP. 28-42. **2017**. PP. 28-42. DOI: 10.1002/masy.201700018

3. Hana Macková, Zdeněk Plichta, Helena Hlídková ,Ondřej Sedláček, Rafal Konefal, <u>Zhansaya Sadakbayeva</u>, Miroslava Dušková-Smrčková, Daniel Horák, Šárka Kubinová. Reductively degradable poly(2-hydroxyethyl methacrylate) hydrogels with oriented porosity for tissue engineering // *ACS Applied Materials & Interfaces*. Vol. 9. **2017**. PP. 10544-10553. DOI: 10.1021/acsami.7b01513

4. Martin Přádný, Miroslava Dušková-Smrčková, Karel Dušek, Olga Janoušková, <u>Zhansaya Sadakbayeva</u>, Miroslav Šlouf, Jiří Michálek. Macroporous 2-hydroxyethyl methacrylate hydrogels of dual porosity for cell cultivation: morphology, swelling, permeability, and mechanical behavior // *Journal of Polymer Research*. Vol. 21. Issue 11. **2014**. PP. 579-591. DOI: 10.1007/s10965-014-0579-0

5. <u>Zhansaya Sadakbayeva</u>, Evgeny Karpushkin, Miroslava Dušková-Smrčková, Martina Nevoralová, Miroslav Vetrík, Miroslav Šlouf, Karel Dušek. Highly swollen poly(glycerol methacrylate) hydrogels: stumbling blocks in morphology imaging with cryo-SEM (in preparation).

6. <u>Zhansaya Sadakbayeva</u>, Dana Kubies, Martin Přádný, Miroslava Dušková, Jakub Širc, Šlouf Miroslav, Michálek Jiří, Filová Elena, Havlíková Jana, Bačáková Lucie. Macroporous hydrogels based on 2-hydroxyethyl methacrylate: the effect of pore size, charge and mechanical properties on cell proliferation (in preparation).

Other articles:

1. S. Kudaibergenov, Zh. Adilov, D. Berillo, G. Tatykhanova, <u>Zh. Sadakbayeva</u>, Kh. Abdullin, I. Galaev. Novel macroporous amphoteric gels: Preparation and characterization // *eXPRESS Polymer Letters*. Vol.6. No.5. **2012.** PP. 346–353.

2. Kudaibergenov S.E., Sadakbayeva Zh.K., Tatykhanova G.S., Medard N., Seitov A.S., Abdullin K.A. Organosoluble polyelectrolyte-surfactant complexes // *Macromolecular Symposia*. Vol. 317-318. Issue 1. **2012.** PP. 7-17.

3. Gulnur S. Tatykhanova, Zhansaya K. Sadakbayeva, Dmitriy Berillo, Igor Galaev, Khabib A. Abdullin, Zheksenbek Adilov, Sarkyt E. Kudaibergenov. Metal Complexes of Amphoteric Cryogels Based on Allylamine and Methacrylic Acid // *Macromolecular Symposia*. Vol. 317-318. Issue 1. **2012.** PP. 18–27.

4. D.A. Panchuk, Zh.K. Sadakbayeva, D.V. Bagrov, A.V. Bol'shakova, L.M. Yarysheva, I.B. Meshkov, A.M. Muzafarov, A.L. Volynskii, N.F. Bakeev. Estimating the strain-strength characteristics of nanothick nonmetallic coatings deposited onto poly(ethylene terephthalate) films // *Polymer Science Series A*. Vol. 53, Issue 4. **2011.** PP. 303-310.

5. D.A. Panchuk, Zh.K. Sadakbayeva, D.V. Bagrov, A.S. Kechek'yan, A.V. Bol'shakova, S.S. Abramchuk, L.M. Yarysheva, A.L. Volynskii, N.F. Bakeev. Specific features of surface structuring during deformation of plasma-treated polymer films // *Polymer Science Series A*. Vol. 52. Issue 8. **2010.** PP. 794-800.

6. A.L. Volynskii, D.A. Panchuk, Zh.K. Sadakbayeva, A.V. Bol'shakova, L.M. Yarysheva, N.F. Bakeev. Evaluation of the stress-strain properties of surface layers in plasma-treated polymers // *High Energy Chemistry*. Vol. 44. Issue 4. **2010.** PP. 341-346.

7. Volynskii A.L., Panchuk D.A., Sadakbayeva Zh.K., Bol'shakova A.V., Kechek'yan A.S., Yarysheva L.M., Bakeev N.F. Formation of a regular microrelief in deformation of plasma-treated polymer films // *Doklady Physical Chemistry*. Vol. 427. **2009.** PP. 133-135.

8. D.A. Panchuk, Zh.K. Sadakbayeva, E.A. Puklina, A.V. Bol'shakova, S.S. Abramchuk, L.M. Yarysheva, A.L. Volynskii, N.F. Bakeev. The structure of interfacial layer between the metallic coating and the polymer substrate // *Nanotechnologies in Russia*. Vol. 4. Issue 5-6. **2009.** PP 340-348.

Patents:

1. Innovation Patent of the Republic of Kazakhstan № KZ 30944 (from 15.03.**2016**): A method of synthesis of composite hydrogel "pig" for pipeline cleaning. Sadakbayeva Zh.; Blagikh E.; Gabsattarova G.; Didukh A.; Aldiyarov T.; Nasibulin M.; Kudaibergenov S.

2. Innovation Patent of the Republic of Kazakhstan № KZ 30943 (from 15.03.**2016**):
A method of synthesis of composite hydrogel "pig" for pipeline cleaning.
Sadakbayeva Zh.; Blagikh E.; Zhumaly A.; Nurakhmetova Zh.; Klivenko A.

3. Innovation Patent of the Republic of Kazakhstan № KZ 24371 (from 15.08.**2011**):
Mechanical method of obtaining silver nanoparticles. Kudaibergenov S.; Abdullin
Kh.; Ermolayev V.; Ibrayeva Zh; Sadakbayeva Zh.; Tatykhanova G.

4. Innovation Patent of the Russian Federation № RU 2411258 (from 19.01.**2009**):
Method of formation of the microrelief on the polymeric films surfaces. Bolshakova
A.; Yarysheva L.; Volynskii A.; Panchuk D.; Sadakbayeva Zh.; Kechek'yan A.;
Bazhenov C.; Bakeev N.

List of presentations

Contributed talks:

1. Workshop "Career in Polymers III", Prague, Czech Republic, July 16, 2011
Zh. Sadakbayeva, M. Dušková-Smrčková, K. Dušek: Hydrogels based on sequential
interpenetrating networks: swelling and mechanical properties (Best Lecture Award).

2. 21st Annual Student Conference Week of Doctoral Students, Faculty of
Mathematics and Physics, Charles University in Prague, Prague, Czech Republic,
May 30, 2012
Zh. Sadakbayeva, M. Dušková-Smrčková, K. Dušek: Interpenetrating network
hydrogels.

3. EU FP7 People Nanopoly meeting, Prague, Czech Republic, April 23, 2012
Zh. Sadakbayeva, M. Dušková-Smrčková, K. Dušek: Interpenetrating network
hydrogels.

4. EU FP7 People Nanopoly meeting, Porto, Portugal, September 19, 2012
Zh. Sadakbayeva, M. Dušková-Smrčková, K. Dušek: Interpenetrating network
hydrogels based on homogeneous hydrogels with various cross-linker concentration.

5. Macro Treats Its Talents, Institute of Macromolecular Chemistry AS CR, Prague,
Czech Republic, December 3, 2012
Zh. Sadakbayeva, M. Dušková-Smrčková, K. Dušek: Interpenetrating network
hydrogels: preparation and mechanical responses.

6. EU FP7 People Nanopoly meeting, Zurich, Switzerland, April 30, 2013
Zh. Sadakbayeva, M. Dušková-Smrčková, K. Dušek: The concept of reinforcement
of macroporous polymer scaffolds by double network formation.

7. Colloquium XXIII, Institute of Macromolecular Chemistry AS CR, Prague, Czech Republic, February 10-13, 2014

Zh. Sadakbayeva, M. Dušková-Smrčková, K. Dušek: Microstructures hydrogels with double network structure.

8. Individual seminar in the frame of seminar cycles of Education and Information Center of the Institute of Macromolecular Chemistry AS CR, Prague, Czech Republic, May 7, 2015

Zh. Sadakbayeva, M. Dušková-Smrčková, K. Dušek: Hydrogels with interpenetrating network structure.

9. 23rd Polymer Networks Group Meeting, Stockholm, Sweden, June 19-23, 2016

Zhansaya Sadakbayeva, Miroslava Dušková-Smrčková, Adriana Šturcová, Miloš Steinhart, Karel Dušek: IPN hydrogels of poly(2-hydroxyethyl methacrylate) and poly(2,3-dihydroxypropyl methacrylate) with tunable deformation responses.

Conference abstracts published in scope of the PhD work:

1. POLYCHAR 20 World Forum on Advanced Materials, Dubrovnik, Croatia, 26-30 March, 2012. Book of abstracts. P2.25.

Zh. Sadakbayeva, M. Dušková-Smrčková, K. Dušek: Interpenetrating networks based hydrogels (Carl Klason Prize for an Outstanding Student Presentation).

2. 7th International Conference on Nanostructured Polymers and Nanocomposites, 24-27 April, 2012, Prague, Czech Republic. Book of abstracts. P. 364.

Zh. Sadakbayeva, M. Dušková-Smrčková, K. Dušek: Interpenetrating network hydrogels.

3. 7th International Conference on Nanostructured Polymers and Nanocomposites, 24-27 April, 2012, Prague, Czech Republic. Book of abstracts. P. 303.

Kubies D., Přadný M., Michálek J., Šlouf M., Sadakbayeva Zh., Dušková M., Filová E., Havlíková J., Bačáková L.: HEMA-based macroporous hydrogels: the effect of mechanical properties, charge and pore size of and behavior of MG63 osteogenic cells.

4. TERMIS World Congress 2012, Vienna, Austria, 5-8 September, 2012. Journal of Tissue Engineering and Regenerative Medicine. Vol. 6. Issue 1. P. 205.

Kubies D., Přadný M., Michálek J., Šlouf M., Sadakbayeva Zh., Filová E., Havlíková J., Bačáková L.: The effect of chemical composition, pore size and mechanical properties of macroporous hydrogels on behavior of MG63 osteogenic cells.

5. European Polymer Congress EPF 2013, Pisa, Italy, 16-21 June, 2013. Book of abstracts. P2-139.

Zh. Sadakbayeva, M. Dušková-Smrčková, K. Dušek: Interpenetrating network hydrogels: monomer crosslinking in presence of polymeric network.

6. 22nd Polymer Networks Group Meeting and the 10th Gel Symposium 2014, Tokyo, Japan, 10-14 November 2014. Book of abstracts. KL18. P. 26.

K. Dušek, M. Dušková-Smrčková, Zh. Sadakbayeva, A. Choukourov, J. Šomvarský: Swelling and elasticity of constrained networks.

7. 22nd Polymer Networks Group Meeting and the 10th Gel Symposium 2014, Tokyo, Japan, 10-14 November 2014. Book of abstracts. CT23a. P. 83.

M. Dušková-Smrčková, Zh. Sadakbayeva, K. Dušek: Rheology and swelling of double-network hydrogels.

8. 23rd Polymer Networks Group Meeting, Stockholm, Sweden, 19-23 June 2016. Book of abstracts. O-33.

Zhansaya Sadakbayeva, Miroslava Dušková-Smrčková, Adriana Šturcová, Miloš Steinhart, Karel Dušek: IPN hydrogels of poly(2-hydroxyethyl methacrylate) and poly(2,3-dihydroxypropyl methacrylate) with tunable deformation responses.

9. 23rd Polymer Networks Group Meeting, Stockholm, Sweden, 19-23 June 2016. Book of abstracts. O-9.

Miroslava Dušková-Smrčková, Zhansaya Sadakbayeva, Miloš Steinhart and Karel Dušek: Interpenetrating Network Hydrogels: Roles and Fates of Network 1 and Network 2.

10. ACS National Meeting & Exposition /254./. Washington, USA, 20-24 August 2017. Program Book. Washington: American Chemical Society. 2017. PMSE-40.

Dušková-Smrčková M., Sadakbayeva Zh., Steinhart M., Šturcová A., Pfleger J., Dušek K.: Interpenetrating polymer network hydrogels based on poly(2-hydroxyethyl methacrylate): morphology effects on formation, swelling, optical, and mechanical properties.